University of Antwerp
LMPH | Laboratory of Microbiology, Parasitology and Hygiene

Faculty of Pharmaceutical, Biomedical and Veterinary Sciences

Department of Biomedical Sciences

Characterizing the bone marrow as a parasitological niche responsible for antileishmanial treatment failure

Karakterisering van het beenmerg als niche voor *Leishmania* en oorzaak van behandelingsfalen

Thesis submitted to obtain the degree of
Doctor in Biomedical Sciences at the University of Antwerp

Laura DIRKX

May 2023, Antwerp

Promotors:

Prof. dr. Guy Caljon
Prof. dr. Louis Maes

ISBN: 9789057287879

Depot number: D/2023/12.293/11

Front cover design: Laura Dirkx

The research described in this thesis was carried out in the Laboratory of Microbiology, Parasitology and Hygiene (LMPH) at the University of Antwerp, Belgium. The study was funded by an FWO-sb grant.

Dissertation submitted to obtain the degree of Doctor in Biomedical Sciences at the University of Antwerp, Belgium to be defended by

Laura DIRKX

Promotors, University of Antwerp

Prof. dr. Guy Caljon — Promotor

Laboratory of Microbiology, Parasitology and Hygiene (LMPH)

Prof. dr. Louis Maes — Promotor

Laboratory of Microbiology, Parasitology and Hygiene (LMPH)

Members of the PhD Committee, University of Antwerp

Prof. dr. Kristel Sleegers — Chair

Centrum voor Moleculaire Neurologie

Prof. dr. Tom Vanden Berghe — Member

Pathophysiology

External members of the PhD Jury

Prof. dr. ir. Stefan Magez

Department of Bio-engineering Sciences, Vrije Universiteit Brussel, Belgium

Laboratory for Biomedical Research, Ghent University Global Campus, South Korea

Prof. dr. Ana Tomás

Molecular Parasitology Group, Instituto de Investigação e Inovação em Saúde (i3S), Universidade do Porto, Portugal

Prof. dr. ir. Yann Sterckx

Laboratory of Medical Biochemistry, University of Antwerp, Belgium

"Whatever you do in life will be insignificant,

but it is very important that you do it."

- Mahatma Gandhi

Table of content

Abbreviations

µg	microgram
µL	microliter
µm	micrometer
µM	micromolar
γ-GCS	gamma-glutamylcystein synthetase
4-IPP	4-iodo-6-phenylpyrimidine

A

ATP	adenosine triphosphate
ACK	ammonium-chloride-potassium
ACR	Arsenate reductase
AmB	amphotericin B deoxycholate
APC	allophycocyanin
APC-Cy7	allophycocyanin cyanine 7
AQP	aquaglyceroporin

B

BCR	B cell receptor
b.i.d./BID	twice a day
BLI	bioluminescent imaging
BM	bone marrow
BMDM	bone marrow-derived macrophages
BSA	bovine serum albumin
BW	body weight

C

cAMP	cyclic adenosine monophosphate
CD	cluster of differentiation
CO_2	carbon dioxide
CL	cutaneous leishmaniasis
CLP	common lymphoid progenitors
CMP	common myeloid progenitors
Ct	cycle threshold
CXCL12	CXC-motive chemokine ligand 12
CXCR4	CXC-motive chemokine receptor 4
Cys	cysteine

D

DAPI	4', 6-diamidine-2'-phenylindole dihydrochloride
DAT	direct agglutination test
DC	dendritic cell
DEG	differentially expressed genes
DMEM	Dulbecco's Modified Eagle Medium
DMSO	dimethyl sulfoxide
DNA	deoxyribonucleic acid
DND*i*	Drugs for Neglected Diseases *initiative*
dpi	days post-infection

E

EC_{50}	effective concentration 50%

EDTA	ethylenediaminetetraacetic acid
Eef2	eukaryotic translation elongation factor 2
e.g.	exempli gratia (for example)
ELISA	enzyme-Linked Immunosorbent Assay
EVs	extracellular vesicles

F

FACS	fluorescence-activated cell sorting
FMO	fluorescence minus one
FoB	follicular B cell
FSC	forward scatter

G

GFP	green fluorescent protein
GM-CSF	granulocyte macrophage colony-stimulating factor
GMP	granulocyte monocyte progenitors
GOI	genes of interest
GP63	glycoprotein 63
GPCR	G-protein coupled receptors
GSH	glutathione

H

h	hours
HDT	host directed therapy
HEPES	4-(2-hydroxyethyl)-1-piperazine-ethanesulfonic acid

HIF-1	hypoxia inducible factor 1
HIV	Human Immunodeficiency Virus
HRP	Horseradish peroxidase
HOMEM	hemoflagellate-modified essential medium
hpi	hours post-infection
HSC	hematopoietic stem cells
HSPC	hematopoietic stem/progenitor cells

I

IC_{50}	inhibitory concentration 50 %
i.e.	id est (that is)
IFN	interferon
Ig	immunoglobulin
IL	interleukin
i.m. / IM	intramuscular
iNOS	inducible nitric oxide synthase
i.p. / IP	intraperitoneal
ns	not significant
IVIS	*in vivo* imaging system
i.v. / IV	intravenous
iFCS	inactivated fetal calf serum
iNOS	inducible nitric oxide synthase

K

kDa	kilodalton

KO	knock-out
KC	Kupffer cells

L

L-AmB	liposomal amphotericin B
LdMT	*L. donovani* miltefosine transporter
LdROS3	subunit of the LdMT transporter
LPG	lipophosphoglycan
LT-HSC	long-term hematopoietic stem cells

M

M	molar
MAPK	mitogen-activated protein kinase
MCL	mucocutaneous leishmaniasis
M-CSF	macrophage colony-stimulating factor
MHC	major histocompatibility complex
MIF	macrophage migration inhibitory factor
MIL	miltefosine
MilliQ	ultrapure water
mL	millilitres
mM	millimolar
MOA	mode-of-action
MOI	multiplicity of infection
MPP	multipotent progenitors
MSC	mesenchymal stem cells

mRNA	messenger ribonucleic acid
MDR	multidrug resistance transporter
MRP1	multidrug resistance-associated protein 1
MRPA	multidrug resistance associated protein A
MW	molecular weight
MZB	Marginal zone B cell

N

NA	not available
NADP	nicotinamide adenine dinucleotide phosphate
NADPH	reduced nicotinamide adenine dinucleotide phosphate
Nb	nanobody
NEAA	nonessential amino acids
NETs	neutrophil extracellular traps
NF-κB	nuclear transcription factor kappa B
NK	natural killer cell
NKT	natural killer T cell
nm	nanometres
NO	nitric oxide
NTD	neglected tropical disease

O

ODC	ornithine decarboxylase
Orn	ornithine

P

PALS	periarteriolar lymphoid sheath
PAMP	pathogen-associated molecular patterns
PBS	phosphate buffered saline
PCR	polymerase chain reaction
PE	Phycoerythrin
PE-Cy7	phosphatidylethanolamine cyanine 7
Pen/Strep	penicillin/streptomycin
PerCP	peridinin chlorophyll protein
PKDL	post-kala-azar dermal leishmaniasis
PMM	paromomycin
p.o. / PO	per os / per oral
PPG	proteophosphoglycan
PSG	promastigote secretory gel
Put	putrescine

Q

qPCR	quantitative polymerase chain reaction

R

RGS	regulator of G-protein signaling
RLU	relative luminescence units
RNA	ribonucleic acid
RNAi	ribonucleic acid interference
rRNA	ribosomal ribonucleic acid

RNI	reactive nitrogen intermediates
RoA	route of administration
ROI	region of interest
ROS	reactive oxygen species
RPMI	Roswell Park Memorial Institute
RT-qPCR	real-time quantitative PCR

S

Sb	antimonials
SbIII	trivalent antimony
SbV	pentavalent antimony
SD	standard deviation
SDF-1	stromal cell-derived factor-1
SEM	standard error of the mean
SI	selectivity index
s.i.d./SID	Semel in die (once daily)
siRNA	small interfering RNA
SL	spliced leader
SS	spermidine synthase
SSC	side scatter
SPF	Specific Pathogen Free
spp.	species
ST-HSC	short-term hematopoietic stem cells

T

Ta	annealing temperature
TLR	toll-like receptor
Tm	melting temperature
TNF	tumour necrosis factor
Tregs	regulatory T cells
TDR1	thiol-dependent reductase 1
TR	trypanothione reductase
T[SH2]	trypanothione

U

UA	University of Antwerp
u.d.	undetected

V

v/v	volume/volume
VL	visceral leishmaniasis

W

WHO	World Health Organization
wpi	weeks post-infection
WT	wild type

AIMS AND OUTLINE

Aims and outline

Visceral leishmaniasis (VL) is a major **neglected tropical disease**, caused by protozoan parasites of the genus *Leishmania*, and transmitted by the bite of female sand flies. However, do not let the word 'tropical' mislead you; VL is also endemic to certain European countries **[1]**.

More than 1 billion people live in endemic areas in Central and South America, Asia, Africa and Southern Europe and are at risk of infection **[2]**. The number of effective chemotherapeutics to cure leishmaniasis is scarce and all currently available drugs have many disadvantages, such as severe toxic side effects, high costs, the need for parenteral administration requiring hospitalization, the emergence of drug resistance and **increasing treatment failure rates [3]**. To date, relapse rates with miltefosine and antimonials are up to 20% and 38%, respectively, within 12 months after treatment **[4-6]**.

Treatment failure is often associated with drug resistance, although microorganisms can also be impervious to drugs without the acquisition of genetic mutations. The occurrence of viable non-replicating cells, also known as persister-like cells, is common among bacteria and has also been described for *Plasmodium*, *Toxoplasma*, *Trypanosoma* and *Mycobacterium* **[7]**. **Persistent infections** can arise in different tissues and cells throughout the host, referred to as **sanctuary sites or niches**, such as hepatocytes (*P. vivax*), skeletal muscle (*T. gondii*), adipose tissue (*T. cruzi*) and the bone marrow (*M. tuberculosis*) **[8-12]**. Some of these niches give protection against active immunity and drug action **[7]**. Besides persistence linked to cellular niches, treatment failure can also be associated with parasitic adaptive modifications. In response to stress, some microorganisms adopt a **quiescent stage** characterized by a metabolic divergence from proliferation, increasing survival chances **[13]**. Recently, a form of quiescence was discovered in cutaneous leishmaniasis strains **[14]**.

Besides the therapeutic challenges, vaccine development as a prophylactic approach is mostly hampered by insufficient knowledge of parasite pathogenesis and the complexity of protective immune responses. Although much research on the protective role of innate immunity during VL is conducted **[15-17]**, B cells have been largely overlooked as contributors in the antileishmanial immune response, and little effort has been invested to decipher how VL influences **B lymphopoiesis**. Additionally, many infections such as African trypanosomiasis, malaria and measles, can hamper **pre-existing memory B cells** and thereby impair the humoral immune response against previous infections **[18-23]**, a detrimental disease outcome not yet investigated during VL.

Given these premises, the general aims of this thesis were:

(*i*) to unravel the origin of **post-treatment relapse** and make an in-depth analysis of the specific cellular tropism of *Leishmania* in the bone marrow niche,

(*ii*) to evaluate post-treatment parasite characteristics and define **parasite quiescence** in relation with relapse,

and

(*iii*) to better understand the impact of VL on **B cell lymphopoiesis** and humoral immunity, and characterize the **B cell-pathogen interaction**.

Chapter I of this PhD thesis provides an introduction on the causative agents of (visceral) leishmaniasis (**Chapter I.I**), a detailed overview of the available treatment options and their drawbacks (**Chapter I.II**), and the current knowledge on the immunopathogenesis of VL (**Chapter I.III**).

Chapters II-V focus on the bone marrow as a cellular niche, unravelling the origin of relapse with the discovery of a novel and extremely susceptible host cell, the long-term hematopoietic stem cell (LT-HSC) (*Aim 1*). In view of the increasing

relapse, potency of new chemical entities against parasites in this cellular niche should ideally be part of the preclinical data package. These chapters are dedicated to the characterization of LT-HSC as VL niche during infection and treatment failure (**Chapter II**) and the molecular decryption and therapeutic exploitability of the *StemLeish* transcriptional profile (**Chapter III**). To explore the propagation of traits associated with therapeutic failure, parasites originating from the bone marrow niche, *i.e.* post-treatment parasites and quiescent versus non-quiescent parasites, were characterized in terms of infectivity and sand fly transmissibility (*Aim 2,* **Chapter IV**). **Chapter V** aims to better understand the immunopathological impact of VL on bone marrow homeostasis, with its effects on B lymphopoiesis and pre-existing B cell memory (*Aim 3*).

Finally, all obtained results are discussed and put into a broader perspective in **Chapter VI** while contemplating on future endeavors.

INTRODUCING *LEISHMANIA*

CHAPTER I

I.I Leishmaniasis

Leishmaniasis: now hiring

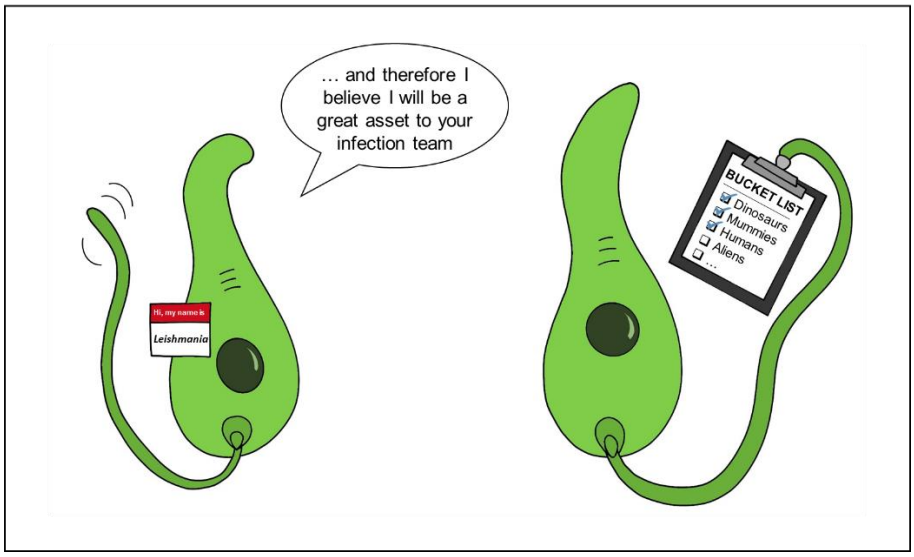

I. Introducing *Leishmania*

I.I General introduction: leishmaniasis

1. Leishmaniasis throughout (pre)history

Did you know that 100 million years ago, even dinosaurs could get infected by *Leishmania*? Indeed, the oldest discovery of a *Leishmania*-like species was found inside a blood-filled female of a now extinct sand fly species, preserved in two fossil ambers of prehistorical times **[24, 25]**.

Despite the primeval occurrence of the pathogen, the first report of the disease in human history was millions of years later on a papyrus scripture in ancient Egypt **[26]** and confirmed by detecting *Leishmania* DNA in mummies **[27]**. From 2000 BCE until the 20th century CE, leishmaniasis carried many names from 'Nile pimple' in Egypt to 'Dum dum fever' in India (**Table 1.1**), until the discovery of the causing pathogen by the Scottish pathologist William Boog Leishman and the Irish doctor Charles Donovan in 1903 instigating the name 'Leishman-Donovan bodies' **[28, 29]**.

Table 1.1. History of leishmaniasis nomenclature. Reviewed in **[30]** and extended using **[31-35]**.

"I have been called many names over many lifetimes"

Name	Time	Place
Nile Pimple	1500 BCE	Egypt
Balkh sore	10th century	Afghanistan
Uta/Espundia	16th century	Peru
White leprosy	16th century	Ecuador/Peru
Oriental sore	18th century	Aleppo, Syria
Aleppo evil/boil	18th century	Aleppo, Syria
Baghdad/Jericho/Delhi boil	19th century	Baghdad/Jericho/Delhi
Kala-azar	1827	India
Dum dum fever	1827	India
Burdwan fever	1858	Bengal
Leishman-donovan bodies	1903	India
Leishmania spp.	Now	Everywhere

It is even speculated that in biblical history, the boils sent by Jehovah through Moses as described in the Old Testament, are referring to the 'Nile pimple' and thus leishmaniasis **[36]**, indicating again how infamous this disease has been and remains to date.

My deepest gratitude to those reading my thesis on the battle against leishmaniasis disease and treatment failure.

2. Geographical distribution and epidemiology

There is no consensus on the geographical origin of leishmaniasis and several hypotheses are discussed **[30]**. Nevertheless, the current global spread of the disease is undebatable.

To date, leishmaniasis can be contracted in 98 countries around the world, mainly in South and Central America, Africa, Asia, and southern Europe (**Figure 1.1**) **[37]**. More importantly, the last decade the disease has been spreading to non-endemic areas in part due to deforestation, migration, and climate change, forcing and enabling the expansion of the sand fly vector **[38, 39]**. In 2020, Belgium reported 27 imported human cases of leishmaniasis **[37]**.

Despite its widespread distribution, in 2020 more than 90% of new reported cases occurred in only 10 countries: Brazil, China, Ethiopia, Eritrea, India, Kenya, Somalia, South Sudan, Sudan and Yemen **[2]**. Leishmaniasis is often deemed a disease of the poor, as factors contributing to an increased incidence include poor housing conditions and low economic status **[40]**. The last decade, high endemic countries such as India, Nepal and Bangladesh committed to eliminate leishmaniasis as a public health problem, as such the incidence has decreased substantially **[41]**.

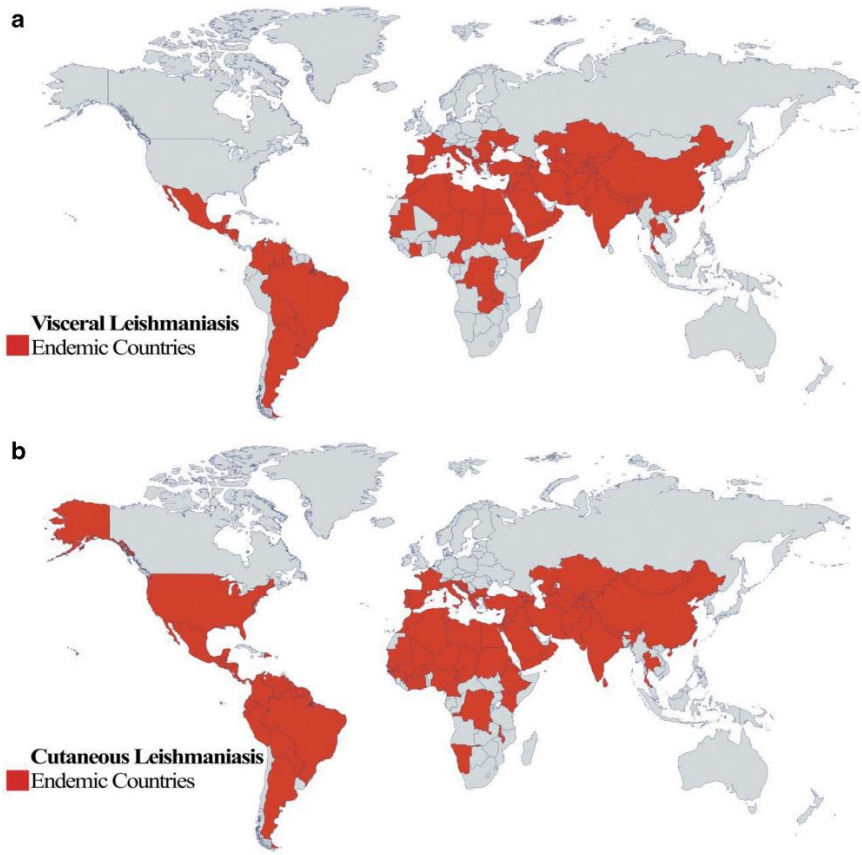

Figure 1.1. Status of endemicity of leishmaniasis. (a) visceral and **(b)** cutaneous leishmaniasis are the most common clinical manifestations (*vide infra*) **[42]**.

Currently, an estimate of 12 million people are infected and over one billion people are at risk of contracting leishmaniasis. About 700,000 to 1 million new cases are reported yearly and approximately 50,000 people die annually due to leishmaniasis **[43, 44]**. However, asymptomatic infections are common in endemic areas and the seroprevalence can go up to 60% **[45]**, suggesting the true disease burden is greatly underestimated.

Collectively, leishmaniasis is a notorious disease of worldwide concern, yet it is still amongst the top 10 'most neglected' tropical diseases (NTDs) in the world as they mostly affect impoverished communities **[46]**. Amongst all parasitic diseases, mortality from leishmaniasis is second only to malaria **[47]**.

3. The *Leishmania* parasite

Now that the antiquity, cosmopolitan nature and profound importance of leishmaniasis are established and your interest is piqued, this next part will focus on the question: what is leishmaniasis?

3.1 Life cycle

Leishmaniasis is a vector-borne disease caused by obligate intracellular protozoan parasites of the *Leishmania* genus **[48]**. Approximately 53 *Leishmania* species are known of which 31 infect mammalian hosts and at least 20 of them are of medical importance in humans **[49]**. The parasites are transmitted by the bite of female bloodsucking sand flies of the genus *Phlebotomus* or *Lutzomyia* **[50, 51]**.

Leishmania parasites exist in two major morphological forms in their life cycle; an extracellular flagellated promastigote within the sand fly's gut (**Figure 1.3, a**) and an obligate intracellular non-flagellated amastigote within phagocytic cells of the mammalian host (**Figure 1.3, b**) **[47]**.

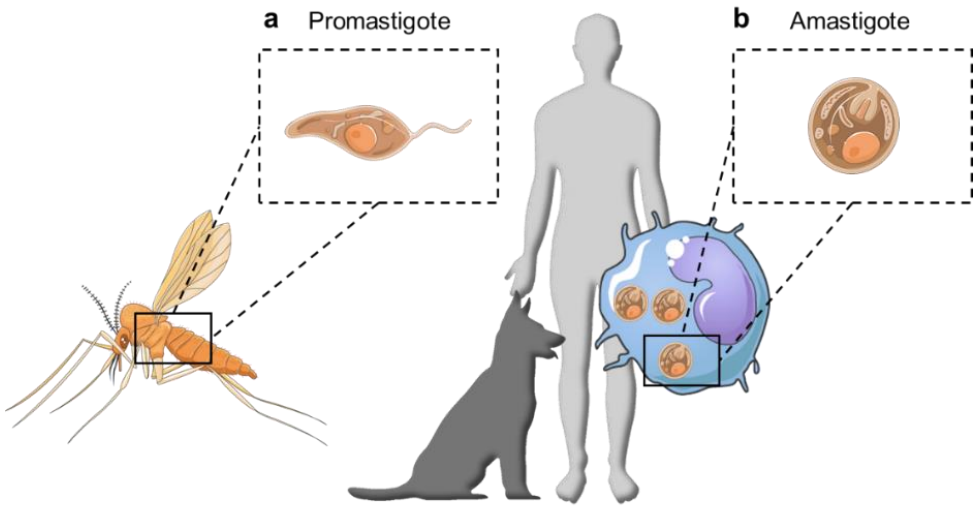

Figure 1.3. Two morphological stages of *Leishmania*. (a) Extracellular promastigote with a well-developed anterior flagellum, exists in the sand fly gut. **(b)** Intracellular amastigote within phagocytic cells of the mammalian host. Figure was created using Servier Medical Art.

Infected sand flies inoculate or even regurgitate metacyclic promastigotes, *i.e.* the infective stage, into the skin when biting a mammalian host (1), together with a variety of antigenic salivary components **[52]**. Inoculated promastigotes are taken up by host phagocytic cells, whereby monocyte-derived cells are most common. Within phagocytes, promastigotes transform into amastigotes that exist within a parasitophorous vacuole or phagolysosome (2), a membrane-bound endosomal compartment that is developed after fusion of phagosomes and lysosomes **[53, 54]**. Amastigotes develop and multiply by simple division within the phagocyte (3) until they are released by cell lysis in order to infect novel host cells (4). Sand flies become infected when ingesting cells containing amastigotes (5). The associated decrease in temperature and increase in pH, triggers the transformation into the procyclic promastigote form that quickly multiplies in the sand fly midgut (6-7). Promastigotes eventually migrate to the proboscis and differentiate to the infective metacyclic stage (8), thus completing the *Leishmania* life cycle (**Figure 1.4**) **[55, 56]**.

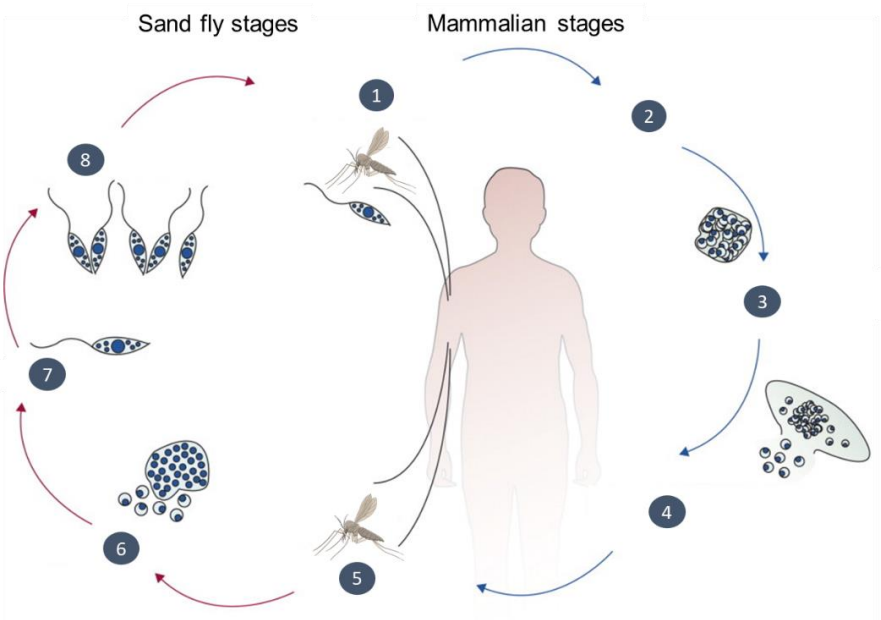

Figure 1.4. *Leishmania* life cycle. (1) Sand fly takes a blood meal and regurgitates promastigotes into skin, (2) promastigotes are phagocytosed by macrophages and neutrophils, (3) promastigotes transform into amastigotes inside macrophages, (4) amastigotes multiply, (5) sand fly takes a blood meal, (6) ingestion of parasitized cell, (7) amastigotes transform into promastigote stage in gut, and (8) divide in gut and migrate to the proventriculus and proboscis. Adapted from **[57]**.

Depending on the *Leishmania* species, the duration of the life cycle in vectors varies from 4 to 18 days. Low temperatures will extend the duration of the life cycle whereas high temperatures will shorten it **[58]**.

a) Promastigote (**Figure 1.3, a**)

Promastigotes are the extracellular 15–20 μm long flagellated *Leishmania* stage within the sand fly. Their well-developed flagellum provides motility and helps the parasite to attach to the sand fly gut **[42]**.

b) Amastigote (**Figure 1.3, b**)

Amastigotes are the obligate intracellular 3–5 μm long non-flagellated *Leishmania* form within cells of the mammalian host myeloid lineage. Their non-functional flagellum barely extrudes from the cell body and renders the amastigotes immobile. They are also known as the Leishman-Donovan bodies, with the typical and distinguishable kinetoplast, a structure consisting of mitochondrial DNA that can be stained and visualized separately from the *Leishmania* nucleus in infected clinical specimens **[47]**. In a lab environment, this stage survives best at 37°C and can transform back into promastigotes by lowering the temperature **[59]**.

3.2 Reservoirs

Natural 'reservoir' hosts of infectious diseases are responsible for maintaining the disease in nature. Hence, control and elimination of the disease largely depends on targeting of infection in the reservoir. For this, efficient screening, vaccination and/or providing protection using insecticides have been suggested **[60]**.

There are two main sources of human leishmaniasis; zoonotic leishmaniasis in which the reservoir hosts are wild animals, commensals or domestic animals, and anthroponotic leishmaniasis in which the reservoir host is human **[61]**. Depending

on the *Leishmania* species, various other susceptible hosts are identified besides humans (*i.e.* 'principal' hosts). The main and most known domestic reservoirs for leishmaniasis are dogs **[62]**. It is therefore imperative that dogs are vaccinated against leishmaniasis – yes, there is a vaccine for dogs **[63]**, but more on this later – before traveling to endemic areas such as Southern Europe.

3.3 The sand fly vector

The sand fly is the only recognized vector responsible for the transmission of *Leishmania*. This noiseless arthropod is only 2–3 mm long and characteristically positions its wings at a 40° angle to the abdomen (typical V-shape, **Figure 1.5**) **[64]**. As such, they are limited in their flying ability and travel mostly by jumping flights (also referred to as 'hopping') and stay close to the ground **[65, 66]**. Most sand flies are active from dusk till dawn, although biting indoors and in daylight is not excluded **[64]**. Besides, only female sand flies require a blood meal next to nectar in order to reproduce **[67]**.

The uptake of parasites by the blood-feeding sand fly is assisted by the cutting action of the mouth parts. Sand flies are pool feeders, *i.e.* they inflict a small wound into which the blood flows from superficial capillaries **[61]**.

Figure 1.5. Blood-fed female sand fly. Image from in-house *Lutzomyia longipalpis* sand fly colony at Laboratory of Microbiology, Parasitology and Hygiene (LMPH), University of Antwerp. Notice the pale 'sandy' color, from which the fly derived its name.

3.4 Clinical manifestations

The diseases manifest in three main clinical presentations depending on the interaction of the *Leishmania* species (**Table 1.2**), host genetic factors and immune response.

(a) Cutaneous leishmaniasis (CL)

CL is the most common form of leishmaniasis and causes skin lesions, mainly ulcers, on exposed parts of the body, leaving life-long scars that lead to stigmatization **[68]**. Lesions develop as a papule over weeks to months at the sand fly's biting site, and enlarges to a nodule that ulcerates slowly over the following few months **[57]**. The lesions usually tend to heal spontaneously within a year **[36]**. In some areas, acquiring CL at least once in a lifetime is very common, and is therefore referred to as 'al okht', translating from Arabic to 'little sister', because "everybody has one" **[35]**.

(b) Mucocutaneous leishmaniasis (MCL)

MCL leads to partial or total destruction of the cartilage and soft tissue (mucous membranes) of the nose, mouth, oropharynx, nasopharynx and eyelids; often resulting in an extensive disfiguration of the face **[69]**, stigmatization and social isolation.

(c) Visceral leishmaniasis (VL)

VL, also known as kala-azar or black fever, is the most lethal disease form and is fatal when left untreated. It is characterized by remittent fever, weight loss, enlargement of the spleen and liver (termed hepatosplenomegaly), and anemia. Overall pancytopenia (*i.e.* reduction in the number of blood cells) is the main reason for disease lethality, causing hemorrhages and an increased susceptibility to secondary infections **[70, 71]**. My PhD research focused on VL, and the current treatment and immunopathogenesis of the disease will be further elaborated in Chapters I.II and I.III.

The incubation period of leishmaniasis varies according to the clinical form of disease, but is generally 2 weeks (or less) to 2 months for CL, 3 to 9 months for VL, and over 2 years for MCL **[69]**.

Despite the well-recognized classification, there is not always a clear distinction between VL and CL. Indeed, certain parasite species that generally cause CL (e.g. *L. major*) can visceralize in rare cases **[72]**. The reverse is also observed: the visceral species *L. infantum* and *L. donovani* can be dermatotropic and cause localized cutaneous lesions **[73, 74]**. A specific dermal complication that can develop after *L. donovani* VL infection is known as post-kala-azar dermal leishmaniasis (PKDL), in which the parasites persist in the skin after treatment causing highly infectious yet self-healing lesions that usually disappear within a year **[75]**.

3.5 Taxonomy

Leishmania parasites belong to the order of the Kinetoplastida and family of Trypanosomatidae, as such they are closely related to *Trypanosoma* parasites **[76]**. Classification of leishmaniasis is done either according to the world regions in which they occur, the location of the development in the sand fly vector or according to the spectrum of clinical manifestations (*i.e* CL, MCL or VL as described above) (**Table 1.2**).

Old World leishmaniases are transmitted by *Phlebotomus spp*. and exist in the Eastern Hemisphere. New World leishmaniases are transmitted by *Lutzomyia spp*. and are endemic to the Western Hemisphere **[77]**.
In the sand fly vector, parasites establish either (i) in the hindgut, *i.e.* hypopylaria, referred to as the subgenus *Sauroleishmania*, (ii) anterior to the pylorus, *i.e.* suprapylaria, subgenus: *Leishmania*, or (iii) in the hindgut and pylorus, *i.e.* peripylaria, subgenus: *Viannia* **[78]**.

In experimental research, specific *Leishmania* strains are referred to using the World Health Organization (WHO) code for newly isolated strains. An example is

MHOM/FR/96/LEM3323. This label gives information about (1) the host from which the strain was isolated (MHOM: M for Mammalia followed by HOM for *Homo*), (2) the country where the infection was contracted (FR: France), (3) the year the strain was isolated (1996) and (4) the first laboratory identification of the strain (LEM3323) **[79]**.

Table 1.2. Summary of the clinical manifestations of different *Leishmania* species and their geographical distribution. In blue are the species used in this project. Adapted from **[42]**.

Species	Disease	Geographical distribution
L. donovani	VL, PKDL	India, Nepal, Bangladesh, Sri Lanka, East Africa
L. infantum (or *L. chagasi*)	VL, PKDL	Mediterranean Basin, central and west Asia, Latin-America
L. major	CL	North Africa, central and west Asia
L. tropica	CL	Central and west Asia, western India
L. aethiopica	CL	Ethiopia and Kenya
L. braziliensis	CL, MCL	Argentina, Belize, Bolivia, Brazil, Colombia, Costa Rica, Ecuador, French Guyana, Guatemala, Honduras, Nicaragua, Panama, Peru, Venezuela
L. amazonensis	CL, MCL	Bolivia, Brazil, Colombia, French Guyana, Paraguay
L. mexicana	CL	Belize, Colombia, Costa Rica, Dominican, Ecuador, El Salvador, Guatemala, Honduras, Mexico, USA
L. yucumensis	CL	Bolivia
L. llanosmartini	CL, MCL	Bolivia
L. guyanensis	CL, MCL	Brazil, French Guyana, Guyana, Venezuela
L. lainsoni	CL	Brazil
L. naiffi	CL	Brazil, French Guyana
L. shawi	CL	Brazil
L. colombiensis	CL	Colombia, Venezuela
L. panamensis	CL, MCL	Colombia, Costa Rica, Honduras, Nicaragua, Panama
L. aristedesi	CL	Panama
L. peruviana	CL	Peru
L. garnhami	CL	Venezuela
L. pifanoi	CL	Venezuela
L. venezuelensis	CL	Venezuela

3.6 Prevention

Vector control strategies are based on indoor residual spraying, long-lasting insecticide-treated nets, and environmental management. However, it is generally assumed that the sand fly vector mainly bites outdoors and there is no evidence for the effectiveness of outdoor insecticide spraying **[48]**.

Vaccination studies have been ongoing for many decades, however, to date still no human vaccine exists. The only promising candidate is ChAd63-KH, a third-generation vaccine encoding two antigens of *L. donovani*, KMP-11 and HASPB **[80]**. In contrast, since 2011 a canine leishmaniasis vaccine, CaniLeish (Virbac, France) was licensed in the European Union for protection of dogs against *L. infantum* infection. It requires yearly boosting and decreases rather than eliminates the risk of acquiring leishmaniasis **[63]**. Nowadays, three canine leishmaniasis vaccines are commercially available.

Leishmania vaccine development is mostly hampered by insufficient knowledge of parasite pathogenesis and the complexity of protective immune responses (see Chapter I.III). Promising results from experimental human VL vaccine trials and the practice of "leishmanization" **[81]** provide strong evidence for the scientific feasibility of an effective vaccine against human VL.

3.7 Diagnosis

In general, leishmaniasis is diagnosed by demonstrating the presence of amastigotes in clinical specimens using direct microscopic examination or molecular analysis based on nuclear or kinetoplast DNA amplification. Recently, a new RNA real-time quantitative PCR assay was developed targeting the conserved and highly expressed spliced-leader (SL) mini-exon sequence **[82]**, which specifically allows the detection of viable parasites.

For microscopic examination, the sensitivity depends on the tissue: >90% in the spleen, 50–80% in bone marrow (BM) and even lower in lymph node aspirates.

Hence, splenic aspirates are considered the golden standard, although the procedure has a high risk of hemorrhage **[48]**.

In the field, two serological tests are available to detect circulating antibodies against VL in blood or serum: the direct agglutination test (DAT) **[83]** and the immunochromatographic rK39 lateral flow test **[84]** with sensitivities around 90-95%. These tests are simple to perform, cost-effective, stable at room temperature, rapid, and therefore widely implemented for the diagnosis of VL in resource-limited countries **[85]**. However, these tests are unreliable after antileishmanial treatment and can only be properly interpreted considering the clinical history of the patient **[48]**.

I.II Anti-leishmanial treatment (failure)

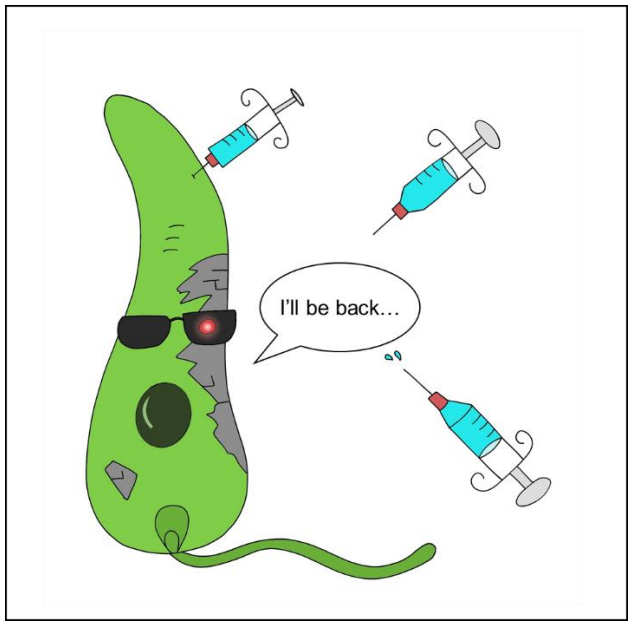

Part of this chapter has been published:

Gert-Jan Wijnant[1], Franck Dumetz[2], **Laura Dirkx[3]**, Dimitri Bulté[3], Bart Cuypers[4], Katrien Van Bocxlaer[5] and Sarah Hendrickx[3]*. Tackling Drug Resistance and Other Causes of Treatment Failure in Leishmaniasis. *Frontiers in Tropical Diseases* 2022, doi.org/10.3389/fitd.2022.837460.

[1] Department of Cellular and Molecular Pharmacology, Louvain Drug Research Institute, Université Catholique de Louvain, Brussels, Belgium
[2] Institute for Genome Sciences, University of Maryland, Baltimore, MD, United States
[3] Laboratory of Microbiology, Parasitology and Hygiene (LMPH), Department of Biomedical Sciences, University of Antwerp, Antwerp, Belgium
[4] Adrem Data Lab, Department of Computer Science, University of Antwerp, Antwerp, Belgium
[5] Department of Biology, York Biomedical Research Institute, University of York, York, United Kingdom

I. Introducing *Leishmania*

I.II Anti-leishmanial treatment (failure) of VL

1. Current treatment options

VL belongs to the most neglected diseases, thus it is not surprising that only few therapeutic options are currently available. Moreover, because VL mainly affects the poorest developing countries, pharmaceutical industries are not eager to prioritize drug development for this indication **[86]**. The current antileishmanial treatment is limited to only a handful of commercial drugs, including pentavalent antimonials (Sb), miltefosine (MIL), paromomycin (PMM) and amphotericin B. The latter exists in two formulations: the free deoxycholate form (AmB) and the liposomal formulation (L-AmB) with lower toxicity **[87]** (**Figure 1.6**, overview on the mode of action).

However, the current treatments do not meet the standards to entirely cure VL and display severe limitations such as toxicity, high production cost, decreased efficacy, difficulty in administration, and most importantly the emergence of resistance (**Table 1.3**). Additionally, regional differences in therapeutic efficacy are observed, hence every region depends on different treatment strategies, highlighting the challenges of current VL treatment **[70, 86]**.

The high VL mortality rate dictates the need for novel and effective drug therapy and over the past decades, there has been an evolution from Sb monotherapy to treatment with new chemical entities and combination therapies to improve efficacy and prevent emergence of resistance **[87]**. Ideally, a treatment should be oral, safe and effective with a low cost and short course of maximum 10 days **[88]**.

Table 1.3. Current antileishmanial drugs. Abbreviations: route of administration (RoA), antimonials (Sb), miltefosine (MIL), paromomycin (PMM), amphotericin B (AmB), liposomal amphotericin B (L-AmB), intravenous administration (IV), intramuscular administration (IM), per os (PO).

Drug	RoA	Action mechanism	Adverse effects / limitations	
Sb	IV, IM	Elevated ROS levels, inhibition macromolecular biosynthesis in amastigotes	Cardiotoxicity, hepatotoxicity, nausea, vomiting, weakness, myalgia, abdominal colic, diarrhoea, skin rash, long treatment duration	[86, 87, 89-92]
MIL	PO	Interference with mitochondrial function and lipid metabolism	Teratogenic, gastrointestinal disturbances, nephrotoxicity, long treatment duration, expensive	[86, 87, 89, 90, 92-94]
PMM	IM	Interference with protein synthesis, inhibition respiration	Hepatotoxicity, ototoxicity, low efficacy	[86, 87, 92]
AmB	IV	Disruption parasitic membrane	Nephrotoxicity, hypokalemia, anaemia	[86, 87, 89, 90, 92]
L-AmB	IV	Disruption parasitic membrane	Fever, nausea, dorsal pain, vomiting, headache, mild nephrotoxicity, expensive	[87, 90, 92]

In general, most patients affected by VL respond well to treatment. However, successful treatment of VL with complete parasite eradication remains notoriously challenging **[95]**. Of increasing concern is the rise of antiparasitic drug resistance and treatment failure for all current antileishmanial drugs **[87, 96]**.

Drug resistance and treatment failure are no synonyms. Drug resistance is acquired by the parasite due to a variety of mechanisms, involving emergence of genetic mutations giving rise to a lower parasite susceptibility to the drug **[59]**. Treatment failure, however, can be the result of numerous parameters, either related to the parasite (tissue or cellular niches, fitness, virulence, quiescent forms), host (immunity, HIV co-infection, nutritional status, age, gender), or drug (dose, dosing frequency, treatment duration, pharmacokinetics, pharmaceutical quality, compliance) **[97]**. Inversely, when viable parasites survive upon treatment failure they can be exposed to residual subtherapeutic drug levels, hereby increasing the risk for the emergence of drug resistance **[98]**.

2. Drug resistance and treatment failure

In broad and general terms, drug resistance in leishmaniasis can be described as the decrease in the activity of a compound against a population of *Leishmania* parasites to which they were previously susceptible, consequently leading to the need for higher drug doses or even complete clinical drug ineffectiveness at the maximal safe or tolerated drug dose **[97]**. It should not be confused with drug tolerance, which is an innate feature related to intrinsic metabolic properties of certain species or life cycle stages that renders them naturally less sensitive to a certain drug **[99]**.

2.1 Parasite-related factors

The *Leishmania* parasite is known for its remarkable genomic plasticity and constant rearrangement, resulting in variations in gene copy number, clusters of genes, or even whole chromosomes **[100, 101]**. As a result, mosaic aneuploidy is not only widespread in *Leishmania* but is also an essential adaptive mechanism that allows a certain genome structure to be quickly selected in the face of adverse conditions, such as drug pressure **[102-105]**.

The acquisition of such resistance mechanisms can be associated with either (i) decreased drug uptake, (ii) increased drug efflux, (iii) enzymatic drug inactivation, (iv) improved cellular mechanisms to deal with drug-induced stress of cell damage, and/or (v) changes in the expression, abundance or drug binding affinity of the primary therapeutic target **[106]** (**Figure 1.6**). These changes, however, might not only impact the parasite's drug susceptibility but also the parasite fitness, which is defined as the parasite's virulence and its propensity to spread in the environment **[107]**. Detailed drug resistance mechanisms at the level of the parasite fall outside the scope of this thesis, however, Figure 1.6 summarizes the current scientific knowledge on mode of action and mechanisms of resistance for the available antileishmanial reference drugs Sb, MIL, AmB and PMM.

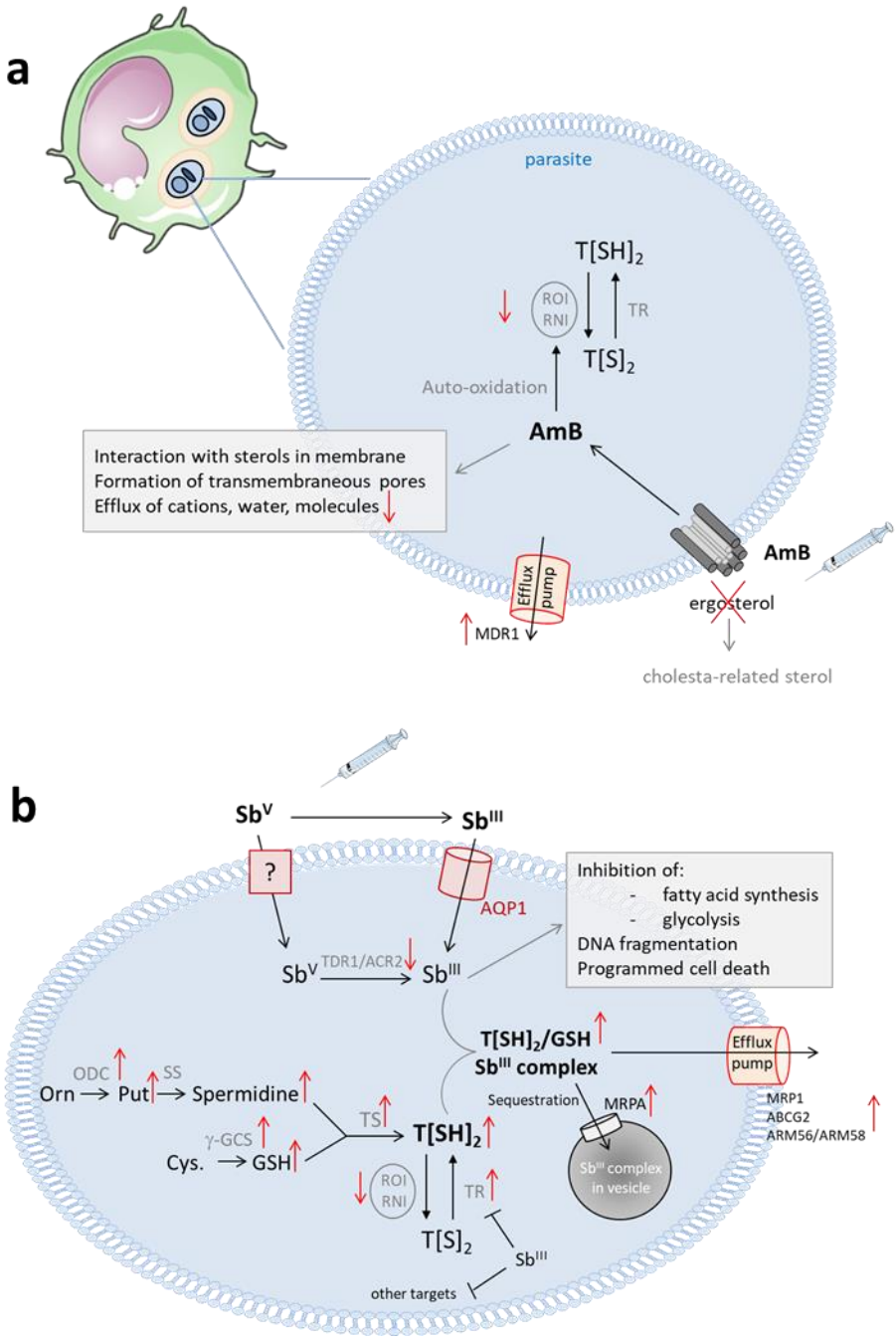
a
parasite
T[SH]2
ROI
RNI
TR
T[S]2
Auto-oxidation
AmB
Interaction with sterols in membrane
Formation of transmembraneous pores
Efflux of cations, water, molecules
AmB
Efflux pump
MDR1
ergosterol
cholesta-related sterol
b
SbV
SbIII
?
AQP1
SbV
TDR1/ACR2
SbIII
Inhibition of:
- fatty acid synthesis
- glycolysis
DNA fragmentation
Programmed cell death
T[SH]2/GSH
SbIII complex
Efflux pump
MRP1
ABCG2
ARM56/ARM58
ODC
SS
Orn
Put
Spermidine
Sequestration
MRPA
SbIII complex in vesicle
γ-GCS
Cys.
GSH
TS
T[SH]2
ROI
RNI
TR
T[S]2
SbIII
other targets

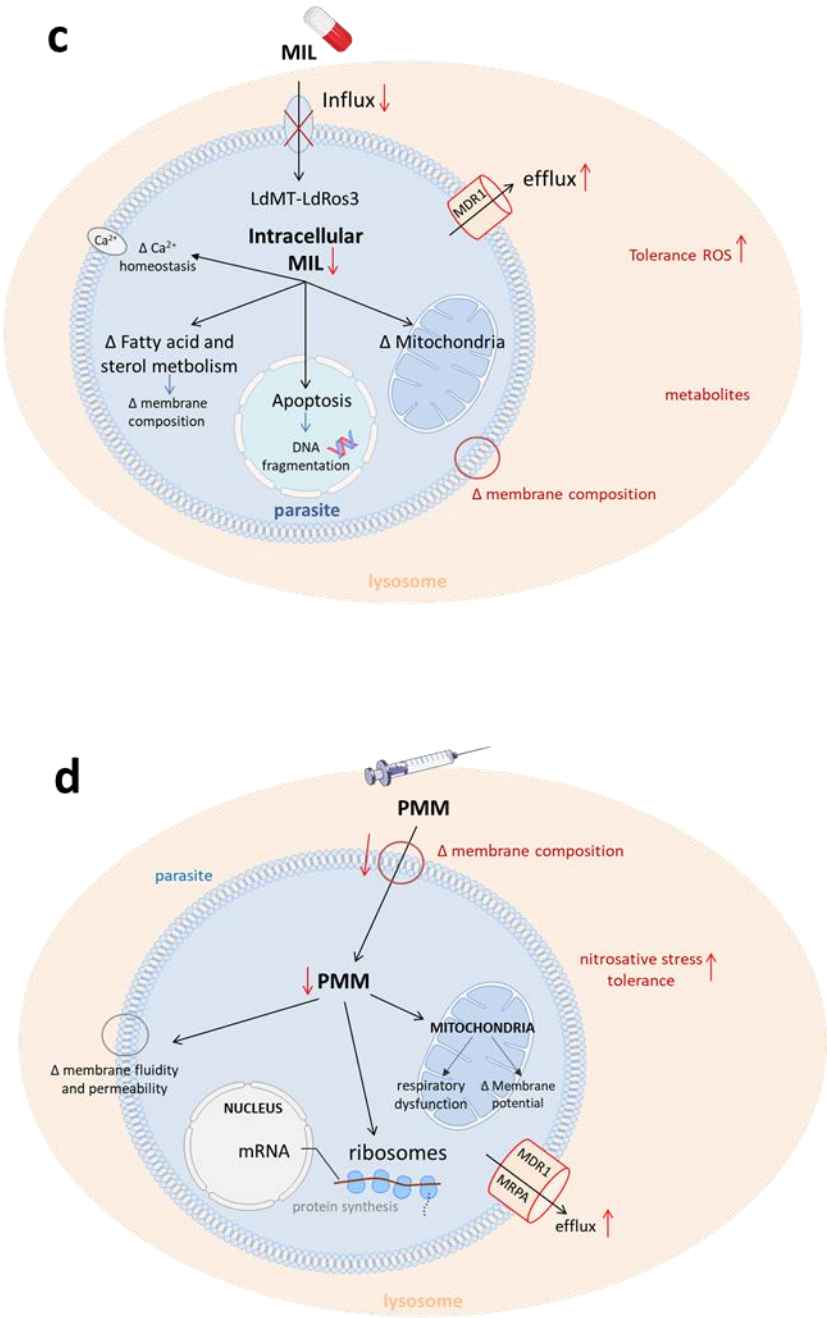

Figure 1.6. Schematic overview of the mechanisms of action and resistance of the antileishmanial reference drugs. Left corner: infected host cell with amastigotes in phagolysosomes. Resistance mechanisms are shown in red. **(a)** The mechanism of action of amphotericin B. AmB Amphotericin B; Cys cystein; γ-GCS gamma-glutamylcystein synthetase; GSH glutathione; Orn ornithine; ODC ornithine decarboxylase; Put putrescine; RNI reactive nitrogen intermediates; ROI reactive oxygen intermediates; SS spermidine synthase; TR trypanothione reductase; T[SH2] trypanothione; **(b)** The mechanism of action of antimonials. (ACR

Arsenate reductase; AQP aquaglyceroporin; Cys cysteine; γ-GCS gamma-glutamylcysteine synthetase; GSH glutathione; NADP nicotinamide adenine dinucleotide phosphate; NADPH reduced nicotinamide adenine dinucleotide phosphate; Orn ornithine; ODC ornithine decarboxylase; Put putrescine; RNI reactive nitrogen intermediates; ROI reactive oxygen intermediates; SS spermidine synthase; SbIII trivalent antimony; SbV pentavalent antimony; TDR1: Thiol-dependent reductase 1; TR trypanothione reductase; T[SH2] trypanothione); **(c)** The mechanisms of action for miltefosine. (LdMT *L. donovani* miltefosine transporter; LdROS3 subunit of the LdMT transporter; MIL miltefosine; MDR multidrug resistance transporter 1); **(d)** The mechanism of action of paromomycin. (PMM paromomycin; MDR1 multidrug resistance transporter 1; MRP1 multidrug resistance-associated protein 1; MRPA multidrug resistance associated protein A). Figure developed as part of review **[108]**.

Alternatively, the intracellular amastigotes could be in a quiescent or metabolically inactive state. In a recent review on protozoan persister-like cells, dormant forms of several Trypanosomatids are described and linked to drug treatment failure **[7]**.

As last, the inherent virulence of the infecting (polyclonal) parasite population can stimulate a different kind of immunological response in the host **[109, 110]**. It is known that *Leishmania* parasites produce virulence factor proteins, such as glycoprotein 63 (GP63), amastin or A2 protein to trick the immune system into inducing a weaker response. GP63 specifically provides parasite resistance to complement-mediated lysis and facilitates promastigote engulfment by macrophages **[111]**. Amastin is a surface glycoprotein vital for parasite intracellular multiplication and survival **[112, 113]**. A2 is a stress response protein specifically expressed on VL parasites and has a role in visceralization **[114]**.

2.2 Host-related factors

Host-related factors include immune response, pharmacokinetics, co-infections, genetics, and environment **[97]**.

a) Immune response

The current leishmaniasis treatment strategy focuses primarily on chemotherapeutic drugs, neglecting the importance of the host immune response. However, as an obligate intracellular parasite residing within immune cells, *Leishmania* infection involves a complex interplay between the host and parasite and is classified as an

immune-mediated disease **[115]**. Various types of immune responses are observed during different *Leishmania* spp. infections **[115]**, contributing to variable drug efficacy and acquisition of disease or drug resistance. Moreover, antileishmanial drugs are supported by an effective immune response, e.g. antimonials are less effective in immunocompromised individuals **[116]**. Hence, drug efficacy could be enhanced or compromised by the host's immune response, and immunotherapy could be crucial for the development of new treatments or to improve the efficacy of the current ones **[17]**.

Aside from drug resistance induced by genetic changes in the parasites themselves, therapeutic failure can occur by various other parameters, e.g. if the drug does not reach the appropriate sites of infection **[117]**, or when the parasites reside in protective niches **[7]**. Such niches or sanctuary sites are defined as cells or tissues that allow the pathogens to survive and escape treatment or the immune response. Niches have been described for many pathogens across the microorganism spectrum, e.g. adipose tissue for *T. cruzi* **[9]**, hepatocytes for *P. vivax* **[11]**, stem cells for *M. tuberculosis* **[8]** and primary skeletal muscle cells for *T. gondii* **[10]**. Besides residing in different tissues, *Leishmania* has been described to infect different types of cells: amastigotes have not only been found in phagocytic immune cells, but also in fibroblasts **[118]**, keratinocytes **[119]**, hepatocytes **[120]** and stem cells **[121]**. These specific infection sites could be linked to treatment failure as these niches have biological properties that provide opportunities for the pathogen to evade immune responses and drug action **[122]** (**Figure 1.7**).

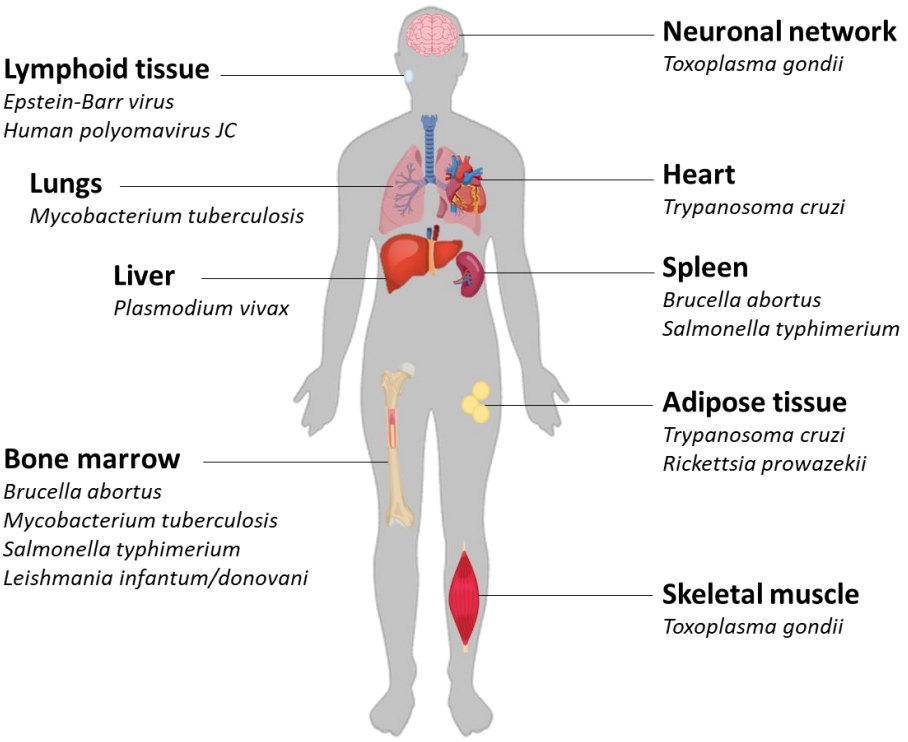

Figure 1.7. Tissue or cellular niches of specific pathogens. Several sanctuary sites have been described for pathogens the last decade **[8, 9, 11, 123-135]**. Figure developed using BioRender.com.

Besides benefiting from the protective properties of these cell or tissue niches, the intracellular parasites can induce modifications to the immune system or alter the infected host cell characteristics, all of which render parasites less responsive to treatment. For example, Sb failure has been linked to extra immune suppression caused by upregulation of the anti-inflammatory cytokine IL-10 produced by regulatory T cells (Tregs) **[136-138]**. This has also been related to induced overexpression of the host cell multidrug resistance-associated protein 1 (MRP1) to export Sb which diminishes the total levels reaching the parasites **[139]**. MIL has been described to enhance monocytic function, such as inducing phagocytosis and increasing oxidative burst. In addition, MIL increases the number of $CD4^+$ T cells, which is associated with the necessary Th1 response during infection **[140]**. MIL also increases IFN-γ responsiveness of macrophages by inducing the upregulation of the IFN-γ receptor, all of which shifts the immune response to Th1 type **[141]**.

b) HIV and other co-infections

As leishmaniasis is an immune mediated disease, co-infections can play a role in shaping the defensive immune response. Patients with immunodeficiencies can be particularly hard to cure **[142]**.

The most notoriously challenging co-infection of VL is human immunodeficiency virus (HIV). In general, HIV co-infection is associated with higher initial treatment failure and relapse rates due to immune exhaustion and chronic immune stimulation. In short, HIV infection decreases the number of $CD4^+$ T cells which allows the development of VL. Immunosenescence is detected, characterized by exhaustion of immune resources and the presence of senescent $CD4^+$ and $CD8^+$ T cells **[143]**. HIV co-infected VL patients are ideal candidates for the development of resistance due to the low efficacy of antileishmanials, the possibility of more adverse effects and a higher relapse rate. The recurrent relapses may select resistant clones that could contribute to the spread of drug resistance, especially in anthroponotic settings **[144]**.

Particularly with antimonials, low efficacy, pronounced side effects and increased mortality is observed in patients with HIV co-infection **[145]**. A recent systematic review of treatment of HIV-VL patients observed that L-AmB was the most commonly used drug with an overall cure rate of 68% **[146]**. Data of MIL in HIV co-infected patients are mainly with *L. infantum* in southern Europe where it has shown not to be very efficacious **[147]**. Although an initial cure rate of 64% was achieved, all patients relapsed **[148]**. Among HIV-VL patients in Ethiopia, MIL was safer but less effective than Sb **[149]**. To protect the few available drugs from the development of resistance, combination therapy appears to be a logical option. A retrospective analysis with a co-infected population in Bihar, India that received L-AmB and MIL for 14 days resulted in good tolerance, safety and efficacy **[150]**. For HIV-VL patients, secondary prophylaxis to prevent relapse is key. Unfortunately, the use of maintenance therapy has not yet been optimized and has only a partial

effect. A recent example in Ethiopian HIV-VL patients where pentamidine was used as secondary prophylaxis, the relapse-free survival rate at 2 years was only 58.3% **[151]**.

The knowledge of non-HIV immunosuppressive conditions is more fragmented and is mostly based on case reports or small case studies. The majority of reported non-HIV immunosuppressive conditions is related to organ transplantation, rheumatology, hematology and oncology **[116]**. The available data seem to suggest that, in comparison to HIV co-infected VL patients, the treatment efficacy is higher and recurrence rates are lower, but still not as good as in immunocompetent patients **[152]**. As with HIV co-infected VL patients, other immunocompromised VL patients experience relatively high rates of potentially life-threatening toxicity with Sb's **[153]**. Surprisingly, many VL patients remain relapse-free without secondary prophylaxis and despite the ongoing use of immunosuppressive medication **[154]**.

c) Geographic region

Regional variation in response to treatment has been extensively described **[155]**, accordingly regional differences in drug resistance are encountered as well.

Pentavalent antimonials are ineffective to treat VL in the Indian subcontinent due to the development of resistance **[156]**. In contrast, it is effective in other parts of the world especially in Africa **[157]**. MIL has been used successfully to treat VL in India, but efficacy in Africa is low **[149]** and failed in a clinical trial in Brazil. The 40% relapse rate in Brazil was associated with the absence of the MIL sensitivity locus **[158]**. PMM monotherapy has been shown to be highly variable between geographical regions with high efficacy in Indian VL patients **[159]** but failing to show a similar efficacy in Eastern Africa. Within Eastern Africa, large geographical variability in efficacy has been observed, with lowest efficacy in sites in Sudan (14.3% and 46.7%) compared with Kenya (80.0%), Northern Ethiopia (75.0%), and Southern Ethiopia (96.6%) **[160]**. A recent study comparing Indian and African VL

patients concluded that the differences in PMM efficacy could not be explained by differences in pharmacokinetics **[161]**.

Several factors lay the foundation of regional differences in drug efficacy and resistance. Demographic changes following movement of infected people from endemic rural regions to sprawling capitals lead to increasing incidence and resistance spreading of leishmaniasis **[162]**. Poor socioeconomic conditions seem to be a fundamental contributing factor for Sb resistance in the North Bihar region of India **[163]**. Host genetic diversity linked to geographical background needs to be considered, although few studies were conducted in this field. Additionally, the *Leishmania* strains themselves should be considered. Parasites with varying Sb susceptibility coexist in the field and also influence the variable responses that occur in different geographical areas **[164]**. Lastly, the environment plays an important role in drug resistance. Bihar is the only region where arsenic contamination of drinking water coexists alongside endemic VL and where widespread resistance to SbV occurs. The selection for resistance in infected individuals exposed to environmental arsenic results in cross-resistance to the related metalloid Sb **[165]**. A universal concern is climate change, more specifically global warming contributing to the expansion of the disease to new geographical areas and possibly the (re-)emergence of resistance **[166]**. The epidemiological and clinical context of any given endemic region can thus influence drug efficacy.

d) Genetics (age, gender, …)

Host genetic factors play a crucial role in determining pathogenicity, susceptibility but also treatment failure. Response differences between individuals are common for most drugs, and these are clearly observed for leishmaniasis **[99]**.

The role of cytokines and host genetics in determining susceptibility or resistance to leishmaniasis has recently gained more interest **[167]**. Various cytokines, e.g. IFN-γ, IL-2, IL-12, and TNF-α play an important role during protection, while some other cytokines, e.g. IL-10, IL-6, IL-17, TGF-β, and others are associated with

disease progression **[168]**. Textbook examples come from studies in mice with different genetic backgrounds and diverging immune responses to leishmaniasis infection, e.g. BALB/c and C57BL/6 mice are susceptible, while SV/129 mice are resistant **[169]**. Although BALB/c and C57BL/6 are considered susceptible, intrinsic differences linked to the inherent immune response are observed: C57BL/6 mice display a predominant Th1 cytokine response conferring a more resistant phenotype; conversely BALB/c mice trigger an initial Th2 response which renders them susceptible to infection with continuous parasite multiplication and tissue damage **[170]**.

Age and gender are other important factors related to disease progression and treatment failure. It has long been described that males have a certain predisposition to VL, both for *L. donovani* **[171-173]** and *L. infantum* **[174-176]**, although gender differences relating to specific behavior, activities, access to health care and societal roles of men and women were speculated to be confounding factors. A recent study in the Indian subcontinent described a male predominance of VL unrelated to socio-cultural differences **[177]** in which it is speculated that biological factors such as hormones, including sex hormones, can modulate the immune system and influence the response to infection. Several animal studies in leishmaniasis have described higher susceptibility to disease and worse disease outcomes in male animals **[178, 179]**. This gender effect is age-dependent and more pronounced post-pubertal. The underlying physical factors for the male susceptibility remain to be understood, although serum cytokine concentrations in infected mice showed higher levels of IL-12 in females, whereas males had significantly higher levels of TNF-α and IL-10 **[180]**.

Pre-pubertal children exhibit an increased risk for disease development and treatment failure **[6]**. For MIL, young age and male gender were associated with increased risk of VL relapse, suggesting that the mechanism of relapse is mainly related to immunological factors and/or drug exposure (pharmacokinetics) **[181]**.

Besides age and gender, other host-related factors have been associated with treatment failure, such as patient non-compliance **[6]**. Low drug exposure, as described for MIL in VL patients, correlates with treatment failure **[182]**. In Brazil, Rodrigues *et al.* even associated treatment failure with a body weight above 68 kg **[183]**.

c. Drug-related factors

The role of subtherapeutic drug exposure due to poor pharmacokinetics or pharmaceutical quality of the medication should also be considered.

Recently, intracellular parasite survival was demonstrated in different immune cell types in granulomatous lesions, which may shield the pathogen from drug exposure and lead to the adaptation of intracellular amastigotes into a reversible, quiescent stage with limited metabolic activity and replication **[184, 185]**, hence potentially altering drug tolerance. The likelihood of *Leishmania* to survive drug exposure due to inadequate drug penetration (and/or due to a switch to a 'drug-tolerant phenotype') is an important concern because drug tolerance is presumed to be a precursor of "classic" genotypic resistance in many bacterial infections **[186]**.

A particularly important pharmacokinetic property in the context of resistance emergence is the elimination half-life. For example, the plasma half-life for MIL and L-AmB both exceed 5 days **[187, 188]**, causing them to linger in the body at subtherapeutic concentrations for weeks after treatment, a major concern when viable "persister" parasites remain present in the host. Subtherapeutic drug exposure has already been linked to treatment failure, in particular responsible for age-related differences **[182, 189-191]** and the adverse effect of antiviral therapy on lower plasma exposure for MIL and AmB in HIV-VL patients **[192]**. Lastly, the use of poor pharmaceutical quality products can also result in subtherapeutic drug exposure and increased risks of drug resistance and treatment failure **[193, 194]**.

3. VL post-treatment relapse

Recurrent disease occurs because of re-infection or relapse. The former results from the exogenous infection with a pathogenic strain that can be distinct from the organism that caused the original infection. The latter is defined as the recurrence of symptomatic disease after apparent cure **[195]**.

A particularly alarming situation is the occurrence of post-treatment relapse for all known antileishmanial drugs. Relapse rates of up to 7% for L-Amb **[196]**, 20% for MIL **[6]** and 38% for Sb **[4]** have been reported in the last decade. Even combination therapy, such as Sb and PMM showed a relapse rate of 6% **[197]**. Relapse rates for VL are also increasing considerably. In South-Sudan, VL relapse as a proportion of all VL cases increased by 6.5% per annum, from 5.2% during 2001–2003 to 14.4% during 2016–2018 **[198]**. The only plausible indicator of definitive cure after treatment is the absence of clinical relapse at 6 or even 12 months.

It can be appreciated that relapse poses an increasing problem, and little is known about its origin, cause, or mechanism. Monitoring patients and relapse should be a primary concern. Recent transcriptomic studies on peripheral blood of HIV-VL co-infected patients holds promise in identifying prognostic immunological response signatures behind clearance or persistence of parasites after treatment. Adriaensen *et al.* observed a distinctive pattern of disease remission in successfully cured HIV-VL co-infected patients and the complete lack of it in treatment failure cases. Subsequently, a 4-gene signature was identified to discriminate treatment success at 4 weeks with a sensitivity of 84% and a specificity of 85% **[199]**.

4. Future: host-directed therapies

Chemotherapeutics or targeted therapies act by blocking essential biochemical or signaling pathways that are indispensable for *Leishmania* parasite growth and survival **[155]**. Alternatively, immunotherapy involves the use of biological molecules or compounds to modulate immune responses and can be applied in combination with antiparasitic drugs.

The plethora of approaches to modulate immune responses with cytokines, small molecule agonists/antagonists and humanized monoclonal antibodies elicited a growing interest in applying host-directed therapies (HDTs) to infectious diseases **[200]**. HDTs are a group of strategies that interfere with host mechanisms that are necessary for pathogen survival and/or stimulate the immune response to eliminate pathogens. Such an approach bypasses existing limitations of conventional treatments, such as the risk of parasites developing resistance **[201]**. Over the last decades, various approaches of immunotherapies or targeted therapies have been developed and applied in the treatment of human leishmaniasis.

Examples of HDTs during VL infection include the combination of IL-12 and SbV, which helped in the recovery of animals infected with *L. donovani* **[202]**. Other studies focused on promoting the production of nitric oxide (NO), IL-12 **[203]** and reactive oxygen species (ROS) **[204]**, resulting in improvement of immune response and promoting healing. However, there is still a lot to learn about strengths and weaknesses. For example, to be successful HDTs should not overstimulate the immune response or block protective immune responses necessary to control the pathogen of other infections **[200]**.

With the ever emerging risk of drug resistance and the much slower development of new antileismanial drugs, redirecting our focus to combining drugs with the enhancement of the host immune system could proof promising for the future.

I.III Immunopathogenesis of VL

***Leishmania* as masters of immune evasion**

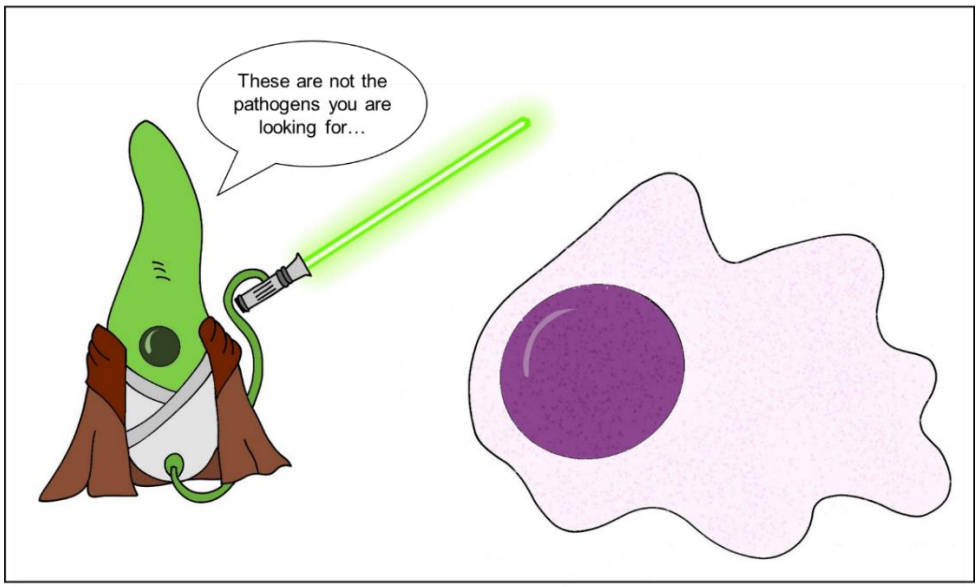

I. Introducing *Leishmania*

I.III Immunopathogenesis of VL

1. Infection tropism

As an obligate intracellular pathogen, *Leishmania* is known to persist in host cells that support its growth and consequently induce several protective or detrimental immune responses.

a) Tissue tropism

Leishmania parasites primarily colonize the liver, spleen, skin, lymph nodes and bone marrow (BM). At the level of the liver, parasites mainly colonize Kupffer cells, *i.e.* resident liver macrophages, resulting in hyperplasia and hypertrophy **[205]**. VL is associated with the emergence of liver granulomatous inflammation representing the tissue expression of a successful T-cell dependent immune response **[206, 207]**. While the liver embodies an acute resolving infection, the spleen displays a chronic unresolved state of infection caused by persistent VL parasites. Here, the parasite initiates an immunologic cascade of overwhelming dendritic cell activation, loss of stromal cells, complete splenic disorganization, and priming of macrophages to a disease-amplifying phenotype **[208]**. In the BM, a contradiction between hyperplasia and peripheral cytopenia's is observed, partially attributed to the increased destruction of mature blood cells in the periphery **[209]**.

b) Cell tropism

As already mentioned cellular niches for VL comprise not solely phagocytic cells (monocytes, macrophages, neutrophils and dendritic cells). Stromal cells (fibroblasts), keratinocytes and adipocytes have also been described to be susceptible hosts for *Leishmania* **[52, 210]**. However, macrophages remain the foremost infected host cells **[211]**. These cellular niches are thought to play a role

in escaping the immediate host immune response and subsequent elimination **[210]** in addition to other immune evasive strategies of *Leishmania* parasites (*vide infra*).

2. Immunopathogenesis in target organs

In general, the resolution of VL disease requires both $CD8^+$ and $CD4^+$ T cell participation with IFN-γ and NO production, *i.e.* a Th1 response. Regrettably, most knowledge on the immunopathology of VL is acquired in laboratory animal models, such as mice. Of note is that mice are considered subclinical or self-limiting models for VL as they control the disease in contrast to humans **[169]**. Extrapolation to the human host should therefore be attempted with caution. Data on HIV-VL co-infections already highlighted the importance of $CD4^+$ T cells, as decreased numbers of $CD4^+$ T cells facilitates the development of VL **[143]**.

a) Early events in the skin

The immunopathogenesis of leishmaniasis starts in the skin when the parasites are introduced by the bite of an infected sand fly. Skin damage caused during the probing and biting events induces the release of cytokines and chemokines that will attract leukocytes to the injured tissue **[212]**. This recruitment is reinforced by sand fly saliva **[213]**, gut microbiota **[214]** and a proteophosphoglycan-rich gel (Promastigote Secretory Gel, PSG) secreted by *Leishmania* promastigotes **[215]**. Mostly neutrophils and inflammatory monocytes are initially recruited to the infection site. During the first 24 hours, most parasites are engulfed by neutrophils that dominate the infection site as 'first responders'. Subsequently, inflammatory monocytes and skin-resident macrophages phagocytose the infected apoptotic neutrophils that act as 'Trojan horses'. The engulfment of promastigotes is mostly mediated by classical membrane-bound phagocytic receptors such as the complement (CR1 and CR3), mannose/fucose (MR) and fibronectin receptors. To initiate phagocytosis, several promastigote surface proteins are implicated such as

lipophosphoglycan (LPG), the metalloprotease GP63 and proteophosphoglycans (PPGs) **[216]**.

Phagocytosed *Leishmania* parasites are able to survive and multiply within macrophages, hence establishing infection and promoting parasite spread (**Figure 1.8**) **[217]**. Within 6-8 weeks, skin granulomas are established that control the local infection **[218]**. By that time, however, the disease has already spread to other target organs.

b) Cidal response in the liver

Epithelioid granulomas in various stages of maturation have been found in liver and spleen biopsies of asymptomatic patients **[205]**. As described above, splenomegaly, lymphadenopathy and varying degrees of hepatomegaly are the hallmarks of the progressive stage of VL. This pathology accompanies the failure of the host's granulomatous response to control the parasitic load **[208]**.
Control of hepatic infection in mice requires the development of inflammatory granulomas around infected Kupffer cells (KCs). Briefly, the infection of KCs initiates the process of granulomatous inflammation. Hepatic natural killer T cells (NKTs) migrate toward infected KCs and their interaction triggers the recruitment of mononuclear cells to the liver. Early parasite proliferation in KCs is associated with decreased levels of IL-12 and IFN-γ and up-regulation of anti-inflammatory cytokines TGF-β and IL-10 **[216]**. Various cell types, predominantly T cells, are recruited to infected KC foci within the liver with granulomas developing in size and cellularity in an asynchronous manner over the first 4 weeks post-infection. During this stage, increased levels of proinflammatory cytokines are produced, such as TNF-α, IFN-γ, and IL-12 that activate infected cells to generate ROS and NO to begin clearing the parasite burden. As parasites are cleared from individual infected KC foci, cells emigrate as part of resolution of the granuloma, and returns the liver to its original pre-infection state. As such, hepatic granulomatous inflammation resolves by 8 weeks post-infection in mice (**Figure 1.8**) **[219]**.

c) Ineffective response in the spleen

Rapid proliferation of parasites is observed in the liver during the first four weeks post-infection. In contrast, parasite growth in the spleen seems to be slower **[220]**. In this lymphoid organ, a heterogeneous immune response occurs with the production of both pro- and anti-inflammatory cytokines such as IL-12, IFN-γ, IL-10 and TGF-β (**Figure 1.8**) **[216]**. In contrast with its regulated role in resolving the liver infection, the excessive production of TNF-α and IL-10 in the spleen appear to mediate parasite proliferation and chronic infection. These disproportionate cytokines levels majorly contribute to an aberrant relocation of dendritic cells, which affects their interaction with T cells and the development of an antigen-specific response **[208]**. In addition, a complete splenic anatomical and functional disorganization compromises the role of short-lived plasma cells that usually provide an essential survival trait by the production of nonspecific, polyreactive antibodies that efficiently contain infectious agents until the antigen-specific immune reaction occurs in the germinal center (GC). Given the high parasite loads in the spleen and the complications of splenomegaly, splenectomy appears to minimize the effects of severe VL in humans **[221]**.

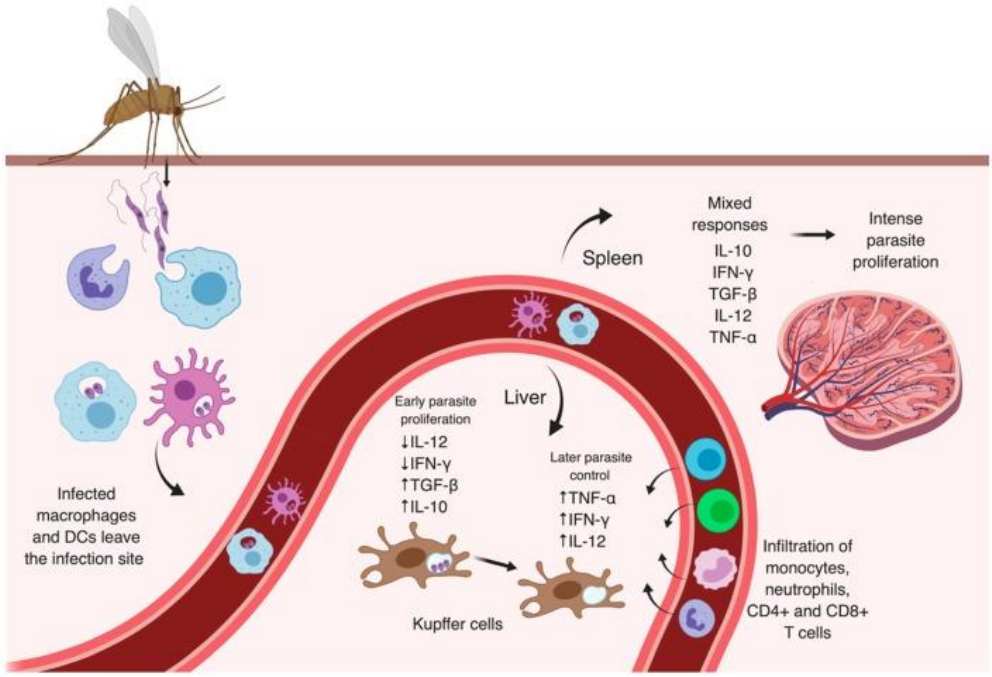

Figure 1.8. Overview of mechanisms leading to parasite dissemination and proliferation in VL. Parasites inoculated into the dermis by the sand fly vector are captured by innate immune cells, such as neutrophils, macrophages and dendritic cells (DCs). Infected cells leave the infection site and disseminate parasites to liver and spleen. In the liver, early parasite proliferation in Kupffer cells is associated with decreased levels of IL-12 and IFN-γ and up-regulation of anti-inflammatory cytokines. Later, with infiltration of monocytes, neutrophils, $CD4^+$, and $CD8^+$ T cells in liver granulomas, increased levels of proinflammatory cytokines are observed, and infected cells are able to eliminate parasites. However, a heterogeneous pro- and anti-inflammatory responses in the spleen seems to affect the interaction of antigen-presenting cells with T cells and induce intense proliferation of parasites in this lymphoid organ. Figure reprinted from **[216]**.

d) Exhaustion in the BM

The BM is the primary site of hematopoiesis producing all major cell lineages from a pool of committed precursors. Emergency hematopoiesis is a stress-induced response necessary to support the body in eliminating a pathogenic intruder. Upon VL infection, significant histological and morphological alterations can be observed, which includes erythroid and histiocytic hyperplasia, an increased number of plasma cells and hemophagocytosis **[222]**. *Leishmania* modifies the host's BM emergency response to promote its own proliferation and allow continued persistence of infection. Indeed, most long-term hematopoietic stem cells (LT-

HCS) enter cell cycle, correlating with functional exhaustion. More specifically, HSC are guided to differentiate into non-classical myeloid progenitors, with a regulatory suppressor cell-like phenotype that is more permissive to parasite infection **[223, 224]**. Effective HSC differentiation depends on hypoxia inducible factor 1 (HIF-1) degradation, however, during VL infection HIF-1 is stabilized and thus may contribute to the myelodysplastic phenomena observed in VL **[208]**. HIF-1 is also involved in driving the polarization towards M2-like macrophages, which are more susceptible to infection **[225] (Figure 1.9)**. Another target in the BM are stromal macrophages, which upon infection preferentially support increased levels of myelopoiesis as a consequence of the selective induction of granulocyte macrophage colony-stimulating factor (GM-CSF) and TNF-α production **[226]**. Additionally, rapid HSC migration from the BM to the circulation is observed **[227]**. Given that the BM acts as a site of infection, T cells are also recruited in high numbers, more specifically TNF-dependent $CD4^+$ IFN-γ^+ T cells, resulting in progressive HSC exhaustion **[224]** and erosion of the erythropoietic niche **[228]**. During infection, sustained activation of the Pi3k/Akt pathway (involved in a.o. apoptosis, proliferation, growth) with induction of autophagy and HIF-1 stabilization maintain the conditions needed for parasite survival **[229]**. Indeed, this reaction increases available glucose, reduces immune reaction, and prolongs the life span of the infected cell **[208]**.

In general, the BM has remained a neglected organ in VL infection studies and little is known about the immunopathology in humans. The observed structural abnormalities, marked stem cell exhaustion and cytopenia's certainly warrant further research **[209, 223]**.

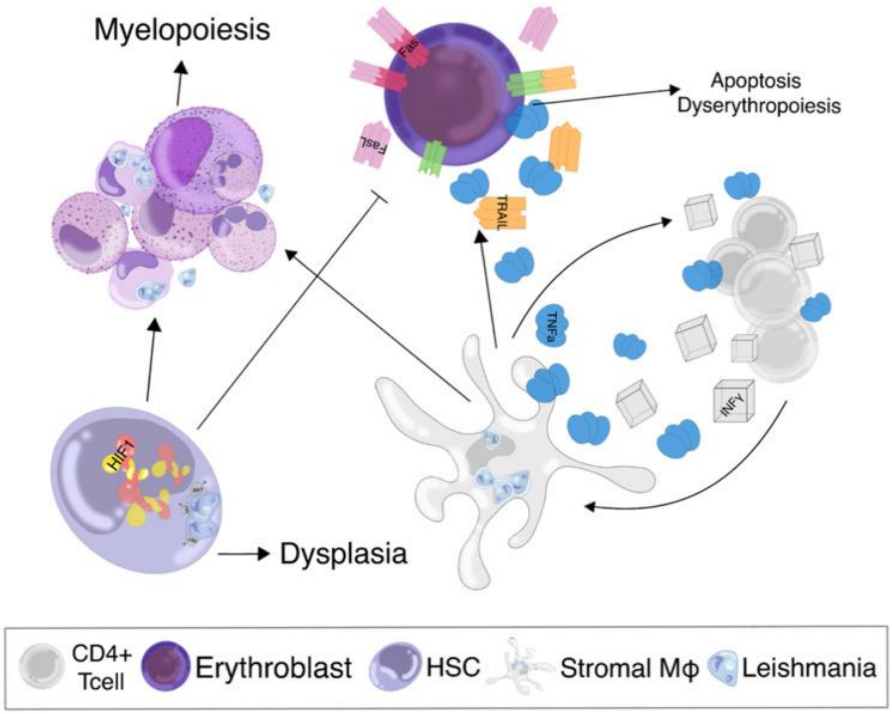

Figure 1.9 Effect of *Leishmania* infestation on the BM. Parasite-infected stromal macrophages (stromal Mφs) secrete large amounts of TNF-α that stimulate bystander $CD4^+$ T cells to acquire an effector phenotype marked by INF-γ release. The proinflammatory microenvironment causes the hematopoietic stem cells (HSCs) to differentiate into the myeloid lineage. Both phenomena cause skewing of hematopoiesis toward myelopoiesis at the expense of the erythroid lineage, largely contributing to VL-associated anemia. Furthermore, infection of HSCs leads to Akt docking on the parasitophorous vacuole membrane and thereafter phosphorylation and activation. Activation of Akt further leads to oxygen-independent HIF1 stabilization inside the HSCs, which translates to acquired myelodysplasia. Figure reprinted from **[208]**.

3. Immune evasion

Leishmania is able to persist in host cells by evading or exploiting a whole range of immune mechanisms of the host aiming to ensure survival, some of which are listed in **Table 1.4**. As already elaborated, promastigotes establish and differentiate in a parasitophorous vacuole or phagolysosome, which is accompanied by a modification of the intracellular environment. To survive, promastigotes must ensure evasion of the macrophage antimicrobial mechanisms and harsh intracellular conditions, including the acidic pH, elevated temperature and increased oxidative/nitrosative stress. This is achieved by a protective intrinsic property of

promastigotes by synthesizing abundant membrane-bound LPG. This LPG acts by disrupting phagosomal lipid microdomains, leading to a reduction of phagosome fusogenicity towards endosomes and lysosomes. In other words, they delay or inhibit endosomal maturation by transiently preventing fusion of the phagosome with the lysosome **[230]**. Hence, promastigotes create an intracellular phagosomal niche that fails to acidify and trigger microbicidal machinery such to assure sufficient time to transform into amastigotes **[210, 231, 232]**. Once transformed, several mechanisms are employed to survive inside the phagolysosome, such as interference with cell signaling cascades involved in synthesis of microbicidal factors. One of these mechanisms leads to the deactivation of the ROS production machinery, possibly by preventing NADPH oxidase assembly and subsequent superoxide production **[230, 233]**. Via this mechanism, *Leishmania* is able to avoid cellular oxidative stress. Another evasion strategy involves the regulation of the nuclear transcription factor kappa B (NF-$\varkappa$B) expression and evasion of complement-mediated lysis by the GP63 surface metalloproteinase **[234]**. NF-$\varkappa$B is a key player in the initiation of innate immune responses by regulating expression of important mediators, including cytokines, chemokines and secondary inflammatory mediators, such as the inducible nitric oxide synthase (iNOS). Studies revealed that *Leishmania* negatively regulates iNOS expression and subsequently causes lower NO levels, favoring infection establishment and survival **[235, 236]**.

Furthermore, *Leishmania* parasites are known to modulate cytokines and chemokines and related receptors in an attempt to modify cellular activation and recruitment in the tissue microenvironment **[237]**. *Leishmania* is capable of attenuating T cell mediated immune responses by causing defective antigen presentation, which is achieved by suppressing the presentation of leishmanial antigen-loaded major histocompatibility complex molecules (MHC) on the surface of antigen presenting cells. More specifically, parasites interfere with the loading of antigens onto MHC class II molecules or cause antigen sequestration **[230]**. A

chronic murine model of VL also revealed that *L. donovani* prevents DC migration to splenic areas rich of T cells, due to TNF-α and IL-10 mediated-inhibition of chemokine receptor CCR7. This receptor is essential for the recruitment of DCs and T cells to the periarteriolar lymphoid sheath (PALS) and hence for the physical interaction between these two immune cells, which is crucial for a successful cellular immunity against infection. This spatial segregation of DCs and T cells partly mediates the immunosuppression that is responsible for an increased susceptibility to secondary infections **[238]**.

Notably, this is only a brief summary of the evasion strategies that *Leishmania* possesses, but many more exist contributing to the success of *Leishmania* infections.

Table 1.4. Immune evasion strategies targeting specific physiological mechanisms.

Biological process	Virulence factors/mechanisms
Phagosome maturation	LPG preventing phagosome fusion towards endosome and lysosome
Signal transduction	Interference with microbicidal synthesis: ➢ Deactivation of ROS production machinery ➢ Negative regulation of iNOS by inhibition of NF-ϰB ➢ Evasion of complement-mediated lysis and inactivation of NF-ϰB by GP63
Antigen presentation	Defective antigen presentation via: ➢ Suppression of antigen-loading on MHC-II ➢ Antigen sequestration
Mediator release	TNF-α and IL-10 mediated inhibition of CCR7 dependent DC migration

4. B cell immune response: the double-edged sword

The interest in B cells during VL was sparked by the high titers of both *Leishmania*-specific and non-specific antibodies in patients, suggesting that a humoral immune response develops during infection **[239]**.

In the BM, common lymphoid progenitor cells (CLP) can give rise to pre-pro B cells that further differentiate into pro B cells, pre B cells and finally immature B cells that highly express IgM **[18, 240]**. During the development of B cells in the BM, the different B cell subsets undergo a positive and negative selection

procedure, mainly involving their B cell receptor (BCR) **[18, 241]**. For the completion of their development, immature B cells migrate to secondary lymphoid organs such as the spleen where they enter as T1 transitional B cells **[240, 242, 243]**. Here, they differentiate into T2 B cells which can further mature into follicular B (FoB) or marginal zone B (MZB) cells. Located in the white pulp of the spleen, FoB forming primary B cell follicles can get activated via proteins and glycoproteins in a T cell dependent way and give rise to short-lived plasma cells which produce high affinity antibodies, long-lived plasma cells or memory B cells that are important during reinfections. MZB surround the white pulp outside the splenic marginal sinus and give rise to short-lived and long-lived plasma cells in a T cell independent way **[18, 242]**.

Due to *Leishmania*'s intracellular nature, B cells have not been considered as an important contributor to the protective immune response. However, recent studies have shown that B cells do play protective roles **[244]**. A first role of B cells leading to a protective immune response is the production of antibodies. Three mature B cell subtypes, namely FoB, B1 and MZB cells, respond to initial antigen contact by differentiating into antibody-secreting cells that produce high-affinity antibodies. These antibodies have a neutralizing capacity and can activate the complement system **[245, 246]**. Studies in India and Nepal showed that these anti-leishmanial antibodies can persist for more than 15 years after cure **[247, 248]**. Besides antibody production, B cells also participate in antigenic presentation. This can result in activation of T cells which will skew towards a Th1 response **[245]**. In addition to T cell activation, antigen-presenting B cells are also involved in increased antigenic uptake by dendritic cells, leading to increased antigen presentation and stimulation of a Th1 protective immune response **[244, 249]**. A last role for B cells leading to protection is the production of various pro-inflammatory and anti-inflammatory cytokines. These cytokines participate in maintaining tissue structure and organisation **[245]**.

Although B cells will normally help to clear the pathogen, *Leishmania* is able to manipulate B cell responses. Hypergammaglobulinemia is one of the many symptoms associated with *Leishmania* infection. Studies of patients show that active disease is associated with the production of large amounts of parasite non-specific and autoreactive antibodies of IgM and IgG isotypes **[245, 250]**. Hypergammaglobulinemia has been linked to the production of IL-10 and type I IFN by activated B cells **[251, 252]**. Furthermore, Miles *et al.* showed that high IgG levels are predictive of disease in humans as IgG immune complexes enhance IL-10 production by macrophages which is associated with disease aggravation. Moreover, anti-leishmanial treatment resulted in a decrease in IgG levels and disease resolution **[253]**. Murine models corroborate that B cells and antibodies can contribute to exacerbation of disease. Indeed, B-cell deficient mice are more resistant to *L. donovani* infection with decreased liver burdens and the absence of a splenic infection **[254]**. After administering anti-leishmanial antibodies, the B-cell deficient mice became more susceptible to VL infection **[255]**. B cell-deficient mice also displayed an increased cytotoxicity of $CD8^+$ T cells and increased numbers of IFN-γ producing $CD4^+$ T cells **[251]**.

To conclude, B cells have a dual role during VL as they can both promote or control disease pathology **[245]**.

Table 1.5. Modulation of B cell functions by VL. Adapted from **[245]**.

VL modulation	**Effect**	
Induction of polyclonal B cell activation	Highly activated B cells ➢ Antibody secretion ➢ Low-affinity antibodies ➢ Autoantibodies	
Induction of B cell cytokine production	IL-10	Inhibits INF-γ secretion by T cells
	IFN-I	Enhances cytokine production and antibody secretion

Long-term hematopoietic stem cells as sanctuary niche with a unique transcriptional signature during treatment failure in visceral leishmaniasis

CHAPTER II

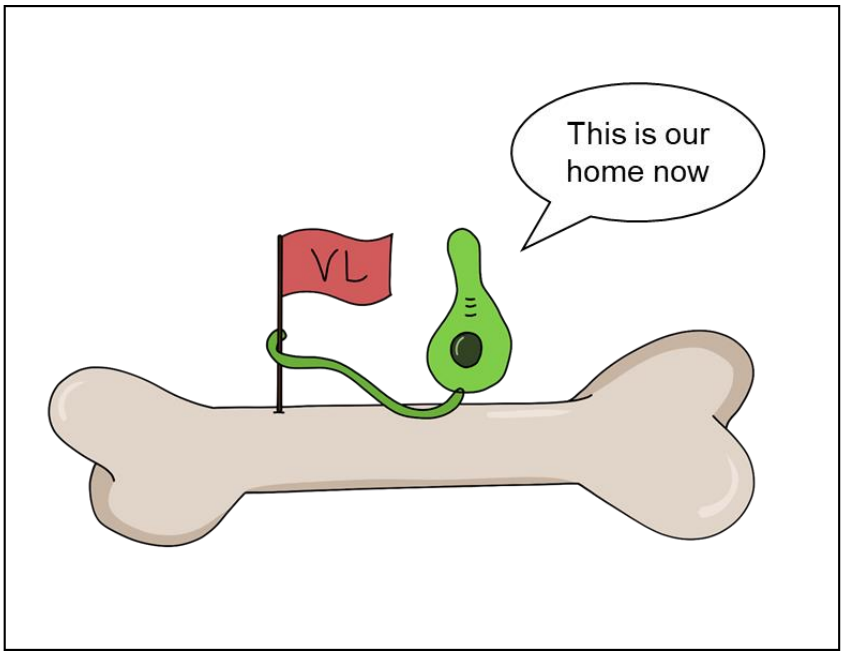

Part of this chapter has been published in:

Laura Dirkx[1], Sarah Hendrickx[1], Margot Merlot[1], Dimitri Bulté[1], Marick Starick[2,3], Jessy Elst[4], André Bafica[3], Didier G. Ebo[4], Louis Maes[1], Johan Van Weyenbergh[2], Guy Caljon[1]*. Long-term hematopoietic stem cells as a parasite niche during treatment failure in visceral leishmaniasis. *Communications Biology* 2022, 5, 626. doi:10.1038/s42003-022-03591-7.

[1] Laboratory of Microbiology, Parasitology and Hygiene (LMPH), Infla-Med Centre of Excellence, University of Antwerp, Antwerp, Belgium.
[2] Clinical and Epidemiological Virology, Department of Microbiology, Immunology and Transplantation, Rega Institute of Medical Research, KU Leuven, Leuven, Belgium.
[3] Laboratory of Immunobiology, Department of Microbiology, Immunology and Parasitology Federal University of Santa Catarina, Florianopolis, Brazil.
[4] Department of Immunology – Allergology – Rheumatology, Faculty of Medicine and Health Science and the Infla-Med Centre of Excellence, University of Antwerp, Antwerp University Hospital, Antwerp, Belgium.
* Corresponding author.

II. Long-term hematopoietic stem cells as sanctuary niche with a unique transcriptional signature during treatment failure in visceral leishmaniasis.

II.1 Abstract

Given the discontinuation of various first-line drugs for VL, large-scale *in vivo* drug screening, immunophenotyping and a systems biology approach were combined to study therapeutic failure. Infections with double bioluminescent/fluorescent *Leishmania infantum* and *L. donovani* reporter lines identified long-term hematopoietic stem cells (LT-HSC; Lin^- $Sca1^+$ $cKit^+$ $CD48^-$ $CD150^+$) as a hospitable cellular niche in the BM that serves as a source of relapse. LT-HSC were found to become readily infected, a feature confirmed for human hematopoietic stem cells (hHSPC), with low nitric oxide and reactive oxygen species levels, harboring enormous parasite burdens increasing antileishmanial drug tolerance. Infected LT-HSC displayed a unique transcriptional '*StemLeish*' signature defined by upregulated TNF/NF-kB and RGS1/TGF-β/SMAD/SKIL signaling, and a downregulated oxidative burst. Cross-species and cross-omics analyses demonstrated significant overlap with human VL and HIV co-infected blood transcriptomes and with epigenetic and transcriptional *in vivo* signatures of both human and experimental tuberculosis. In summary, the identification of LT-HSC as a drug- and oxidative stress-resistant niche, undergoing a conserved transcriptional reprogramming underlying *Leishmania* persistence and treatment failure, may open new therapeutic avenues for both leishmaniasis and tuberculosis.

II.2 Background information

Successful curative treatment of VL is notoriously challenging. A particularly alarming situation is the increasing number of VL infections that are inadequately responding to any of the known antileishmanial drugs **[96]**. To date, antimony (Sb)

and miltefosine (MIL) monotherapy against VL have been discontinued in the Indian subcontinent due to an increase in the number of treatment failures and/or relapses, with a staggering paromomycin (PMM) relapse rate of 17% and MIL relapse rates up to 20% within 12 months after treatment **[5, 6]**. In general, treatment failure occurs frequently and treatment options become critically compromised **[87].** Associations are often sought with drug resistance, although microorganisms can also be impervious to drugs without acquisition of genetic mutations. The formation of viable non-replicating cells, also known as persister-like cells, is common among bacteria and has also been described for *P. falciparum* and *P. vivax*, *T. gondii*, *T. cruzi, Leishmania* spp. and *M. tuberculosis* **[7]**. Persistent infections can occur in different tissues and cells throughout the host, such as hepatocytes (*P. vivax*), skeletal muscle and neurons (*T. gondii*), adipose tissue (*T. cruzi*) and the BM (*M. tuberculosis*) **[8-12]**. Some of these niches give protection against active immunity and drug action **[7]**. Within the BM, VL parasites are renowned to elicit emergency hematopoiesis with consequent exhaustion of hematopoietic stem cells (HSC) **[223, 224, 256]** and induction of leucopenia, neutropenia, thrombocytopenia and anemia **[209]**.

Own historical drug evaluation data triggered the hypothesis that treatment is generally less effective in the BM hence representing a reservoir site from where relapse can occur. To date, *Leishmania* spp. have been extensively reported to reside primarily within macrophages and dendritic cells **[211]** and case studies document infested macrophages in BM aspirates **[257-259]**. However, the exact pre- and post-treatment tropism in the BM has not yet been exhaustively described. In this study, LT-HSC were found to become readily infected and to display a lower sensitivity to a range of antileishmanial drugs, which was unrelated to efflux pumps. This indicates that infection of LT-HSC may not only allow escape from the host immune response but also from antileishmanial drug action. Our cross-species multi-omics analysis revealed a unique but evolutionary conserved RGS1/TGF-β/SKIL signaling-driven *StemLeish* gene signature, which significantly overlapped

with epigenetic and transcriptional *in vivo* signatures of both clinical and experimental tuberculosis. This unique *StemLeish* gene signature corresponded to a functional *RGS1*^{high}*TNFAIP3*^{high}*NOS2*^{low} profile in both *Leishmania*- and mycobacteria-infected HSC, with decreased levels of reactive oxygen species (ROS) and nitric oxide (NO) that represent important effector molecules involved in intracellular pathogen killing **[260, 261]**. In summary, this study identified a protective cellular niche of persistent *Leishmania* parasites in the BM. Given the current field situation of increasing post-treatment relapse rates, our findings warrant for advanced pharmacodynamic and novel drug exploration.

II.3 Materials and methods

Ethical statement

The use of laboratory rodents was carried out in strict accordance with all mandatory guidelines (EU directives, including the Revised Directive, 2010/63/EU on the Protection of Animals used for Scientific Purposes that came into force on 01/01/2013, and the declaration of Helsinki in its latest version) and was approved by the Ethical Committee of the University of Antwerp, Belgium (UA-ECD 2019–04). Human BM aspirate rest samples, obtained as a diagnostic sample without a written informed consent, were available for *in vitro* infection experiments following approval by the Committee of Medical Ethics UZA-UA (B3002021000027).

Leishmania parasites

The *L. infantum* strain MHOM/FR/96/LEM3323, with an inherent Sb resistance, was obtained from an HIV-positive patient from the Languedoc area in Southern France and kindly provided by CNRL (Montpellier, France). The *L. donovani* strain MHOM/ET/67/L82 was isolated from an Ethiopian VL-patient. Both were modified to express bioluminescent (PpyRE9) and/or fluorescent (DsRed) reporter proteins (LEM3323 WT^{PpyRE9}, LEM3323 WT$^{PpyRE9/DsRed}$ and Ldl82 WT$^{PpyRE9/DsRed}$) **[262]**. Promastigotes were sub-cultured twice weekly at 25°C in hemoflagellate-

modified minimal essential medium (HOMEM, Gibco), supplemented with 10% inactivated fetal calf serum (iFCS), 200 mM L-glutamine, 16.5 mM $NaHCO_3$, 40 mg/L adenine, 3 mg/L folic acid, 2 mg/L D-biotin and 2.5 mg/L hemin. The number of passages was kept as low as possible to maintain parasite virulence.

Laboratory animals

Female BALB/c mice (6-8 weeks old) and female golden hamsters (BW 90-97g) were purchased from Janvier (Genest-Saint-Isle, France) and accommodated in individually ventilated cages in pathogen-free conditions. They were provided with food for laboratory rodents (Carfil, Arendonk, Belgium) and water *ad libitum*. Animals were subdivided in experimental groups based on simple randomization. Mice were kept in quarantine for at least 5 days before starting the experiment. Euthanasia was performed in CO_2 chambers followed by cervical dislocation, and tissues were collected under aseptic conditions.

Primary mouse cells

Mouse BM was collected from BALB/c mice using two distinct techniques, based on pilot studies comparing alternative methods in terms of yield and quality. For both techniques, mice were sacrificed, and hind legs aseptically removed. Isolated femurs and tibias were cleaned by removing soft tissue from the bone using 70% ethanol-soaked cloth and tweezers.

For the crushing technique, the protocol was adapted from Lo Celso and Scadden **[263]**. Briefly, bones were crushed with mortar and pestle in ammonium-chloride-potassium (ACK) buffer (0.15 M NH_4Cl, 1.0 mM $KHCO_3$, 0.1 mM Na_2EDTA) for erythrocyte lysis. Single cell suspensions were obtained by filtering through MACS® SmartStrainers (100 μm, Miltenyi Biotec), centrifuged at 500×*g* for 10 min (4°C) and resuspended in phosphate-buffered saline (PBS) + 0.2% bovine serum albumin (BSA). For efficient depletion of mature lineage-positive hematopoietic cells and to specifically isolate the preferred lineage-negative cells (*i.e.*

undifferentiated progenitor cells), the Direct Lineage Cell Depletion Kit (Miltenyi Biotec) was employed according to manufacturer's instructions. Following lineage depletion, cells were counted in PBS and resuspended in PBS + 0.2% BSA buffer to 2×10^7 cells/mL. Cells were kept on ice during all procedures.

The centrifugation method was adjusted from the protocol described by Amend *et al.* **[264]** and Dobson *et al.* **[265]** and used for subsequent macrophage and dendritic cell differentiation. Briefly, a 0.5 mL microcentrifuge tube was perforated at the bottom with a 21G needle and nested inside a 1.5 mL tube (both from Eppendorf). After collection of femurs and tibias, one proximal end (knee epiphysis) was cut-off and placed in the 0.5 mL tube. Nested tubes were centrifuged in a microcentrifuge at 10,000×*g* for 15 sec. Both long bones became white and a large visual pellet was observed in the 1.5 mL tube. This pellet was then resuspended in ACK buffer for erythrocyte lysis.

To obtain BM-derived macrophages (BMDM), cells were centrifuged at 500×*g* for 10 min at 4°C, resuspended in Roswell Park Memorial Institute (RPMI) medium (Gibco) and divided over Petri dishes (Starstedt) supplemented with BM medium [RPMI 1640 medium with 10% (v/v) iFCS, 1% non-essential amino acids (NEAA), 1% sodium pyruvate, 1% L-glutamine, 50 U/mL penicillin, 50 µg/mL streptomycin (all from Gibco) and 15% L929 supernatant with M-CSF]. Following a 6-day incubation at 37°C with 5% CO_2, the macrophages were collected by replacing the BM medium with ice cold dissociation buffer [PBS with 1% 0.5 M ethylenediaminetetraacetic acid (EDTA) and 2% 1 M 4-(2-hydroxyethyl)-1-piperazine-ethanesulfonic acid (HEPES)]. After detachment, the macrophage cell suspension was centrifuged at 500×*g* for 10 min and resuspended in RPMI medium. The number of macrophages was counted in PBS using a KOVA® counting chamber. Cells were seeded in a 96-well plate (3×10^4 cells/well) or a 24-well plate (1×10^6 cells/well) and incubated for 24 h at 37°C with 5% CO_2 to allow adherence of the BMDMs.

To differentiate BM cells into dendritic cells (BMDCs), cells were cultured in Petri dishes in DC medium [RPMI 1640 supplemented with 10% (v/v) iFCS, 2 mM Glutamax, 20 mM HEPES, 50 U/mL penicillin, 50 µg/mL streptomycin, 50 µM 2-mercaptoethanol (all from Gibco) with 200 U/mL recombinant murine granulocyte-macrophage colony-stimulating factor (GM-CSF; Peprotech)], followed by a 9-day incubation at 37°C with 5% CO_2 during which the medium was refreshed twice. After 9 days of differentiation with GM-CSF, preheated DC medium was used to recover the semi-adherent BMDC fraction which is reported to contain most $CD11c^+$ and MHC-II^{hi} DCs **[266]**. Following a 10 min centrifugation at 500×*g*, cells were resuspended in DC medium and counted in PBS using a KOVA® counting chamber. Cells were then plated in a 24-well plate (1×10^6 cells/well) and incubated at 37°C with 5% CO_2.

Primary human BM cells

Human BM aspirate was obtained from the iliac crest using BD Vacutainer® Plastic K3EDTA Tubes, initially collected for diagnostics, and delivered as residual sample. The BM was subjected to erythrocyte lysis twice using ACK buffer. Single cell suspensions were obtained by filtering through MACS® SmartStrainers (100 µm, Miltenyi Biotec), centrifuged at 300×*g* for 10 min (4°C) and resuspended in PBS + 0.2% BSA. Cells were counted in PBS and diluted to a concentration of 2×10^7 cells/mL for flow cytometric analysis. Cells were kept on ice during these procedures.

In vitro and *in vivo* visceral *Leishmania* infections

Parasite density was assessed by counting parasites in PBS using a KOVA® counting chamber. For *in vitro* infections, cell monolayers were co-cultured with stationary-phase promastigotes of *L. infantum* or *L. donovani* at a multiplicity of infection (MOI) of 5 for a minimum of 24h at 37°C with 5% CO_2. In some experiments, amastigotes were purified from 96h infected macrophages and used to initiate infection at a MOI of 5. For *in vivo* infection, stationary-phase parasites were centrifuged for 10

min at 4,000×*g* (25°C) and resuspended to 1×10^9 parasites/mL in sterile RPMI medium. Mice were infected intravenously (i.v.) in the lateral tail vein with 1×10^8 parasites in 100 µL of RPMI medium.

In vivo bioluminescent imaging (BLI)

Animals were monitored using *in vivo* BLI at selected time points. Imaging was performed 3 min after intraperitoneal (i.p.) injection of 150 mg/kg D-Luciferin (Beetle Luciferin Potassium Salt, Promega) in the IVIS® Spectrum In Vivo Imaging System under 2.5% isoflurane inhalation anesthesia using 15 min exposure. Images were analyzed using LivingImage v4.3.1 software by drawing regions of interests (ROIs) around specific organs to quantify the luminescent signal as relative luminescence units (RLU).

Paromomycin post-treatment relapse model

Paromomycin sulfate salt (PMM, Sigma-Aldrich) stock solution was dissolved in MilliQ® at a concentration of 70mg/mL. Mice were infected i.v. with 1×10^8 metacyclic promastigotes of LEM3323 WT^{PpyRE9}. Starting from 3 days post infection (dpi), mice were treated i.p. for 5 consecutive days with 350 mg/kg s.i.d. PMM.

Compound evaluation in the Syrian golden hamster model

For all compounds historically evaluated and reported in this study **[267]**, the following screening protocol was performed: hamsters were allocated to experimental units of 5 to 6 animals based on live body weight at the start of the experiment. *L. infantum* (MHOM/MA(BE)/67) amastigotes obtained from the spleens of heavily infected donor hamsters were purified using two centrifugation steps and diluted to prepare an infection inoculum containing 2×10^7 amastigotes/100µL PBS. The infection inoculum was administered intracardially (i.c.). Amastigote burdens in the different target organs (liver, spleen, BM) were determined 10 days after the last treatment (*i.e.* day 35 of the experiment). The organs of individual animals were weighed (except BM); impression smears were

Giemsa-stained for microscopic evaluation of amastigote burden, expressed as LDU (= mean number of amastigotes/cell × organ weight in mg). A minimum of 500 nuclei was counted. Percentage reduction compared to the burdens in the vehicle-treated infected control animals (VIC) was used as a measure for drug activity.

Promastigote back-transformation

BM cells were mechanically disrupted to release the intracellular amastigotes in HOMEM promastigote medium. At 25°C, amastigotes readily transform back into proliferative promastigotes **[59]**.

Intracellular NO and ROS staining

To detect NO and ROS, DAF-FM Diacetate (4-amino-5-methylamino-2',7'-difluorofluorescein diacetate) and CM-H_2DCFDA were used respectively (both from ThermoFischer Scientific). Stock solutions were prepared at 5 mM in dimethyl sulfoxide (DMSO) stored at -20°C, and diluted immediately prior to use. Cells were incubated in pre-warmed PBS containing either probe in a final working concentration of 5 μM. After 30 minutes at 37°C with 5% CO_2, the loading buffer was removed and cells were incubated for 15 minutes in dye-free medium at the same temperature to allow complete de-esterification of the intracellular diacetates. Cells were further processed for flow cytometry as described below.

Flow cytometry

Cell suspensions (2×10^7/mL concentration) were treated with FcγR-blocking agent (anti-CD16/32, clone 2.4G2, BD Biosciences) for 15 min, followed by a washing step using 500×*g* centrifugation and resuspension in PBS + 0.2% BSA buffer. Next, cells were incubated for 20 min at 4°C with a mix of fluorescent conjugated anti-mouse antibodies (**Table 2.1**) at optimized concentrations. DAPI Staining Solution (Miltenyi Biotec) was used to assess viability. Cells were measured by flow cytometry using MACSQuant® Analyzer 10 (Miltenyi Biotec) and analyses were

performed using FlowLogic™ Software (Miltenyi Biotec) following specific gating strategies (**Figure 2.1**, **Table 2.2**), confirmed with fluorescence minus one (FMO) controls.

Fluorescence-activated cell sorting (FACS)

Cell suspensions were processed as above (flow cytometry) prior to cell sorting using a specific antibody mix (**Table 2.3**). Cells were sorted using FACSMelody™ (BD Bioscience) following specific gating strategies (**Figure 2.1**, **Table 2.2**), confirmed with fluorescence minus one (FMO) controls and compensated using single stains. The quality of sorting was confirmed by analyzing post-sort samples.

Page 76: Figure 2.1. Flow cytometry gating strategy. (a) BM cells were separated into lineage positive (Lin^+) and negative (Lin^-) cells using negative magnetic sorting. For both fractions, a cell gate was selected in a SSC-A versus FSC-A plot, followed by a gating on singlets in a FSC-H versus FSC-A plot. Lin^+ live ($DAPI^-$) $CD45^+$ cells were further characterized as neutrophils ($CD11b^+$ $Ly\text{-}6G^+$), monocytes ($Ly\text{-}6C^{hi}$) and macrophages (SSC^{lo}, $Ly\text{-}6C^-$, $F4/80^+$). Lin^- live ($DAPI^-$) cells were either plotted as cKit versus Sca1 or as CD105 versus CD271 to allow identification of hematopoietic stem cells or mesenchymal stem cells, respectively. $cKit^+Sca1^+$ cells were further characterized as LT-HSC ($CD48^-$ $CD150^+$), ST-HSCs ($CD48^-$ $CD150^-$), MPP2 ($CD48^+$ $CD150^+$), and MPP3 ($CD48^+$ $CD150^-$). $cKit^+Sca1^-$ cells were identified as CMP/GMP. $CD105^+CD271^+$ cells were further characterized as MSCs ($CD90.2^+$). **(b)** BM cells were differentiated into dendritic cells or macrophages using GM-CSF or L929, respectively. For both subsets, a cell gate was selected in a SSC-A versus FSC-A plot, followed by gating on singlets in a FSC-H versus FSC-A plot and a live ($DAPI^-$) selection as in (a). $CD45^+$ cells were further characterized as macrophages ($CD11b^+$ $F4/80^+$), and $CD11c^+$ cells as dendritic cells ($CD11b^-$ $F4/80^-$ $MHC\text{-}II^{hi}$). **(c)** Human BM aspirate was treated twice with erythrocyte lysis buffer, a SSC low cell gate was selected in a SSC-A versus FSC-A plot, followed by gating on singlets in a FSC-H versus FSC-A plot. Live ($DAPI^-$) cells were further characterized as HSCs ($CD45^{lo}$ $CD34^+$) and $CD45^{hi}$ cells ($CD45^{hi}$ $CD34^-$).

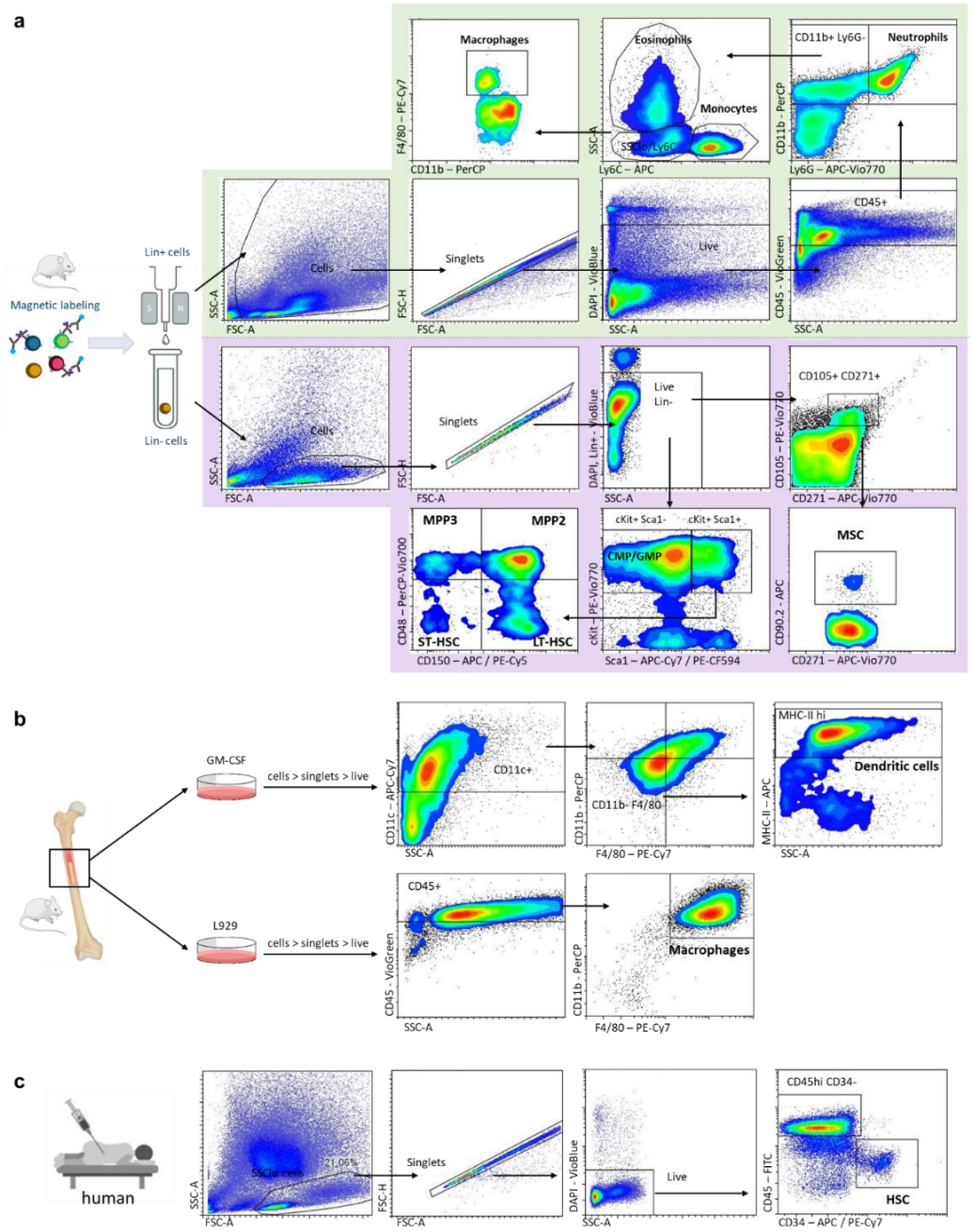
a
Magnetic labeling
Lin+ cells
Lin- cells
Cells
Singlets
Live
CD45+
Macrophages
Eosinophils
Monocytes
SSChi Ly6C+
CD11b+ Ly6G-
Neutrophils
F4/80 – PE-Cy7
CD11b – PerCP
Ly6C – APC
Ly6G – APC-Vio770
SSC-A
FSC-A
FSC-H
DAPI - VioBlue
CD45 - VioGreen
Live Lin-
CD105+ CD271+
DAPI, Lin+ - VioBlue
CD105 – PE-Vio770
CD271 – APC-Vio770
MPP3
MPP2
ST-HSC
LT-HSC
CD48 – PerCP-Vio700
CD150 – APC / PE-Cy5
cKit+ Sca1-
cKit+ Sca1+
CMP/GMP
cKit – PE-Vio770
Sca1 – APC-Cy7 / PE-CF594
MSC
CD90.2 - APC
b
GM-CSF
L929
cells > singlets > live
CD11c+
CD11c – APC-Cy7
CD11b- F4/80-
CD11b - PerCP
F4/80 – PE-Cy7
MHC-II hi
Dendritic cells
MHC-II – APC
CD45+
Macrophages
CD45 - VioGreen
c
human
SSCla cells
21,06%
CD45hi CD34-
HSC
CD45 – FITC
CD34 – APC / PE-Cy7

Table 2.1. Cell markers to differentiate mouse BM cells by flow cytometry using MACSQuant® Analyzer 10. Abbreviations: long-term (LT) and short-term (ST) hematopoietic stem cell (HSC), multipotent progenitor (MPP), common myeloid progenitor (CMP), granulocyte monocyte progenitor (GMP).

Cell surface marker	Fluorophore	Clone N°	Manufacturer	Dilution
LT-HSC, ST-HSC, MPP2, MPP3, CMP, GMP				
cKit	PE-Vio770	REA791	Miltenyi Biotec	1:50
CD150	APC	REA299	Miltenyi Biotec	1:11
CD48	PerCP-Vio700	HM48-1	Miltenyi Biotec	1:100
CD34	FITC	REA383	Miltenyi Biotec	1:50
Ter119	VioBlue	Ter-119	Miltenyi Biotec	1:11
Gr-1	VioBlue	REA810	Miltenyi Biotec	1:500
CD11b	VioBlue	REA592	Miltenyi Biotec	1:500
TCR-β	VioBlue	REA318	Miltenyi Biotec	1:100
B220	VioBlue	REA755	Miltenyi Biotec	1:500
CD335	VioBlue	REA815	Miltenyi Biotec	1:50
Sca-1	APC-Cy7	D7	BD Biosciences	1:40
Monocytes, macrophages, neutrophils, eosinophils				
Ly6C	APC	AL-21	BD Biosciences	1:200
Ly6G	APC-Vio770	REA526	Miltenyi Biotec	1:100
CD11b	PerCP	M1/70	BioLegend®	1:400
F4/80	PE-Cy7	BM8	BioLegend®	1:200
CD45	VioGreen	REA737	Miltenyi Biotec	1:200
Mesenchymal stem cells				
CD105	PE-Vio770	REA1058	Miltenyi Biotec	1:50
CD271	APC-Vio770	REA648	Miltenyi Biotec	1:11
CD34	FITC	REA383	Miltenyi Biotec	1:50
Ter119	VioBlue	Ter-119	Miltenyi Biotec	1:11
Gr-1	VioBlue	REA810	Miltenyi Biotec	1:500
CD11b	VioBlue	REA592	Miltenyi Biotec	1:500
TCR-β	VioBlue	REA318	Miltenyi Biotec	1:100
B220	VioBlue	REA755	Miltenyi Biotec	1:500
CD335	VioBlue	REA815	Miltenyi Biotec	1:50
Dendritic cells				
CD11b	PerCP	M1/70	BioLegend®	1:400
F4/80	PE-Cy7	BM8	BioLegend®	1:200
CD11c	APC-Cy7	REA791	Miltenyi Biotec	1:100
MHC-II	APC	M5/114.15.2	Miltenyi Biotec	1:100
Human HSC and CD45^{hi} cells				
CD45	FITC	REA747	Miltenyi Biotec	1:140
CD34	APC	581	BioLegend®	1:20

Table 2.2. Characteristic cell surface markers for the identification of mouse BM cells with flow cytometry. Abbreviations: long-term (LT) and short-term (ST) hematopoietic stem cell (HSC), multipotent progenitor (MPP), common myeloid progenitor (CMP), granulocyte monocyte progenitor (GMP).

Cell Type	Flow cytometry markers
Mouse	
MSC	Lin^- $CD105^+$ $CD271^+$ $CD90.2^+$
LT-HSC	Lin^- Sca^+ $cKit^+$ $CD150^+$ $CD48^-$
ST-HSC	Lin^- Sca^+ $cKit^+$ $CD150^-$ $CD48^-$
MPP2	Lin^- Sca^+ $cKit^+$ $CD150^+$ $CD48^+$
MPP3	Lin^- Sca^+ $cKit^+$ $CD150^-$ $CD48^+$
CMP / GMP	Lin^- Sca^- $cKit^+$ $CD34^+$
Monocytes	$CD45^+$ $CD11b^+$ $Ly6C^{Hi}$ $Ly6G^-$ $F4/80^{Lo}$
Macrophages	$CD45^+$ $CD11b^+$ $Ly6C^{Lo}$ $Ly6G^-$ $F4/80^+$
Neutrophils	$CD45^+$ $CD11b^+$ $Ly6C^+$ $Ly6G^+$ $F4/80^-$
Dendritic cells	$CD11c^+$ $CD11b^-$ $F4/80^-$ $MHC\text{-}II^{Hi}$
Human	
hHSPC	SSC^{Lo} $CD45^{Lo}$ $CD34^+$
$CD45^{hi}$ cells	$CD45^{hi}$ $CD34^-$

Table 2.3. Cell markers to differentiate BM cells by flow cytometry using FACSMelody™. Abbreviations: long-term (LT) and short-term (ST) hematopoietic stem cell (HSC), multipotent progenitor (MPP), common myeloid progenitor (CMP), granulocyte monocyte progenitor (GMP).

Cell surface marker	Fluorophore	Clone N°	Manufacturer	Dilution
Mouse LT-HSC, ST-HSC, MPP2, MPP3, CMP, GMP				
cKit	PE-Vio770	REA791	Miltenyi Biotec	1:50
CD150	PE-Cy5	TC15-12F12.2	BioLegend®	1:80
CD48	PerCP-Vio700	HM48-1	Miltenyi Biotec	1:100
CD34	FITC	REA383	Miltenyi Biotec	1:50
Ter119	VioBlue	Ter-119	Miltenyi Biotec	1:11
Gr-1	VioBlue	REA810	Miltenyi Biotec	1:500
CD11b	VioBlue	REA592	Miltenyi Biotec	1:500
TCR-β	VioBlue	REA318	Miltenyi Biotec	1:100
B220	VioBlue	REA755	Miltenyi Biotec	1:500
CD335	VioBlue	REA815	Miltenyi Biotec	1:50
Sca-1	PE-CF594	D7	BD Bioscience	1:40
Human HSC, $CD45^{hi}$ cells				
CD45	FITC	REA747	Miltenyi Biotec	1:140
CD34	PE-Cy7	581	BioLegend®	1:20

Epifluorescence and conventional microscopy

After cell sorting, LT-HSC were collected on slides by Cytospin™ followed by Giemsa or fluorescence staining. For fluorescence, both LT-HSC and BM-derived macrophages were fixed using 2% paraformaldehyde for 15 min at ambient temperature, followed by two washes with PBS. Cell nuclei were stained with DAPI (4', 6-diamidine-2'-phenylindole dihydrochloride) solution (Sigma-Aldrich) for 2 min at ambient temperature. Finally, a drop of DABCO (1,4-diazabicyclo[2.2.2]octane, mixture of 70% glycerol and PBS) was added and analysis was performed using a fluorescence microscope (Zeiss Axio Observer Z1 epifluorescence microscope) with a ×63 oil objective lens and ZEN software 2.3 pro. For conventional microscopy, both LT-HSC and BM-derived macrophages were fixed using methanol and stained with Giemsa. To confirm intracellular amastigote multiplication and thus remove extracellular promastigotes as potentially confounding factor, media with horse serum (as opposed to bovine serum) was used according to **[268]**.

RNA isolation

Total RNA was extracted from *L. infantum* infected mouse liver and spleen tissue using RNeasy Plus Mini kit, and BM using QIAamp® RNA Blood Mini kit (both from Qiagen), according to manufacturer's instruction. To exclude gDNA, an additional step using gDNA elimination columns (Monarch®) was performed. RNA samples were stored in aliquots at -80°C until qPCR analysis.

Real-time quantitative PCR

The primer sequences and RT-qPCR conditions for Spliced-Leader RNA (SL-RNA) were derived from **[82]**. The Step One Plus real-time PCR system (Applied Biosystems) was used for all real-time qPCR assays and melt curve analyses. RT-qPCR were performed in a 20 µL reaction mixture containing 10 µL of 2× SensiFAST SYBR Hi-ROX One-Step mix (Bioline), 1 µL of each primer (10µM

final concentration), 0.2 µL of reverse transcriptase, 0.4 µL of RNAse inhibitor, 4 µL of RNA template, and 3.4 µL of PCR water. Each assay was run in duplicate together with a blank control. Threshold cycles (Ct) were defined as the fractional cycle number at which the fluorescence passed the fixed threshold. Ct values were extracted by using the StepOne™ software v2.3. The mRNA expression of each gene was calculated relative to the expression of the housekeeping gene (Eef2 - *eukaryotic translation elongation factor 2)* (**Table 2.4**). After normalization, the relative expression levels were analyzed by using GraphPad software 7.0.

Table 2.4. Overview of the used primers.

Name	Sequence	Tm (°C)*
Eef2_F	TGTCAGTCATCGCCCATGTG	57.6
Eef2_R	CATCCTTGCGAGTGTCAGTGA	57.1
SL-RNA_F	AACTAACGCTATATAAGTAT	42.6
SL-RNA_R	CAATAAAGTACAGAAACTG	43.1

*Melting temperatures of primers.

NanoString digital transcriptomics and bioinformatic analyses

Cell lysates (from approximately 10,000 LT-HSC or macrophages, triplicates for both infected and uninfected conditions) for nCounter (NanoString) analysis were prepared using RNeasy Lysis buffer (RLT buffer, Qiagen). Cell lysates were hybridized to 800 unique capture/reporter pairs (50 bp each) targeting 742 immune transcripts and 20 housekeeping genes as defined in the Mouse Myeloid Innate Immunity nCounter® panel, as well as 6 positive and 8 negative control probes (all from NanoString). Results were sequentially corrected for background (negative control probes), technical variation (positive control probes) and RNA content (housekeeping genes) using nSolver 4.0 (NanoString), followed by differential expression and pathway enrichment analysis (Rosalind (www.rosalind.bio), MSigDb **[269]**), in conjunction with publicly available datasets (GEO (https://www.ncbi.nlm.nih.gov/geo/), ToppCell (toppcell.cchmc.org), ImmGen (www.immgen.org), ImmuCo **[270]**).

Drug susceptibility determination

Used concentrations of reference drugs (PMM, Sb, MIL) were selected according to Maes *et al.* **[271]**. After 120 hours of drug exposure at 37°C and 5% CO_2, both LT-HSC and BMDMs were fixed with methanol and stained with Giemsa to microscopically determine the number of intracellular amastigotes per nucleus, the percentage of infection and the infection index. LT-HSC (3×10^4 cells in 200 µL RPMI medium) were collected on slides by Cytospin™ to enable processing for Giemsa staining. To confirm intracellular amastigote multiplication and thus remove extracellular promastigotes as potentially confounding factor, horse serum was used according to **[268]**.

Efflux susceptibility assay

The efflux pump inhibitor verapamil (MDR and MRP inhibitor, Sigma-Aldrich) was formulated in 100% DMSO at 20 mM. The stock solution was further diluted in demineralized water and administered in a concentration of 8 µM based on **[272]**. In all assays, the final in-test concentration of DMSO did not exceed 1%. Dilutions of the reference drugs, PMM (120 µM), MIL (7.5 µM), and Sodium stibogluconate (SSG, 35 eq. Sb) were added either with or without verapamil. After 96 hours of drug and inhibitor exposure at 37°C and 5% CO_2, both LT-HSC and BMDM were processed as described above, and reduction in amastigote burden in the treated cells was compared to that of the untreated control cells.

Statistical analysis

Statistical analyses were performed using GraphPad® Prism version 7.00 and version 9.0.1. Tests were considered statistically significant if $p < 0.05$. BLI data were analyzed using a Mann-Whitney test (two-tailed). Organ burden reductions in golden Syrian hamsters were subjected to a Wilcoxon matched-pairs signed rank test (two-tailed). Statistical analysis for back-transformation was based on a 2-way ANOVA using titration endpoints with positive back-transformations as measure

of viable parasite presence. Differences in amastigote multiplication were determined applying a multiple *t* test (two-tailed). Infection parameters (MFI, % infection and infection index) were compared using a Kruskal-Wallis test. Induction of ROS and NO using MFI data were subjected to multiple *t* tests (two-tailed) after outlier analysis (ROUT, Q = 1%). Statistical analysis for experiments using Giemsa staining were performed using a Mann-Whitney test.

II.4 Results

Bone marrow as a niche for persistent VL parasites

By means of *in vivo* bioluminescence imaging (BLI), we developed a reproducible post-treatment relapse model in BALB/c mice using PMM exposure. After 5 consecutive days of 350 mg/kg *s.i.d.* intraperitoneal (i.p.) injections of PMM, a significant decrease of parasite burdens in the liver, spleen and BM was obtained (**Figure 2.2a**) indicating that PMM is able to reach these infection sites. However, low-level BM burdens above the detection threshold remained at the end of treatment as evidenced by imaging at a high sensitivity scale. In animals with the highest BM signal, bioluminescent signals also appear in the spleen (**Figure 2.2b**). These burdens re-emerged in the absence of drug pressure indicating that BM represents a niche where parasites can survive treatment. Subsequently, parasites were able to recolonize target organs with BLI signals increasing from 2-3 weeks post-treatment (wpt) onwards in the spleen. Remarkably, the liver seems to be protected from recolonization (**Figure 2.2c**). As BLI is a semi-quantitative method, RT-qPCR was performed to address the sensitivity of imaging different organs showing that burdens are relatively underestimated in the BM compared to the spleen, possibly due to the low perfusion rate or lower accessibility of the BM for the D-luciferin substrate **[273]** (**Figure 2.3b**). Besides the BALB/c model, the golden Syrian hamster model of symptomatic progressive VL was used as it is considered more representative for human VL and appropriate for studying drug efficacy and relapse. Own historical laboratory data in the early curative VL hamster

model using diverse experimental compounds and reference drugs revealed that the BM was indeed the most difficult to clear. In extreme cases, no drug activity was recorded in the BM at all (**Figure 2.2d** and **[267]**). For instance, the 8-aminoquinoline analogs Sitamaquine (compound 10) and Tafenoquine (compound 86) were found to be inactive in the BM at effective concentrations in the liver **[267]**.

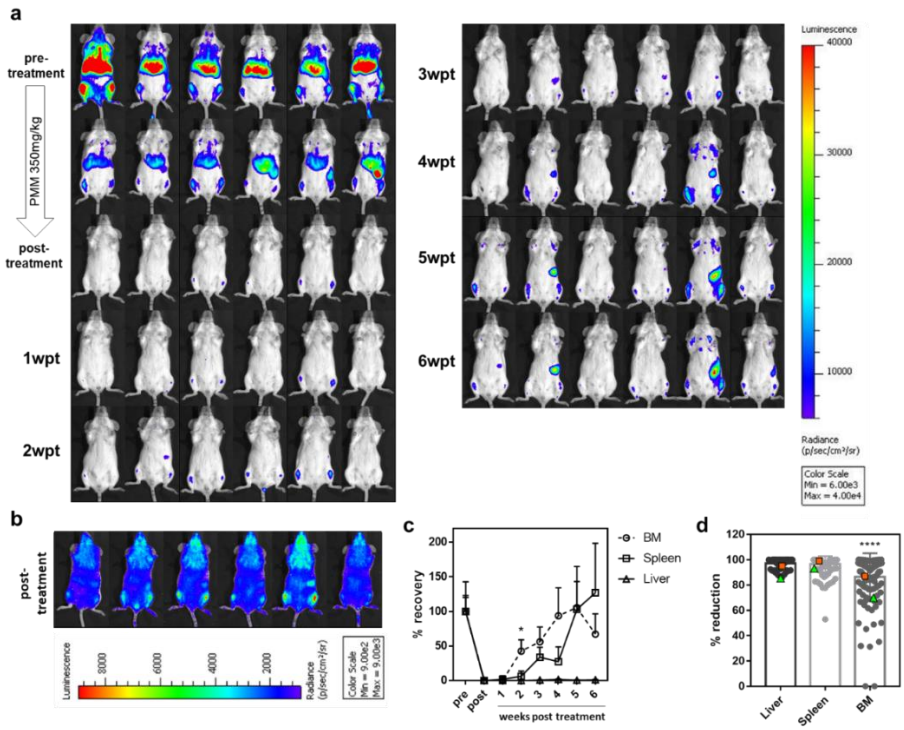

Figure 2.2. Reproducible post-treatment relapse model using sub-curative paromomycin identifies the BM as niche for treatment failure. (a) *In vivo* bioluminescent imaging (BLI) using an exposure time of 15 min of LEM3323 WT^{PpyRE9} infected BALB/c mice at 1-6 weeks post-treatment (wpt) at 350 mg/kg PMM s.i.d. IP for 5 days. **(b)** BLI (with sensitivity scale) at the end of treatment. **(c)** Mean relative luminescence units (RLU) values of BM and spleen during the first 6 weeks of LEM3323 WT^{PpyRE9} infection in BALB/c mice, where 100% is the pre-treatment RLU and 0% the post-treatment RLU. Results are expressed as mean ± SEM, Mann-Whitney test (two-tailed), *p ≤0.05. **(a-c)** Groups consist of 3-6 BALB/c mice (three independent experiments). **(d)** Reduction in parasite burden after treatment of golden Syrian hamsters with a broad set (n = 90) of antileishmanial test compounds; treatments with >85% clearance in the liver were considered therapeutically relevant. As a reference, squares (orange) depict results with MIL and triangles (green) represent SSG treatment. Wilcoxon matched-pairs signed rank test (two-tailed), ****p ≤0.0001.

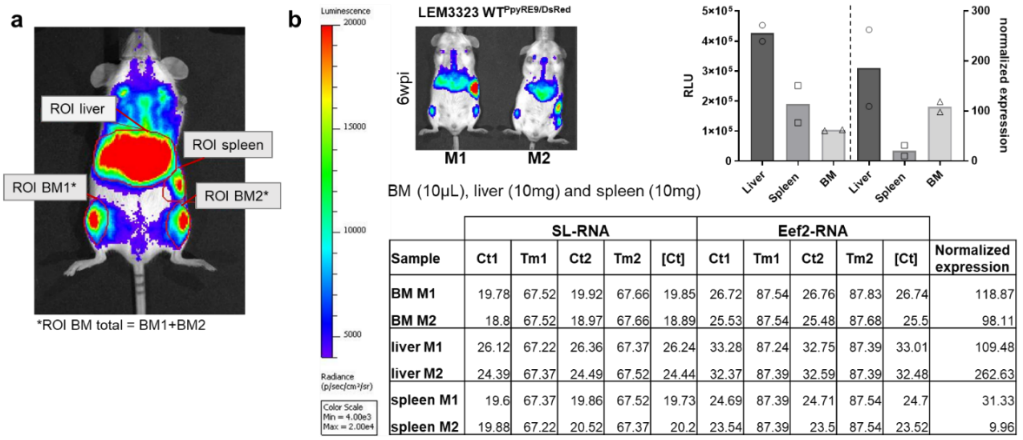

	SL-RNA					Eef2-RNA					
Sample	Ct1	Tm1	Ct2	Tm2	[Ct]	Ct1	Tm1	Ct2	Tm2	[Ct]	Normalized expression
BM M1	19.78	67.52	19.92	67.66	19.85	26.72	87.54	26.76	87.83	26.74	118.87
BM M2	18.8	67.52	18.97	67.66	18.89	25.53	87.54	25.48	87.68	25.5	98.11
liver M1	26.12	67.22	26.36	67.37	26.24	33.28	87.24	32.75	87.39	33.01	109.48
liver M2	24.39	67.37	24.49	67.52	24.44	32.37	87.39	32.59	87.39	32.48	262.63
spleen M1	19.6	67.37	19.86	67.52	19.73	24.69	87.39	24.71	87.54	24.7	31.33
spleen M2	19.88	67.22	20.52	67.37	20.2	23.54	87.39	23.5	87.54	23.52	9.96

Figure 2.3. (a) regions of interest (ROI) to calculate relative luminescence units. **(b)** Quantitative analysis of BLI imaging using RT-qPCR shows an underestimation of BM infection. Representative example of mice infected for 6 weeks (6wpi) with LEM3323 WT$^{PpyRE9/DsRed}$ imaged with BLI and subsequently sacrificed to perform RT-qPCR on the liver, spleen and BM. Normalized expression based on SL-RNA, which represents the parasite RNA, and Eef2 as the control for mouse RNA. Results are based on two independent repeats, 2 BALB/c mice per group.

Identification of specific BM cell niches for viable *Leishmania* parasites during infection and upon relapse

Progenitor and stem cells only represent 0.01% of the total BM, hence requiring enrichment for analysis in the complex pool of BM cellular constituents **[274]**. To identify the specific BM cell subsets in which the parasites reside *in vivo*, a two-step enrichment was performed combined with a staining for specific markers (**Figure 2.4a**). Cells harboring a DsRed^{+} fluorescent signal from *Leishmania* strain were flow sorted, stained and analyzed excluding lineage positive cells (Ter-119, Ly-6C/G, CD11b, TCR-β, B220, CD335) as second enrichment step. Here, *Leishmania* sensitive BM cells were identified, *i.e.* LT-HSC (Lin^{-} Sca1^{+} cKit^{+} CD48^{-} CD150^{+}) and to a lesser extent multipotent progenitors 2 (MPP2; Lin^{-} Sca1^{+} cKit^{+} CD48^{+} CD150^{+}). As *in vivo* infection in the BM only comprises 0.07 ± 0.03% of total cells, detection of infected stem cells is scarce and easily overlooked (**Figure 2.4b**). In figure 4b all DsRed^{+} cells are shown to illustrate the presence of events that correspond to extracellular amastigotes (46.26% ± 2.14% in infected mice, 62.23% ± 13.17% in relapsed mice), lineage positive cells (13.63% ± 0.03% in infected mice,

9.04% ± 3.97% in relapsed mice) and lineage negative cells (15.76% ± 3.30% in infected mice, 13.44% ± 2.63% in relapsed mice) that mainly consist of LT-HSC (67.33% ± 13.15% in infected mice, 77.14% ± 2.40% in relapsed mice). Although the occurrence of extracellular amastigotes could be the consequence of the sorting and centrifugation procedure, this has also been described in BM smears of patients together with the presence in lineage positive cells **[275, 276]**. The release of extracellular amastigotes that survived drug treatment could next initiate reinfection of BM cells. The percentage *in vivo* LT-HSC infection was calculated to be 20.04% ± 7.67%, in a comparable range to what is observed in *ex vivo* infections of LT-HSC (*vide infra*). For relapsed mice after PMM treatment, *in vivo* infection in the BM is 0.05% ± 0.01% of total cells, and the percentage LT-HSC infection is 6.67% ± 0.97% (**Figure 2.4b**).

Giemsa staining also revealed that LT-HSC, with confirmed post-sort purity of 95.3% (**Figure 2.5a**), harbored more parasites than MPP2 (**Figure 2.4c**). To additionally confirm amastigote viability in the various BM cells of infected and relapsed mice, a promastigote back-transformation assay was performed as most reliable indicator of viability **[59]**. A formal link and the relative contribution of LT-HSC during infection and relapse *in vivo* was thus explored using cell sorting of lineage positive cells and various stem cell types from the BM of infected/treated mice. After PMM treatment, LT-HSC and MPP2 were still found to harbor viable parasites, whereas no viable parasites could be recovered from sorted lineage positive cells (**Figure 2.4d**). Similar results were obtained at 3, 4 and 5 weeks post-treatment and coincided with the gradual detection of relapse by BLI. Promastigote back-transformation, which provides more accurate data than the $dsRed^+$ signals on parasite viability, unequivocally demonstrated that LT-HSC reproducibly harbored high numbers of viable parasites post-treatment (**Figure 2.4d**).

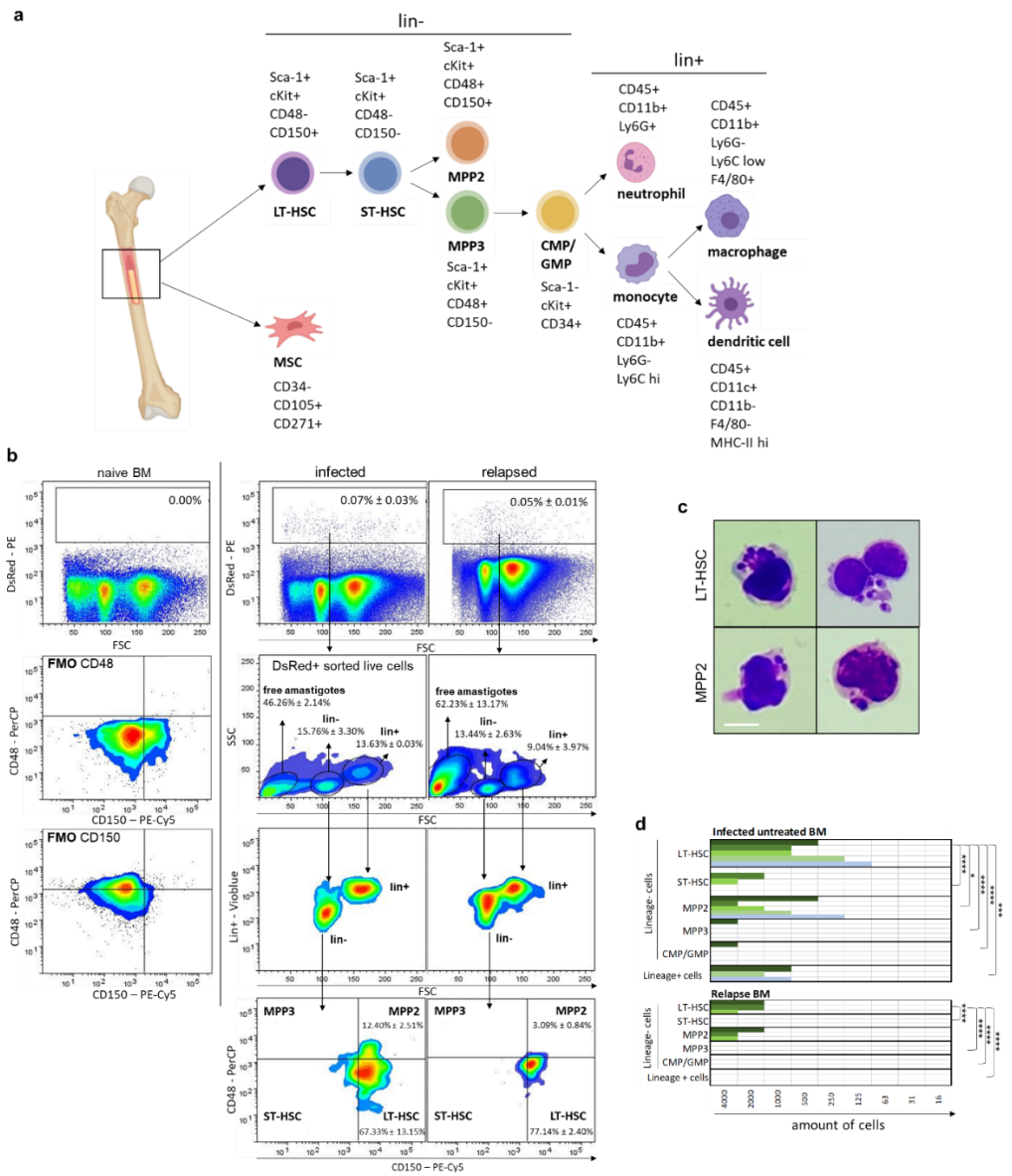

Figure 2.4. Identification of LT-HSC and MPP2 as niche for viable parasites during infection and following treatment failure. (a) Specific markers for BM cell subsets: long-term hematopoietic stem cell (LT-HSC), short-term HSC (ST-HSC), multipotent progenitor (MPP), common myeloid progenitor (CMP), granulocyte-monocyte progenitor (GMP), mesenchymal stem cells (MSC). **(b)** Cell sorting of DsRed^{+} BM cells of LEM3323 WT$^{PpyRE9/DsRed}$ infected BALB/c mice to enrich the infected sample, followed by re-measuring with markers as described in (a) and gated on LSK cells, *i.e.* Lin^{-}, Sca-1^{+} and cKit^{+} cells. Fluorescence minus one (FMO) controls are displayed to confirm the gates. Representative plots and frequencies of DsRed^{+} cells (mean ± SD) are shown of two independent experiments per condition (n = 4), performed at 4 wpi (infected) and 5 wpt (relapsed). **(c)** Giemsa-stained LT-HSC and MPP2 cells sorted from LEM3323 WT$^{PpyRE9/DsRed}$ infected BALB/c mice (6wpi). Scale bar = 10 µm. **(d)** Results of promastigote back-transformation

assays after FACS of an indicated number of cells (LT-HSC, ST-HSC, MPP2, MPP3, CMP/GMP and Lin$^+$ cells) from infected untreated mice (top panel, pooled results of 4, 5 and 6 wpi) and relapsed mice after PMM treatment (bottom panel, pooled results of 3, 4 and 5 wpt). Colored bars represent independent experiments ($3 \leq n \leq 5$) and positive back-transformation. Statistical significance levels using titration endpoints are indicated (2-way ANOVA, multiple comparisons). *p <0.05, ***p <0.001, ****p <0.0001. The diagram in (a) was generated using Biorender.com.

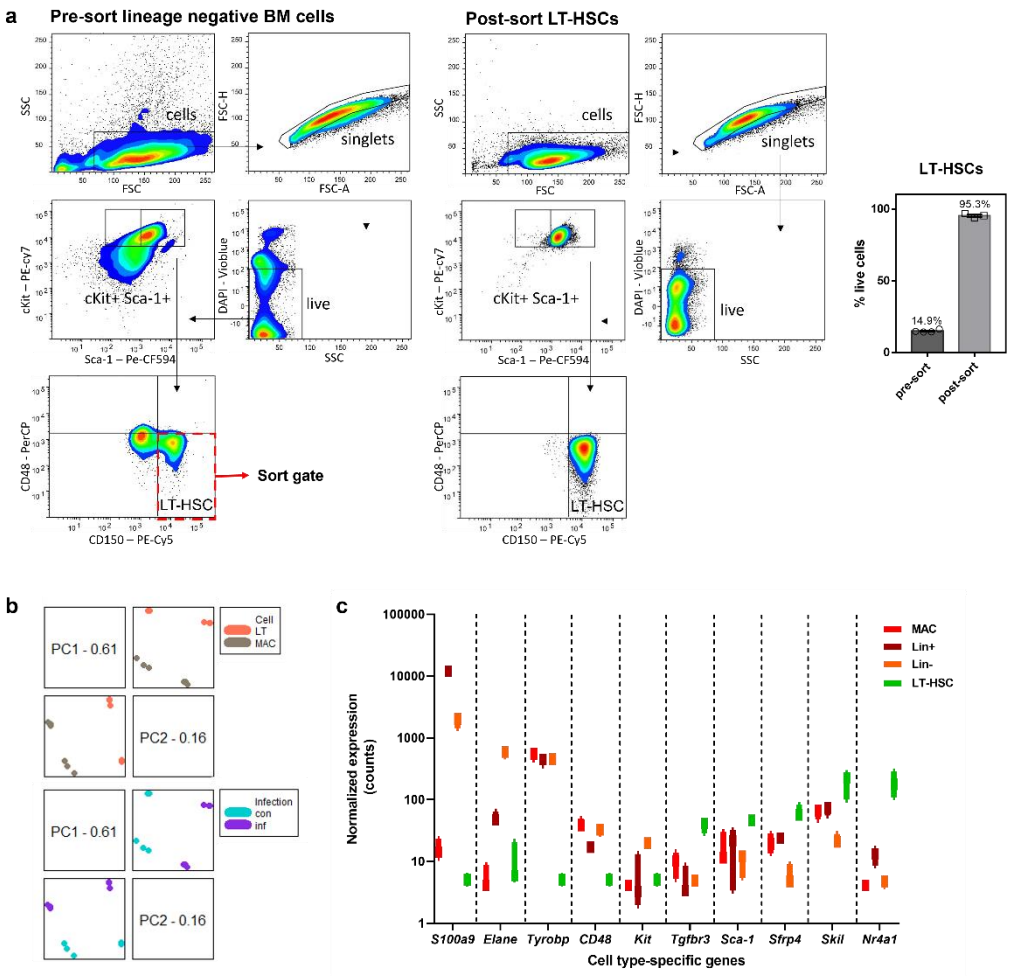

Figure 2.5. Purity assessment of post-sort LT-HSC. (a) Lineage depleted BM of naïve BALB/c mice was sorted for LT-HSC and re-measured to assess the purity of sorting with FACSMelody. **(b)** PCA analysis of the nCounter digital transcriptomics data revealing distant clustering of the LT-HSC and macrophage samples, confirming purity of the sorted samples. **(c)** Quantification of post-sorting purity using cell type-specific transcripts for Lin$^-$, MAC, Lin$^+$ and LT-HSC, including established (*S100a9*, *Elane*, *CD48*, *Kit*) and novel markers identified by nCounter analysis (*Tyrobp*, *Tgfbr3*, *Sfrp4*, *Skil*, *Nr4a1*). Based on the 7 most significant transcripts, the maximum contamination of purified LT-HSC with MAC, Lin$^+$ or Lin$^-$ cells was 0.0009%, 0.001% and 0.8%, respectively.

LT-HSC are exceptionally susceptible host cells to VL infection

To further investigate the intrinsic susceptibility of BM cell subsets to *Leishmania* infection, stem cells were isolated by negative immunomagnetic selection, followed by *ex vivo* infection with *Leishmania*. Lineage negative BM cells were co-cultured with metacyclic *L. infantum* (LEM3323 WT$^{PpyRE9/DsRed}$) promastigotes for 24, 48 and 72 hours, followed by flow cytometry analysis. Compared to the various BM cell subsets, LT-HSC were more readily infected with *Leishmania*, both in terms of proportion of infected cells (% of infection) and number of amastigotes per cell based on the DsRed median fluorescence intensity (MFI) (**Figure 2.6a**, **Figure 2.7a**). Interestingly, the MFI of infected LT-HSC increased over time compared to T_0 (24 hpi) implying that these cells are highly permissive for amastigote multiplication, in contrast to the stagnating parasite burdens in MPP2 cells (**Figure 2.6b**). This intracellular amastigote multiplication was confirmed by Giemsa staining in a comparative experiment using horse and bovine serum (**Figure 2.6c**), the former known to remove extracellular promastigotes as potentially confounding factor to determine intracellular multiplication **[268]**. Compared to BM-derived macrophages and dendritic cells as established host cells for *Leishmania*, LT-HSC infection rates were lower (± 20%, comparable to *in vivo* infection) whereas the MFI was substantially higher, hence representative of considerably higher intracellular burdens (**Figure 2.6d**). Strikingly high amastigote burdens were further revealed in sorted LT-HSC using immunofluorescence and Giemsa analyses (**Figure 2.6e and f**). The DsRed signal was more variable amongst the amastigotes in LT-HSC which may indicate the occurrence of quiescence in a subset of the parasites. The high susceptibility of LT-HSC was confirmed using the *L. donovani* Ldl82 WT$^{PpyRe9/DsRed}$ strain (**Figure 2.8a-d**) and using amastigotes of both *L. infantum* LEM3323 WT$^{PpyRE9/DsRed}$ and *L. donovani* Ldl82 WT $^{PpyRE9/DsRed}$ (**Figure 2.7b**). Cross-species confirmation using human BM aspirates from three different healthy donors confirmed heavy VL infection of hHSPC ($CD45^{lo}$ $CD34^{+}$) after *in vitro* infection comparable to the observations in mouse LT-HSC (**Figure 2.6g**).

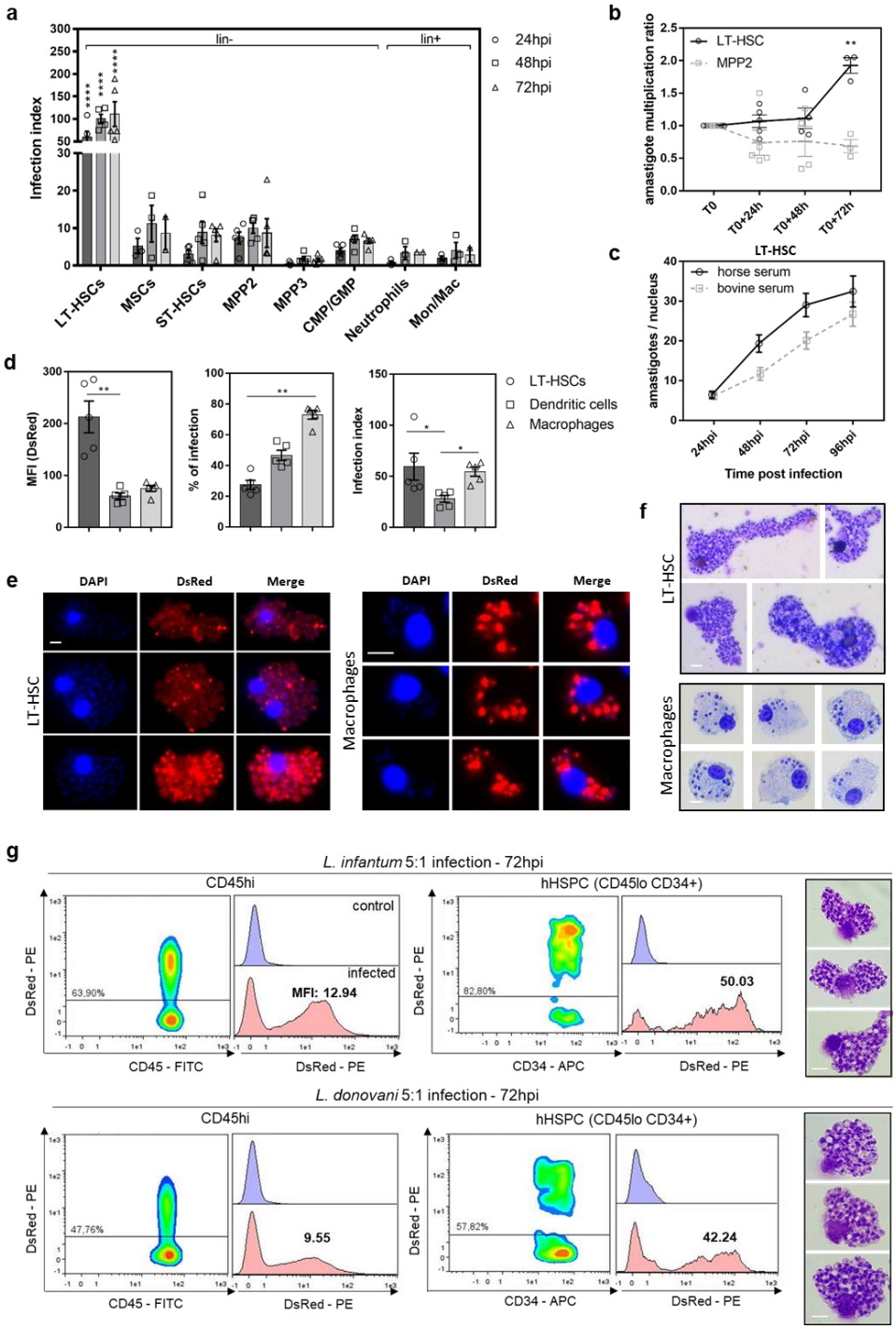

Figure 2.6. ***Ex vivo*** **LT-HSC are most susceptible to VL infection** ***in vitro*****. (a)** *Ex vivo* LEM3323 WT$^{PpyRE9/DsRed}$ infection of lineage depleted BM collected from BALB/c mice: infection index representing DsRed MFI × % of infection. Statistical comparisons were made between LT-HSC and all other groups, for each time point. **(b)** Evolution over time of the DsRed MFI indicating

intracellular parasite expansion (amastigote multiplication ratio) in two BM cell subsets: LT-HSC and MPP2. **(c)** Additional confirmation of amastigote multiplication using horse serum versus bovine serum on LEM3323 WT$^{PpyRE9/DsRed}$ infected sorted LT-HSC – amastigotes per nucleus microscopically counted after Giemsa staining (n = 30 cells). **(d)** Comparison of MFI, % infection and infection index between BM-derived dendritic cells and macrophages and LT-HSC. **(e)** Immunofluorescence microphotograph of LEM3323 WT$^{PpyRE9/DsRed}$ infected (120 h) BM-derived macrophages and sorted LT-HSC with nuclei/kinetoplasts stained with DAPI (blue) and DsRed signal from LEM3323 WT$^{PpyRE9/DsRed}$ (red), scale bar = 10 μm. **(f)** Giemsa staining of infected BM-derived macrophages and sorted LT-HSC, scale bar = 10 μm. **(g)** DsRed plots of CD45^{hi} and hHSPC (CD45^{lo} CD34^{+}) BM subsets and histogram of representative results for three human BM aspirates, *ex vivo* infected for 72h using either *L. infantum* (LEM3323 WT$^{PpyRE9/DsRed}$) or *L. donovani* (Ldl82 WT$^{PpyRE9/DsRed}$) promastigotes. % of infection and median fluorescence intensity (MFI) is provided in the individual plots. Giemsa confirmation of infection of hHSPCs, at 72 hpi, with both *L. infantum* and *L. donovani* promastigotes, is shown on the right. Scale bar = 10 μm. **(a-g)** Days/hours post-infection (dpi/hpi), median fluorescence intensity (MFI), mesenchymal stem cell (MSC), long-term hematopoietic stem cell (LT-HSC), short-term hematopoietic stem cell (ST-HSC), multipotent progenitor (MPP), common myeloid progenitor (CMP), granulocyte-monocyte progenitor (GMP), monocyte/macrophage (Mon/Mac), human hematopoietic stem cell (hHSPC). Results are shown as mean ± SEM and are based on at least three independent experiments ($3 \leq n \leq 5$). Statistical significance was found with two-tailed tests, *i.e.* 2-way ANOVA in (**a**), multiple *t* test illustrating a difference between LT-HSC and MPP2 in (**b**), and Kruskal-Wallis in (**d**). *p <0.05, **p <0.01, ****p <0.0001.

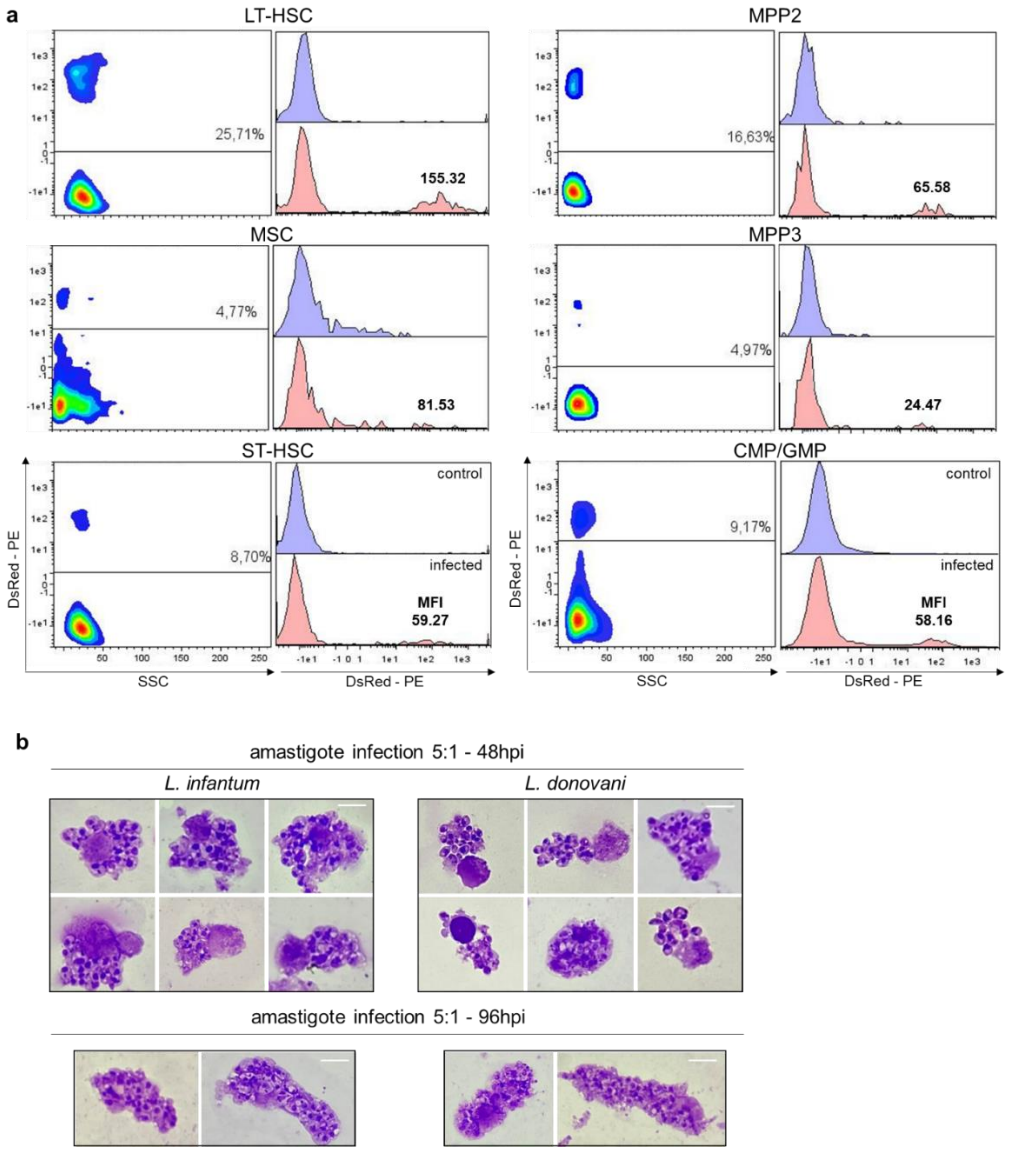

Figure 2.7. (a) DsRed plots of all lineage negative BM subsets and histogram of representative result for Figure 3. Percentage of infection and MFI is provided on plots. Median fluorescence intensity (MFI). **(b)** Confirmation of amastigote infection of LT-HSC, both 48 and 96hpi, using both *L. infantum* (LEM3323 WT$^{PpyRE9/DsRed}$) and *L. donovani* (Ldl82 WT$^{PpyRE9/DsRed}$) amastigotes purified from peritoneal macrophages 96hpi. Scale bar = 10 μm.

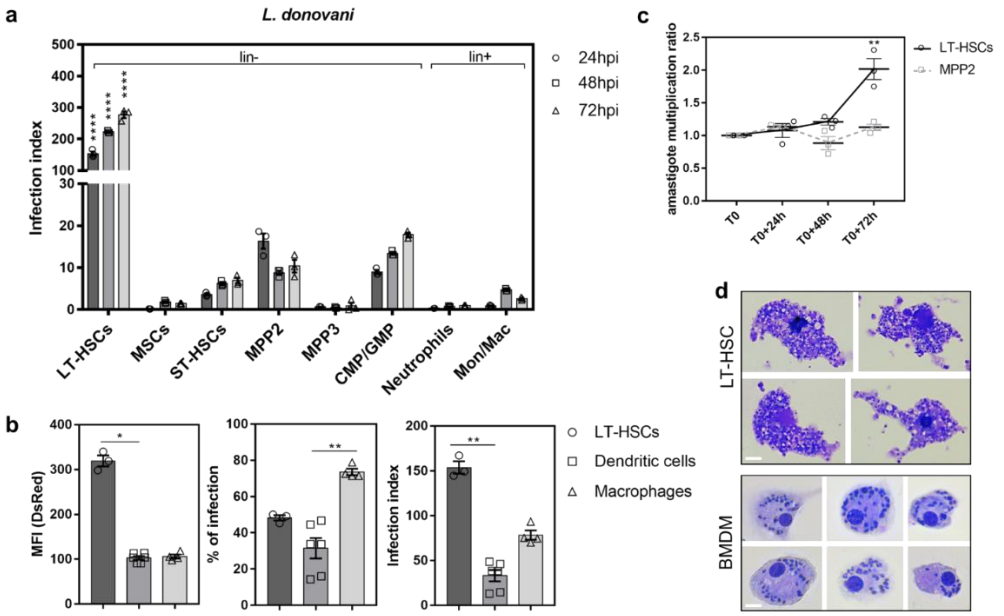

Figure 2.8. LT-HSC are most susceptible to VL infection *ex vivo*. (a) *Ex vivo* Ldl82 WT$^{PpyRE9/DsRed}$ infection of lineage depleted BM collected from BALB/c mice: infection index representing DsRed MFI × % of infection. Statistical comparisons were made between LT-HSC and all other groups, for each timepoint. **(b)** Evolution over time of the intracellular parasite burden (amastigote multiplication ratio) in two BM cell subsets: LT-HSC and MPP2s. **(c)** Comparison of MFI, % infection and infection index between BM-derived dendritic cells and macrophages and LT-HSC, **(d)** Giemsa staining of Lld82 WT$^{PpyRE9/DsRed}$ infected BM-derived macrophages and sorted LT-HSC 120hpi. Scale bar = 10 μm. **(a-d)** Days post-infection (dpi), median fluorescence intensity (MFI), mesenchymal stem cell (MSC), long-term hematopoietic stem cell (LT-HSC), short-term hematopoietic stem cell (ST-HSC), multipotent progenitor (MPP), common myeloid progenitor (CMP), granulocyte-monocyte progenitor (GMP), monocyte/macrophage (Mon/Mac). Results are shown as mean ± SEM and are based on at least three independent repeats ($3 \leq n \leq 6$). Statistical significance was found with two-tailed tests, *i.e.* 2-way ANOVA in (**a**), Kruskal-Wallis in (**b**), and multiple t test in (**d**). *p <0.05, **p <0.01, ****p <0.0001.

LT-HSC represent an oxidative stress- and drug-resistant sanctuary for viscerotropic *Leishmania spp.*

Given the importance of reactive nitrogen and oxygen radicals as antiparasitic response, their production in LT-HSC was examined using flow cytometry including all necessary fluorescence minus one controls to assure specificity and exclude autofluorescence. From 24 hours of *ex vivo* infection onwards, intracellular NO and ROS levels notably declined ($p < 0.0001$) in $DsRed^+$ LT-HSC compared to naïve cells or DsRed- cells within the same well (**Figure 2.9a**). In contrast, NO and ROS levels were elevated or stable in infected macrophages (**Figure 2.9b**).

To further document LT-HSCs as a privileged cellular niche for *Leishmania*, their sensitivity to PMM, MIL and SSG was tested. Sorted LT-HSC and BM-derived macrophages were infected and drug-exposed for 120h at two concentrations selected based on previous research **[271]**. In comparison to macrophages, *L. infantum* and *L. donovani* parasites remain more abundant in LT-HSC after treatment with PMM, MIL and SSG (**Figure 2.9c**). As the percentage of reduction remains similar between the two host cell types, it is particularly the extreme amastigote burden that impedes parasite elimination from LT-HSCs rather than an intrinsic cellular drug resistance phenotype (**Figure 2.9d**). High-level expression of efflux pumps on stem cells could potentially contribute to the enhanced tolerance to drugs **[277]**. The role of efflux pumps in LT-HSC was assessed by co-incubation with the efflux pump inhibitor verapamil, as previously described **[272]**. Verapamil inhibits efflux mediated by both multi-drug resistance protein (MDR) and multi-drug resistance associated protein (MRP), which are often implicated in resistance. Co-administration of verapamil (8 μM) (**Figure 2.9e**) did not enhance susceptibility of LT-HSC to most reference drugs except for SSG, a known substrate of efflux transport **[278]**. Through the use of verapamil, SSG efflux was shown to be more prominent in LT-HSC than in macrophages confirming previous reports of higher efflux pump expression levels in progenitors **[122]**. Nevertheless, parasite burden

on a per-cell basis was significantly higher in LT-HSC *vs.* macrophages for all three drugs, confirming the *in vivo* relapse data and implicating LT-HSC as highly permissive host cells that support post-treatment survival of the intracellular parasites.

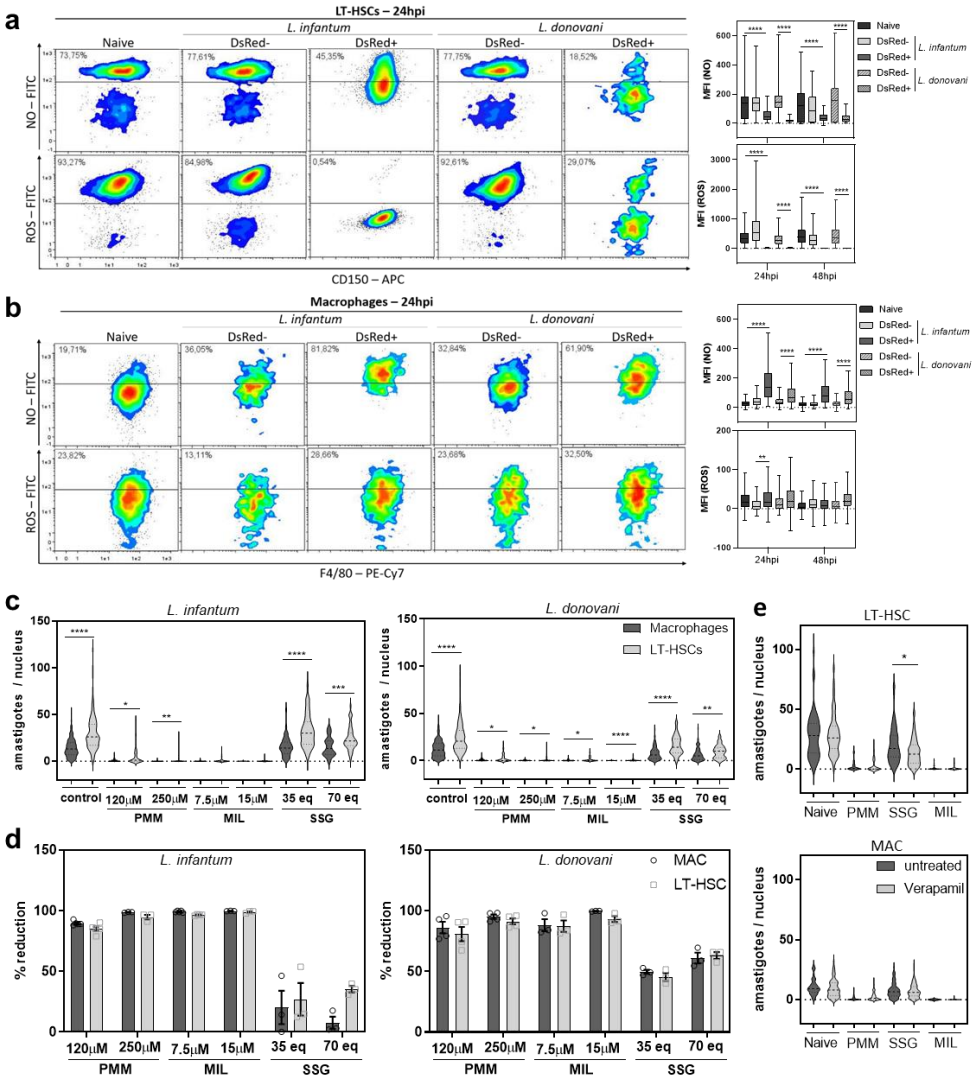

Figure 2.9. LT-HSC represent an oxidative stress- and drug-resistant sanctuary for viscerotropic *Leishmania spp.* (a-b) ROS and NO levels, determined using CM-H_2DCFDA and DAF-FM diacetate, are decreased in *ex vivo* infected stem cells. Density plots of LT-HSC (a) and macrophages (b) at 24h post infection (hpi) with fluorescent signal of NO (top rows) and ROS (bottom rows). Graph represents the MFI of these plots at 24h and 48h post infection. Representative dot plots with corresponding graphs of three independent experiments with similar

results are shown. Multiple *t* tests (two-tailed) after outlier analysis (ROUT, Q = 1%), boxplots represent minimum, maximum, median and 75% and 25% percentiles, $155 \leq n \leq 16250$, $^{**}p < 0.01$, $^{****}p < 0.0001$. **(c)** Sorted LT-HSC infected with *L. donovani* Ldl82 WT$^{PpyRE9/DsRed}$ in a 5:1 ratio and treated for 120h. Representative plots of two independent experiments for PMM (120 μM and 250 μM), MIL (7.5 μM and 15 μM) and SSG (35 eq. Sb and 70 eq. Sb) are shown. Confirmatory results with PMM, MIL and SSG on *L. infantum* LEM3323 (with inherent Sb resistance) in two independent experiments. Results are expressed as mean ± SEM. Mann-Whitney test, $45 \leq n \leq 250$, $^{*}p < 0.05$, $^{**}p < 0.01$, $^{****}p < 0.0001$. **(d)** Percentage of reduction compared to untreated controls is shown, calculated from the data shown in (c). **(e)** Effect of 120h co-incubation of verapamil (8 μM) with PMM (120 μM), MIL (7.5 μM) and SSG (35 eq. Sb) on *L. infantum* LEM3323 WT$^{PpyRE9/DsRed}$ (with inherent Sb resistance) infected (5:1) sorted LT-HSC and BM-derived macrophages. Results are based on three independent experiments. Mann-Whitney test, $60 \leq n \leq 100$, $^{*}p < 0.05$.

Leishmania infantum infection of LT-HSC triggers a unique *StemLeish* transcriptional profile characterized by TNF/NF-κB and RGS1/TGF-β/SMAD/SKIL signaling

To unravel the molecular basis for the high susceptibility and map the comprehensive impact of infection on HSC functionality, nCounter digital transcriptomics was used on *ex vivo* infected LT-HSC in comparison with BM-derived macrophages, using the Mouse Myeloid Innate Immunity panel from Nanostring. As shown in a heat map of 736 genes (**Figure 2.10a**), the overall transcriptional profile of macrophages was only modestly affected by infection (as previously demonstrated by **[279]**) whereas a strong effect was observed in LT-HSC. PCA analysis (**Figure 2.5b**) and evaluation of cell type-specific transcripts (**Figure 2.5c**) revealed distant profiles of the LT-HSC and macrophage samples, further supporting the very high purity of the sorted cells. A total of 101 genes were differentially expressed in LT-HSC (73 up- and 28 down-regulated, **Figure 2.10b** and [a] from **[280]**) in contrast to 49 differentially expressed genes in macrophages (38 up- and 11 down-regulated, [b] from **[280]**). Of the 15 up-regulated genes shared between LT-HSC and macrophages, 9 corresponded to *Leishmania* transcripts whereas only 6 were host genes (*Arf6*, *Atf3*, *Calr*, *Ctsd*, *Itgb1*, *S100a10*). Downregulated genes (**Figure 2.10b**) included notably monocyte/macrophage lineage marker *Cd68*, transcriptional regulator *Cepba*, genes involved in IL-4/IL-13 signaling and *Nos2* (**Figure 2.10b**), corroborating our *in vitro* assays (**Figure 2.9**).

None of the downregulated genes were shared between LT-HSC and macrophages, further confirming the divergent response to infection in both cell types. A systems biology analysis of LT-HSC upregulated genes revealed significant enrichment of several hallmark gene sets ([c] from **[280]**), curated pathways ([d] from **[280]**) and transcription factor motifs ([e] from **[280]**). The most predominant pathways were TNF/NF-κB, TFG-β/SMAD/SKIL and MAPK signaling as well as oxidative damage/reactive nitrogen and oxygen species detoxification, and p53-mediated apoptosis (**Figure 2.10b, lower right panel**), all of which have previously been demonstrated in either human or experimental VL **[261, 279, 281-285]**.

However, nCounter profiling also revealed several highly up-regulated LT-HSC genes that have not yet been described in *Leishmania spp.* infections, such as *Rgs1*, *Twistnb*, *Ell2*, *Vav1*. Three orthogonal approaches argue in favor of a new HSC transcriptional program (further referred to as 'StemLeish'), rather than a *Leishmania*-triggered differentiation of LT-HSC to one or more specific leukocyte subsets. First, *in silico* cell type deconvolution of *Leishmania*-infected *vs.* uninfected LT-HSC demonstrates down-regulation of major leukocyte subsets, but not total leukocytes (*pan*-leukocytes quantified as $CD45^+$) (**Figure 2.10c** and [f] from **[280]**). Second, quantification of the 65-gene *StemLeish* up-regulated subset across all currently known leukocyte subsets (including several HSC subsets) analyzed by RNAseq in the comprehensive ImmGen data set (**Figure 2.10d**), demonstrated significant downregulation in all subsets (except thioglycolate-induced inflammatory neutrophils, for which a null result was obtained, *i.e.* no significant up- or down-regulation). Similar results were obtained for *StemLeish* down-regulated genes (**Figure 2.11a** and [g-h] from **[280]**). Third, transcription factor enrichment demonstrated 'classical' pro-inflammatory NF-κB and AP-1 (Jun/Fos) transcription factors, but also Skil, Mef2c, Foxf2, Bach2 ([e] from **[280]**) which have not been previously described in either experimental or human leishmaniasis.

We therefore further investigated the *StemLeish* gene signature in large publicly available transcriptomic datasets (ImmuCo) of purified mouse leukocyte subsets. In

agreement with our results, *Rgs1*, *Skil*, *Ell2*, *Cebpa* and *Twistnb* were confirmed as highly expressed in murine HSCs isolated from >600 animals (**Figure 2.10e**). We next verified how both genes might be regulated in HSC differentiation towards myeloid, lymphoid and erythroid lineages. *Rgs1* was found to be significantly positively correlated with *Ell2* and *Skil* in purified HSCs. In line with our nCounter digital transcriptomics data, *Rgs1* negatively correlated in purified HSCs to the master transcriptional regulator *Cebpa* ($p = 1.4\times10^{-60}$), a driver of myeloid and particularly neutrophil differentiation. In addition, *Twistnb* was also negatively correlated ($p = 9.1\times10^{-26}$) to *Cd68* transcript levels in macrophages. Taken together, overexpression of *Rgs1* and transcription factors *Twistnb/Vav1/Smad2/Ell2/Atf3* characterize a *StemLeish* transcriptional program in LT-HSC that differs from previously described transcriptional reprogramming triggered by *Leishmania spp* **[223, 227, 279, 281, 282]**.

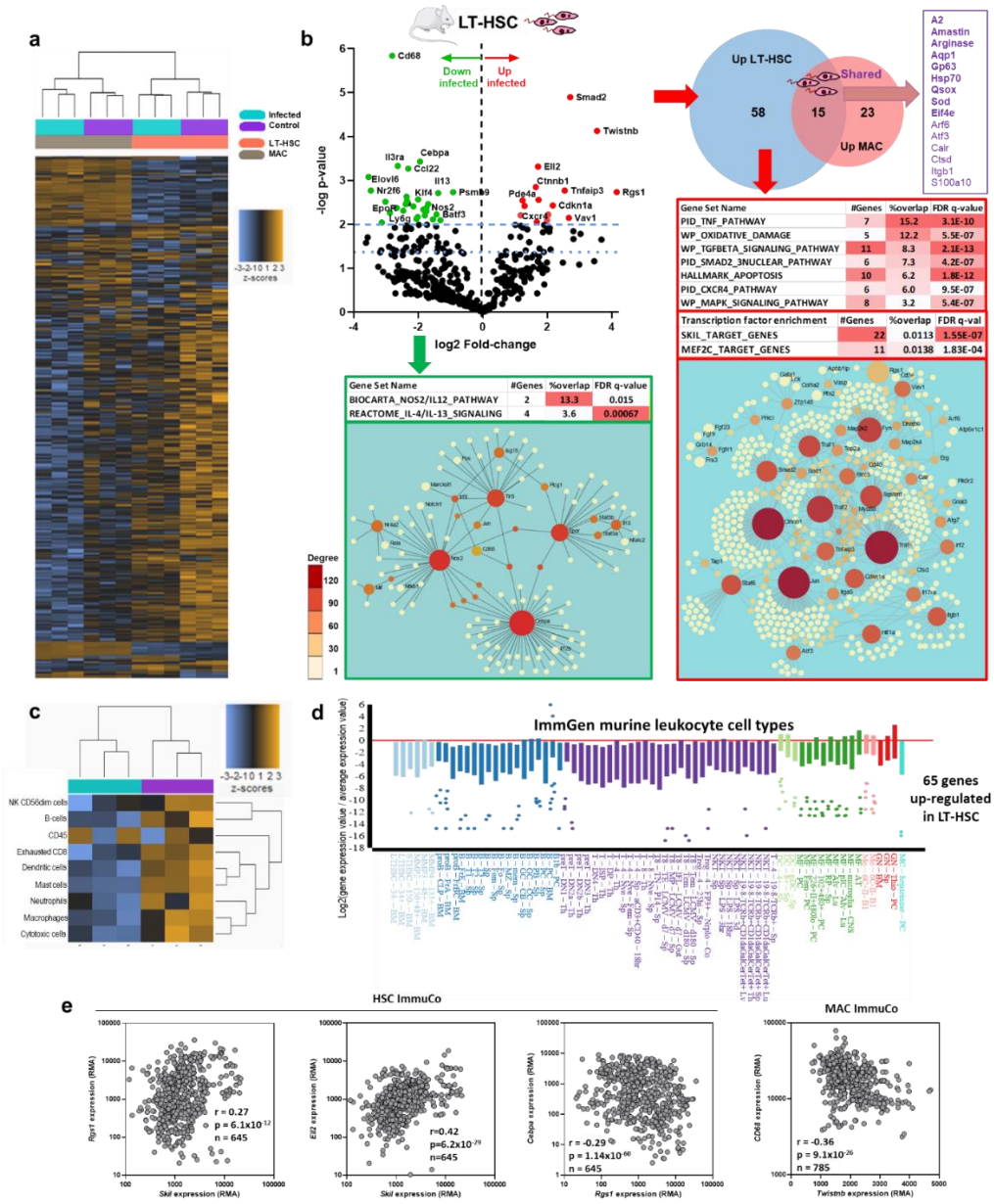

Figure 2.10. ***L. infantum*** **infection of LT-HSC triggers a unique StemLeish transcriptional profile characterized by RGS1/TGF-β/SMAD/SKIL signaling. (a)** Heatmap of 736 host and pathogen transcripts above the detection threshold and quantified by nCounter digital transcriptomics in control *vs. L. infantum*-infected LT-HSC (Lin$^-$cKit$^+$Sca1$^+$CD48$^-$CD150$^+$) and macrophages, purified as detailed in Methods. **(b)** Volcano plot (upper left panel) and systems biology analysis of differentially expressed genes (DEG, upper left) in LT-HSC. Venn Diagram of overlapping DEG in LT-HSC *vs.* macrophages (upper right panel). Enrichment of pathways, transcription factor motifs (MSigDb), and network analysis (NetworkAnalyst 3.0) in up-regulated (lower right panel) and down-regulated (lower left panel) genes in LT-HSC. Genes are colored

according to node degree (number of connections)[286]. **(c)** *In silico* cell type deconvolution (nSolver) of *Leishmania*-infected *vs.* uninfected LT-HSC demonstrates down-regulation of major leukocyte subsets, but not total leukocytes (*pan*-leukocytes quantified as $CD45^+$). **(d)** Quantification of the 65-gene StemLeish up-regulated subset across all leukocyte subsets (analyzed by single-cell RNAseq) in the ImmGen data set demonstrates significant downregulation in all subsets except thioglycolate-induced inflammatory neutrophils. **(e)** Validation of the StemLeish signature (*Rgs1/Skil/Ell2/Cebpa/Twistnb*) in large independent murine LT-HSC and macrophage datasets (ImmuCo; $n = 645$ and $n = 785$ mice respectively), analyzed using Spearman's correlation between up- *vs.* down-regulated StemLeish genes. Data are shown as RMA (Robust Microarray Average), with a conservative detection limit at RMA>100. The highly significant positive correlations (after FDR correction) between genes upregulated in StemLeish (*Rgs1/Skil/Ell2*, two left panels) confirm that these genes are co-regulated in a quantitative manner across a large number of independent samples. A negative correlation (two right panels) was found between the up-regulated *Rgs1* and *Twistnb* transcription factors, and the down-regulated *Cebpa* transcription factor and *Cd68* macrophage lineage marker. Clipart used in diagram (b) was obtained from Servier Medical Art (https://smart.servier.com).

Page 100: Figure 2.11. Systems biology analysis of DEG in LT-HSC. (a) Genes down-regulated in LT-HSC upon infection with *L. infantum* are not significantly over- or under-expressed in any current known murine leukocyte subset in the exhaustive ImmGen database. **(b)** The $RGS1^{high}$ macrophage gene signature (recently characterized in COVID19 patients) is significantly enriched for all clinical aspects of human visceral leishmaniasis (shaded in blue), in addition to the COVID-19/ respiratory tract infectious disease clinical phenotype (unshaded). All enrichment data originate from MSigDB, human Phenome gene set database. **(c)** *Rgs1* mRNA is detectable in purified human progenitor ($CD34^+$) and total PBMCS, and highly expressed in specific mature leukocyte subsets (Tregs, several CD4 memory subsets, CD8 central/effector memory cells, plasmacytoid and myeloid DCs).

a

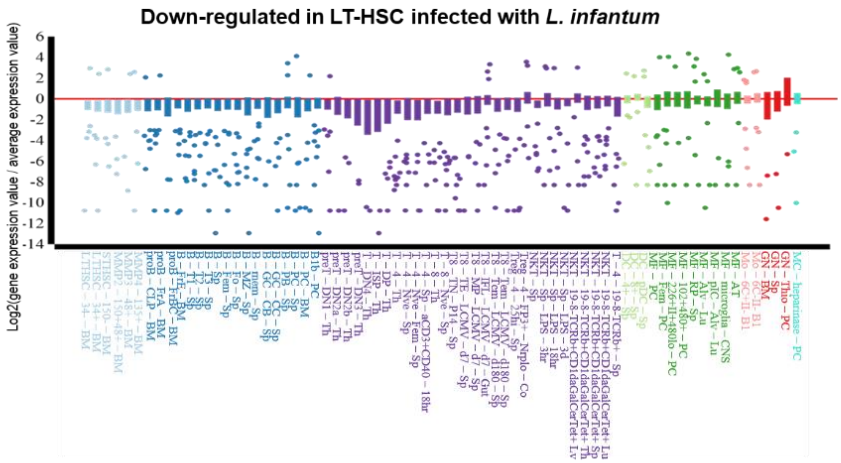

b

Gene Set Name	#Genes	%overlap	FDR q-val
ABNORMAL_MACROPHAGE_MORPHOLOGY	6	18.2	3.4E-07
CACHEXIA	4	6.7	1.6E-03
SKIN_RASH	7	6.1	1.4E-05
SKIN_ULCER	7	6.0	1.4E-05
PULMONARY_FIBROSIS	4	5.7	2.5E-03
WEIGHT_LOSS	10	3.7	2.9E-06
PNEUMONIA	6	3.0	1.4E-03
FEVER	9	3.0	4.2E-05
SPLENOMEGALY	10	2.9	1.7E-05
ABNORMALITY_OF_HUMORAL_IMMUNITY	7	2.8	6.2E-04
ABNORMAL_LEUKOCYTE_COUNT	9	2.5	1.1E-04
ABNORMALITY_OF_THE_UPPER_RESPIRATORY_TRACT	9	2.3	1.7E-04
ABNORMAL_INFLAMMATORY_RESPONSE	21	2.3	2.8E-10
RESPIRATORY_TRACT_INFECTION	12	2.1	1.8E-05
HEPATOMEGALY	10	2.0	1.7E-04
RECURRENT_RESPIRATORY_INFECTIONS	8	1.7	2.9E-03
ABNORMALITY_OF_BLOOD_AND_BLOOD_FORMING_TIS	20	1.7	2.4E-07
DECREASED_BODY_WEIGHT	14	1.1	1.1E-03

c

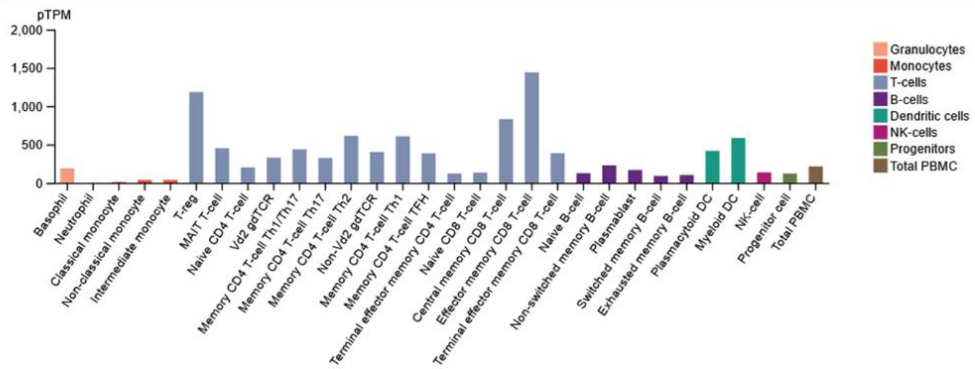

A conserved *StemLeish* gene signature recapitulates cross-species epigenetic and transcriptional signatures of visceral leishmaniasis and tuberculosis

Following identification of the *StemLeish* gene signature, we next sought to investigate a possible presence of this signature in three independent cohorts of human VL (patients from Brazil **[282]**, from India **[287]** and HIV co-infected VL patients from Ethiopia **[199]**) considering the fold-changes of DEG between untreated patients with active disease and post-treatment blood samples. The Venn diagram (**Figure 2.12a, upper left panel**) illustrates the overlap between murine *StemLeish* and human VL signatures, with notable conservation of the *Rgs1/Tnfaip3/Atf3* signature. Detection of the *StemLeish* signature in blood of VL patients supports the notion that HSC migrate from the BM to the circulation during VL **[227]**. Human Phenotype Ontology (MSigDb) enrichment analysis reveals that the *StemLeish* signature phenocopies the complete clinical picture of human VL (**Figure 2.12a, lower left panel**), with a significant cross-species correlation (Spearman) in the fold-changes of shared DEG (**Figure 2.12a, right panel),** including in the cohort with HIV co-infection.

Additional in depth cross-species and cross-pathology comparison revealed a specific overlap of the *StemLeish* gene signature with the "*RGS1*^{high}" macrophage signature recently identified by single-cell RNAseq in COVID-19 patients (**Figure 2.12b**) **[288]** and with the *in vivo* interstitial macrophage subset IM2 (interstitial macrophage subset 2) during murine mycobacterial infection (**Figure 2.12c**). Strikingly the *RGS1*^{high} macrophage gene signature is also significantly enriched for all clinical aspects of human VL (Human Phenotype Ontology, **Figure 2.11b**). In addition, IM2 share the concurrent up- (*Rgs1/Tnfaip3/Nfil3/Skil*) and downregulation (*Mif/Nos2*) of *StemLeish* signature genes in *Mtb*-infected lungs. As can be deduced from **Figure 2.12d** (Venn Diagram, left panel), DEG are broadly shared between human pathologies (TB, VL and "RGS1^{high}" macrophages in COVID-19) and both murine (*StemLeish*) and human (*M. tuberculosis*-infected CD34^{+}) HSC gene signatures (significant overlap for each pairwise comparison,

hypergeometric test $p < 0.05$). Moreover, prominently enriched signaling pathways in *StemLeish* (TNF/TGF-β signaling, inflammatory response, oxidative stress and p53 signaling/apoptosis) as well as transcription factors binding sites (SKIL/MEF2c) are almost universally shared across species (mouse, human) and across relevant *in vitro* and *in vivo* biological/clinical VL and tuberculosis settings (**Figure 2.12d, right panel**). In agreement with enrichment of several SARS-COV-2 and COVID-19 pathways across leishmaniasis and tuberculosis (TB) data sets, both our *StemLeish* and the *RGS1^{high}* macrophage COVID gene signatures are significantly up-regulated *in vivo* upon conversion of latent into active TB (**Figure 2.12e**), as shown by reanalysis of RNAseq data of a large prospective cohort **[289]**. However, using non-overlapping gene sets for *StemLeish* and *RGS1^{high}* macrophages (**Figure 2.12e**), we found that both transcriptional signatures represent independent early events (detectable at an average of >200 days before diagnosis, data not shown) in TB pathogenesis. Thus, our meta-analysis underscores the broad clinical relevance of the *StemLeish*/*RGS1^{high}* signature and suggests its possible use as a predictor of both *Leishmania spp.* and *M. tuberculosis* dissemination as well as therapeutic failure.

Finally, we compiled existing epigenetic, transcriptional and genomic data for the prominent *StemLeish* gene *Rgs1* (**Figure 2.12f**), demonstrating similar epigenetic regulation of open chromatin (ATAC-Seq, DNAse I hypersensitive sites) in human undifferentiated $CD34^+$ HSC *vs.* HSC induced towards myeloid differentiation. The open chromatin regions in differentiated HSC (indicated as CD34-) correspond to increased transcription (**Figure 2.12f**) and are conserved in all currently used animal models of leishmaniasis and/or tuberculosis (rhesus macaque, mouse, hamster, dog), but not in zebrafish. However, the enhancer region upstream of *Rgs1* (containing the MEF2C binding site) is highly conserved among all vertebrates. Similar correlations between epigenetic and transcriptomic profiles were obtained for the other prominent *StemLeish* genes (**Figure 2.13**).

Rgs1 transcription is generally very low in embryonic stem cells (**Figure 2.12f, Figure 2.11c**) but reexamination of published single-cell RNAseq data **[290]** from cord blood confirmed the presence of a *RGS1*^{high} phenotype in several human CD34^{+} HSC subsets. More specifically, *RGS1*^{high} cells were frequent among Erythro-Myeloid Precursors (EMP), Lymphoid/Myeloid Precursors (LMPP7) and HSC in a metabolically active state (**Figure 2.12g**, HSC/Met. state). Collectively, these data underscore that the *StemLeish* gene signature corresponds to an evolutionary conserved, cross-species and cross-pathology epigenetic and transcriptional program with significant clinical implications for both VL and tuberculosis.

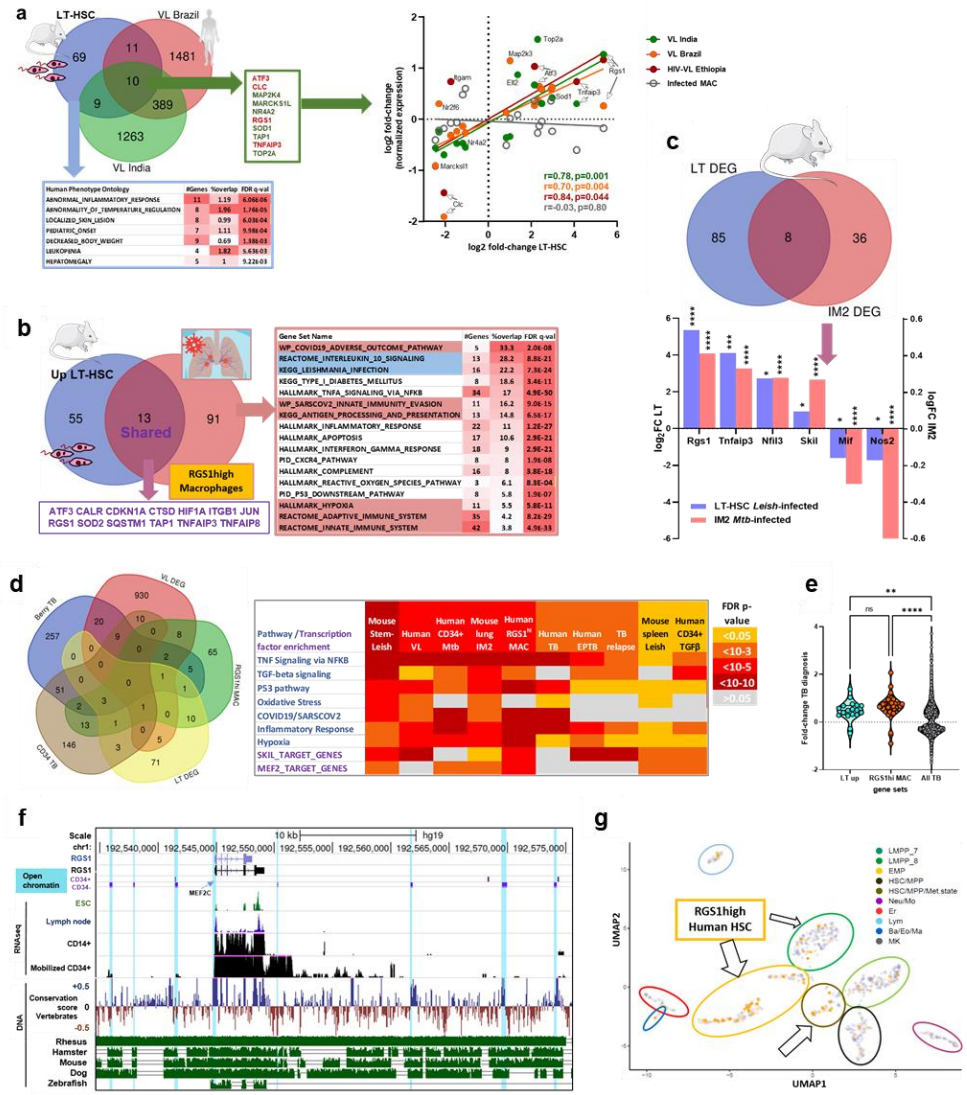

Figure 2.12. An evolutionary conserved *StemLeish* gene signature recapitulates cross-species epigenetic and transcriptional signatures of visceral leishmaniasis and tuberculosis. **(a)** *In vivo* validation of *StemLeish* signature in three independent cohorts of human VL patients from Brazil, from India and HIV+VL co-infected patients from Ethiopia, all fold-changes of DEG from untreated patients with active disease *vs.* post-treatment blood samples. Venn diagram (upper left panel) shows overlap between murine and human signatures. Human Phenotype Ontology (MSigDb) enrichment analysis indicates the *StemLeish* signature phenocopies the complete clinical picture of human VL (lower left panel). Significant correlations (Spearman) between *StemLeish* and human VL DEG in all three cohorts (right panel). **(b)** The *StemLeish* gene signature significantly overlaps with the *RGS1^{high}* macrophage signature recently identified by single-cell RNAseq in COVID-19 patients (left panel) which independently recapitulates various immunological features of human VL (right panel). **(c)** Overlap with the transcriptional signature in IM2 (interstitial macrophage subset 2) in *Mtb*-infected murine lungs revealing concurrent up-(*Rgs1*/*Tnfaip3*/*Nfil3*/*Skil*) and downregulation (*Mif*/*Nos2*) of *StemLeish* signature genes. **(d)** Venn

diagram (left panel) shows differential overlaps in a cross-species cross-pathology comparison between human TB ("Berry TB" signature, **[291]**), human VL ("VL DEG", **[282]**) and three cell-based signatures [*StemLeish* (LT DEG, this study), human CD34$^+$ cells infected with *Mtb* **[292]**, and the COVID-19 *RGS1^{high}* macrophage signature **[288]**]. Enriched signaling pathways and transcription factors binding sites (SKIL/MEF2c) in gene promoters are strongly shared across species (mouse, human) and relevant *in vitro* and *in vivo* biological/clinical settings of VL and tuberculosis (right panel). **(e)** Both *StemLeish* and *RGS1^{high}* macrophage gene signatures are significantly upregulated, as compared to all other DEG observed ("All TB") during the *in vivo* conversion of latent into active TB, as shown by reanalysis of whole blood RNAseq data of a large prospective cohort **[289]**. (***p* <0.01, *****p* <0.0001) **(f)** Integrated epigenetic, transcriptomic and genomic analysis of the *Rgs1* locus, visualized in UCSC Gene browser. Open chromatin regions (DNase I Hypersensitive Sites) in purified CD34$^+$ HSC (indicated as CD34$^+$) and HSC undergoing myeloid differentiation (indicated as CD34-) are indicated by light blue shades. Transcriptomic data (RNAseq) represent mapped reads present in purified CD14$^+$ *vs.* purified mobilized CD34$^+$ cells, with embryonic stem cells (ESC) and lymph node RNAseq data plotted for comparison. Genomic data show conservation score across 100 different vertebrate species (blue: conserved, brown: not conserved), with leishmaniasis and tuberculosis model species (rhesus macaques, mouse, hamster, dog, zebrafish) plotted individually (green panels below), as compared to the human reference genome. **(g)** Reanalysis of single-cell RNAseq data **[290]** using UMAP (Unifold Mapping) revealed presence within purified human CD34$^+$ cells of an *RGS1^{high}* phenotype in several progenitor subsets [Erythro-Myeloid Progenitors (EMP), Lymphoid/Myeloid Progenitors (LMPP7), HSC in a metabolically active state (HSC/Met. state)]. Arrows demonstrate clusters containing *RGS1^{high}* cells (orange vs. gray *RGS1^{low}* cells). Arrow sizes are proportional to the frequency of *RGS1^{high}* cells.

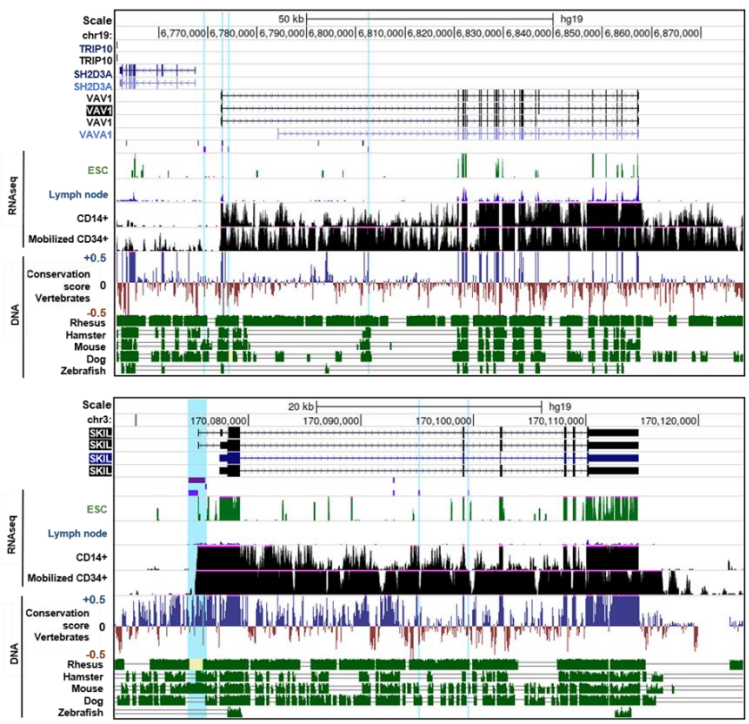

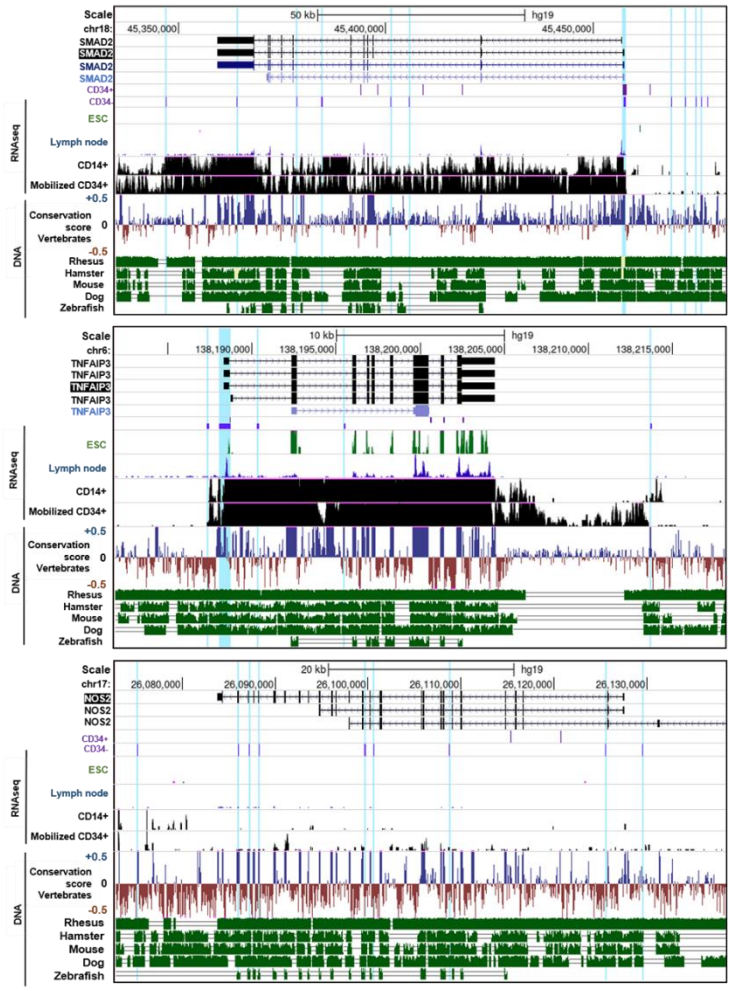

Figure 2.13. *StemLeish* gene epigenomic/transcriptional regulation and genomic conservation. Integrated epigenetic, transcriptomic and genomic analysis of the *Vav1*, *Skil*, *Smad2*, *Tnfaip3* and *Nos2* loci, visualized in UCSC Gene browser. Open chromatin regions (DNase I Hypersensitive Sites) in purified CD34$^+$ HSC (indicated as CD34$^+$) and HSC undergoing myeloid differentiation (indicated as CD34$^-$) are indicated by light blue shades. Transcriptomic data (RNAseq) represent mapped reads present in purified CD14$^+$ *vs.* purified mobilized CD34$^+$ cells, with embryonic stem cells (ESC) and lymph node RNAseq data plotted for comparison. Genomic conservation score across 100 different vertebrate species (blue: conserved, brown: not conserved), with leishmaniasis and tuberculosis model species (rhesus macaques, mouse, hamster, dog, zebrafish) plotted individually (green panels below), as compared to the human reference genome.

II.5 Discussion

Many infectious diseases are complicated by post-treatment clinical reactivation, and protective tissues or cellular niches have recently gained increasing awareness. A well-known example is the liver that can be colonized by dormant or hypnozoite stages of *P. vivax*. These stages are less susceptible for antimalarial therapies and can reactivate **[11, 293]**. The adipose tissue has been described as a hiding place for *Trypanosoma* species, which may be less amenable for drug treatment due to a low tissue perfusion rate **[9, 294]**. In the present study, the importance of the BM as a relapse-prone niche during VL was unveiled. For both the adipose tissue **[295]** and the BM **[273]** low perfusion rates have been described. In addition, drug concentrations within an organ can diverge at a cellular level. Zhao *et al.* **[296]** have shown that HSC can differently respond to chemotherapy based on their position in the BM and distance to the blood vessel. The possibility of the BM as sanctuary site was already indicated in 2014 by a rare clinical case of VL after allogeneic BM transplantation from an asymptomatic Portuguese donor **[258]**. Our data using 90 different antileishmanial compounds whereby various degrees of efficacy were achieved in the BM is considerable. Whereas several compounds prove to be highly effective in this niche, others were only poorly active. For instance, at effective doses for the liver, the 8-aminoquinoline analogs Tafenoquine and Sitamaquine cannot effectively penetrate the BM, which is in line with the rather poor/variable efficacy in Phase II clinical trials **[297]**.

Parasite replication at systemic sites such as the BM is characteristic for the progressive disease course of VL. Chronic *L. donovani* infection studies in mice revealed that emergency hematopoiesis is induced, a stress response that activates HSC and results in hematological alterations **[224]**. Besides *Leishmania*, the BM was identified as an antibiotic-protective niche for *M. tuberculosis* where it was shown that *Mtb* can infect $CD271^+$ BM mesenchymal stem cells (MSC) *in vitro* and *in vivo* in the presence or absence of antibiotic pressure **[132]**. It was also demonstrated

that even after prolonged treatment, *Mtb* survived in $CD271^+$ MSC **[8]** as well as it replicates within HSC **[291]**. Apart from MSC and HSC, presence of *Mtb* in LT-HSC has been documented in both human and mouse latent TB infections **[134, 292]**. Moreover, $CD34^+$ LT-HSC were recently confirmed as the main *in vivo* reservoir of circulating mycobacteria in a large cohort of *M. tuberculosis* and *M. bovis* infected individuals **[298]**.

HSC are progenitor cells that continuously replenish all blood cell types and can be classified in two subsets according to their long-term or short-term self-renewal capacity. Long-term HSC ($Lin^-Sca1^+cKit^+CD48^-CD150^{+)}$ can regenerate over a longer period of time and will subsequently differentiate into short-term HSC ($Lin^-Sca1^+cKit^+CD48^-CD150^-$) and multipotent progenitors (MPP2: $Lin^-Sca1^+cKit^+CD48^+CD150^+$ and MPP3/4: $Lin^-Sca1^+cKit^+CD48^+CD150^-$). MPP lack self-renewal capacity but can further differentiate in lineage committed cells such as common lymphoid progenitors (CLP) or common myeloid progenitors (CMP). MPP2 mostly give rise to pre-megakaryocyte-erythroid progenitors (PreME) and pre-megakaryocyte progenitors (PreMeg), whereas MPP3/4 cells differentiate into CMP and granulocyte-monocyte progenitors (GMP) **[299-302]**. MSC ($CD90.2^+CD105^+CD271^+$) are distinct from HSC as they shape the BM stroma by differentiating in adipocytes, osteoblasts, osteoclasts, fibroblasts, endothelial cells and smooth muscle cells **[303]**. LT-HSC reside in the immune privileged niche of the BM **[304]** and have been characterized as relatively quiescent stem cells (in the G0 phase of cell cycle) with the capacity of self-renewal **[274, 305, 306]**. During chronic VL infection, most LT-HSC were found to have entered cell cycle (G0 to G1) correlating with functional exhaustion. More specifically, HSC were skewed to differentiate into non-classical myeloid progenitors with a regulatory suppressor cell-like phenotype that is more permissive to parasite infection **[223]**. Modification of the host's BM emergency response thus enables *Leishmania* to promote its own proliferation and allows continued infection. Lopes *et al.* **[122]** recently described the importance of the BM stroma and showed that *L. infantum* is capable of infecting

$CD45^+$ BM cells and $CD271^+CD45^-$ MSC *in vitro* and *in vivo*. In a study by Pinto *et al.* that did not include a progenitor enrichment **[224]**, no infected LT-HSC were detected after 28 days of infection with Td-Tomato transgenic *L. donovani*. In contrast, an *in vitro* study by Carvalho-Gontijo *et al.* **[121]** documented the presence of *L. infantum* in human $CD34^+$ stem cells. According to Cotterell *et al.* **[226]**, $CD34^+$ progenitor cells do not appear to be targets for *Leishmania* infection. An important difference between $CD34^+$ progenitors and LT-HSC in mice, is that LT-HSC are $CD34^-$, a phenotype already acknowledged for a few decades **[224, 307, 308]**. Despite the apparent controversy, our study further pinpointed the exact tropism of visceral *Leishmania* species in the various stem cell and progenitor subsets *in vitro* and *in vivo*, using specific enrichment steps. Parasite loads differed substantially in these cell types with single parasites in BM monocytes whereas macrophages and myeloblasts can harbor multiple **[223]**. In our study, mouse LT-HSC and human HSPC were found to accommodate excessive burdens of parasites. Our data also show that LT-HSC prominently harbor viable parasites after drug treatment *in vitro* and *in vivo*. It deserves emphasis that the detection of a fluorescent protein expressed by transgenic parasites revealed to be an unreliable indicator of viable parasite presence. The higher *in vitro* clearance from macrophages and the reduction of viable parasite to undetectable levels in Lin^+ cells following *in vivo* treatment suggest that LT-HSC more than stromal macrophages play a prominent role in the process of treatment failure. This does not exclude the possible involvement of other sanctuary cells, such as the MPP2 cells that also retain viable parasites. Spatial information about host cell tropism and fate of released amastigotes and infected cells will be helpful to shed more light on the dynamic processes that occur just after treatment. It has already been described that some intrinsic properties of stem cells may provide opportunities for the pathogen to evade immune responses and drug action, e.g. by avoiding the induction of cytotoxic T cell responses and by enhanced drug efflux **[122, 274]**. Although SSG efflux transport was more prominent in LT-HSC, cell-intrinsic differences of drug

responsiveness are not limited to drug efflux and likely relate to the vast differences in intracellular amastigote burdens. Based on a large *in vivo* drug evaluation effort (**Figure 2.2d**), drug discovery activities should preferably include this particular BM niche during early discovery phase. Drugs with favorable pharmacokinetic properties to target the BM would potentially be more effective in targeting the LT-HSC burdens to prevent persistence and post-treatment relapse.

Besides the implications for drug discovery, the fundamental biology of parasite interaction with these cells deserves further exploration. Transcriptomic profiling of infected LT-HSC and cross-species systems biology analysis of large publicly available datasets revealed a unique *Leishmania*-triggered gene signature in LT-HSC, *StemLeish*, containing several host genes not previously associated with either experimental or human leishmaniasis (*Rgs1*, *Twistnb*, *Ell2*, *Vav1*). The LT-HSC gene signature also phenocopies transcriptional blood profiles of human VL, including HIV-VL co-infection, which may be the result of HSC migration from the BM to the circulation **[227]**. Although further mechanistic work will be necessary, our data mining approach shows that *Rgs1* and *Twistnb* are *bona fide* HSC genes and suggest they might function as antagonists of myeloid (neutrophil and macrophage) differentiation (**Figure 2.10d**). However, only Rgs1 and Vav1, Ell2 and Smad2 transcription factors were shared with murine models and human cohorts of tuberculosis. Notably, although the novel *StemLeish* signature overlaps with DEG identified in *M. tuberculosis*-infected human $CD34^+$ cells, it is radically different from the previously identified *IFN/IL6/CEBP* gene module in three ways. First, the combined pro-inflammatory TNF/NFkB and anti-inflammatory TGF-β/SMAD/SKIL signaling pathways are uniquely enriched in *StemLeish* and driven by specific transcription factors (**Figure 2.10b**). Second, the *StemLeish* transcriptional and epigenetic signature is strongly conserved among mammals, including rodents (**Figure 2.12f**), whereas the previously identified *IFN/IL6/CEBP* gene module is evolutionary recent and probably primate-specific **[292]**. Third, the *StemLeish* transcriptional program does not drive

myeloid/monocytic differentiation (**Figure 2.10c-d**), in contrast to the *IFN/IL6/CEBP* gene module **[292]**.

Another evolutionary conserved host response is the production of reactive oxygen and nitrogen species, a prominent and thoroughly regulated antileishmanial response of macrophages aimed at killing the parasite without damaging the host cell. These oxidative mechanisms are in part stimulated by phagocytosis and involve various signaling and effector molecules. NO is one of the major reactive species in macrophages produced by inducible nitric oxide synthase (iNOS, encoded by the *Nos2* gene) **[17]** which mediates intracellular killing of *Leishmania* **[309]**. The effects of ROS are variable amongst *Leishmania* species: some are susceptible to their action (*L. donovani* **[310]**, *L. major* **[311]**), while others appear resistant (*L. guyanensis* **[312]**, *L. amazonensis* **[313]**). Interestingly, our experiments demonstrate substantially decreased levels of *Nos2* gene expression and of both NO and ROS in infected LT-HSC, creating a more hospitable environment for parasite survival and multiplication. These results were paralleled by a functional $Rgs1^{high}Tnfaip3^{high}Nos2^{low}$ *in vivo* transcriptional profile in *Mtb*-infected IM2 interstitial alveolar macrophages, further highlighting the similarities between both murine models. Balanced ROS levels are known to be pivotal for naïve LT-HSC to maintain stem cell function and hematopoietic homeostasis. Stem cells in the BM also reside in a relatively hypoxic environment where low ROS and NO levels sustain a quiescent state and support self-renewal capacity **[314]**. In the event of ROS induction, stem cell differentiation is triggered and can lead to HSC exhaustion **[315]**. Similarly, NO stimulation induces the expansion of HSC and commitment to the myeloid progeny **[316]**.

In summary, our *in vivo* and *ex vivo* data demonstrate that LT-HSC in the BM represent an oxidative stress- and drug-resistant protective niche in VL. A unique LT-HSC *StemLeish* transcriptional profile was triggered by viscerotropic *Leishmania* infection, which recapitulated the *in vivo* blood profiles of human VL as well as

tuberculosis and includes potential therapeutic targets. Our results bring fundamental insights into host-pathogen interactions, but also highlight that drug discovery efforts will need to be tweaked to be effective against intracellular pathogens residing in this highly permissive host cell.

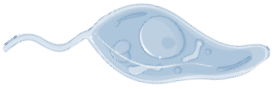

Exploration of the therapeutic and diagnostic potential of the *StemLeish* transcriptional signature in visceral leishmaniasis

CHAPTER III

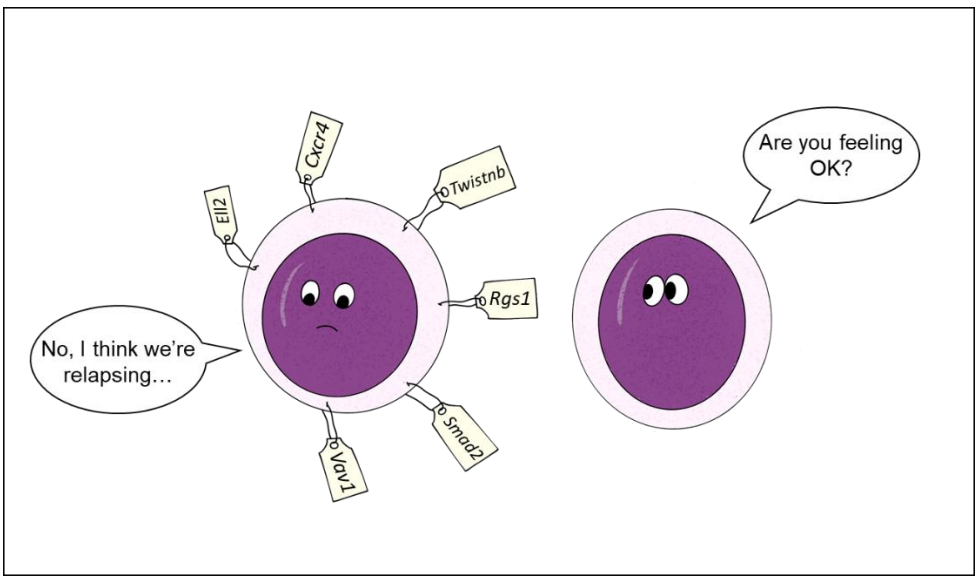

Acknowledgements:

Yasmine Nicolaes[1], my master thesis student working on this project. My gratitude for the assistance with interconnectivity qPCRs and LT-HSC sorts.
Benoit Stijlemans[2], for providing anti-CXCR4 nanobodies.

[1]Laboratory of Microbiology, Parasitology and Hygiene (LMPH), Infla-Med Centre of Excellence, University of Antwerp, Antwerp, Belgium.
[2]Laboratory of Cellular and Molecular Immunology (CMIM), Vrije Universiteit Brussel (VUB), Brussels, Belgium

III. Exploration of the therapeutic and diagnostic potential of the *StemLeish* transcriptional signature in visceral leishmaniasis.

III.1 Abstract

Effective therapeutics to cure VL are scarce, and asymptomatic disease and post-treatment relapse occur frequently and remain unpredictable. Both strongly advocate for the need of disease and relapse preventing therapeutics and prognostic tools. Recently, infected BM LT-HSC were described to express the *StemLeish* gene signature and to provide a sanctuary niche for high burdens of quiescent VL parasites. Here, knockdown of major differential *StemLeish* genes *Rgs1, Cxcr4, Ell2, Vav1* and *Twistnb,* confirmed their importance in regulating LT-HSC infection, yet not affecting the occurrence of quiescence under the used experimental conditions. Silencing *Cxcr4* partially restored the downregulated *Nos2* in infected LT-HSC, suggesting a central role of this gene in shaping the LT-HSC niche. A decreased infection burden was also demonstrated by *in vitro* pharmacological CXCR4 inhibition using plerixafor, 4-IPP and an anti-CXCR4 nanobody. *In vivo* therapeutic exploration showed that inhibition of CXCR4 may have both beneficial or detrimental effects depending on the used antagonist, emphasizing a pivotal balancing role in infection and pathology during VL. Transcriptional studies in mouse infection and relapse models provide a first indication of *Cxcr4* as a biomarker for infection in blood and BM. The annotation in this study of the *StemLeish* genes as highly influential during VL offers a basis for future development of potential biomarkers and exploration of relapse preventing therapeutics.

III.2 Background information

In the vertebrate host, *L. donovani* and *L. infantum* can propagate as amastigotes in monocyte-derived cells of the liver, spleen and BM, and eventually cause life-threatening complications **[207, 317, 318]**. Successful curative treatment of VL is scarce and the number of treatment failures for most antileishmanial drugs is increasing **[5, 6, 87, 96, 196, 319]**. Additionally, many VL patients are known to remain asymptomatic **[320, 321]** with unpredictable disease emergence. Currently there are no preventive therapeutics nor prognostic tools to predict symptomatic disease or relapse.

To understand the basis of therapeutic failure, former studies investigated parasitic niches as possible origins of disease recrudescence **[122, 322] (Chapter II)**. In the BM, LT-HSC were found to become heavily infected with *L. infantum* and *L. donovani*, also confirmed in human hematopoietic stem and progenitor cells (hHSPC). *In vivo*, these infected stem cells harbor relatively more viable parasites after relapse in comparison to other cells in the BM **[322] (Chapter II)**. In *ex vivo* settings, infected LT-HSC were confirmed to better tolerate antileishmanial drugs and to respond with decreased nitrogen oxide (NO) and reactive oxygen species (ROS) levels. Parasites in this cellular niche were also found to rapidly develop features of quiescence, a metabolic state known to increase tolerance to drug exposure (**Chapter IV**). Transcriptomic profiling of infected LT-HSC and cross-species systems biology analysis of large publicly available datasets revealed a unique *Leishmania*-triggered gene signature in LT-HSC, containing several novel host genes not previously associated with either experimental or human leishmaniasis: *Rgs1*, *Cxcr4*, *Smad2*, *Ell2*, *Vav1, Twistnb* **[322] (Chapter II)**. Underscoring the important physiological role of some of these genes, *Rgs1* and *Cxcr4* attenuate LT-HSC migration from the BM **[323-327].** *Cxcr4*, which encodes a well-known G-protein-coupled receptor (GPCR) for the endogenous chemokine CXCL12 **[328, 329]**, participates in the protection of HSC from oxidative stress and regulates HSC

retention in the BM and subsequent migration **[330]**. The novel LT-HSC gene signature also phenocopies transcriptional blood profiles of human VL **[227]**, including HIV-VL co-infection associated with frequent treatment failure **[322] (Chapter II)**.

Following identification and molecular characterization of LT-HSC as cellular niche for persistence of *Leishmania spp.*, further scrutiny of the upregulated *StemLeish* genes in this study sheds new light on the host-parasite interaction. Indeed, specific gene silencing of *Rgs1, Cxcr4, Ell2, Vav1* and *Twistnb* but not *Smad2* confirmed the importance of the *StemLeish* signature in the establishment of the extreme parasite load in LT-HSC but not in the occurrence of quiescence. A decreased infection burden was also demonstrated by pharmacological inhibition of CXCR4 by the FDA-approved plerixafor and anti-CXCR4 nanobodies (Nbs). Administration of plerixafor to *L. infantum* infected BALB/c mice notably decreased the liver and spleen peak, and combination treatment with paromomycin delayed the occurrence of relapse but could not overcome it. Ultimately, these results provide insights regarding new potential drug targets and biomarkers in the battle against VL disease and relapse.

III.3 Materials and methods

Ethical statement

The use of laboratory rodents was carried out in strict accordance with all mandatory guidelines (EU directives, including the Revised Directive 2010/63/EU on the Protection of Animals used for Scientific Purposes that came into force on 01/01/2013, and the declaration of Helsinki in its latest version) and was approved by the Ethical Committee of the University of Antwerp, Belgium (UA-ECD 2019–04).

Leishmania parasites

The *L. infantum* strain MHOM/FR/96/LEM3323 was kindly provided by CNRL (Montpellier, France) and modified to express bioluminescent (PpyRE9) and fluorescent (DsRed) reporter genes integrated into the 18S rDNA locus (LEM3323 WT$^{PpyRE9/DsRed}$) **[262]**. Promastigotes were sub-cultured twice weekly at 25°C in hemoflagellate-modified minimal essential medium (HOMEM, Gibco), supplemented with 10 % inactivated fetal calf serum (iFCS), 200 mM L-glutamine, 16.5 mM $NaHCO_3$, 40 mg/L adenine, 3 mg/L folic acid, 2 mg/L D-biotin and 2.5 mg/L hemin. The number of passages was kept as low as possible to maintain parasite virulence.

Laboratory animals

Female BALB/c mice (6-8 weeks old) were purchased from Janvier (Genest-Saint-Isle, France) and accommodated in individually ventilated cages in pathogen-free conditions. They were provided with food for laboratory rodents (Carfil, Arendonk, Belgium) and water *ad libitum*. Animals were subdivided in experimental groups based on simple randomization. Mice were kept in quarantine for at least 5 days before starting the experiment. Euthanasia was performed in CO_2 chambers followed by cervical dislocation, and tissues were collected under aseptic conditions.

Primary mouse cells

Mouse BM was collected from BALB/c mice using two distinct techniques; crushing **[263]** for sorting of LT-HSC, and centrifugation **[264]** to obtain BM-derived macrophages, both are described in **Chapter II**. After collection, cell suspensions were subjected to ammonium-chloride-potassium (ACK) buffer (0.15 M NH_4Cl, 1.0 mM $KHCO_3$, 0.1 mM Na_2EDTA) for erythrocyte lysis. Single cell suspensions were obtained by filtering through MACS® SmartStrainers (100 µm, Miltenyi Biotec), centrifuged at 500×*g* for 10 min (4°C) and resuspended in phosphate-buffered saline (PBS) + 0.2% bovine serum albumin (BSA) for LT-HSC

isolation or Roswell Park Memorial Institute (RPMI) medium (Gibco) for macrophage differentiation. The former was subjected to the Direct Lineage Cell Depletion Kit (Miltenyi Biotec) according to manufacturer's instructions, counted in PBS using a KOVA® counting chamber and resuspended in PBS + 0.2% BSA buffer to 2×10^7 cells/mL. The latter was divided over Petri dishes (Starstedt) supplemented with BM medium [RPMI 1640 medium with 10% (v/v) iFCS, 1% non-essential amino acids (NEAA), 1% sodium pyruvate, 1% L-glutamine, 50 U/mL penicillin, 50 µg/mL streptomycin (all from Gibco) and 15% L929 supernatant with M-CSF]. Following a 6-day incubation at 37°C with 5% CO_2, macrophages were collected by replacing the BM medium with ice cold dissociation buffer [PBS with 1% 0.5 M ethylenediaminetetraacetic acid (EDTA) and 2% 1 M 4-(2-hydroxyethyl)-1-piperazine-ethanesulfonic acid (HEPES)]. After detachment, the macrophage cell suspension was centrifuged at 500×*g* for 10 min and resuspended in RPMI medium. The number of macrophages was counted in PBS using a KOVA® counting chamber. Cells were seeded in a 96-well plate (3×10^4 cells/well) and incubated for 24 h at 37°C with 5% CO_2 to allow adherence of the BMDMs. Cells were kept on ice during procedures.

In vitro and *in vivo* visceral *Leishmania* infections

Parasite density was assessed by counting parasites in PBS using a KOVA® counting chamber. For *in vitro* infections, cell monolayers were co-cultured with stationary-phase promastigotes of *L. infantum* at a multiplicity of infection (MOI) of 5 for a minimum of 24h at 37°C with 5% CO_2. For *in vivo* mouse infection, stationary-phase parasites were centrifuged for 10 min at 4,000×*g* (25°C) and resuspended to 1×10^9 parasites/mL in sterile RPMI medium. Mice were infected intravenously (i.v.) in the lateral tail vein with 1×10^8 parasites in 100 µL of RPMI medium. Animals were monitored using *in vivo* BLI at selected time points. Imaging was performed 3 min after intraperitoneal (i.p.) injection of 150 mg/kg D-Luciferin (Beetle Luciferin Potassium Salt, Promega) in the IVIS® Spectrum In Vivo Imaging

System under 2.5% isoflurane inhalation anesthesia using 15 min exposure. Images were analyzed using LivingImage v4.3.1 software by drawing regions of interests (ROIs) around specific organs to quantify the luminescent signal as relative luminescence units (RLU).

To purify amastigotes from infected cells, suspensions were centrifuged at 400×*g* for 10 min and in PBS + 0.2% BSA. Host cell membranes were disrupted by 3 passages through a 25G needle. Amastigotes were collected in the supernatant after centrifugation at 250×*g* for 10 min and subsequently pelleted at 3,000×*g* for 10 min and resuspended in 100 µL PBS+0.2% BSA for analysis by flow cytometry.

In vitro and *in vivo* pharmacological inhibition studies

Isolated cells were treated with the small molecule CXCR4 antagonist AMD3100 (plerixafor, Mozobil® from Abcam), 4-iodo-6-phenylpyrimidine (4-IPP, EMD Millipore Corp) or anti-CXCR4 Nbs to obtain final concentrations of respectively 5 µg/mL dissolved in MilliQ® or 7.05 µg/mL (25 µM), 14.11 µg/mL (50 µM) dissolved in dimethylsulfoxide (DMSO) and 100 µg/mL dissolved in PBS. Anti-mouse CXCR4 Nb VUN415 was obtained from Prof. Martine J Smit (Vrije Universiteit Amsterdam). Drugs or Nbs were administered 24 hours after infection for 72 hours after which cells were processed for microscopy as described below. For Nb blocking, sorted LT-HSC were treated for 12 hours with 100 µg/mL anti-CXCR4 Nbs before infection lasting 72 hours.

For treatment of mice, plerixafor was dissolved in MilliQ® at 1 mg/mL. For pre-treatment, 10 mg/kg plerixafor was administered i.p. 2 hours before infection to allow peak distribution **[331]**. For single treatment, mice at 1-3 weeks post-infection (wpi) with confirmed parasite burdens by BLI, were treated i.p. at 10 mg/kg s.i.d. for 5 consecutive days. For combination treatment, paromomycin sulfate salt (PMM, Sigma-Aldrich) stock solution was dissolved in MilliQ® at 70 mg/mL. Again after confirmed infection by BLI, mice were treated for 5 consecutive days at 350 mg/kg s.i.d. PMM (i.p.) and 5 mg/kg s.i.d. plerixafor (s.c.). For 4-IPP

treatment, the drug was dissolved in DMSO at 1 mg/mL and administered i.p. for 3 days at 5 mg/kg s.i.d.

Flow cytometry and fluorescence-activated cell sorting (FACS)

Cell suspensions (2×10^7/mL) were treated with FcγR-blocking agent (anti-CD16/32, clone 2.4G2, BD Biosciences) for 15 min, followed by a 20 min incubation at 4°C with FITC-conjugated anti-CXCR4 antibody (Miltenyi Biotec) at 1:50 dilution. DAPI Staining Solution (Miltenyi Biotec) was used to assess viability. Cells were measured by flow cytometry using MACSQuant® Analyzer 10 (Miltenyi Biotec) and analyses were performed using FlowLogic™ Software (Miltenyi Biotec).

Sorting of mouse LT-HSC was performed and quality confirmed as described in **Chapter II [322]**. Briefly, cell suspensions were processed as above prior to cell sorting using a specific antibody mix (**Table 2.3, Chapter II**). Cells were sorted using FACSMelody™ (BD Bioscience) following specific gating strategy (**Figure 2.1, Chapter II**), confirmed with fluorescence minus one (FMO) controls and compensated using single stains. After cell sorting, LT-HSC were collected on slides by Cytospin™ followed by Giemsa staining after fixation with methanol.

RNA isolation

Total RNA was extracted from *L. infantum* infected mouse liver and spleen tissue using RNeasy Plus Mini kit, and BM, blood and infected LT-HSC using QIAamp® RNA Blood Mini kit (both from Qiagen), according to manufacturer's instruction. To exclude gDNA, an additional step using gDNA elimination columns (Monarch®) was performed. RNA samples were stored in aliquots at -80°C until qPCR analysis. RNA from samples stored in DNA/RNA shield™ (Zymo Research) at -80°C were extracted using the Maxwell® RSC simplyRNA blood kit (Promega) following manufacturer's instructions and using Maxwell® RSC instrument.

Real-time quantitative PCR

The primer sequences and RT-qPCR conditions for Spliced-Leader RNA (SL-RNA) were derived from **[82]**. The Step One Plus real-time PCR system (Applied Biosystems) was used for all real-time qPCR assays and melt curve analyses. RT-qPCR were performed in a 20 μL reaction mixture containing 10 μL of 2× SensiFAST SYBR Hi-ROX One-Step mix (Bioline), 1 μL of each primer (10 μM final concentration), 0.2 μL of reverse transcriptase, 0.4 μL of RNAse inhibitor, 4 μL of RNA template, and 3.4 μL of PCR water. Each assay was run in duplicate together with a blank control. Threshold cycles (Ct) were defined as the fractional cycle number at which the fluorescence passed the fixed threshold. Ct values were extracted by using the StepOne™ software v2.3. The mRNA expression of each gene was calculated relative to the expression of the housekeeping gene for mouse (Eef2 - *eukaryotic translation elongation factor 2*) (**Table 3.1**). After normalization, the relative expression levels were analyzed by using GraphPad software 7.0.

Table 3.1. Overview of the used primers. Melting temperature (Tm) as provided in Primer-BLAST.

Name	Sequence	Tm (°C)*
Eef2_F	TGTCAGTCATCGCCCATGTG	57.6
Eef2_R	CATCCTTGCGAGTGTCAGTGA	57.1
SL-RNA_F	AACTAACGCTATATAAGTAT	42.6
SL-RNA_R	CAATAAAGTACAGAAACTG	43.1
Rgs1_mouse_F	ATCCATTCACTTCAGTGGAGC	58.0
Rgs1_mouse_R	ATCTGCCCTGCAATACCACA	59.4
CXCR4_mouse_F	TCCAACAAGGAACCCTGCTTC	57.5
CXCR4_mouse_R	TTGCCGACTATGCCAGTCAAG	57.5
Smad2_mouse_F	AGGTTTCACACCGGAAAGGG	60.2
Smad2_mouse_R	CGCAGTTTTCGATTGCCTTGA	60.1
Vav1_mouse_F	TGTGCATCTCTGGTATGCGG	57.4
Vav1_mouse_R	GTCCCATCAGAACGGTTGGT	57.3
Ell2_mouse_F	CGAGACTGGCCAGGTTACAG	60.1

Ell2_mouse_R	GGAGATGAGGCAGCGTCTTT	60.1
Twistnb_mouse_F	CTATTCGTGCTTGGTGGCTG	59.3
Twistnb_mouse_R	GGACACCTAAAAGGCTCTCGG	60.4
Nos2_mouse_F	TCCTGGACATTACGACCCCT	57.7
Nos2_mouse_R	AGGCCTCCAATCTCTGCCTA	57.8

*Melting temperatures of primers.

DsiRNA mediated gene silencing

LT-HSC were sorted as described above at a density of 1×10^4 cells/well in 96-well plates. Cells were transfected with 10 nM 27-mer DsiRNA (Dicer-substrate siRNA) targeting *Rgs1, Cxcr4, Smad2, Ell2, Vav1* or *Twistnb* or with the included negative control DsiRNA (TriFECTa® RNAi kit, Integrated DNA Technologies) in Opti-MEM® Reduced Serum medium (Thermo Fischer). Lipofectamine® RNAiMAX Reagent (Life Technologies) was used as transfecting reagent. After 24 h, cells were infected with *L. infantum* (MOI of 5), as described above, and incubated for 72 h at 37°C with 5% CO_2. Cells were then processed for RT-qPCR to determine the specific transcript levels (used primers: **Table 3.1**), or for Giemsa staining to microscopically evaluate intracellular amastigote burdens.

Statistical analysis

Statistical analyses were performed using GraphPad® Prism version 9.0.1. Tests were considered statistically significant if p <0.05. Gene silencing and Giemsa staining results were tested using Mann-Whitney test. BLI data was tested using 2-way ANOVA. 4-IPP and plerixafor treatment experiments *in vitro* were statistically tested using one-way ANOVA with Tukey's multiple comparisons test. MFI after gene silencing, protein inhibition or nanobody inhibition was statistically compared using ordinary one-way ANOVA.

III.4 Results

Silencing of *StemLeish* genes significantly reduces parasite burden in LT-HSC

The contribution of *StemLeish* genes to the establishment of high amastigote burdens in sorted LT-HSC was studied using successful silencing of *Rgs1, Cxcr4, Smad2, Ell2*, *Vav1* and *Twistnb* with 27-mer Dicer-substrate small interfering RNA (DsiRNA) (**Figure 3.1a,b**). Despite rather limited silencing levels based on RT-qPCR, *Rgs1, Cxcr4, Ell2, Vav1* and *Twistnb* silencing significantly reduced the intracellular parasite burden (p<0.0001, **Figure 3.1c,d**). These observations unequivocally demonstrate that upregulation of *Rgs1, Ell2, Vav1, Twistnb* and especially *Cxcr4* is highly influential in shaping LT-HSC as a privileged niche for VL parasites, highlighting the importance of these genes as potential therapeutic targets. Considering that most *StemLeish* genes are likely intertwined in interacting pathways (**Figure 3.2**), impeding one gene may alter the expression of others. To comprehensively map the impact of RNA interference, RT-qPCR analysis was used across the selected gene panel in infected LT-HSC treated with DsiRNA. An overall reduction of all *StemLeish* genes can be observed after *Ell2* silencing. Additionally, *Rgs1* and *Cxcr4* expression show a general downregulation after silencing of any *StemLeish* genes. Moreover, an increase of *Ell2* expression is observed after *Cxcr4* silencing (**Figure 3.1e, Figure 3.3**). As described in **Chapter II [322]**, NO/ROS levels are decreased in infected LT-HSC as is *Nos2* expression. Interestingly, silencing of *Cxcr4* and to a lesser extent *Vav1* and *Twistnb* partially restores *Nos2* expression in infected LT-HSC (**Figure 3.1f**).

Recently, quiescent parasites were discovered inside infected LT-HSC (**Chapter IV**). We set out to investigate whether *StemLeish* genes contribute to the induction of this dormant metabolic state. However, incubating primary LT-HSC sorted from mouse BM for 24 hours at 37°C either or not in the presence of DsiRNA significantly reduced the intracellular numbers of quiescent parasites. Under these

experimental conditions, no difference was observed in *in situ* parasite quiescence in non-silenced *vs* silenced infected LT-HSC (**Figure 3.1g**).

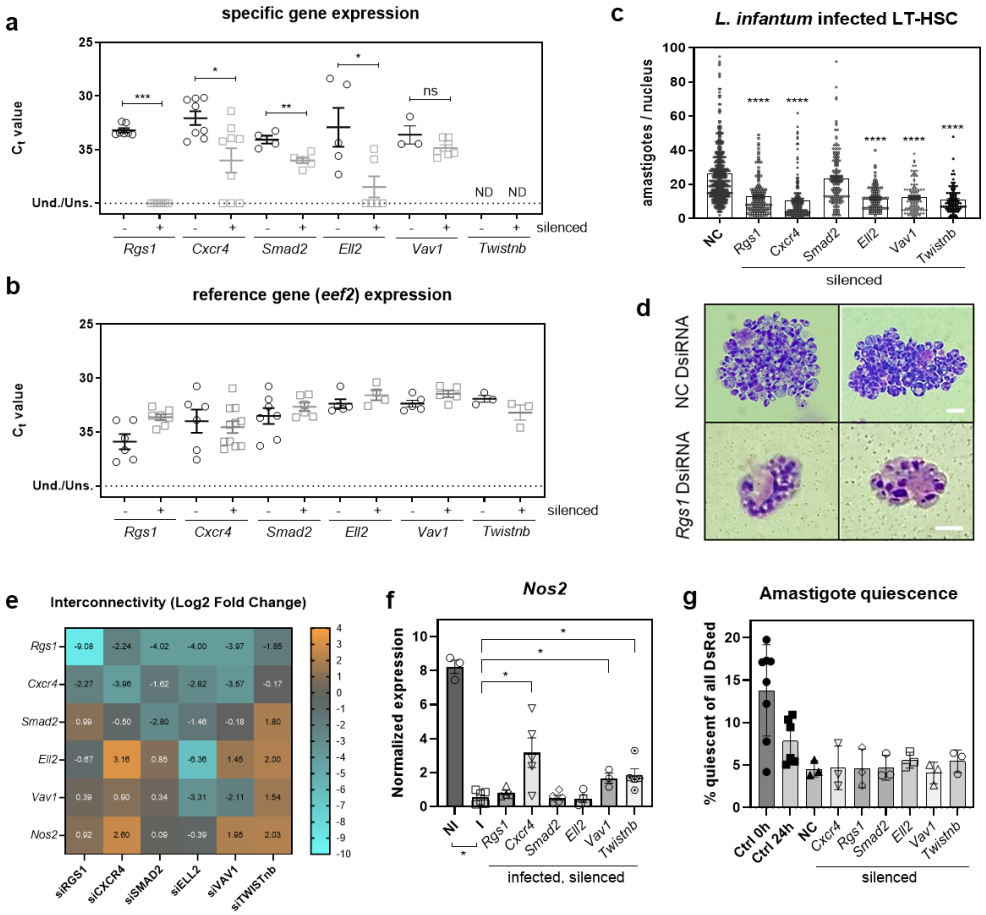

Figure 3.1. *StemLeish* silencing in LT-HSC results in a significantly decreased parasite burden. Sorted LT-HSC (10,000 / well) were transfected with 10 nM 27-mer DsiRNA (control or *StemLeish gene*-specific) using Lipofectamine® RNAiMAX reagent for 24 h, followed by infection with *L. infantum* LEM3323 WT$^{PpyRE9/DsRed}$ in a 5:1 ratio for 72 h. **(a)** RT-qPCR targeting the genes of interest *Rgs1, Cxcr4, Smad2, Ell2, Vav1* and *Twistnb* and **(b)** the reference gene *Eef2* to detect specific gene silencing in DsiRNA-treated, infected LT-HSC. Used primers are indicated in table 1. *Twistnb* levels could not be detected (ND) due to technical limitations. Mann-Whitney test, *p <0.05, **p <0.01. **(c)** Amastigotes per nucleus were counted microscopically after Giemsa staining. These results are based on three independent experiments. Mann-Whitney test, 150 ≤ n ≤ 200, ****p <0.0001. Negative control nonspecific DsiRNA (NC). **(d)** Giemsa staining of representative infected LT-HSC subjected to control or *Rgs1*-silencing as example of the microscopic assessment. Nonspecific control DsiRNA (NC). Scale bar = 10 µm. **(e)** Interconnectivity between silenced *StemLeish* genes shown as log2 fold change relative to the nonspecific DsiRNA control. Prefix 'si'

stands for silenced. **(f)** Effect of *StemLeish* gene silencing on recovery of *Nos2*. Non-infected LT-HSC (NI), infected LT-HSC (I). Mann-Whitney test, $*p < 0.05$. **(g)** Effect of *StemLeish* gene silencing on occurrence of quiescence as seen in Chapter III. Genes were silenced immediately post-sort, infected 24h later with *L. infantum* LEM3323 WT$^{PpyRE9/DsRed}$ and measured 48h post silencing (24h post-infection) using FACSMelody. Controls are amastigotes recovered from LT-HSC infected immediately (0h) and 24h post-sort. All results are based on at least three independent experiments and expressed as mean ± SEM.

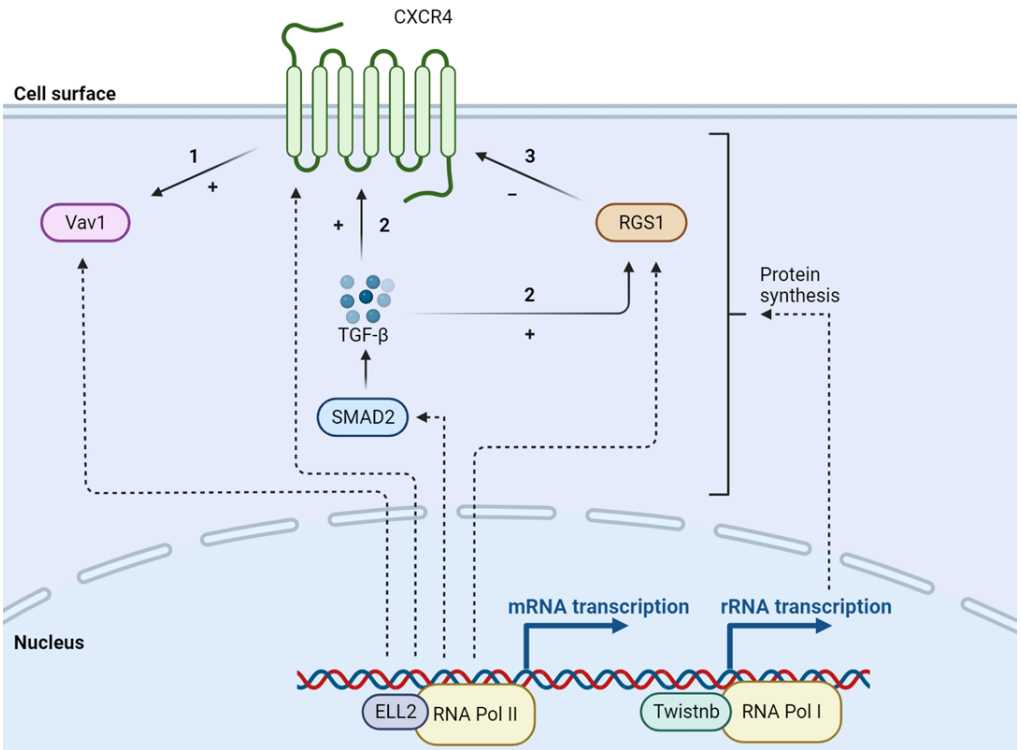

Figure 3.2. *StemLeish* gene product interactions. Overview of the different interactions between the proteins encoded by the GOI. **(1)** It has been described that CXCL12/CXCR4 signaling leads to the downstream activation of Vav1 **[332, 333]**. **(2)** SMAD2 plays an essential role in the TGF-β pathway and increased TGF-β signaling levels have been discovered to result in an upregulated expression of both *Cxcr4* and *Rgs1* **[323, 334, 335]**. **(3)** RGS1 is known to affect GPCR and has been discovered to inhibit CXCL12/CXCR4 signaling **[323, 325-327]**. Established protein association (full arrows), potential protein association (dotted arrows). Figure created with ©BioRender 2022 Online Software.

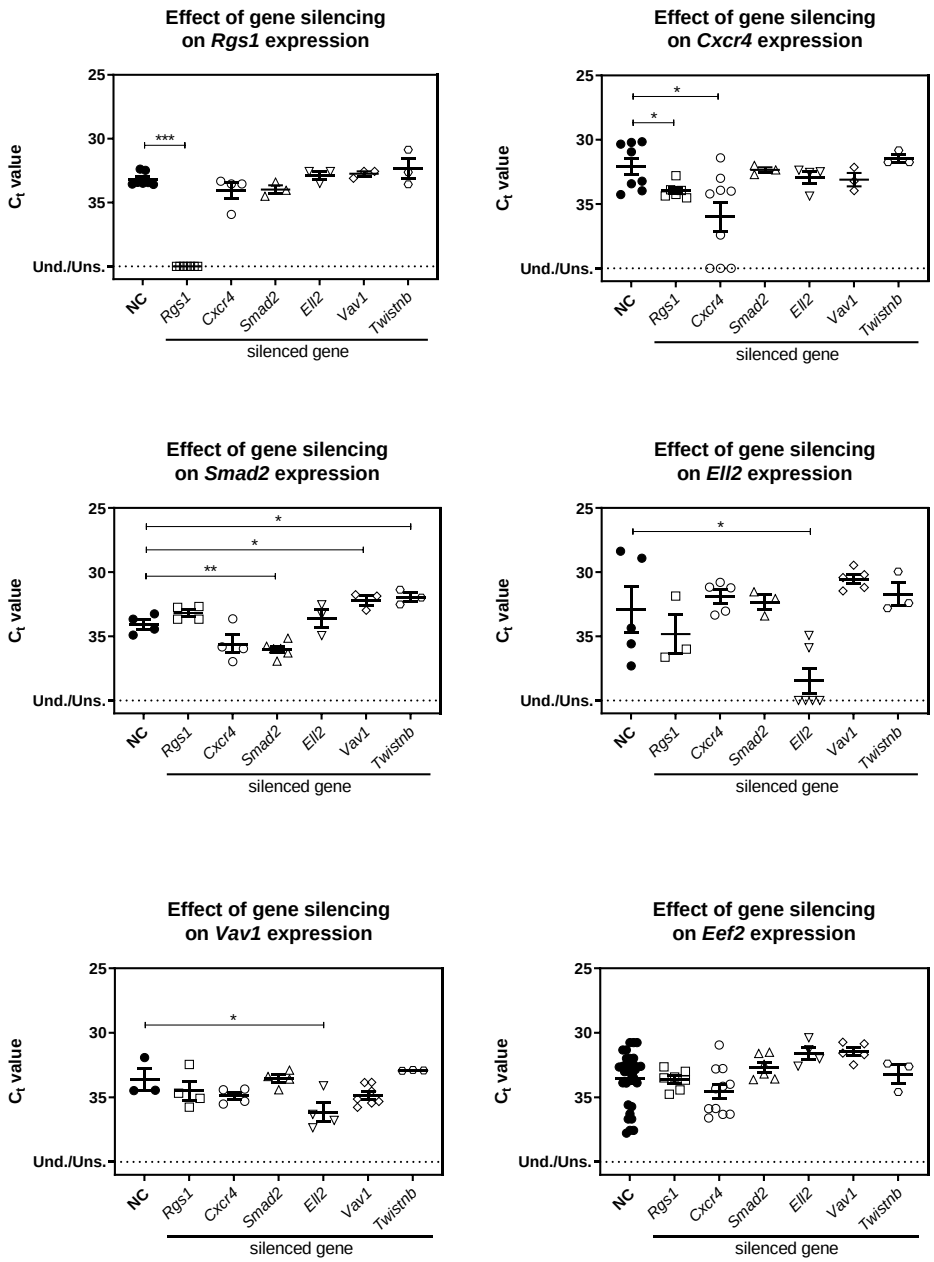

Figure 3.3. Effect of gene silencing on specific *StemLeish* gene interconnectivity after gene silencing. Infected LT-HSC sorted from mouse BM and subjected to gene silencing using siRNAs for *Rgs1* (a), *Cxcr4* (b), *Smad2* (c), *Ell2* (d) or *Vav1* (e) for 24h and infected with *L. infantum* LEM3323 $WT^{PpyRE9/DsRed}$ for 72h prior to RNA extraction. Shown is the C_t value compared to the non-silenced baseline using aspecific dsiRNA, *i.e.* negative control (NC). Mann-Whitney test one-tailed, * p <0.05, ** p <0.01, *** p <0.001.

Exploration of *StemLeish* gene *Cxcr4* as putative therapeutic target and biomarker of infection

Following identification of multiple relevant genes in the establishment of LT-HSC infection with viscerotropic *Leishmania spp.*, it was sought whether pharmacological inhibition could reduce the parasite susceptibility of LT-HSC. Since *Cxcr4* was identified as the most influential gene, coincidently encoding a surface receptor, its potential as therapeutic target and biomarker was evaluated. First, DsiRNA-mediated silencing of this gene was confirmed at protein level (**Figure 3.6a**). Second, plerixafor and 4-IPP were tested, two pharmacological CXCR4 inhibitors that antagonize the CXCR4/CXCL12 and CXCR4/macrophage inhibitory factor (MIF) interaction, respectively. 4-IPP additionally blocks binding of the parasitic MIF homologue **[336]**. Third, the use of mouse CXCR4-specific Nb VUN450 **[337]** was explored. Reduction of CXCR4 surface exposure was confirmed after 72h of plerixafor treatment (**Figure 3.4a**), albeit less pronounced than the effect of gene silencing. LT-HSC treatment with 5 μg/mL plerixafor, after 24h of *ex vivo* infection significantly reduced parasite burdens compared to untreated controls (p <0.0001, **Figure 3.4b**). Inhibition of CXCR4 using 25 μM or 50 μM 4-IPP also resulted in a decreased parasite load (p <0.0001, **Figure 3.5a**). Effects of both inhibitors were more apparent in LT-HSC than in macrophages.

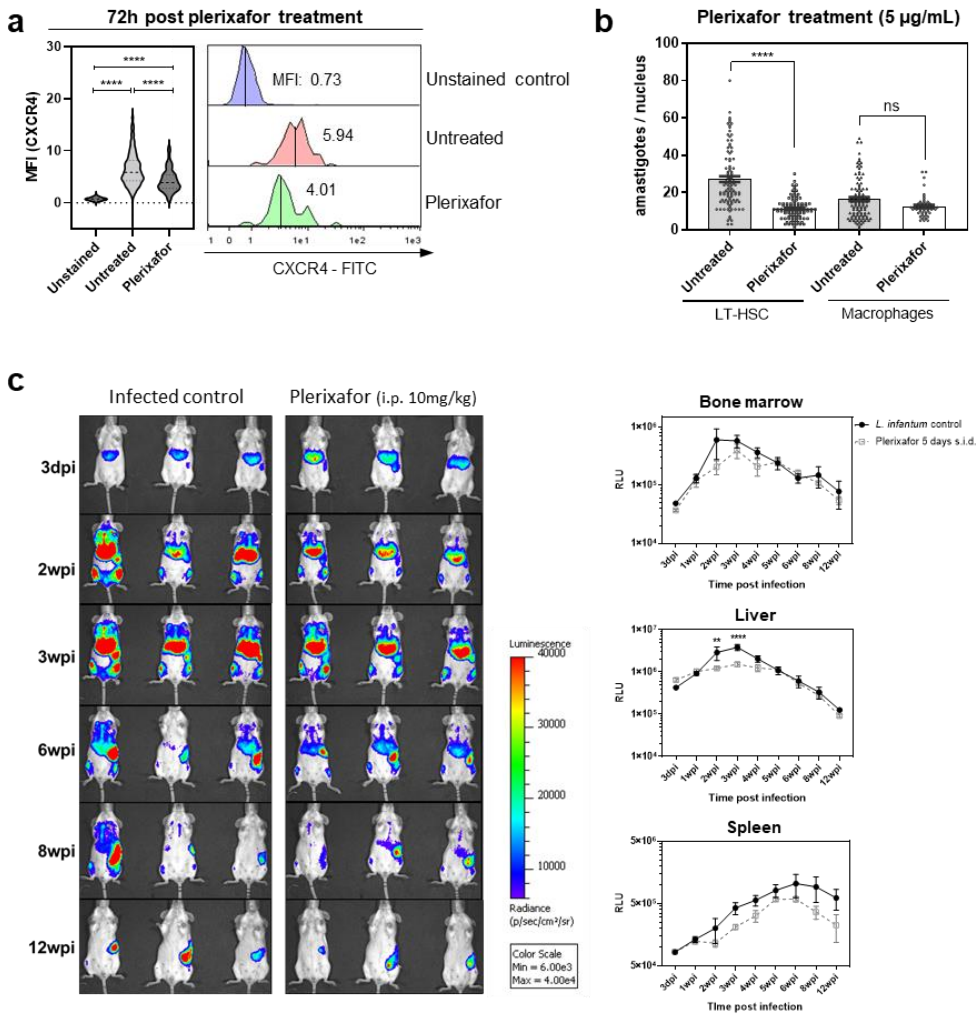

Figure 3.4. ***In vivo*** **application of CXCR4-antagonist plerixafor during VL. (a)** Effect of 72h plerixafor treatment (5 µg/mL) on CXCR4 protein level measured by flow cytometry. Ordinary one-way ANOVA, ****p <0.0001. **(b)** LT-HSC sorted from BALB/c mice (10,000/well) and infected with *L. infantum* LEM3323 WT$^{PpyRE9/DsRed}$ for 24h, exposed to 5 µg/mL plerixafor for 72h. The parasite load per nucleus was determined using Giemsa staining. Results are expressed as mean ± SEM. One-way ANOVA with Tukey's multiple comparisons test, ****p <0.0001. **(c)** Treatment of *L. infantum* infected BALB/c mice with 10 mg/kg s.i.d. (i.p.) plerixafor for 5 consecutive days starting from 3 days post-infection (dpi). Relative luminescence units (RLU) of parasite burden in BM, liver and spleen. Groups consist of 3 mice. 2-way ANOVA, *p <0.05.

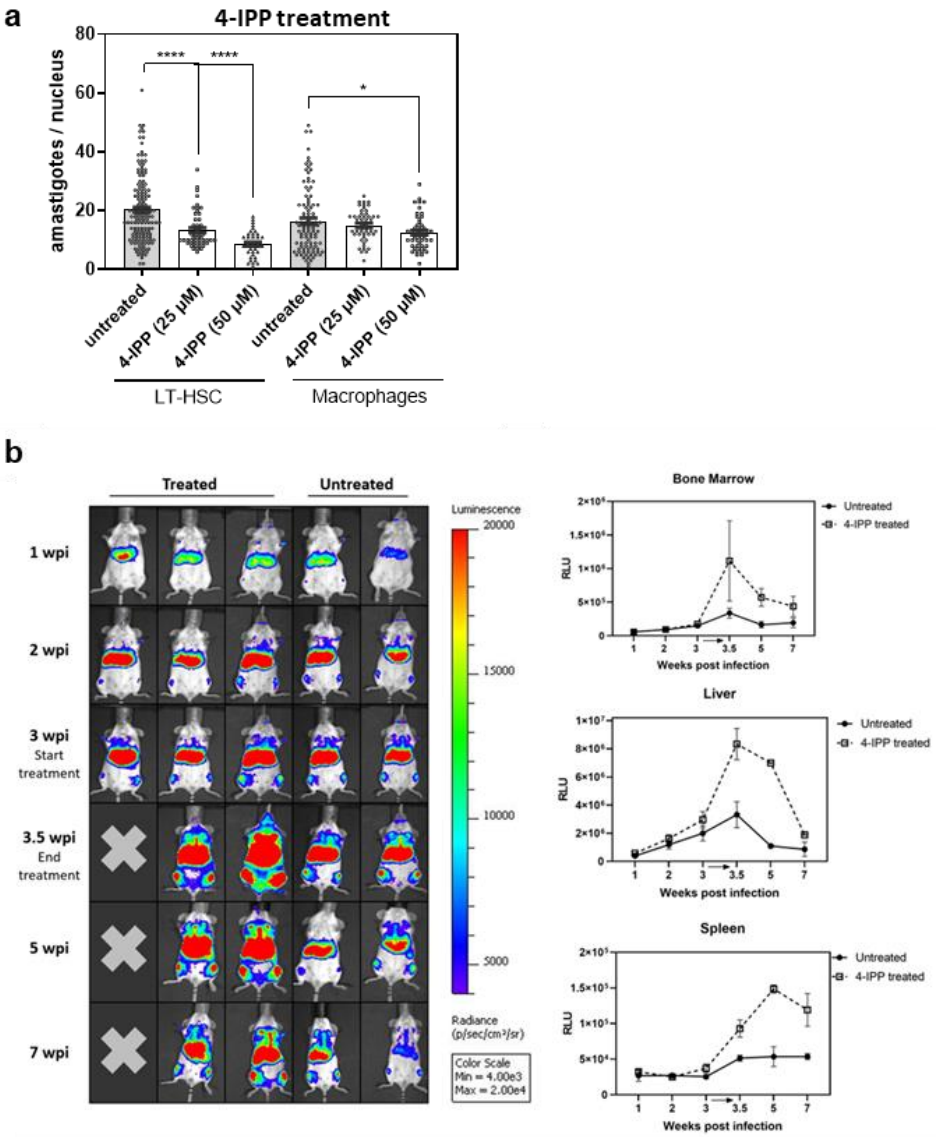

Figure 3.5. Treatment with CXCR4-antagonist 4-IPP is promising *in vitro*, but exacerbates disease *in vivo*. (a) Sorted LT-HSC from BALB/c mice (10,000/well) and infected with *L. infantum* LEM3323 WT$^{PpyRE9/DsRed}$ for 24h were exposed to 25 µM or 50 µM 4-IPP for 72h. The parasite load per nucleus was determined using Giemsa staining. Results are expressed as mean ± SEM. One-way ANOVA with Tukey's multiple comparisons test, **p* <0.05, *****p* <0.0001. **(b)** *In vivo* bioluminescence imaging (BLI) during a 15 min exposure period of *L. infantum* LEM3323 WT^{PpyRE9}-infected BALB/c mice at 1-7 weeks post-infection (wpi). At 3 wpi, daily treatment with 5 mg/kg 4-IPP i.p. was initialized for 3 consecutive days. Mean relative luminescence units (RLU) values of BM (top panel), liver (central panel) and spleen (bottom panel). Results are expressed as mean ± SEM.

In vitro use of anti-CXCR4 Nb VUN450 affected CXCR4 surface detection with antibodies (**Figure 3.6b**). Moreover, pharmacological intervention with the Nb as pre-infection blocking agent or as post infection treatment also reduced parasite loads as observed with plerixafor (**Figure 3.6c**). These observations show that pharmacological inhibition of CXCR4 with various reagents has a direct impact on the LT-HSC niche, warranting further *in vivo* evaluation.

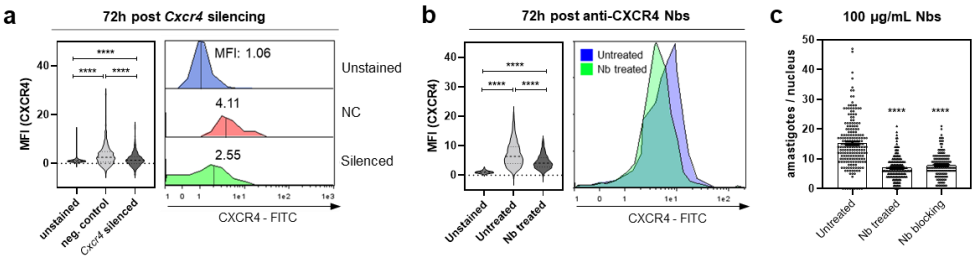

Figure 3.6. *StemLeish* genes with focus on Cxcr4 as potential therapeutic target. (a) Silencing on protein level measured with flow cytometry after 72h of DsiRNA administration of *L. infantum* infected LT-HSC. Ordinary one-way ANOVA, ****p <0.0001. **(b)** Effect of anti-CXCR4 Nb treatment on *L. infantum* infected LT-HSC was assessed 72h after treatment and measured with flow cytometry. Ordinary one-way ANOVA, 1613 < n < 4994, ****p <0.0001. **(c)** Sorted LT-HSC were infected with *L. infantum* for 24h and treated with 100 µg/mL anti-CXCR4 Nb VUN450 for 72h, or blocked with 100 µg/mL anti-CXCR4 Nb VUN450 for 12h before infection. Amastigotes per nucleus were counted microscopically after Giemsa staining. Mann-Whitney test, 100 < n < 200, ****p <0.0001. Results are based on three independent experiments.

Treatment with plerixafor (10 mg/kg s.i.d., i.p.) of infected mice for 5 days to block the CXCR4/CXCL12-axis tends to moderately reduce the parasite burdens in the liver (p = 0.0064) and to a lesser extend in BM and spleen (**Figure 3.4c**). Given the limited effect in monotherapy, plerixafor (5 mg/kg s.i.d., s.c.) was also evaluated in a combination treatment with PMM (350 mg/kg s.i.d., i.p.) for 5 days. This resulted in an initial increase of splenic parasite burdens that rapidly decreased after treatment termination. Considering the relapse kinetics in the BM and spleen, inclusion of plerixafor could not overcome relapse (**Figure 3.7a**). Pre-treatment of mice 2 hours before infection with a single i.p. injection of 10 mg/kg plerixafor also temporarily increases the spleen peak (**Figure 3.7b**), suggesting that treatment increased BM cell dissemination to the blood and spleen **[338]**. Unexpectedly,

simultaneous *in vivo* inhibition of the CXCR4/CXCL12- and CXCR4/MIF-axis using 4-IPP (5 mg/kg s.i.d., i.p.) for 3 days increased parasite burdens more than 3-fold and exacerbated disease symptoms, consequently leading to atypical animal behaviour (ephemeral episodes of piloerection, abdominal writhing, staggering, orbital tightening and gasping) and even death within the experimental group (**Figure 3.5b**). The large differences depending on the antagonist used, emphasize the pivotal role of *Cxcr4* in balancing infection and pathology during VL.

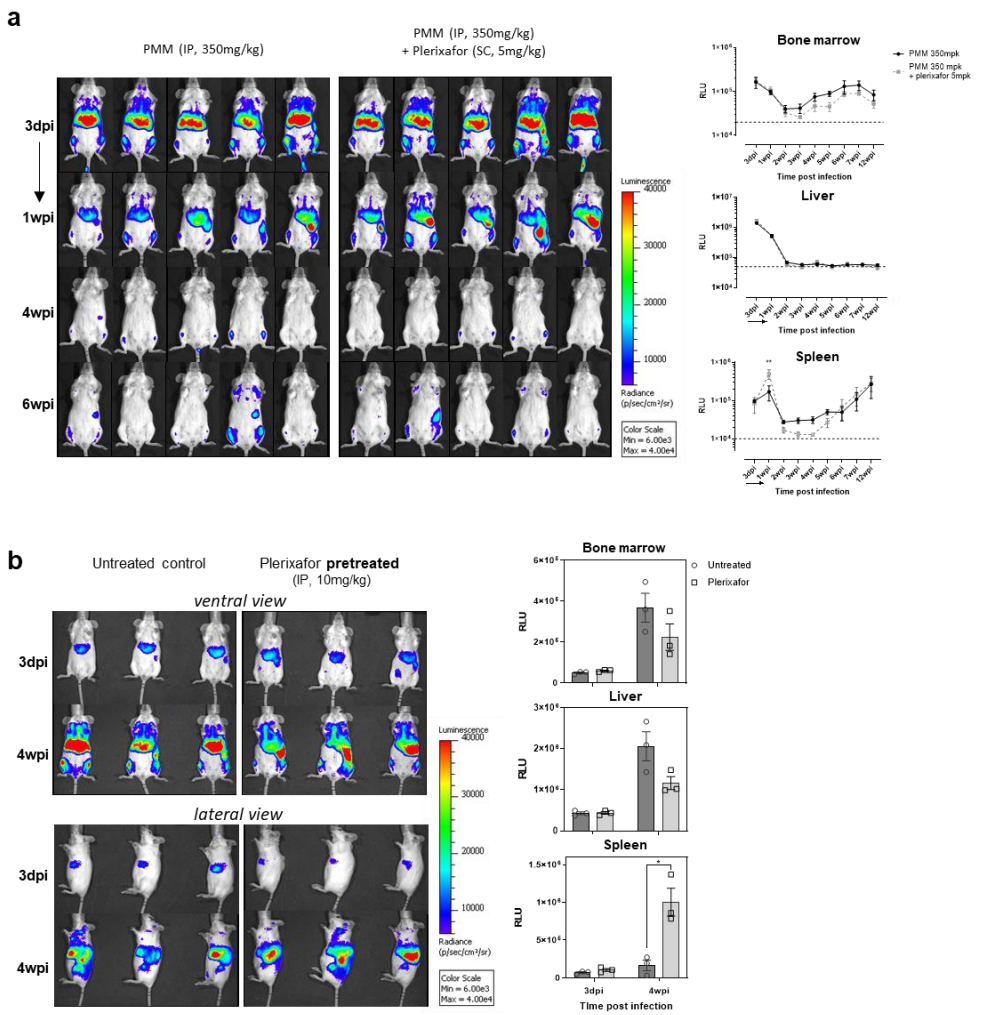

Figure 3.7. ***In vivo*** **application potential of plerixafor during VL. (a)** Combination treatment of 5 mg/kg plerixafor s.i.d. (s.c.) and 350 mg/kg paromomycin (PMM) s.i.d. (i.p.) for 5 consecutive days starting from 3 dpi and measured with BLI. Relative luminescence units (RLU) of parasite burden in BM, spleen and liver. Groups consist of 5 mice. $^{**}p < 0.01$. **(b)** Pretreatment of one i.p.

injection of 10 mg/kg plerixafor 2h before infection of BALB/c with *L. infantum* LEM3323 WT$^{PpyRE9/DsRed}$ and measured with BLI. Relative luminescence units (RLU) of parasite burden in BM, spleen and liver. Groups consist of 3 mice. *p <0.05.

The use of *Cxcr4* as a biomarker of VL infection and relapse was also evaluated by RT-qPCR in blood, spleen and BM tissue of naïve, infected and relapsed mice using the reproducible post-treatment relapse model as described in **Chapter II [322]**. In BM and blood, *Cxcr4* was found to be elevated in infected and relapsed mice with significance in the blood ($p = 0.0173$, **Figure 3.8a**). Moreover, *Cxcr4* expression in relapsed BM appeared positively correlated with infection burden as measured by SL-RNA ($R^2 = 0.9907$, **Figure 3.8b**). More infected tissue samples will be needed to further substantiate this correlation.

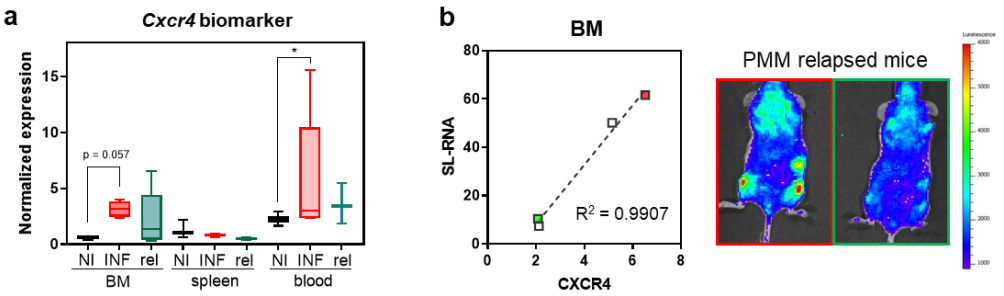

Figure 3.8. *StemLeish* genes with focus on *Cxcr4* as potential biomarker. (a) RT-qPCR of BM, spleen and blood samples from non-infected (NI), *L. infantum* infected (INF) and relapsed (rel) after paromomycin treatment BALB/c mice with *Cxcr4* primers. Mann-Whitney T test, *p <0.05. **(b, left)** Correlation of SL-RNA (*i.e.* infection burden) with *Cxcr4* expression in BM samples. **(b, right)** Bioluminescence images of PMM treated and relapsed mice. Red box refers to red data point in graph, likewise for green.

III.5 Discussion

VL is an opportunistic disease and many patients remain asymptomatic. Reported ratios of asymptomatic individuals and cases of active disease range from 2.6:1 in Sudan to 50:1 in Spain **[320, 321]**. Moreover, little is known about the triggers for active disease. The same occurs in treated patients who redevelop symptoms after apparent cure. Relapse rates of up to 7% for liposomal amphotericin B (LAmB) **[196]** and up to 20% for miltefosine **[6]** have been reported for VL in the last decade. Asymptomatic individuals and pre-relapse patients most likely harbor quiescent parasites in cellular niches awaiting (re)colonization, such as the LT-HSC niche in the BM **([322] Chapter II, Chapter IV)**. VL relapse patients have a high chance to relapse again; for example, a recent study in Sudan using LAmB revealed that 10% of VL relapse patients experienced a new relapse **[196]**. Therefore, new detection methods are needed not only to provide proper treatment and enable accurate post-treatment follow-up, but also to tackle the dissemination of infection. For this, highly specific biomarkers and new host-directed therapeutic targets may serve these purposes. With the continuous risk of emerging drug resistance and the limited resources for novel anti-leishmanial drug development, combining existing drugs with host immune modulators is holding promise for the future.

The role of the *StemLeish* gene signature was explored in the interaction of *Leishmania* with stem cells in the BM. Stem cells are less amenable to transfection and gene silencing since they are mostly quiescent with reduced metabolic and endocytic activity **[339].** This study opted to use Dicer-substrate siRNAs with greater proven potency at lower concentrations than the widely used canonical siRNAs **[340]**. The obtained RT-qPCR data provided evidence for a heterogenous level of silencing across the different genes under study. It is striking that even limited silencing of *Rgs1, Cxcr4, Ell2* and *Vav1* exerts a profound effect on intracellular parasite numbers. This underscores the prominence by which these genes govern parasitic infection in the LT-HSC niche. Recently, quiescent parasites were discovered inside infected LT-HSC (**Chapter IV**) with increased fitness for

infection and sand fly transmissibility. However, the factors triggering these parasites to become dormant are elusive. We next evaluated whether *StemLeish* host genes were responsible for entry into quiescence. Given that incubating primary LT-HSC from mouse BM in medium with supplemented DsiRNA markedly reduced the intracellular accumulation of quiescent parasites, no definite conclusions could be drawn.

The most influential gene during LT-HSC infection, CXC-motif chemokine receptor 4 (CXCR4), is a well-known chemokine receptor belonging to the GPCRs **[328, 329].** CXC-motive chemokine ligand 12 (CXCL12), also known as Stromal cell-derived factor-1 (SDF-1), serves as endogenous ligand and orchestrates several cellular processes such as migration, proliferation and survival **[329, 341-344]**. Additionally, Zhang *et al.* discovered that the CXCR4/CXCL12 axis participates in the protection of HSC from oxidative stress by keeping ROS levels low **[330]**. Not surprisingly, the observed increased *Cxcr4* expression on infected LT-HSC **[322]** (**Chapter II**) was demonstrated to be linked to the decreased *Nos2* levels, as *Cxcr4* silencing partially restored this oxidative/nitrosative burst. Chemokine receptor signaling is also modulated by Regulator G-protein signaling (RGS) proteins that are highly expressed in the BM and belong to the family of GTPase activating proteins **[326]**. RGS1 is expressed in HSC where it attenuates migration and subsequently participates in HSC maintenance and retention in the BM **[323]**. Overexpression of RGS proteins, including RGS1, inhibits CXCL12-directed migration through negative regulation of the CXCR4/CXCL12 axis and desensitization of CXCR4 **[323, 325-327]**. Combined upregulation of *Cxcr4* and *Rgs*1 in the BM during VL infection may help to retain infected LT-HSC with a low oxidative burst in the BM, contributing to parasite persistence.

CXCR4 is also responsive to MIF (Macrophage migration inhibitory factor), a pleiotropic cytokine that mediates arrest of immune effector migration from infected sites by receptor desensitization **[345]**. Alternatively, it binds to its cognate

receptor CD74 and promotes cell persistence by suppression of p53 and Bad/FoxoA3-induced apoptosis of immune effector cells **[346]**. In *Leishmania*-infected LT-HSC, *Mif* expression is significantly decreased **[322] (Chapter II)**. This suppression is likely to benefit the parasite as the pro-inflammatory role of MIF was shown to control cutaneous *Leishmania* infection **[347]**. In line with downregulated *Nos2*-levels in LT-HSC, MIF-deficient mice have an impaired ability to produce NO and ROS in response to IFN-γ. MIF has received particular interest during protozoal infections because parasites such as *Leishmania* even express one or more MIF orthologues **[348, 349].** These parasitic MIFs can also occupy the CD74 receptor and induce ERK1/2 phosphorylation in macrophages while blocking p53 phosphorylation and NO-induced apoptosis **[336]** and can promote dendritic cell-mediated T-cell exhaustion and prolonged parasite persistence **[350, 351]**.

SMAD proteins play a significant role in TGF-β signaling which is a crucial pathway in immune surveillance and response during infection **[352]**. Abundant TGF-β production and signaling has been associated with human VL progression as this cytokine has potent immunosuppressive effects in infectious diseases **[168, 353]**. Several findings imply that a rise in *Smad2* expression is associated with increased TGF-β signaling and may promote parasitic survival and growth in infected LT-HSC through upregulation of *Rgs1* and *Cxcr4* **[323, 334, 335]**. Surprisingly, silencing *Smad2* did not alter parasite burden in LT-HSC which may be because silencing is moderately less efficient than for most other *Stemleish* genes. Moreover, as the *Smad2* gene product belongs to a family of structurally related proteins, silencing of *Smad2* may have resulted in compensatory upregulation of another *Smad*-gene.

The Vav family forms a group of signal transduction proteins that function both as guanosine exchange factors and adaptor molecules. *Vav1* displays a more restricted gene expression compared to other *Vav* genes as it is primarily detected in hematopoietic cells **[354-357]**. Vav proteins participate in the regulation of various biological responses including cell morphology, motility and gene expression **[354]**.

Studies suggest that the downstream interaction of CXCR4 with Vav1 plays a considerable role in the migratory behavior of leukocytes **[332, 333]** indicating again that upregulation of both *Cxcr4* and *Vav1* during LT-HSC infection may lead to increased retention in the BM.

The *Stemleish* genes *Twistnb* and *Ell2* are involved in transcription. *Twistnb*, also referred to as *Polr1f* (RNA Polymerase I Subunit F), is a transcription factor gene that encodes for DNA-directed RNA polymerase I subunit RPA43. *Ell2* encodes for the RNA polymerase II (RNA Pol II) elongation factor ELL2 and regulates the catalytic rate of the RNA Pol II elongation complex **[358]**. Since RNA Pol II transcribes all protein-coding genes and numerous non-coding RNAs in eukaryotic genomes **[359]**, upregulation of *Ell2* in infected LT-HSC can be expected to cause an overall increased transcription. However, silencing *Ell2* did not particularly affect the expression of other *StemLeish* genes.

Considering the abundant effect of *Cxcr4* silencing on parasite burden and the recovery of *Nos2* levels, this gene product may conceptually be an excellent therapeutic target. Application of the small molecule CXCR4 inhibitor plerixafor during VL infection in mice already demonstrated a beneficial reduction of the liver peak and to a lesser extent the spleen and BM burden. In contrast to the *in vitro* data obtained for the inhibitor 4-IPP, *in vivo* treatment of infected BALB/c mice resulted in a rapid and excessive upsurge of infection also eliciting abnormal animal behavior and even death. Given that 4-IPP simultaneously inhibits the CXCR4/CXCL12- and CXCR4/MIF-axes, ablation of host or parasite MIF-mediated immune regulation may underlie the detrimental infection flare-up. Discerning effects of parasite or host MIF would require studies using deficient mouse and parasite models, as explored for cutaneous leishmaniasis **[347, 350]**. Irrespective of the implicated mechanism, we propose that this serendipitous observation for 4-IPP may benefit adaptation of clinical isolates, attenuated parasite lines or newly generated *Leishmania* strains for infection in rodent models.

Besides exploring their role during infection and therapeutic potential, *Stemleish* genes were also explored as biomarkers. For VL, most studied biomarkers are parasite-specific such as peroxiredoxins, cysteine proteinases or A2 proteins **[360]**. Host biomarkers have recently gained more interest to monitor response to treatment, pathogenicity and death. A recent study showed that soluble CD14 is a powerful marker of pathogenicity and death in patients with VL-HIV/AIDS **[361]**. MIF levels were also associated with death in co-infected patients. Two other studies describe IL-10 as an excellent biomarker for therapeutic effectiveness **[362, 363]**. Here, we show that *Cxcr4* is increased in the blood of VL mice and can be measured by RT-qPCR. To further substantiate this biomarker, follow-up studies will be performed in order to determine appropriate cutoffs and evaluate sensitivity and specificity to indicate diagnostic accuracy in mouse models and human samples.

Collectively, the presented findings provide unprecedented fundamental insights into the host-*Leishmania* interactions and a transcriptional program of broad clinical relevance, which we propose as a solid basis for new host-directed therapies in VL and as a repository for novel biomarkers of infection and relapse.

Long-term hematopoietic stem cells trigger quiescence in *Leishmania* amastigotes

CHAPTER IV

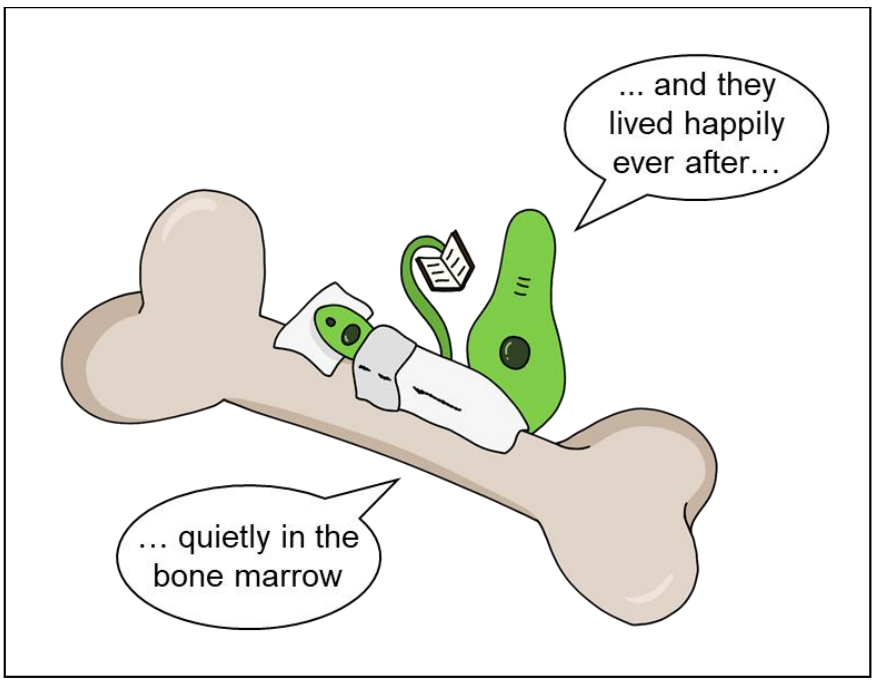

Acknowledgements:

Yasmine Nicolaes[1], for the assistance in LT-HSC sorts
Sarah Hendrickx[1], for the excellent help in sand fly studies
João Luís Reis Cunha[2] and Daniel Jeffares[2], for the analysis of the transcript data
Ben Caljon[3] and Hideo Imamura[3], for the performance of RNA seq and analysis
Yann G.-J. Sterckx[4], for the structural prediction analysis

[1] Laboratory of Microbiology, Parasitology and Hygiene (LMPH), Infla-Med Centre of Excellence, University of Antwerp, Antwerp, Belgium.
[2] Population Genomics, University of York, York, United Kingdom.
[3] Brussels Interuniversity Genomics High Throughput core (BRIGHTcore) platform, Vrije Universiteit Brussel (VUB), Universitair Ziekenhuis Brussel (UZ Brussel), Brussels, Belgium.
[4] Laboratory of Medical Biochemistry (LMB), Infla-Med Centre of Excellence, University of Antwerp, Antwerp, Belgium.

IV. Long-term hematopoietic stem cells trigger quiescence in *Leishmania* amastigotes.

IV.1 Abstract

LT-HSC were identified as a hospitable and relapse prone niche for visceral *Leishmania* parasites in the BM. Using reporter gene expression from an 18S rDNA locus as a read-out, this study unveiled that *L. infantum* and *L. donovani* amastigotes rapidly enter quiescence after an estimated 4-6 divisions in both mouse LT-HSC and human HSPC but not in macrophages. Acquisition of a quiescent phenotype endowed parasites inside LT-HSC with a higher capacity to survive antileishmanial treatment. Parasites that transitioned through such an in situ quiescent stage retained a lower reporter gene expression and displayed an increased cellular infectivity and high transmission capacity through the sand fly vector. Transcriptional profiling of the two metabolic states (quiescent and non-quiescent) in three biologically independent samples revealed a strongly reduced gene expression in quiescent parasites. Most notably, structural constituents of the ribosome and biological processes such as oxidation-reduction and various metabolic processes, including mitochondrial activity, are suppressed in quiescent parasites. A limited set of 26 upregulated genes, mostly without an annotated function, are of particular interest given their predicted involvement as regulators of cell cycle progression and of gene expression at various levels. The herein reported differential gene set constitutes a reliable source for the identification of novel markers and potential drivers of quiescence, a metabolic state bestowing parasites the capacity to escape treatment.

IV.2 Background information

Leishmania parasites alternate between two main morphological forms during their life cycle: a long flagellated extracellular promastigote within the sand fly and a non-

flagellated obligate intracellular amastigote in the vertebrate host that resides within the monocyte-derived cells of the liver, spleen and BM and eventually causes life-threatening complications **[207, 317, 318, 364]**.

The current antileishmanial drugs have many disadvantages and post-treatment relapse rates are increasing **[96]**. In many instances relapse does not relate to reinfection, drug quality, drug exposure or resistance **[98]**, but is rather due to persistence for which mechanistic information is lacking. Persistent infections can occur in a variety of host sanctuary tissues or cellular niches, such as hepatocytes (*P. vivax*), skeletal muscle and neurons (*T. gondii*), adipose tissue (*T. brucei* and *T. cruzi*) and the BM (*M. tuberculosis*) **[8-12]**. In **Chapter II**, LT-HSC in the BM were identified as a relapse niche for VL infection. LT-HSC become readily infected with extreme parasite burdens accompanied with low ROS and NO levels and with higher residual parasite burdens after antileishmanial treatment **[322] (Chapter II)**.

Besides persistence linked to cellular niches, treatment failure can also be associated with the adaptive behavior of parasites. In response to stress, certain microorganisms employ so-called quiescence to increase their chances of survival **[13]**. The quiescent state is characterized by a lowered metabolic activity and renders a microorganism tolerant to antibiotics at the expense of becoming non-proliferative **[365, 366]**. Hence quiescent cells are phenotypic variants of the wildtype and their dormancy can be reversed when stressors are alleviated. Given its discernible clinical implications, microbial quiescence has gained considerable interest and has been the subject of intense research for certain pathogens, especially bacteria **[365-369]**. In contrast, quiescence in *Leishmania* has only recently been discovered and its role in drug tolerance, infection relapse, and general parasite biology remains poorly understood. A recent study demonstrated that *Leishmania* quiescence can be induced by various triggers (e.g. antimonial drug pressure or stationary phase growth **[370]**). Furthermore, transcriptomic and metabolomic analyses of quiescent stages corroborated an overall downregulation of biosynthetic processes as a hallmark of quiescence **[370]**. Despite these important insights, the

molecular determinants orchestrating the phenotypic transition to the quiescent state in *Leishmania* remain thus far unknown.

The present study started with the observation that visceral *Leishmania* amastigotes inside LT-HSC rapidly enter a quiescent state. Although the induction is unrelated to drug pressure, we demonstrate that these quiescent parasites benefit from an enhanced survival of antileishmanial treatment. To better understand the molecular basis underlying amastigote quiescence, we performed an unbiased total RNAseq, which led to the identification of genes that are significantly overexpressed in the LT-HSC-induced quiescent state. Functional annotation of the proteins encoded by these upregulated genes through AlphaFold2 **[371, 372]** structure prediction provide clues on the players involved in attaining the quiescent phenotype in a natural infection model. In addition, we show that transitioning through a quiescent state has a profound impact on parasite infectivity and transmissibility. The results provide mechanistic information on the *in situ* acquisition of quiescence and its downstream effects on parasite biology (survival under drug pressure, infection, and transmissibility). Given its broad relevance across the microbial spectrum, several of the quiescence-associated genes warrant future exploration as positive markers of quiescence/relapse or as putative targets in the transition process.

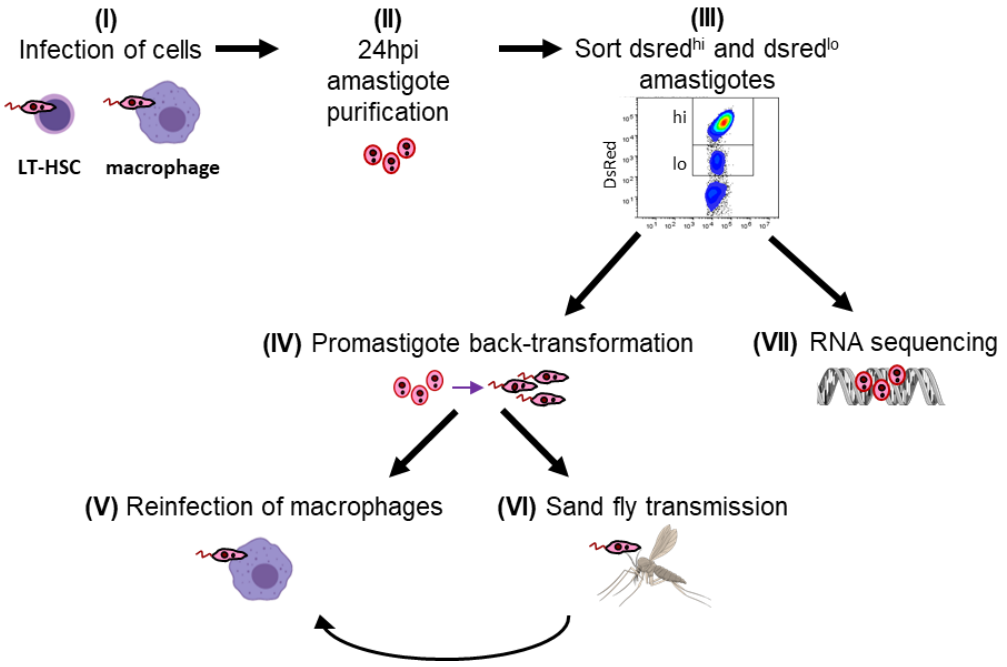

Figure 4.1. Workflow of experiments conducted in this chapter.

IV.3 Materials and methods

Ethical statement

The use of laboratory rodents was carried out in strict accordance with all mandatory guidelines (EU directives, including the Revised Directive 2010/63/EU on the Protection of Animals used for Scientific Purposes that came into force on 01/01/2013, and the declaration of Helsinki in its latest version) and was approved by the Ethical Committee of the University of Antwerp, Belgium (UA-ECD 2019–04). Human BM aspirate rest samples, obtained as a diagnostic sample without a written informed consent, were available for *in vitro* infection experiments following approval by the Committee of Medical Ethics UZA-UA (B3002021000027).

Leishmania parasites

The *L. infantum* strains MHOM/FR/96/LEM3323 and MHOM/ES/2016/LLM2346 were kindly provided respectively by CNRL (Montpellier, France) and by WHOCC (Madrid, Spain), the latter being a recent clinical isolate. The *L. donovani* strain MHOM/ET/67/L82 was isolated from an Ethiopian VL patient. All were modified to express bioluminescent (PpyRE9) and fluorescent (DsRed) reporter genes integrated into the 18S rDNA locus (LEM3323 $WT^{PpyRE9/DsRed}$, LLM2346 $WT^{PpyRE9/DsRed}$ and Ldl82 $WT^{PpyRE9/DsRed}$) **[262, 373]**. Promastigotes were sub-cultured twice weekly at 25°C in hemoflagellate-modified minimal essential medium (HOMEM, Gibco), supplemented with 10 % inactivated fetal calf serum (iFCS), 200 mM L-glutamine, 16.5 mM $NaHCO_3$, 40 mg/L adenine, 3 mg/L folic acid, 2 mg/L D-biotin and 2.5 mg/L hemin. The number of passages was kept as low as possible to maintain parasite virulence.

Laboratory animals and sand fly colony

Female BALB/c mice (6-8 weeks old) were purchased from Janvier (Genest-Saint-Isle, France) and accommodated in individually ventilated cages in SPF conditions. They were provided with food for laboratory rodents (Carfil, Arendonk, Belgium) and water *ad libitum*. Animals were subdivided in experimental groups based on simple randomization. Mice were kept in quarantine for at least 5 days before starting the experiment. Euthanasia was performed in CO_2 chambers followed by cervical dislocation, and tissues were collected under aseptic conditions.

A *Lutzomyia longipalpis* sand fly colony was initiated with the kind help of NIH-NIAID (Prof. Shaden Kamhawi and Prof. Jesus Valenzuela) and maintained at the University of Antwerp under standard conditions (26°C, >75% humidity, in the dark) with provision of a 30% glucose solution *ad libitum* **[374]**. For infection experiments, 3- to 5-day old females from generations 31 to 44 were used.

Primary mouse cells

Mouse BM was collected from BALB/c mice using two distinct techniques, based on pilot studies comparing alternative methods in terms of yield and quality. For both techniques, mice were sacrificed, and hind legs aseptically removed. Isolated femurs and tibias were cleaned by removing soft tissue from the bone using 70% ethanol-soaked cloth and tweezers.

For the crushing technique, the protocol was adapted from Lo Celso and Scadden **[263]**. Briefly, bones were crushed with mortar and pestle in ammonium-chloride-potassium (ACK) buffer (0.15 M NH_4Cl, 1.0 mM $KHCO_3$, 0.1 mM Na_2EDTA) for erythrocyte lysis. Single cell suspensions were obtained by filtering through MACS® SmartStrainers (100 µm, Miltenyi Biotec), centrifuged at 500×*g* for 10 min (4°C) and resuspended in phosphate-buffered saline (PBS) + 0.2% bovine serum albumin (BSA). For efficient depletion of mature lineage-positive hematopoietic cells and to specifically isolate the preferred lineage-negative cells (*i.e.,* undifferentiated progenitor cells), the Direct Lineage Cell Depletion Kit (Miltenyi Biotec) was employed according to manufacturer's instructions. Following lineage depletion, cells were counted in PBS using a KOVA® counting chamber and resuspended in PBS + 0.2% BSA buffer to 2×10^7 cells/mL. Cells were kept on ice during all procedures.

The centrifugation method, adjusted from the protocol described by Amend *et al.* **[264]** and Dobson *et al.* **[265]**, was used for subsequent macrophage and dendritic cell differentiation. Briefly, a 0.5 mL microcentrifuge tube was perforated at the bottom with a 21G needle and nested inside a 1.5 mL tube (both from Eppendorf). After collection of femurs and tibias, one proximal end (knee epiphysis) was cut-off and placed in the 0.5 mL tube. Nested tubes were centrifuged in a microcentrifuge at 10,000×*g* for 15 sec, resulting in a visible pellet in the 1.5 mL tube. This pellet was then resuspended in ACK buffer for erythrocyte lysis.

To obtain BM-derived macrophages (BMDM), cells were centrifuged at 500×*g* for 10 min at 4°C, resuspended in Roswell Park Memorial Institute (RPMI) medium (Gibco) and divided over Petri dishes (Starstedt) supplemented with BM medium [RPMI 1640 medium with 10% (v/v) iFCS, 1% non-essential amino acids (NEAA), 1% sodium pyruvate, 1% L-glutamine, 50 U/mL penicillin, 50 µg/mL streptomycin (all from Gibco) and 15% L929 supernatant with M-CSF]. Following a 6-day incubation at 37°C with 5% CO_2, the macrophages were collected by replacing the BM medium with ice cold dissociation buffer [PBS with 1% 0.5 M ethylenediaminetetraacetic acid (EDTA) and 2% 1 M 4-(2-hydroxyethyl)-1-piperazine-ethanesulfonic acid (HEPES)]. After detachment, the macrophage cell suspension was centrifuged at 500×*g* for 10 min and resuspended in RPMI medium. Cells were seeded in a 96-well plate (3×10^4 cells/well) or a 24-well plate (1×10^6 cells/well) and incubated for 24 h at 37°C with 5% CO_2 to allow adherence of the BMDMs.

Primary peritoneal macrophages were obtained from Swiss mice after inoculation of 1 mL 2% starch solution in PBS. Macrophages were seeded in a 96-well plate (6×10^4 cells/well) and kept at 37°C and 5% CO_2 to allow adhesion. After 48 hours, macrophages were infected as described below.

Primary human BM cells

Human BM aspirate was obtained from the iliac crest using BD Vacutainer® Plastic K3EDTA Tubes, initially collected for diagnostics, and delivered as residual sample. The BM was subjected to erythrocyte lysis twice using ACK buffer. Single cell suspensions were obtained by filtering through MACS® SmartStrainers (100 µm, Miltenyi Biotec), centrifuged at 300×*g* for 10 min (4°C) and resuspended in PBS + 0.2% BSA. Cells were counted in PBS and diluted to 2×10^7 cells/mL for flow cytometric analysis. Cells were kept on ice during these procedures.

In vitro and *in vivo Leishmania* infections

Parasite density was assessed using a KOVA® counting chamber. For *in vitro* infections, macrophages, LT-HSC and human HSPC were co-cultured with stationary-phase promastigotes at a multiplicity of infection (MOI) of 5 for a minimum of 24h at 37°C with 5% CO_2. For *in vivo* infection, stationary-phase parasites were centrifuged for 10 min at 4,000×*g* (25°C) and resuspended to 1×10^9 parasites/mL in sterile RPMI medium. Mice were infected intravenously (i.v.) in the lateral tail vein with 1×10^8 parasites in 100 µL of RPMI medium. Animals were monitored using *in vivo* BLI at selected time points. Imaging was performed 3 min after intraperitoneal (i.p.) injection of 150 mg/kg D-Luciferin (Beetle Luciferin Potassium Salt, Promega) in the IVIS® Spectrum In Vivo Imaging System under 2.5% isoflurane inhalation anesthesia using 15 min exposure. Images were analyzed using LivingImage v4.3.1 software by drawing regions of interests (ROIs) around specific organs to quantify the luminescent signal as relative luminescence units (RLU).

Cell staining, flow cytometry and fluorescence-activated cell sorting (FACS)

Parasite cultures were analyzed on a MACSQuant® Analyzer 10 (Miltenyi Biotec) after a 10 min centrifugation at 4,105×*g* and resuspension in PBS + 0.2% BSA buffer. Analyses were performed using FlowLogic™ Software (Miltenyi Biotec) using a specific gating for singlet parasites expressing dsRed, for which the non-transfected parental parasite line served as a control. In some experiments, parasites were stained with 5-(and 6)-carboxyfluorescein diacetate succinimidyl ester (CFSE; Cell Division Tracker Kit, BioLegend) according to manufacturer's instructions. Briefly, lyophilized CFSE was reconstituted with DMSO to a stock concentration of 5 mM. This stock solution was diluted in PBS to a 5 µM working solution. Promastigotes at a concentration of 10^8 cells/mL were centrifuged at 4,000×*g* for 10 min and resuspended in CFSE working solution for 20 min at 25°C. The staining was quenched by adding 5 times the original staining volume of cell culture medium

containing 10% FBS. Parasites were centrifuged again and resuspended in pre-warmed HOMEM medium for 10 min. After incubation, CFSE labeled parasites were used for infection and determining *in situ* proliferation in macrophages, LT-HSC and human HSPC.

Sorting of mouse LT-HSC and human HSPC was performed, and quality confirmed as described previously **([322], Chapter II)**. Briefly, BM cell suspensions (2×10^7/mL concentration) were treated with FcγR-blocking agent (anti-CD16/32, clone 2.4G2, BD Biosciences) for 15 min, followed by a washing step using 400×*g* centrifugation and resuspension in PBS + 0.2% BSA buffer. Next, cells were incubated for 20 min at 4°C with a mix of fluorescent conjugated anti-mouse antibodies at optimized concentrations. DAPI Staining Solution (Miltenyi Biotec) was used to assess viability. Cells were sorted using FACSMelody™ (BD Bioscience) following specific gating strategies, confirmed with fluorescence minus one (FMO) controls and compensated using single stains. For visualizing infection, LT-HSC were collected on slides by Cytospin™, fixed using methanol and stained for 15 min with Giemsa (Sigma Aldrich). For analysis of dsRed and/or CFSE levels on amastigotes at designated timepoints, infected macrophages and LT-HSC were recovered from the cultures. Cells were centrifuged at 400×*g* for 10 min and in PBS + 0.2% BSA. Host cell membranes were disrupted by 3 passages through a 25G needle. Amastigotes were collected in the supernatant after centrifugation at 250×*g* for 10 min and subsequently pelleted at 3,000×*g* for 10 min and resuspended in 500 μL PBS + 0.2% BSA for analysis by flow cytometry.

RNA isolation and sequencing

Total RNA was extracted from three independent samples of 10,000 sorted $DsRed^{hi}$ amastigotes or quiescent amastigotes (*L. infantum*) obtained from 5,000 sorted and infected LT-HSC. Extraction was performed with the QIAamp® RNA Blood Mini kit (Qiagen), according to the manufacturer's instructions. To exclude gDNA, an additional step using gDNA elimination columns (Monarch®) was performed.

RNA samples were stored in aliquots at -80°C. Unbiased total RNA sequencing was performed at Brightcore using the SMARTer® Stranded RNA-Seq Kit to generate strand-specific RNAseq libraries for Illumina® sequencing. Reads were generated in an S4 run (2×100bp, 200M reads) on an Illumina NovaSeq 6000 apparatus. Alignments of the low input RNAseqs with the *L. infantum* JPCM5 reference genome were made using BWA (Burrows-Wheeler Aligner) and normalization was performed in DESeq2 using the variance stabilizing transformation (VST) in the default unsupervised mode **[375]**. Differential expression analysis was largely based on a workflow using Bioconductor packages in R **[376]**. Euclidean distance between samples was calculated using the R function *dist* and with the Poisson Distance package *PoiClaClu* (https://CRAN.R-project.org/package=PoiClaClu) and visualized in a heatmap using *pheatmap* (https://CRAN.R-project.org/package=pheatmap) and the colorRampPalette function from the RColorBrewer (https://CRAN.Rproject.org/package=RColorBrewer). PCA and Volcano plots were generated using *ggplot2* (https://CRAN.Rproject.org/package=ggplot2) and *ggrepel* (https://cran.r-project.org/web/packages/ggrepel/). Heatmaps of the top 150 differential genes and the top 25 upregulated and 25 downregulated genes were generated using *pheatmap*. Gene Set Enrichment by Ontology Analysis was performed in R, using the topGO library, based on Fisher's exact test. The false discovery rate correction was performed using Benjamini-Hochberg, and the p.adjust function, in R.

Functional annotation through bio-informatics and structure prediction

Insights in differentially expressed genes were obtained by searches for functional annotation or orthologues in TriTrypDB **[377]**. An approach combining bioinformatics and AlphaFold2 **[371, 372]** structure prediction, followed by a structural homology search using the DALI server **[378]** was employed to elucidate the putative roles of the proteins encoded by upregulated quiescence-associated

genes without annotated function. Amino acid sequences were subjected to a search on the InterPro web server (https://www.ebi.ac.uk/interpro/) to find potential functional motifs. Protein structures for all 24 candidates were predicted using Alphafold2 and their (local) quality were critically assessed based on the pLDDT confidence metric (score between 0 and 100 that estimates how well predicted models agree with experimentally determined structures). AlphaFold-Multimer **[379]** was employed for one candidate (LINF_230021900) to generate a structural model of a homodimer and dimer formation was critically assessed based on the predicted aligned errors (PAE) confidence metric. The structural models were then submitted to the DALI web server for a structural homology search and hits were carefully evaluated based on the DALI Z-score and Cα rmsd. Molecular graphics and analyses were performed with UCSF ChimeraX **[380, 381]**.

Sand fly infections and evaluation of parasite load

Sand fly females (*L. longipalpis*) were fed with heat-inactivated heparinized mouse blood containing 5×10^6/mL promastigotes from log-phase cultures through a chicken skin membrane. Groups were randomized by an independent researcher until data analysis to avoid bias. Blood-fed females were separated 24 h after feeding, kept in the same conditions as the colony and dissected on 5, 7, 9, and 12 days post blood meal to microscopically check the presence of parasites. Following disruption of the total gut in 50 µL PBS, the parasite load was quantified microscopically using a KOVA® counting chamber **[382, 383]**. Parasites isolated from sand flies on day 12 post blood meal were cultured in HOMEM promastigote medium supplemented with 5% penicillin-streptomycin, to obtain post sand fly cultures.

Promastigote growth

Promastigote growth curves were made as described before **[384]** to compare the *in vitro* growth of quiescent *vs* non-quiescent strains. After passage through fine needles (21G and 25G) to break clustering, the promastigotes were diluted in PBS

and counted by KOVA® counting chamber. Exactly 5×10^5 log-phase promastigotes/mL were seeded in 5 mL HOMEM and their number was determined by microscopic counting every 24 h for a total of 10 days. Three independent repeats of each strain were run in parallel.

Statistics and reproducibility

Statistical analyses were performed using GraphPad® Prism version 9.0.1. Tests were considered statistically significant if $p < 0.05$. Growth curves were statistically compared using Wilcoxon matched-pairs signed rank test. Parasite load in sand fly infections were tested using Unpaired *t* test. Infectivity in macrophages was tested using Ordinary one-way ANOVA. MFI of DsRed expression was compared using Mann-Whitney test.

IV.4 Results

Leishmania infection of mouse and human stem cells triggers amastigote quiescence

We previously reported that LT-HSC harbor an excessive number of amastigotes in comparison to macrophages **[322] (Chapter II)**. Already after 24 hours of infection, epifluorescence microscopy revealed heterogenous DsRed signals in amastigotes of LT-HSC, in contrast to intramacrophage amastigotes that show a bright DsRed expression (**Figure 4.2a**, microscopic panel adopted from **[322] Chapter II**). Amastigotes were isolated from both cell types and measured via flow cytometry, confirming two distinct DsRed$^+$ amastigote populations (DsRed^{hi} and DsRed^{lo}) in LT-HSC. In contrast, amastigotes purified from infected macrophages cluster in one homogenous DsRed^{hi} population (**Figure 4.2a, right panel**). The decreased DsRed signal indicates reduced expression from the 18S rDNA locus, previously reported as an indicator of reduced metabolic activity and entry into a quiescent state **[14]**. Promastigote back-transformation was used to confirm viability of sorted DsRed^{lo} parasites, the capacity to regain proliferative capacity and

stability of the DsRed^{lo} phenotype. Promastigote back-transformation from sorted amastigotes was very variable with recovery rates ranging from 0.8% to 100% for both LT-HSC and macrophages (**Figure 4.2b**). DsRed expression in the quiescent state remained lowered after transformation into the promastigote form (**Figure 4.2c)** which was also confirmed for derived monoclonal lines. Quiescent parasite cultures lost DsRed-expression after promastigote back-transformation with a frequency between 1.96% (1/51 clones) and 4.76% (2/42 clones) (**Figure 4.3**), suggesting that parasites undergo a rapid evolutionary adaptation response and genetic rearrangements upon entry and exit from quiescence. In contrast, no clones derived from DsRed^{hi} parasites lost the DsRed construct.

In situ amastigote quiescence was shown to occur independently of strain (*L. infantum* LEM3323 or clinical isolate LLM2346) or species (*L. infantum* and *L. donovani*) (**Figure 4.2d**) and was recorded in both mouse LT-HSC and human HSPC (**Figure 4.2e**).

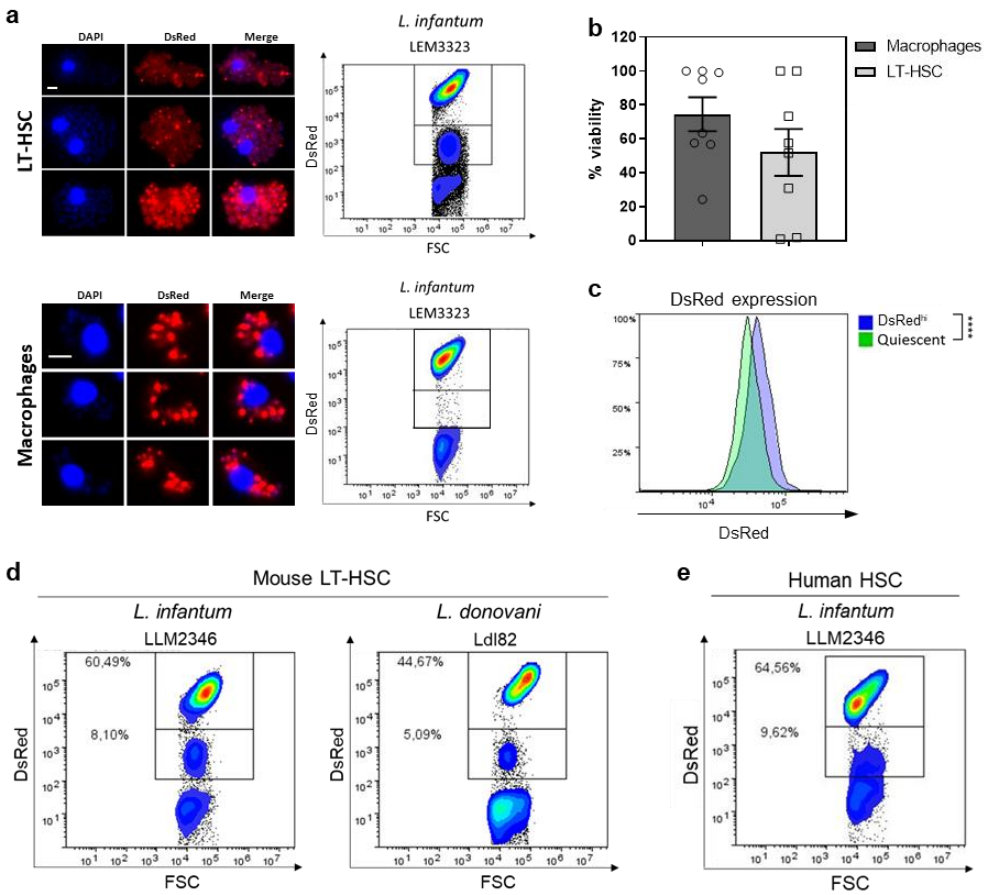

Figure 4.2. *Leishmania* infection of mouse LT-HSC and human HSPC triggers amastigote quiescence. (a) Sorted mouse LT-HSC and BM derived macrophages were infected with *L. infantum* (LEM3323 WT$^{PpyRE9/DsRed}$) and processed for microscopy (microscopic images were published in [322], Chapter II). DAPI (blue), amastigotes (red). Scale bar = 10 µm. Intracellular amastigotes were isolated and measured by flow cytometry. **(b)** Percentage of viable parasites recovered from infected LT-HSC and BM derived macrophages as measured by positive promastigote back-transformation. **(c)** DsRed expression measured by flow cytometry after promastigote back-transformation of DsRed^{hi} and DsRed^{lo} (*i.e.,* quiescent) amastigotes recovered from LT-HSC. **(d)** Amastigotes recovered from infected mouse LT-HSC and measured via flow cytometry. Cells in the left panel were infected with *L. infantum* clinical isolate LLM2346 WT$^{PpyRE9/DsRed}$, right panel with *L. donovani* Ldl82 WT$^{PpyRE9/DsRed}$. **(e)** Amastigotes recovered from *L. infantum* LLM2346 WT$^{PpyRE9/DsRed}$ infected human HSPC.

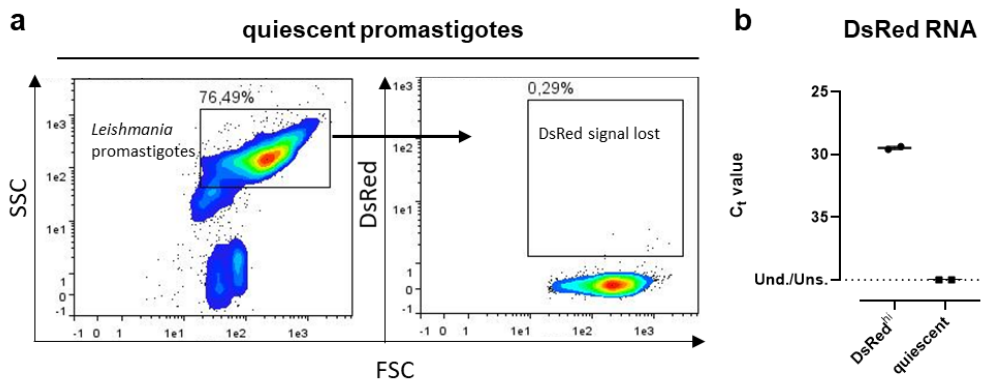

Figure 4.3. Quiescent promastigotes lose DsRed marker. (a) sorted human HSPC were infected for 24 hours with *L. infantum* (LLM1246 WT$^{PpyRE9/DsRed}$). Amastigotes were recovered and measured via flow cytometry. **(b)** RT-qPCR on RNA samples extracted from recovered cultures after promastigote back-transformation from (a).

Amastigotes enter quiescence following *in situ* proliferation in mouse and human stem cells

To uncover why LT-HSC trigger the rapid development of quiescent amastigotes, a CFSE labelling of *L. infantum* LEM3323 promastigotes was performed to assess the number of parasite divisions before entering quiescence (*i.e.*, acquire a DsRed^{lo} phenotype). The number of divisions was calculated based on a 2-fold decline at each division of the CFSE median fluorescence intensity (MFI) (**Figure 4.4a, left panel**). After 6 hours of co-incubation, the DsRed^{hi} amastigote fraction divided about 2 times compared to the control (0 hours), which was comparable to promastigote proliferation in 6-hour *in vitro* cultures. In contrast, the amastigote fraction that would eventually acquire a DsRed^{lo} phenotype displayed a more diverse pattern, ranging between 2, 4 and 6 *in situ* divisions (**Figure 4.4a)**. The highest proportion of amastigotes underwent 6 divisions prior entrance of quiescence (**Figure 4.4b**). These data indicate that the high proliferation rate in LT-HSC is a prevailing trigger. To confirm clinical relevance of these findings, amastigote quiescence was tested in human HSPC using a recent *L. infantum* clinical isolate (LLM2346 WT$^{PpyRE9/DsRed}$). In **Figure 4.4c-d**, CFSE labelling of

promastigotes was again performed to assess the number of divisions. After 24 hours of co-incubation, the DsRed^{hi} fraction divided about 0.5-1 time compared to the control (0 hours), which was comparable to the promastigote culture after 24 hours. The amastigote fraction that ultimately becomes quiescent divided about 4-5 times (**Figure 4.4d**). The observed difference in division rate between LEM3323 and LLM2346 can be linked to intrinsic growth rate differences (**Figure 4.5a, b**). Collectively these data show that *Leishmania* quiescence arises mostly after 4-6 divisions in mouse and human stem cells.

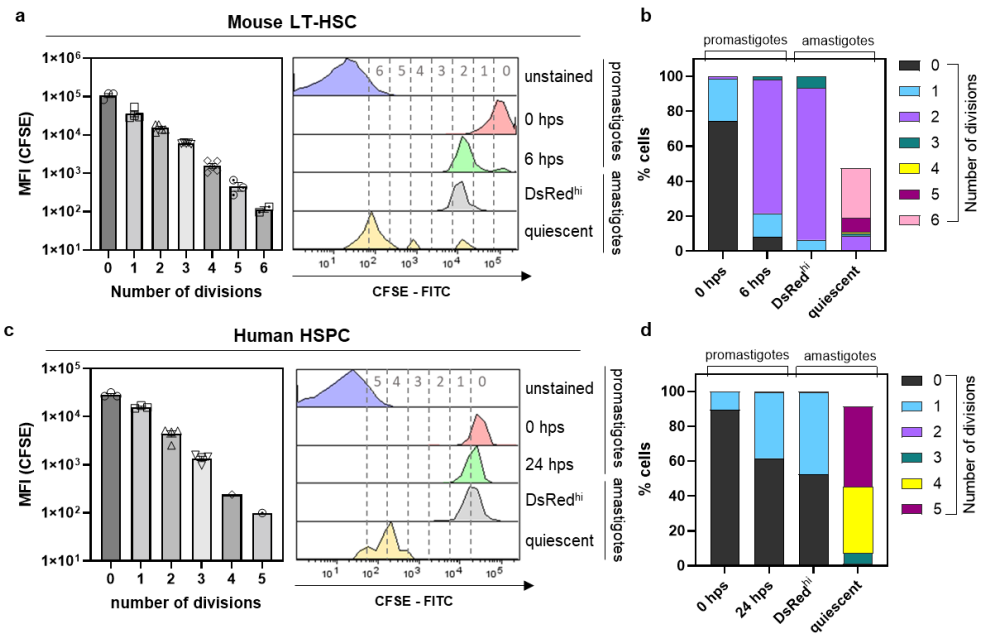

Figure 4.4. Number of divisions to trigger quiescence in amastigotes from mouse LT-HSC and human HSPC. (a) Number of divisions as calculated by CFSE staining and defined by halving of CFSE MFI (left panel). Controls are unstained and CFSE *L. infantum* (LEM3323 WT$^{PpyRE9/DsRed}$) promastigote cultures. Sorted mouse LT-HSC were infected with CFSE labelled *L. infantum* promastigotes and amastigotes were recovered after 6 hours of co-incubation (right panel). **(b)** Percentage of cells in each division range from (a). Results are based on three independent repeats. **(c)** Number of divisions as calculated by CFSE staining and defined by halving of CFSE MFI (left panel). Controls are unstained and CFSE *L. infantum* (LLM2346 WT$^{PpyRE9/DsRed}$) promastigote cultures. Sorted human HSPC were infected with CFSE labelled *L. infantum* promastigotes and amastigotes were recovered after 24 hours of co-incubation (right panel). **(d)** Percentage of cells in each division range from (c). Results are based on three independent repeats.

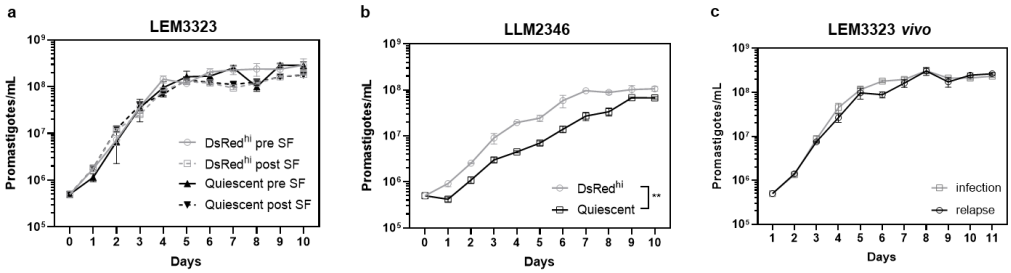

Figure 4.5. Promastigote growth curves remain stable between quiescent and DsRed^{hi} strains. (a) *In vitro* growth curves of LEM3323 promastigotes recovered from quiescent and non-quiescent (DsRed^{hi}) parasites in infected mouse LT-HSC, both before (pre) and after (post) sand fly passage. **(b)** LLM2346 promastigote growth curves *in vitro* of quiescent and non-quiescent (DsRed^{hi}) strains recovered from infected human HSPC. Wilcoxon matched-pairs signed rank test, $^{**}p < 0.01$. **(c)** LEM3323 promastigote growth curves *in vitro* of relapse and infection strains recovered from relapsed and infected BALB/c mice as described above. All results are based on three independent replicates.

Transition through *in situ* quiescence enhances parasite survival, infectivity, and transmission potential

Next, we wondered whether adoption of a quiescent state would have an impact on various aspects of parasite biology. To investigate whether amastigote quiescence in LT-HSC is linked to survival of treatment and consequent occurrence of relapse, sorted/infected cells were treated with 250 μM paromomycin (PMM) or 7.5 μM miltefosine (MIL) for 72 hours before purifying the remaining amastigotes and determining the distribution of quiescent parasites based on DsRed fluorescence by flow cytometry. Drug treatment was found to primarily affect DsRed^{hi} parasites, increasing the proportion of quiescent amastigotes (**Figure 4.6a,b**).

To assess whether going through a reversible quiescent state influences subsequent transmission, sand flies were infected with promastigotes derived from DsRed^{hi} and quiescent amastigotes. In **Figure 4.6c**, parasite load in the gut was compared at different time points, with parasites having transitioned through a quiescent state showing a slightly enhanced sand fly infectivity ($p < 0.05$ at day 12). A similar analysis

was performed for parasites derived from human HSPC, where infectivity in the sand fly vector remained the same (**Figure 4.6e**).

As shown before sand fly passage, quiescent parasites post sand fly showed a lower DsRed signal (**Figure 4.6g**), indicating that some quiescence-associated phenotypic changes are stable after sand fly passage. Infectivity was evaluated by co-incubation with peritoneal macrophages for 96 hours. Interestingly, promastigotes derived from quiescent ($DsRed^{lo}$) amastigotes had a significantly higher infectivity compared to their $DsRed^{hi}$ counterparts ($p < 0.0001$) or the original promastigote culture before LT-HSC passage ($p < 0.0001$). This difference in infectivity was even more pronounced after sand fly passage (**Figure 4.6d**). The infectivity in macrophages was also observed to be significantly higher for promastigotes derived from the quiescent strain recovered from human HSPC ($p < 0.0001$) than for $DsRed^{hi}$ promastigotes (**Figure 4.6f**). The *in vitro* growth curves of LEM3323 and LLM2346 promastigotes comparing quiescent and $DsRed^{hi}$ phenotypes show no significant differences, suggesting that growth rate is not a determining factor contributing to the observed higher infectivity (**Figure 4.5**). These results highlight that a transition through quiescence not only affects treatment but also significantly influences important life cycle features such as infectivity and transmissibility.

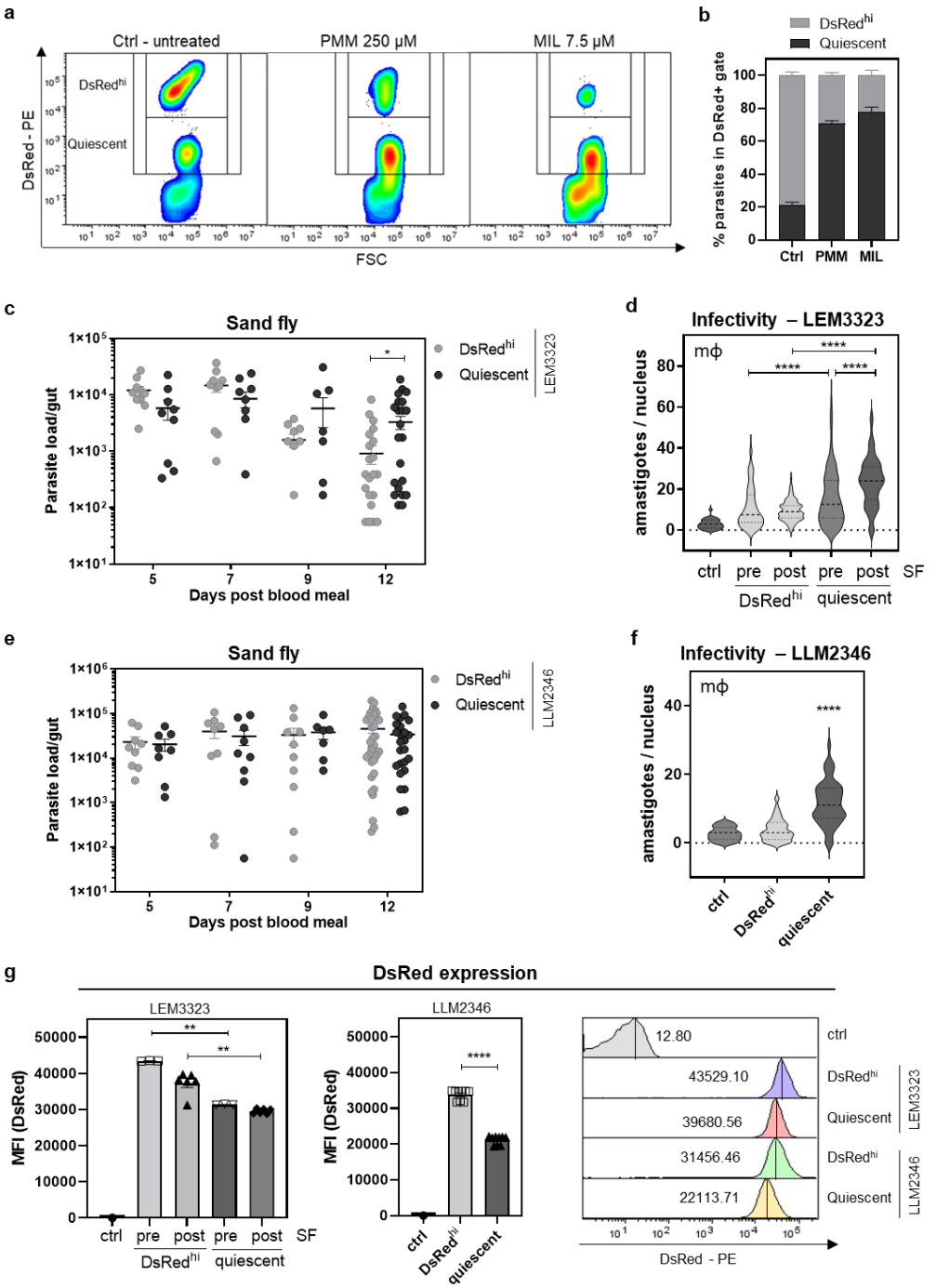

Figure 4.6. Phenotypic characteristics of quiescent amastigotes from LT-HSC. (a-b) Sorted LT-HSC were infected with *L. infantum* (LEM3323 WT$^{PpyRE9/DsRed}$) for 24 hours followed by treatment with 250 µM PMM or 7.5 µM MIL for 72 hours. To compare pre- and post-treatment distribution of quiescent parasites, amastigotes were isolated and remeasured on the FACSMelody.

(c) Sand flies were infected by LEM3323 promastigotes recovered from DsRed^{hi} and quiescent amastigotes in mouse LT-HSC. The parasite load in the gut was assessed at day 5, 7, 9 and 12 after infection (blood meal). Sand fly infections were repeated three independent times. Unpaired *t* test, $10 < n < 30$, $*p < 0.05$. **(d)** LEM3323 promastigotes of a control culture and promastigotes recovered from DsRed^{hi} and quiescent parasites in mouse LT-HSC, pre and post sand fly passage (SF) were co-incubated with peritoneal macrophages for 96 hours and infectivity was assessed with Giemsa staining. The original promastigote culture was used as control and was significantly lower than pre SF DsRed^{hi} ($p < 0.01$), post SF DsRed^{hi} ($p < 0.05$), pre and post SF quiescent ($p < 0.0001$). Ordinary one-way ANOVA, $30 < n < 130$, $****p < 0.0001$. **(e)** Sand flies were infected by LLM2346 promastigotes recovered from DsRed^{hi} and quiescent amastigotes in human HSPC. The parasite load in the gut was assessed at day 5, 7, 9 and 12 after the infectious blood meal. Sand fly infections were repeated three independent times. $10 < n < 34$. **(f)** LLM2346 promastigotes of DsRed^{hi} and quiescent recovered promastigotes from human HSPC were co-incubated with peritoneal macrophages for 96 hours and infectivity was assessed with Giemsa. Mann-Whitney test, $n = 100$, $****p < 0.0001$. **(g)** DsRed expression of LEM3323 DsRed^{hi} and quiescent promastigotes recovered from mouse LT-HSC before or after passage through the sand fly, and LLM2346 DsRed^{hi} and quiescent promastigotes recovered from human HSPC. Mann-Whitney test, $**p < 0.01$. All experiments are expressed as mean ± SEM.

In vivo relapse parasites share characteristics with parasites that transitioned through quiescence

Using a reproducible post-treatment relapse model as described in **Chapter II [322]**, mice were sacrificed at 6 weeks post-infection (4 weeks post PMM treatment) and BM was collected for promastigote back-transformation (**Figure 4.7a**). Infection of mouse peritoneal macrophages revealed an enhanced infectivity of relapse parasites (**Figure 4.7b**) as was found for quiescent parasites. The percentage of reduction after *in vitro* PMM treatment of infected macrophages remained stable for relapse versus the parental parasites, demonstrating that these parasites did not acquire a drug resistant phenotype (**Figure 4.7c**). To check whether the parasites were still infective for sand flies, the gut parasite load was compared at different time points. No significant differences in sand fly parasite loads (**Figure 4.7d**) and *in vitro* promastigote growth (**Figure 4.5c**) were detected. The recorded high fitness of relapse parasites overlaps with the parasite phenotype after transition through a quiescent stage in LT-HSC.

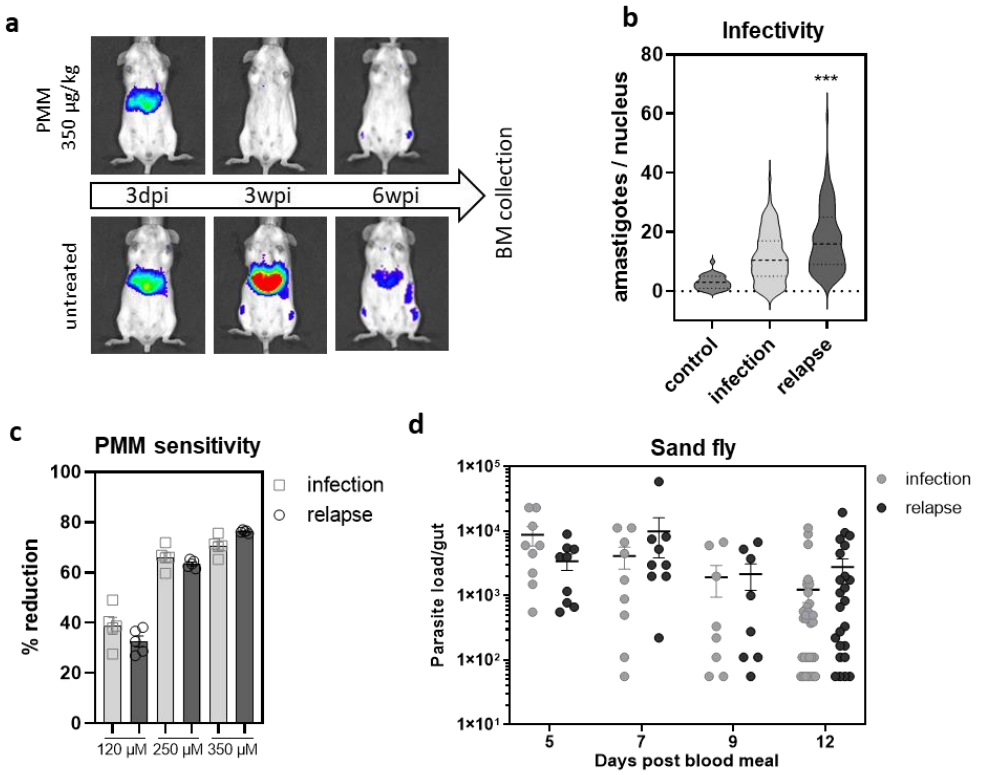

Figure 4.7. Phenotypic characteristics of promastigotes from relapsed BM. (a) BALB/c mice were infected with 10^8 metacyclic promastigotes of *L. infantum* LEM3323 WT$^{PpyRE9/DsRed}$. One group was treated with PMM 350 µg/kg per day (IP) for 5 consecutive days. Infection was followed up by BLI, BM was collected at 6 weeks post-infection (wpi) from untreated and relapsed mice. **(b)** Promastigotes recovered from relapsed BM (relapse) and untreated BM (infection) were co-incubated with peritoneal macrophages for 96 hours and infectivity was assessed with Giemsa. Mann-Whitney test, $n = 100$, $^{***}p < 0.001$. **(c)** Promastigotes recovered from relapsed BM (relapse) and untreated BM (infection) were co-incubated with peritoneal macrophages for 24 hours and treated with 120 µM, 250 µM or 350 µM PMM for 72 hours, infectivity was assessed with Giemsa. **(d)** Sand flies were infected by promastigotes recovered from relapsed BM (relapse) and untreated BM (infection) and the parasite load in the gut from infected flies was assessed at day 5, 7, 9 and 12 after infection (blood meal). Sand fly infections were repeated three independent times. $10 < n < 32$.

In situ quiescent amastigotes undergo vast transcriptional changes and reveal new markers and potential drivers

To unravel the molecular basis for quiescence in LT-HSC amastigotes, unbiased total RNA sequencing was performed on three independent samples of 10,000 DsRed^{lo} (quiescent) and DsRed^{hi} (non-quiescent) amastigotes that were isolated and flow sorted from mouse LT-HSC in three independent infection experiments. Principal component analyses (**Figure 4.8a, b**) revealed distant profiles of the quiescent and DsRed^{hi} samples, supporting the observed difference between both parasite phenotypes. Consistent with a previous quiescence study **[370]**, ribosomal genes were strongly downregulated. The ribosomal genes (194 genes) and transfer RNA (37 genes) were removed for the downstream differential expression analysis. Following trimming of the dataset, 1258 genes were found differentially expressed (*padj* <0.05) in quiescent amastigotes (24 up- and 1234 downregulated, **Figure 4.8c**). Beyond structural constituents of the ribosome, a large proportion of downregulated genes was enriched in biological processes such oxidation-reduction and various other metabolic processes (ATP, carbohydrate derivatives, nucleobase-containing small molecules, L-methionine and ethanolamine biosynthesis), mitochondrial transport, organization and electron transport, cellular protein localization, response to a temperature stimulus and motility (ciliary/flagellar basal body organization) (**Figure 4.9**). The top 25 downregulated genes (5 hypothetical and 20 with annotation), from which 22 were overlapping in all three replicates, may serve as negative markers of quiescence (**Figure 4.8f**, **Table 4.1)**. The previously described absence of an oxidative response to *Leishmania* in the LT-HSC niche and the induction of quiescence may explain why oxidoreductase activity is downregulated **[322] (Chapter II)**.

Interestingly, 24 genes in the quiescent replicates were significantly upregulated considering a log2-fold change and *padj* <0.05 (**Figure 4.8d**), of which 14 showed clear congruence across the three independent biological replicates (**Figure 4.8e, g**). From this list of 24 signature quiescence genes, only 9 have been functionally

annotated, whereas the remaining 15 are labeled as "hypothetical". We reverted to AlphaFold2 structure prediction followed by searches with the DALI server to gain insights into the biological functions of the proteins encoded by these upregulated quiescence-associated genes. Four out of 24 candidates (LINF_230009400, LINF_330016100, LINF_350009900, LINF_350020600) were omitted from further investigation due to poor overall pLDDT scores or the absence of a clear fold in the predicted structures. For those structure predictions characterized by good to excellent overall pLDDT scores, functional annotation was relatively straightforward. For others, functions are proposed based on specific protein regions/domains displaying a reasonable to excellent model quality (e.g., LINF_250022400 and LINF_350025300). The structure-based functional annotation for these proteins is summarized in **Figure 4.10** and **Table 4.2**. The analysis reveals that the proteins encoded by the upregulated quiescence-associated genes are involved in a myriad of cellular processes: metabolism, regulation of gene expression at the RNA level, cell motility and cytoskeleton dynamics, pleiotropic mediators of protein-protein interactions, vesicle transport and autophagosome, and DNA topology and cell cycle control. These results suggest that the phenotypic transition to and/or maintenance of quiescence requires a coordinated cell-wide response.

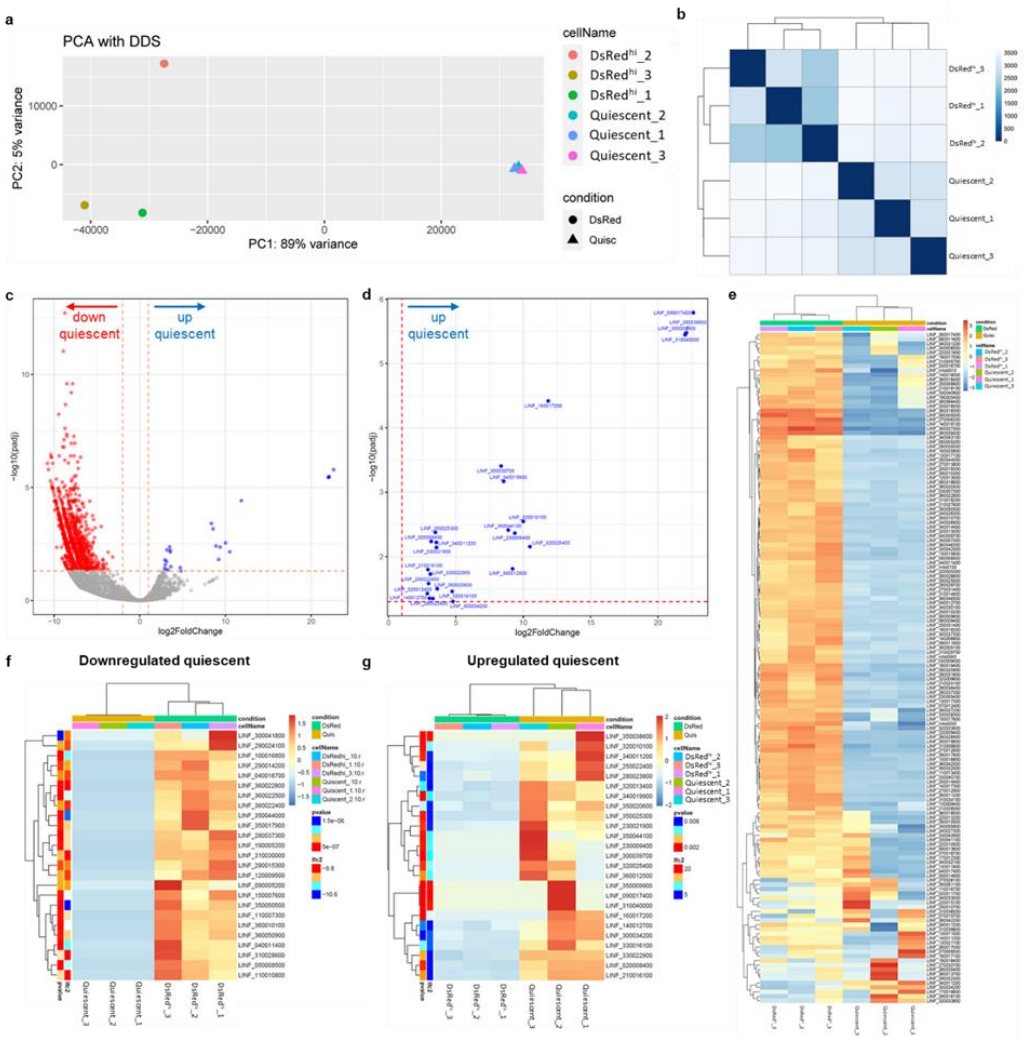

Figure 4.8. RNA seq data from quiescent amastigotes recovered from mouse LT-HSC. (a) Principal component analysis (PCA) of the RNA seq data revealing distant clustering of the independent DsRed^{hi} and quiescent samples. **(b)** Euclidean distance matrix between the samples illustrating the Poisson Distance. **(c)** Volcano plot from quiescent amastigotes displaying significantly up- and downregulated genes. **(d)** Zoom in the top-right section of (c), showing the gene IDS. **(e)** Heatmap of the top 150 differentially expressed genes. **(f)** Top 25 downregulated genes in quiescent amastigotes. **(g)** Top 25 upregulated genes in quiescent amastigotes. **(e-g)** Expression levels are represented with a color scale ranging from blue to red (overexpression). These heatmaps were generated excluding tRNA and transcripts encoding ribosomal proteins.

Table 4.1. Top downregulated genes in quiescent amastigotes. Shaded cells represent congruent downregulation in the three independent biological replicates. Uniprot accession codes are indicated between brackets.

Gene ID	Annotated Function	Putative function*
Transporters/membrane proteins		
LINF_300041800	ATP synthase – epsilon chain – putative	*Has (transmembrane) transporter activity, ligase activity, involvement in metabolic processes such as nucleobase-containing small molecule processes and carbohydrate derivative processes (A0A6L0XK66)
LINF_040011400	Hypothetical protein	*Hypothesized to encode for a cellular membrane component. (A0A6L0WPK2)
LINF_290015300	Hypothetical protein	*Hypothesized to encode for a cellular membrane component. (A0A6L0XIQ7)
LINF_360010100	Hypothetical protein	*Implied to encode for a cellular component part of the mitochondrial respiratory chain complex IV. Potentially involved in the generation of precursor metabolites and energy by taking part in the mitochondrial electron transport from cytochrome c to oxygen. (A0A6L0XW73)
LINF_310028600	CRAL/TRIO domain containing protein – putative	*Cytoskeleton-associated protein described in *L. donovani* **[385]**
Enzymes		
LINF_350017900	Ubiquitin-conjugated enzyme E2 - putative	*Potentially confers transferase activity. (A0A6L0XQ93)
LINF_350044000	T-complex protein 1 - eta subunit - putative	*Has an implicated role in mitochondrial protein import and macromolecular assembly. Potentially involved in the correct folding processes of imported proteins as well as the proper assembly of unfolded polypeptides generated in the mitochondrial matrix under stress conditions. (A0A6L0Y1Z8)
LINF_360050900	Oxidoreductase – putative	*Oxidoreductase activity and implicated in zinc ion binding. (A0A6L0Y2L2)
LINF_110007300	Proteasome alpha 7 subunit – putative	*Multicatalytic proteinase complex involved in ubiquitin-dependent protein catabolic processes. (A0A6L0WK23)
LINF_050008500	Trypanothione reductase	*Disulfide oxidoreductase activity maintaining redox homeostasis needed for parasite survival **[386]**. (A0A6L0WLV7)
LINF_150007600	Lysyl-tRNA synthetase – putative	*Confers lysine-tRNA ligase activity and thus involved in tRNA metabolic processes. Has catalytic activity with the ability to bind RNA nucleotides and is also involved in amino acid metabolic processes.

		(A0A6L0X1S6)
LINF_280037300	Glutamate dehydrogenase – putative	*Oxidoreductase activity, acting on the CH-NH2 group of donors, NAD or NADP as acceptor and thus has a role in the energy metabolism. (A0A6L0XKJ9)
LINF_110010800	Protein kinase – putative	*Potential role in protein kinase activity, ATP binding, protein phosphorylation. (A0A6L0WKT1)
LINF_040016700	fructose-1-6-bisphosphatase	*carbohydrate metabolic process, metal ion binding. (A0A6L0WIH0)
Binding proteins		
LINF_360022500	Universal minicircle sequence binding protein	*Implied to fulfill molecular functions including nucleic acid binding and zinc ion binding. (A0A6L0XWI3)
LINF_360022800	Universal minicircle sequence binding protein	*Implied to fulfill molecular functions including nucleic acid binding and zinc ion binding.
LINF_360022400	Universal minicircle sequence binding protein	*Implied to fulfill molecular functions including nucleic acid binding and zinc ion binding.
LINF_350050500	CS domain containing protein – putative	*Potential molecular function implicated in Hsp90 protein binding and therefore essential proteostasis **[387]**. (A0A6L0XR43)
Histones		
LINF_290024100	Histone H2A - putative	*Implicated as structural constituent of chromatin and therefore structural molecule activity. Potential role in protein heterodimerization processes. (A0A381MN47)
LINF_190005200	Histone H2B	*Implicated as structural constituent of chromatin and therefore structural molecule activity. Potential role in protein heterodimerization processes. (A0A6L0XA47)
LINF_100016800	Histone H3 – putative	*Core histone and structural constituent of the nucleosome/chromatine where it has a role in DNA binding and structuring. (A0A6L0WKL6)
Hypothetical proteins		
LINF_090005200	Hypothetical protein	
LINF_290014200	Hypothetical protein	
LINF_310030000	Hypothetical protein	
LINF_120009500	Hypothetical protein	

Table 4.2. Top upregulated genes in quiescent amastigotes. Shaded cells represent congruent upregulation in the three independent biological replicates. Green shaded cells represent genes for which structural and functional predictions are reliable, blue shaded cells represent genes for which annotating one single function is difficult. Orange shaded cells represent predictions with low confidence.

Gene ID	seq	Annotated Function	Structural homology and predicted function*
DNA topology and cell cycle control			
LINF_210016100	4110	Mis-match repair protein – putative	* DNA binding and mismatch repair
LINF_230021900	921	Hypothetical protein	Centrosomin *Role in regulating cell cycle progression and cell division
LINF_250022400	3507	Hypothetical protein	DNA topoisomerase 2-binding protein, contains 3 BRCT domains (2 clearly predicted and 1 with poor accuracy) and in that regard resembles microcephalin (implicated in chromosome condensation and DNA damage induced cellular response). Interpro accession code IPR001357 *DNA repair, recombination, topology and cell cycle control
LINF_280023800	2823	Hypothetical protein	S-adenosyl-L-methionine-dependent methyltransferases/spermidine synthases/polyamine aminopropyltransferase. Interpro accession code IPR029063 *Pleotropic functions including cell cycle control
LINF_320010100	1152	Hypothetical protein	SWI/SNF and RSC complexes subunit SSR4 / DNA binding (contains a DNA binding domain conserved in some transcription factors and a Zn^{2+} coordination center) *Chromatin remodeling, regulation of transcription
LINF_330016100	1026	Hypothetical protein	* Regulation of gene expression
LINF_350009900	1017	Hypothetical protein	Chromodomain-helicase-DNA-binding protein 1 * Chromatin remodeling
LINF_350025300	4260	Hypothetical protein	Contains well-modelled regions with structural homology to DNA binding domains

Pleiotropic mediators of protein-protein interactions			
LINF_320013400	498	Hypothetical protein	SPRY domain containing protein
LINF_340019900	1041	Hypothetical protein	SPRY domain containing protein
RNA-level regulation of gene expression			
LINF_160017200	354	Hypothetical protein	RNA polymerase II transcription factor B subunit * Regulation of transcription
LINF_300034200	2022	Pentatricopeptide repeat domain containing protein – putative	Large family of modular RNA-binding proteins in kinetoplastids which mediate several aspects of gene expression primarily in mitochondria but also in the nucleus * RNA binding, RNA processing in mitochondria **[388]**
LINF_330022900	993	RNA recognition motif – putative	* RNA binding, post-transcriptional regulation of gene expression (RNA recognition motif)
LINF_350020600	5577	Hypothetical protein	GTP-binding nuclear protein RAN Importing beta-like protein KAP120 * Nuclear translocation of RNA and proteins
LINF_360012500	807	KREPA4 – putative	* RNA binding protein, catalyzing the editing of most mitochondrial mRNAs. KREP4A is essential for editosome integrity and survival of *Trypanosoma brucei* **[389]**
Metabolism			
LINF_020008400	2919	EamA-like transporter family/Triose-phosphate Transporter family/UAA transporter family – putative	Transmembrane transport - Multi-pass membrane protein * Drug/metabolite transporter superfamily * Putative increased tolerance to drugs
LINF_140012700	981	Fatty acid elongase - putative	* Lipid metabolism, *Leishmania* polyunsaturated fatty acid metabolites are implicated in parasite/host interactions (macrophage M2 polarization)
LINF_350044100	1014	Nucleoside diphosphate kinase - putative	NDP kinase (this gene product has two NDP domains and an EF-hand domain to allow dimerization). * Nucleotide metabolism and host cell protection from extracellular ATP **[390]**

Vesicle transport and autophagosome			
LINF_310040000	567	Autophagy protein 10 (ATG10)	Structural homology to ATG3 * Autophagosome formation
LINF_350038600	630	Transport protein particle (TRAPP) subunit - putative	* ER-to-Golgi transport of vesicles, adaptation of cycling cells to stress conditions **[391]**
LINF_230009400	465	Hypothetical protein	* Delivery of tail-anchored (TA) proteins to the endoplasmic reticulum
Cell motility and cytoskeleton dynamics			
LINF_340011200	1749	Hypothetical protein	* Flagellar assembly and stability
LINF_300039700	705	Hypothetical protein	Tropomodulin/leiomodulin/Actin * Regulation cytoskeletal dynamics
LINF_320025400	351	Hypothetical protein	Enhancer of filamentation 1 (focal adhesion domain; bacterial complement inhibitory domain) * Disassembly of the primary cilium/flagellum by activation of Aurora A kinase at the basal body **[392]**

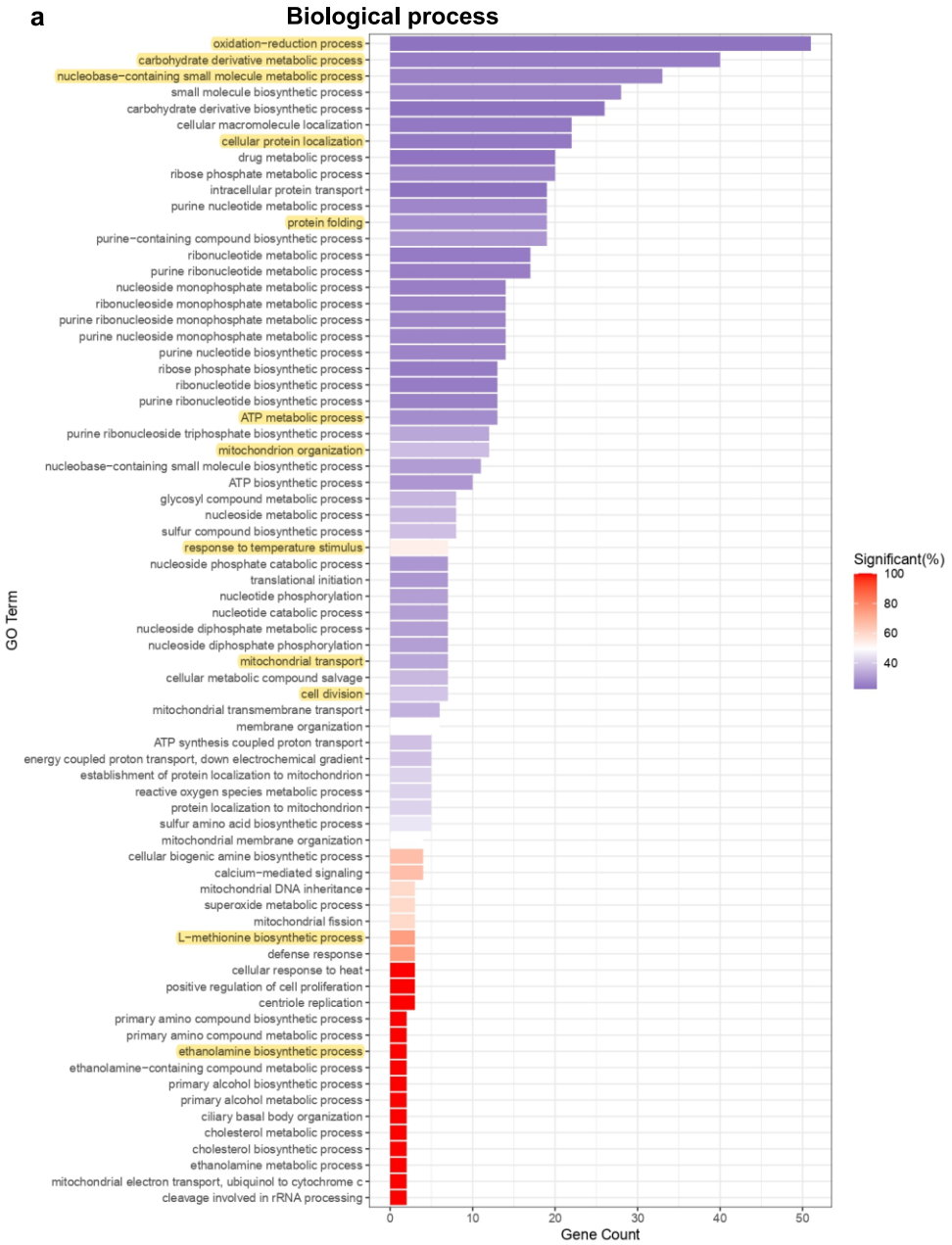
a
Biological process
oxidation−reduction process
carbohydrate derivative metabolic process
nucleobase−containing small molecule metabolic process
small molecule biosynthetic process
carbohydrate derivative biosynthetic process
cellular macromolecule localization
cellular protein localization
drug metabolic process
ribose phosphate metabolic process
intracellular protein transport
purine nucleotide metabolic process
protein folding
purine−containing compound biosynthetic process
ribonucleotide metabolic process
purine ribonucleotide metabolic process
nucleoside monophosphate metabolic process
ribonucleoside monophosphate metabolic process
purine ribonucleoside monophosphate metabolic process
purine nucleoside monophosphate metabolic process
purine nucleotide biosynthetic process
ribose phosphate biosynthetic process
ribonucleotide biosynthetic process
purine ribonucleotide biosynthetic process
ATP metabolic process
purine ribonucleoside triphosphate biosynthetic process
mitochondrion organization
nucleobase−containing small molecule biosynthetic process
ATP biosynthetic process
glycosyl compound metabolic process
nucleoside metabolic process
sulfur compound biosynthetic process
response to temperature stimulus
nucleoside phosphate catabolic process
translational initiation
nucleotide phosphorylation
nucleotide catabolic process
nucleoside diphosphate metabolic process
nucleoside diphosphate phosphorylation
mitochondrial transport
cellular metabolic compound salvage
cell division
mitochondrial transmembrane transport
membrane organization
ATP synthesis coupled proton transport
energy coupled proton transport, down electrochemical gradient
establishment of protein localization to mitochondrion
reactive oxygen species metabolic process
protein localization to mitochondrion
sulfur amino acid biosynthetic process
mitochondrial membrane organization
cellular biogenic amine biosynthetic process
calcium−mediated signaling
mitochondrial DNA inheritance
superoxide metabolic process
mitochondrial fission
L−methionine biosynthetic process
defense response
cellular response to heat
positive regulation of cell proliferation
centriole replication
primary amino compound biosynthetic process
primary amino compound metabolic process
ethanolamine biosynthetic process
ethanolamine−containing compound metabolic process
primary alcohol biosynthetic process
primary alcohol metabolic process
ciliary basal body organization
cholesterol metabolic process
cholesterol biosynthetic process
ethanolamine metabolic process
mitochondrial electron transport, ubiquinol to cytochrome c
cleavage involved in rRNA processing
GO Term
0
10
20
30
40
50
Gene Count
Significant(%)
100
80
60
40

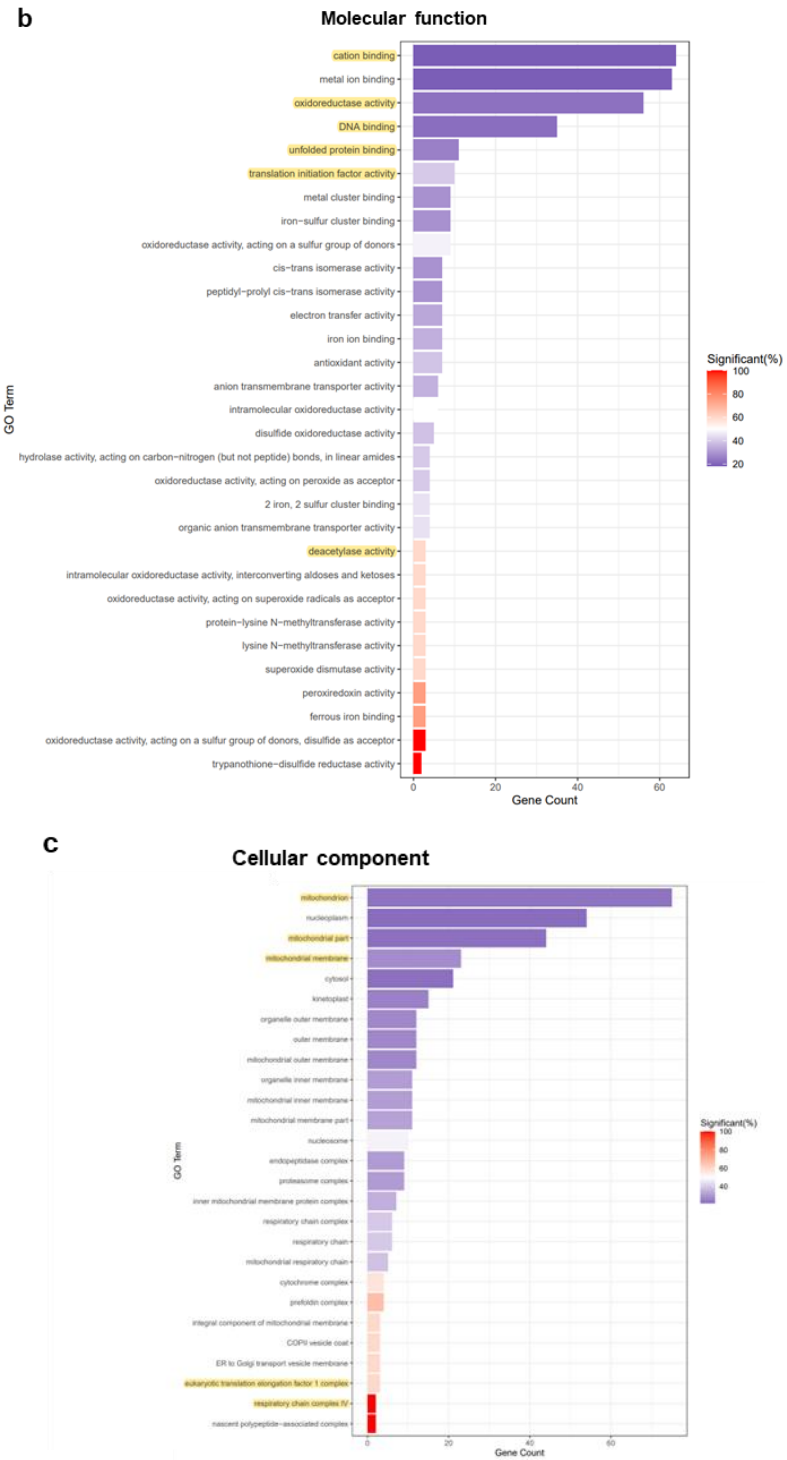

Figure 4.9. GO term analysis of quiescent *Leishmania* amastigotes. Visual representation of GO terms enriched in biological processes **(a)** molecular function **(b)** and cellular components **(c).** Interesting changes are highlighted in yellow.

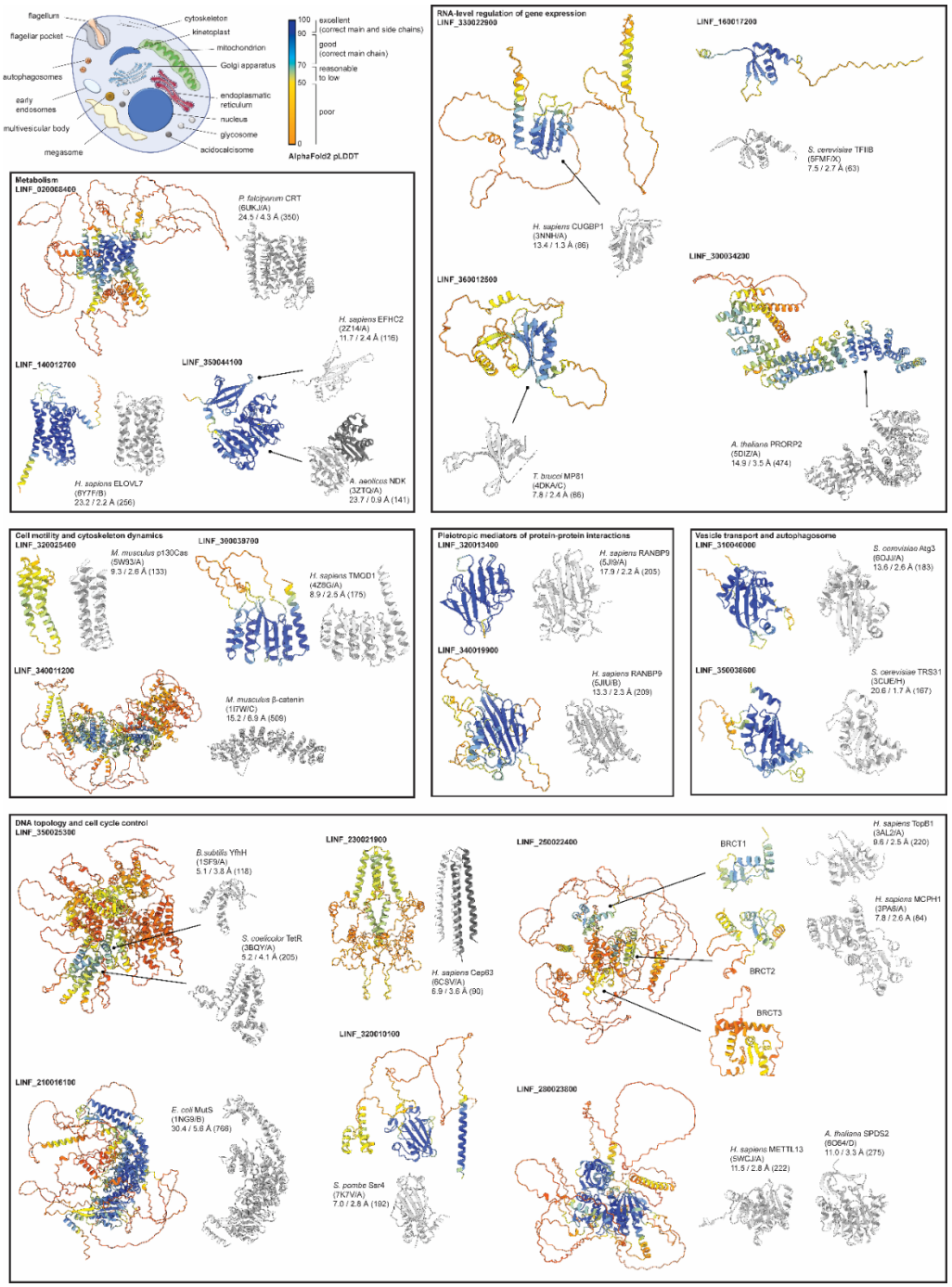

Figure 4.10. Functional annotation of upregulated quiescence-associated genes through AlphaFold2 structure prediction and structural homology searches. The top left corner depicts a cartoon of an amastigote. The boxes contain cartoon representations of the AlphaFold2 structure predictions, which have been grouped together based on their structure-based functional annotation (*cfr.* Table 2). The structures are colored according to the predicted local distance difference test

(pLDDT) score, which reflects (local) model quality. The most representative DALI hits are shown in a cartoon representation and have been colored light grey. The accompanying text provides information on the nature of the DALI hit (first line), the PBD code and chain ID (second line), and the DALI Z-score, Cα rmsd and number of residues included in the structural overlap (third line).

IV.5 Discussion

Current resources for new drug development for VL are scarce. Despite the imminent need to combat the increasing relapse rates, little is known on the underlying cause and suitable methods to study this phenomenon. Notably, post-treatment relapse is mostly not due to reinfection, drug quality, drug exposure or drug-resistant parasites **[6, 98]**, but rather due to persistence of the pathogen. This persistence causing subclinical infections and subsequent relapse has been widely described across the microorganism spectrum **[8-12, 195, 393, 394]**. Generally, two aspects can be the cause of this: pathogens residing in sanctuary sites or niches, or pathogens switching to a quiescent phenotype. The first allows pathogens to survive and escape treatment or immunity without genetic or phenotypic changes. The latter relies on phenotypic diversity, e.g. quiescent or dormant forms **[7]**. Based on our observations, treatment failure in VL most likely results from an intrinsic ability of the *Leishmania* parasite to benefit from both quiescence and the occupation of sanctuary sites. We have previously identified a relapse-prone cellular niche in the BM in which treatment is less effective **[322] (Chapter II)**. Here, we formally link quiescent parasites residing in this particular sanctuary site to drug tolerance.

In literature there is no clear consensus on the definition of persistence or quiescence, and additional synonyms such as dormancy and latency are used interchangeably as conceptually related terms. More commonly, quiescence refers to genetically drug susceptible, dormant (non-growing or slow growing) organisms that survive exposure to a given cidal drug and have the capacity to regrow (or resuscitate and grow) under highly specific conditions **[395]**. Several external triggers may induce quiescence, such as host immunity, drug pressure and/or nutritional and energetic stress **[367, 396]**. Investigation of the physiology of this phenotype *in vivo* is very challenging due to their scarcity and difficulty of detection. A review by Barrett *et al.* envisages several methods to study quiescence such as fluorescent probes, DNA replication probes, sorting of quiescent *vs* replicating cells,

and several omics approaches **[7]**. Studies in various model organisms have been proposed to gain insights in the enigmatic basis of quiescence, such as transgenic fluorescent hypnozoites for *P. vivax* **[397]**, multiple-stress model to study *M. tuberculosis* **[398]**, and GFP reporter gene expression from an 18S rDNA locus in cutaneous leishmaniasis **[14]**.

Quiescence in (cutaneous) leishmaniasis has been observed in several experimental systems since the first observation in 2015 by Kloehn *et al.* **[399]**. A form of quiescence has been described in axenic cultures of cutaneous *Leishmania* strains treated with antimonials or grown under stress conditions **[14, 370]**. A recent study on *L. mexicana* dermal granulomas describes a mosaic of metabolically active and semi-quiescent parasites during acute phases of infection, linking the phenotype to treatment failure **[185]**. Another study uses *in vivo* labeling with 5-bromo-2'-deoxyuridine (BrdU) to visualize persistent slow-growing *L. major* parasites in macrophages in the skin **[400]**. To date, a knowledge gap exists for naturally elicited quiescent parasites recovered from a host cell niche, especially for VL. The present study provides unprecedented insights into quiescence of VL parasites in LT-HSC. The *Leishmania* amastigote stage had already been described as a less active state that may represent an adaptive response to a growth-restrictive intracellular microenvironment in granulomas **[399, 401]**. Here, we compared amastigotes within the common macrophage host cell to those within the LT-HSC niche and found distinct differences. Within LT-HSC, quiescence occurred as quickly as 6 hours after infection following an estimated 4-6 divisions. This indicates that host cell differences and the intracellular parasite proliferation rate determine the occurrence of quiescence.

Characterizing quiescent VL parasites recovered from LT-HSC showed an increased infectivity and a high capacity to colonize the sand fly gut. Consistent with the quiescent phenotype, parasites recovered from the BM of relapsed mice show an increased fitness with an elevated macrophage infectivity combined with a high

sand fly infectivity. This suggests that the selected phenotype, typically associated with transition through a quiescent state, may pose an additional threat to leishmaniasis control programs. An increased infectivity associated with relapse of *L. donovani* infection has already been shown for miltefosine and antimonial treatment in the Indian subcontinent **[98, 402, 403]**. To prevent treatment failure, we advocate that the quiescent state of *Leishmania* should be also considered in the early stages of the drug discovery process.

Transcriptomic analysis of quiescent VL parasites revealed an overall downregulation of RNA, especially ribosomal protein genes, a signature of quiescence well described in literature **[370, 399, 404, 405]**, as ribosome biosynthesis is one of the most energy intensive processes in the cell and thus a measure of the metabolic state. A large proportion of genes was downregulated in quiescent VL parasites, enriched in biological processes such oxidation-reduction and various other metabolic processes (ATP, carbohydrate derivatives, nucleobase-containing small molecules, L-methionine and ethanolamine biosynthesis), mitochondrial transport, organization and electron transport, cellular protein localization, response to a temperature stimulus and motility (ciliary/flagellar basal body organization). Metabolic changes in protozoan persisters are corroborated by other literature reports. Studies have shown that DNA replication, general transcription and protein synthesis are decreased in *Plasmodium spp*. and *Toxoplasma gondii* persisters **[7]**. The artificial axenic amastigote forms of *L. mexicana* and *L. braziliensis* showed downregulated synthesis of ATP, ribosomal components, proteins and alterations in membrane lipids **[14, 401]**. In contrast to many other species, *Leishmania* does not have transcriptional regulation and as such is mainly compensated by post-transcriptional mechanisms by RNA-binding proteins **[406]**. The observed downregulation in translation initiation factor activity, critical for gene expression, together with lower unfolded protein binding could explain the decreased DsRed expression observed in quiescent parasites. The overall downregulated cellular components are related to the energy metabolism

(mitochondrion, mitochondrial part, mitochondrial membrane, respiratory chain complex IV). Mitochondrial gene expression undergoes changes according to the cell culture conditions and has been described to be reduced in an artificial model of quiescence **[370]**.

Although quiescent forms exhibit an overall gene downregulation, some processes are sustained (e.g. oxidation-reduction in *T. gondii*, *M. tuberculosis* and *P. cynomolgi* hypnozoite forms **[407-409]**) or even upregulated (e.g. autophagy, amino acid catabolism, GP63 and amastin surface-like proteins in *L. braziliensis* axenic amastigote forms **[370]**). We also identified genes that were consistently upregulated in our *in situ* quiescence model and our structure-based functional annotation reveals that the encoded proteins are involved in a myriad of cellular processes. Several genes appear to be involved in DNA topology and cell cycle control (LINF_210016100, LINF_230021900 LINF_250022400, LINF_280023800, LINF_320010100, and LINF_350025300). The regulation of gene expression at the RNA level is also involved in acquiring and/or maintaining quiescence and differential transcript data also suggest alterations in RNA editing (LINF_160017200, LINF_300034200, LINF_330022900, LINF_360012500).). As mentioned above, regulation of gene expression for kinetoplastids is by RNA level regulation and editing. Indeed, *Leishmania* is known for its extreme genomic and phenotypic variability, whereby a rapid shift in the gene repertoire is one of the key mechanisms for swift adaptation to changing environments **[105]**, some of which have been associated with increased fitness in stress conditions or drug resistance **[410]**. Interestingly, some upregulated genes are involved in processes such as cell motility and cytoskeleton dynamics (LINF_300039700, LINF_320025400, and LINF_340011200), and vesicle transport and the autophagosome (LINF_310040000 and LINF_350038600). The latter is consistent with autophagy being upregulated in *L. braziliensis* axenic amastigote **[370]**. Two genes encode proteins with an SPRY domain, which is typically found in scaffold proteins involved in functions operating across the cell **[411]**, which is why these were

categorized as pleiotropic mediators of protein-protein interactions. Finally, as expected, only few genes encoding a metabolic function are upregulated in the three independent quiescent samples, including LINF_020008400, LINF_140012700, and LINF_350044100 encoding a drug/metabolite transporter, fatty acid elongase, and nucleoside diphosphate kinase, respectively. The upregulation of a fatty acid elongase has been previously described for quiescent parasites in murine lesions **[399]** and may be important for maintaining a favorable parasite/host interaction as *Leishmania* polyunsaturated fatty acid metabolites are important for macrophage M2 polarization. The functional annotation of an upregulated drug/metabolite transmembrane transporter that may be implicated in conferring quiescent parasites a higher tolerance to antileishmanial treatment. We propose that these upregulated genes participate in entry or maintenance of a quiescent state and may serve as positive markers of quiescence. Both positive and negative transcriptional markers or candidate drivers of entry and/or maintenance of quiescence warrant further investigation using the genetic toolbox available for *Leishmania* and may offer unprecedented insights in the universal problem of quiescence across the microorganism spectrum.

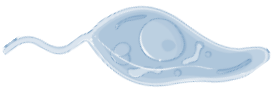

Effect of visceral leishmaniasis on B cell lymphopoiesis and humoral immune memory

CHAPTER V

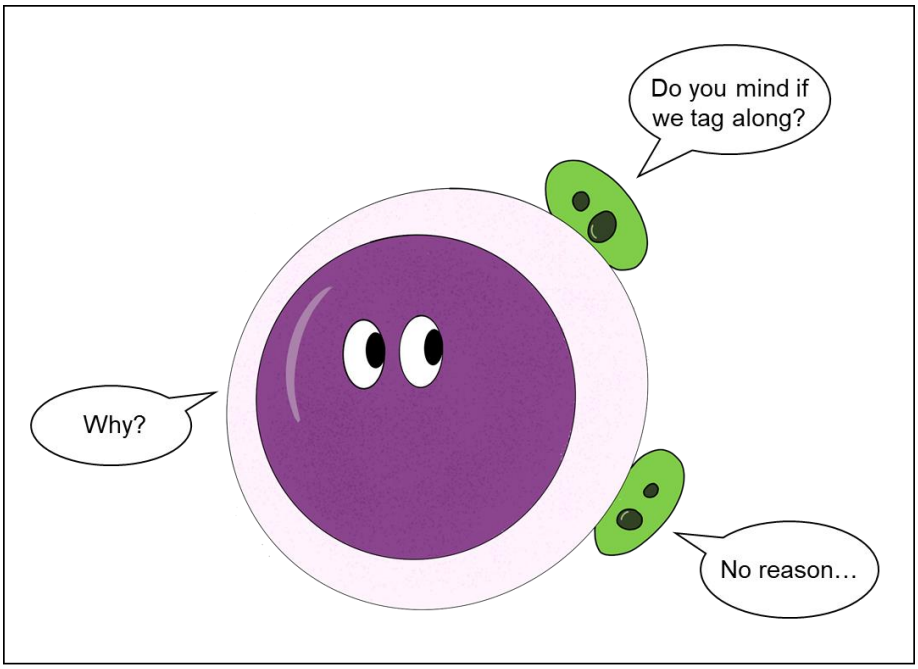

Acknowledgements:

Marlotte Loyens[1], my master thesis student working on this project
Stefan Magez[2], Magdalena Radwanska[2], Moon Sangphil[2], Hien Thi Thu Pham[2], and Thi Thu Hang Nguyen[2], for their excellent guidance in the data analyses

[1]Laboratory of Microbiology, Parasitology and Hygiene (LMPH), Infla-Med Centre of Excellence, University of Antwerp, Antwerp, Belgium.
[2]Laboratory for Biomedical Research, Department of Environmental Technology, Food technology and Molecular Biotechnology, Ghent University Global Campus, South Korea

V. Effect of visceral leishmaniasis on B cell lymphopoiesis and humoral immune memory.

V.1 Abstract

VL causes an uncontrolled infection of internal organs such as spleen, liver and BM and can be lethal when left untreated. To date, no effective vaccines are available for humans, largely due to the complexity of the specific protective immune response against VL, whereby the contribution of B cells has been contentious. Moreover, other related pathogens such as African trypanosomes are known to impair B cell development and deplete vaccine memory. In this study, VL infection was found to increase B cell progenitors in the BM as well as all analyzed B cell subtypes of the spleen, in line with the clinical manifestation of polyclonal hypergammaglobulinemia and the occurrence of autoantibodies during VL. Flow cytometric and microscopic examination identified attachment of viable amastigotes to B cells independent of IgM expression. Using immunization against a fluorescent heterologous antigen, it was shown that VL does not impair immune memory, which is reassuring for vaccination campaigns in VL endemic areas.

V.2 Background information

Despite the distinctive significance of B cells in protective immunity and vaccine development for many infectious diseases, their role during intracellular parasite infections has been explored less extensively. This is also the case for *Leishmania*, a genus of protozoan parasites responsible for leishmaniasis, including the lethal, visceral form of the disease **[412]**. *Leishmania* parasites are transmitted between mammalian hosts by the bites of female sand flies belonging to the genera of *Phlebotomus* or *Lutzomyia* **[413-415]**. In their life cycle, *Leishmania* parasites exist in two major morphological forms: a long flagellated extracellular promastigote within the sand fly and a non-flagellated obligate intracellular amastigote within

mammalian host cells of the myeloid lineage **[55, 56]**. The phagocytosed parasites establish infections by occupying a parasitophorous vacuole or phagolysosome **[53, 54]**.

Leishmania cellular tropism comprises not solely phagocytic cells (monocytes, macrophages, neutrophils and dendritic cells), but also stromal cells (fibroblasts), keratinocytes, adipocytes and recently stem cells have been described to be susceptible host cells **[52, 210, 322]**. Recent studies observed that some splenic B cells interact with surface-attached amastigotes during early *L. donovani* infection, resulting in B cell activation **[251, 252]**. A role of IgM was presumed to provide adhesive pockets and CD21 (complement receptor 2) to enable marginal zone B cells (MZB) to capture parasites **[251]**. Moreover, it has been shown that attached amastigotes can be transferred to other cells **[416]**. Here we show that promastigote co-incubation with B cells from the BM and spleen results in attachment and morphological transformation of *Leishmania* to viable amastigotes independent of IgM expression. However, the question remains whether this is a *bone fide* infection or a distinct association to hijack specific immune cells or to circulate within the host.

Whereas vaccines already contribute to the control of canine leishmaniasis **[417]**, human vaccine development for VL has been ongoing for decades. Different candidates are under evaluation in clinical trials, but none are yet available for implementation **[418]**. Promising results from experimental human VL vaccine trials, and the practice of "leishmanization" **[81]**, provide strong evidence for the scientific feasibility of an effective vaccine against human VL. However, progress is still hampered by insufficient knowledge of parasite pathogenesis and the complexity of protective immune responses. To date, investigations have mostly been skewed to the innate immune response and Th1 cells **[15, 16, 419, 420]**, while the role of B cells during leishmaniasis has always been controversial. Recent studies report that B cells play a dual role during antileishmanial immunity and contribute to both the persistence and elimination of *Leishmania* parasites **[244-246]** (**Figure**

5.1a). On the one hand, B cells exacerbate VL infection as they induce hypergammaglobulinemia, produce non-specific and autoreactive antibodies particularly of the immunoglobulin M (IgM) and IgG isotypes and suppress the generation of effector memory T cells, all due to polyclonal B cell activation **[245, 250, 251, 255]**. On the other hand, B cells activate T cells through antigen presentation, produce various pro- and anti-inflammatory cytokines and yield anti-leishmanial antibodies that have shown to persist for more than 15 years **[245, 247, 248, 421, 422]**.

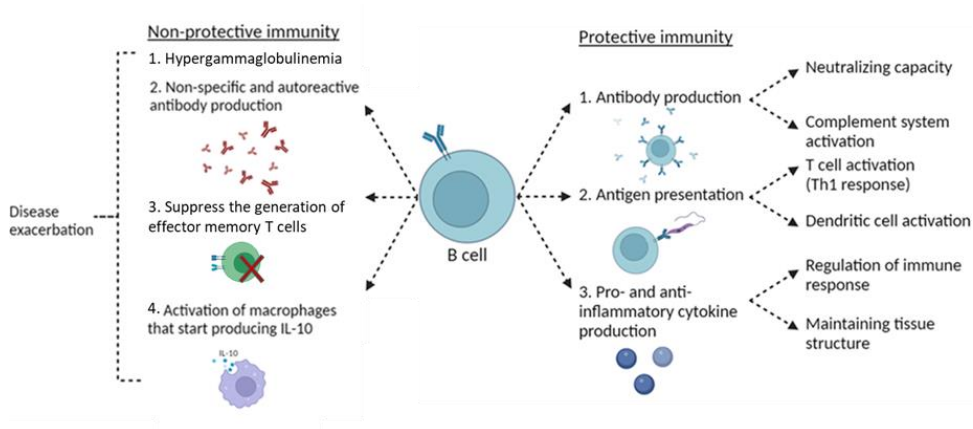

Figure 5.1. B cell immune response. B cells can contribute to the immune response of VL leading to protection or to disease exacerbation. Protective immunity is driven by antibody production, antigen presentation and production of pro- and anti-inflammatory cytokines. Disease exacerbation is the result of hypergammaglobulinemia, production of non-specific and autoreactive antibodies and the activation of macrophages which will produce IL-10. Figure created in BioRender.com

Existing vaccination campaigns against several infectious diseases have no re-exposure strategy, although several extra- or intracellular infections such as African trypanosomiasis **[18, 21, 23, 423]**, malaria **[22, 424]**, measles **[19, 20]** and toxoplasmosis **[425]** can hamper pre-existing memory B cells induced by vaccines or previously encountered infections. Here we show that during early VL infection, B lymphopoiesis is triggered in both BM and spleen and humoral immune memory is not detrimentally affected by the disease.

V.3 Materials and methods

Ethical statement

The animal experiments were carried out in strict accordance with the mandatory guidelines (European Union directive 2010/63/EU on the protection of animals used for scientific purposes and the Declaration of Helsinki) and are approved by the ethical committee of the University of Antwerp (UA-ECD 2019-04).

Laboratory animals

Female BALB/c mice (6-8 weeks old) were purchased from Janvier, France. The animals were group-housed in individually ventilated cages with environmental enrichment material (cardboard house and shredded paper). Food (Carfil, Arendonk, Belgium) and drinking water were available *ad libitum*. To collect tissue, animals were euthanised using a CO_2 induction chamber followed by cervical dislocation.

Parasite cultures

Parasite strains of *L. infantum* and *L. donovani* were transfected to express the fluorescent marker DsRed and/or the bioluminescent marker PpyRE9: (1) LEM3323 $WT^{PpyRE9/DsRed}$ and LEM3323 WT^{PpyRE9} (MHOM/FR/96/LEM3323), derived from a *L. infantum* isolate from a French HIV patient; (2) Ldl82 $WT^{PpYRE9/DsRed}$ (MHOM/ET/67/L82), a *L. donovani* isolate from an Ethiopian VL-patient **[262]**. Promastigotes were grown at 25°C in hemoflagellate modified minimal essential medium (HOMEM, Gibco, Life Technologies) supplemented with 16.5 mM $NaHCO_3$, 200 mM L-glutamine, 40 mg/L adenine solution, 3 mg/L folic acid solution, 2 mg/L D-biotin solution, 2.5 mg/L hemin solution and 10% heat-inactivated foetal calf serum (iFCS) and sub-cultured twice weekly. The number of passages was kept as low as possible to maintain parasite virulence.

Primary mouse cells

Mice were euthanised after which femur, tibia and spleen were aseptically removed. Bones were crushed with mortar and pestle in ammonium-chloride-potassium (ACK) buffer (0.15 M NH_4Cl, 1.0 mM $KHCO_3$, 0.1 mM Na_2EDTA; Medicinal Chemistry Lab) to lyse the red blood cells. The spleen was removed and homogenized with a sterile 10 mL syringe. Both cell suspensions were filtered through a 100 μm MACS® SmartStrainer (Miltenyi Biotec). The red blood cell lysis was stopped by adding complete Roswell Park Memorial Institute medium (RPMI 1640 medium, Gibco, Life Technologies), supplemented with 1% nonessential amino acid (NEAA), 1% Pen/Strep, 1% L-glutamine, 1% sodium pyruvate and 10% iFCS (all from Gibco, Life Technologies). Filtered cell suspensions were centrifuged for 10 minutes at 400×*g* and 4°C, and the pellet was resuspended in complete RPMI medium. The number of cells was counted in phosphate-buffered saline (PBS; Gibco) using a KOVA® counting chamber. Cells were kept on ice during all procedures.

In vitro and *in vivo Leishmania*-infections

Parasite density was assessed by counting parasites in PBS using a KOVA® counting chamber. For *in vitro* infections, BM and spleen cell suspensions were co-cultured with stationary-phase promastigotes of *L. infantum* or *L. donovani* at a multiplicity of infection (MOI) of 5 for a minimum of 2 to 24h at 37°C with 5% CO_2. For *in vivo* infection, stationary-phase parasites were centrifuged for 10 min at 4,000×*g* (25°C) and resuspended to 1×10^9 parasites/mL in sterile RPMI medium. Mice were infected intravenously (i.v.) in the lateral tail vein with 1×10^8 parasites in 100 μL of RPMI medium.

In vivo bioluminescence imaging (BLI)

BLI was performed to monitor animal infections at selected time points. Imaging was performed 3 min after intraperitoneal (i.p.) injection of 150 mg/kg D-Luciferin

(Beetle Luciferin Potassium Salt, Promega) in the IVIS® Spectrum In Vivo Imaging System under 2.5% isoflurane inhalation anaesthesia using 15 min exposure. Images were analyzed using LivingImage v4.3.1 software by drawing regions of interests (ROIs) around specific organs to quantify the luminescent signal as relative luminescence units (RLU).

Immunization with phycoerythrin (PE)

Mice were immunized with the fluorescent protein PE according to Pape *et al.* **[426]**. Briefly, an injection of 50 µL containing 50 µg PE (red fluorescent protein of red algae; Prozyme) dissolved in Imject® Alum (ThermoFisher Scientific), was administered subcutaneously (s.c.) into the hindlimb of noninfected BALB/c mice. This was followed by a booster injection of the same formulation 3 weeks later. After another 3 weeks, half of the immunized mice were infected with *Leishmania* parasites as described above.

Drug formulation and treatment

Three weeks after infection, mice were treated for 5 days with paromomycin sulphate salt (PMM, Sigma-Aldrich), at a dose of 350 mg/kg body weight s.i.d. via intraperitoneal injection. PMM stock solution was dissolved in MilliQ® at 70 mg/mL.

Enzyme-Linked Immunosorbent Assay (ELISA)

ELISA was performed to determine the antibody titters of immunized mice. Briefly, a 96-well plate was coated with 2 µg/mL PE (Prozyme) and incubated overnight at 4°C. The plates were washed with PBS + 0.1% Tween 20 (Sigma-Aldrich) and blocked with PBS + 10% iFCS. Tail vein serum samples were taken from mice and were added to the plates in a 2-fold serial dilution. After an overnight incubation period at 4°C, plates were washed, and a goat anti-mouse horseradish peroxidase (HRP) antibody (Novex) solution was added for 2 hours at 37°C. Next, detection solution containing 3,3',5,5'-tetramethylbenzidine (TMB; Sigma-Aldrich) was

added, dissolved in peroxidase substrate buffer with 75 mM Na_2HPO_4 (Sigma-Aldrich), 44 mM citric acid (Fluka) and 30% H_2O_2 (Emsure). The plates were incubated for 10 minutes at room temperature, after which the reaction was stopped by adding a 1N sulfuric acid solution (H_2SO_4; Sigma-Aldrich). Absorbance was measured at λ 450 nm using a Glomax® Discover Microplate Reader (Promega).

PE enrichment method

To enable quantification of PE-specific B cells by flow cytometry, single cell suspensions from BM and spleen were enriched with magnetic beads according to Pape *et al.* **[426]** and the manufacturer's instructions (Miltenyi Biotec). Briefly, cell suspensions were stained for 20 minutes with PE (Prozyme) at 4°C, followed by washing with PBS + 0.2% bovine serum albumin (BSA, Sigma-Aldrich) and centrifugation for 10 minutes at 400×*g* and 4°C. The cell pellet was resuspended with anti-PE MicroBeads (Miltenyi Biotec) for 15 minutes. Samples were washed with PBS + 0.2% BSA and passed over magnetized LS columns of a MACS Separator (Miltenyi Biotec). The columns were washed with PBS + 0.2% BSA to remove unlabelled cells. Enriched PE-specific cells were then further processed for flow cytometric analysis as described below.

Cell staining, flow cytometry and fluorescence-activated cell sorting (FACS)

BM and spleen cell suspensions were collected and centrifuged at 300×*g* for 10 minutes. The pellet was resuspended in PBS + 0.2% BSA at a concentration of $2x10^7$ cells/mL. Cell suspensions were treated with FcγR-blocking agent (anti-CD16/32, clone 2.4G2, BD Biosciences) for 15 min, followed by incubation for 20 min at 4°C with a mix of fluorescent conjugated anti-mouse antibodies at optimized concentrations (**Table 5.1**). DAPI Staining Solution (Miltenyi Biotec) was used to assess viability.

LysoTracker™ Green DND-26 (green-fluorescent dye, ThermoFisher Scientific) was used for specific lysosome staining using manufacturer's instructions.

LysoTracker™ stock solution was prepared at 1 mM in RPMI medium. Then, a concentration of 75 nM LysoTracker™ was applied to the 24-well plate of BM and spleen samples for 2 hours at 37°C.

Samples were measured by flow cytometry using MACSQuant® Analyser 10 (Miltenyi Biotec). The obtained data were further analyzed with FlowLogic™ software (Miltenyi Biotec). Different B cell subsets express a unique set of cell surface markers that allow distinction (**Figure 5.1b**) **[18, 240, 242, 427]**. The gating strategy (**Table 5.2, Figure 5.2, 5.3 and 5.4**) was based on fluorescence minus one (FMO) controls and compensated using single stains.

To sort B cells, BM and spleen cell suspensions were processed as described above, using CD19 and IgM anti-mouse antibody mix with DAPI as live-death staining. Cells were sorted into a 96-well plate containing HOMEM or RPMI medium for promastigote back-transformation or microscopic analysis respectively, using FACSMelody™ (BD Bioscience) following specific gating strategy based on FMO controls and compensated using single stains. For microscopic visualisation, sorted B cells were collected on slides by Cytospin™ followed by Giemsa staining after fixation with methanol.

Table 5.1. Cell surface markers used for staining of B cell subtypes from BM and spleen samples for analysis by flow cytometry.

Cell surface marker	Fluorophore	Clone	Manufacturer
Mix 1: B cells bone marrow			
Ter119	Vioblue	Ter-119	Miltenyi Biotec
CD11b	Vioblue	REA592	Miltenyi Biotec
Gr1	Vioblue	REA810	Miltenyi Biotec
TCRb	Vioblue	REA318	Miltenyi Biotec
CD335	Vioblue	REA815	Miltenyi Biotec
B220	VioGreen	RA3-6B2	Miltenyi Biotec
CD93	APC-Cy7	REA298	Miltenyi Biotec
IgM	PerCP-Vio700	REA979	Miltenyi Biotec
CD19	Vio Bright FITC	6D5	Miltenyi Biotec
CD43	APC	L11	Miltenyi Biotec
CD138	PE-Cy7	281-2	Biolegend
Mix 2: B cells spleen			

CD23	FITC	B3B4	Miltenyi Biotec
CD21/CD35	PerCP	REA800	Miltenyi Biotec
CD1d	APC	1B1	Miltenyi Biotec
CD138	PE-Cy7	281-2	Biolegend
B220	VioGreen	RA3-6B2	Miltenyi Biotec
CD93	APC-Cy7	REA298	Miltenyi Biotec
Mix 3: Memory B cells bone marrow and spleen			
B220	VioGreen	RA3-6B2	Miltenyi Biotec
CD19	Vio Bright FITC	6D5	Miltenyi Biotec
IgM	PerCP-Vio700	REA979	Miltenyi Biotec
IgG1	APC	X-56	Miltenyi Biotec
IgG2ab	APC	X-57	Miltenyi Biotec
CD205	APC-Fire 750	NLDC-145	Biolegend
CD274	PE-Cy7	10F.9G2	Biolegend

Table 5.2. Cell surface markers used to distinguish B cell subtypes from BM and spleen.

Cell type	Surface markers
Bone marrow	
Pre-pro B	Lin^- ($Ter119^-$, $CD11b^-$, $Gr1^-$, $TCR\beta^-$, $CD335^-$), $B220^+$, $CD19^-$, $CD93^+$, IgM^-, $CD43^+$
Pro B	Lin^- ($Ter119^-$, $CD11b^-$, $Gr1^-$, $TCR\beta^-$, $CD335^-$), $B220^+$, $CD19^+$, $CD93^+$, IgM^-, $CD43^+$
Pre B	Lin^- ($Ter119^-$, $CD11b^-$, $Gr1^-$, $TCR\beta^-$, $CD335^-$), $B220^+$, $CD19^+$, $CD93^+$, IgM^-, $CD43^-$
Immature B	Lin^- ($Ter119^-$, $CD11b^-$, $Gr1^-$, $TCR\beta^-$, $CD335^-$), $B220^+$, $CD19^+$, $CD93^+$, IgM^+, $CD43^-$
Plasma B	Lin^- ($Ter119^-$, $CD11b^-$, $Gr1^-$, $TCR\beta^-$, $CD335^-$), $B220^{low}$, $CD138^+$
Spleen	
Non-mature B	$B220^+$, $CD93^+$
T1 transitional	$B220^+$, $CD93^+$, IgM^{hi}, $CD23^-$
T2 transitional	$B220^+$, $CD93^+$, IgM^{hi}, $CD23^+$
MZB	$B220^+$, $CD93^-$, $CD1d^{hi}$, $CD23^{low}$, $CD21/35^{hi}$
FoB	$B220^+$, $CD93^-$, $CD1d^{low}$, $CD23^{hi}$, $CD21/35^{low}$
Plasma B	$B220^{low}$, $CD138^+$
Memory B cell	$B220^+$, $CD19^+$, $CD205^+$, $CD274^+$, IgM^+/IgG^+

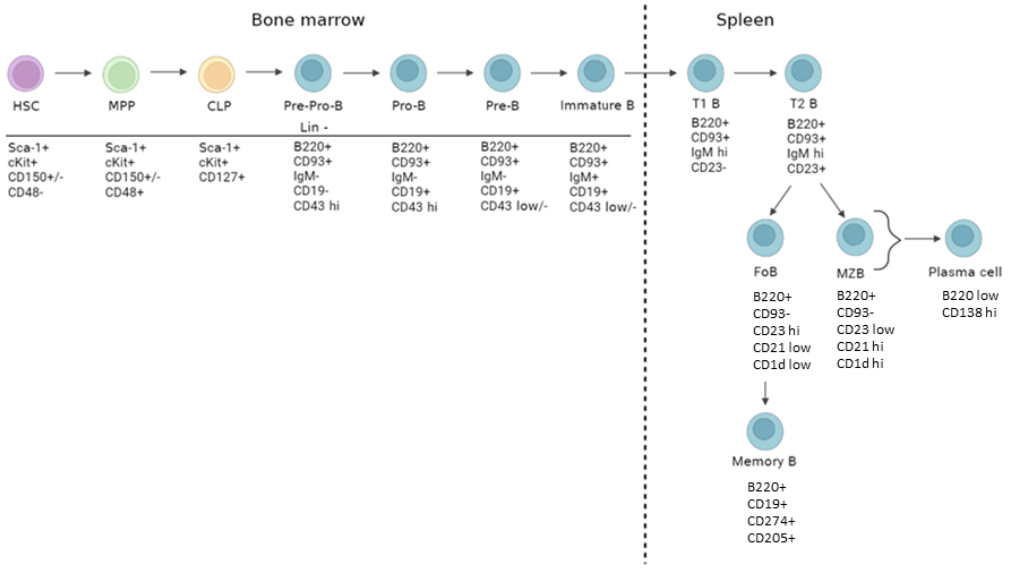

Figure 5.2. Cell surface markers of the different B cell subsets during B lymphopoiesis **[428-430]**. B lymphopoiesis start in the BM with the differentiation of HSC into MPP and CLP, which further differentiate into the different B cell progenitors (Pre-pro-B cells, Pro B cells, Pre B cells) resulting in immature B cells. These migrate to the spleen and develop via transitional stages into FoB and MZB. FoB will develop into memory B cells and plasma cells, whereas MZB will develop only into plasma cells. Lin- (Lineage negative cells: $Ter119^-$, $TCR\beta^-$, $CD11b^-$, $Gr1^-$, $CD335^-$), HSC (hematopoietic stem cell), MPP (multipotent progenitor cell), CLP (common lymphoid progenitor cell), FoB (follicular B cell), MZB (marginal zone B cell). Figure created in BioRender.com.

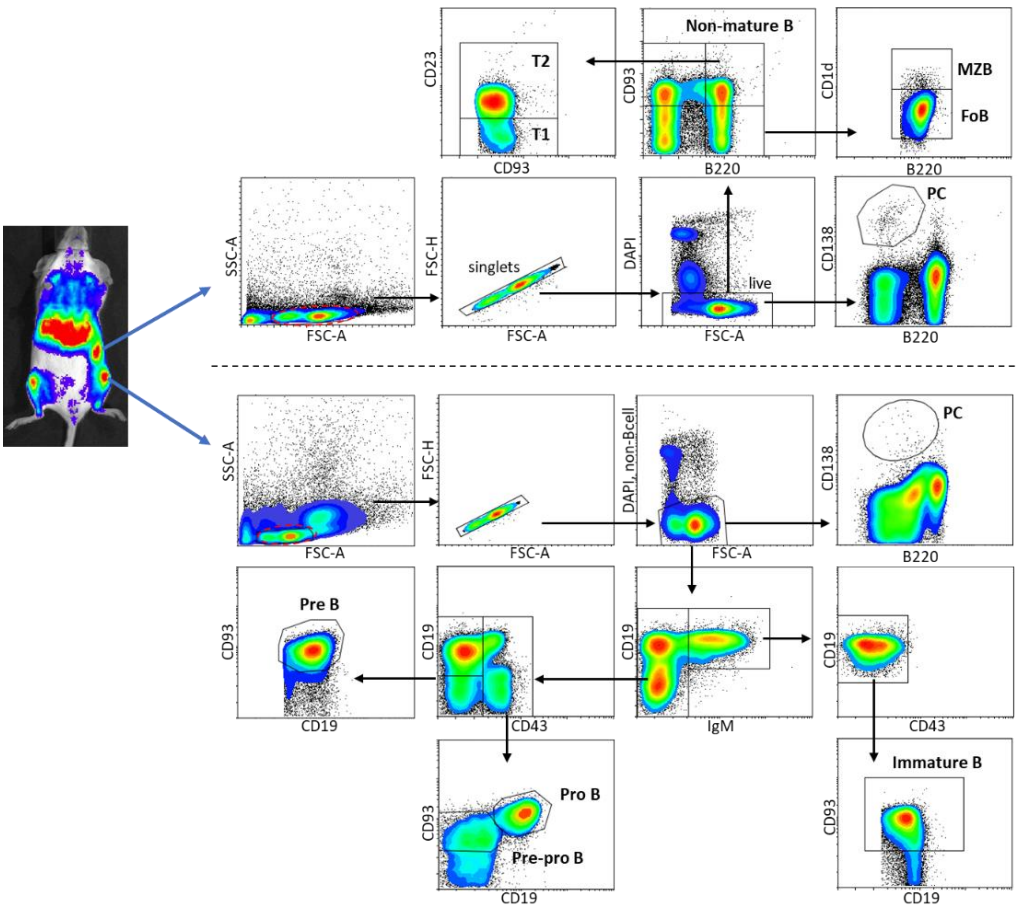

Figure 5.3. Gating strategy for B cell subsets of spleen and BM using flow cytometry. For both spleen and BM, a gating of forward scatter (FSC) and side scatter (SSC) was used to exclude debris and select the cells followed by a gate for singlets in an FSC-H/FSC-A plot. **(a)** A gate for live/death cells in the spleen was used resulting in selection of living cells that are DAPI-. Immature B cells were identified as $B220^{+}CD93^{+}$, followed by specific gating for T1 transitional ($CD23^{-}$) and T2 transitional ($CD23^{+}$) B cells. Identification of plasma cells was done via selection of $B220^{lo}CD138^{hi}$. Additionally, FoB and MZB were selected respectively as $B220^{+}CD93^{-}CD1d^{lo}$ and $B220^{+}CD93^{-}CD1d^{hi}$. **(B)** In BM, living lymphoid cells were selected by exclusion of all $Violblue^{+}$ cells (*i.e.* DAPI, Ter119, Gr-1, CD11b, TcR-β, and CD335). Plasma cells were further identified by selecting $B220^{lo}CD138^{hi}$ cell subsets. Immature B cells were gated as $CD19^{+}IgM^{+}CD43^{-}$ cells. Gating for pre-pro B cells, pro B cells and pre B cells was used by respectively selecting $CD19^{-}IgM^{-}CD43^{+}CD93^{+}$, $CD19^{+}IgM^{-}CD43^{+}CD93^{+}$ and $CD19^{+}IgM^{-}CD43^{+}CD93^{+}$ cells.

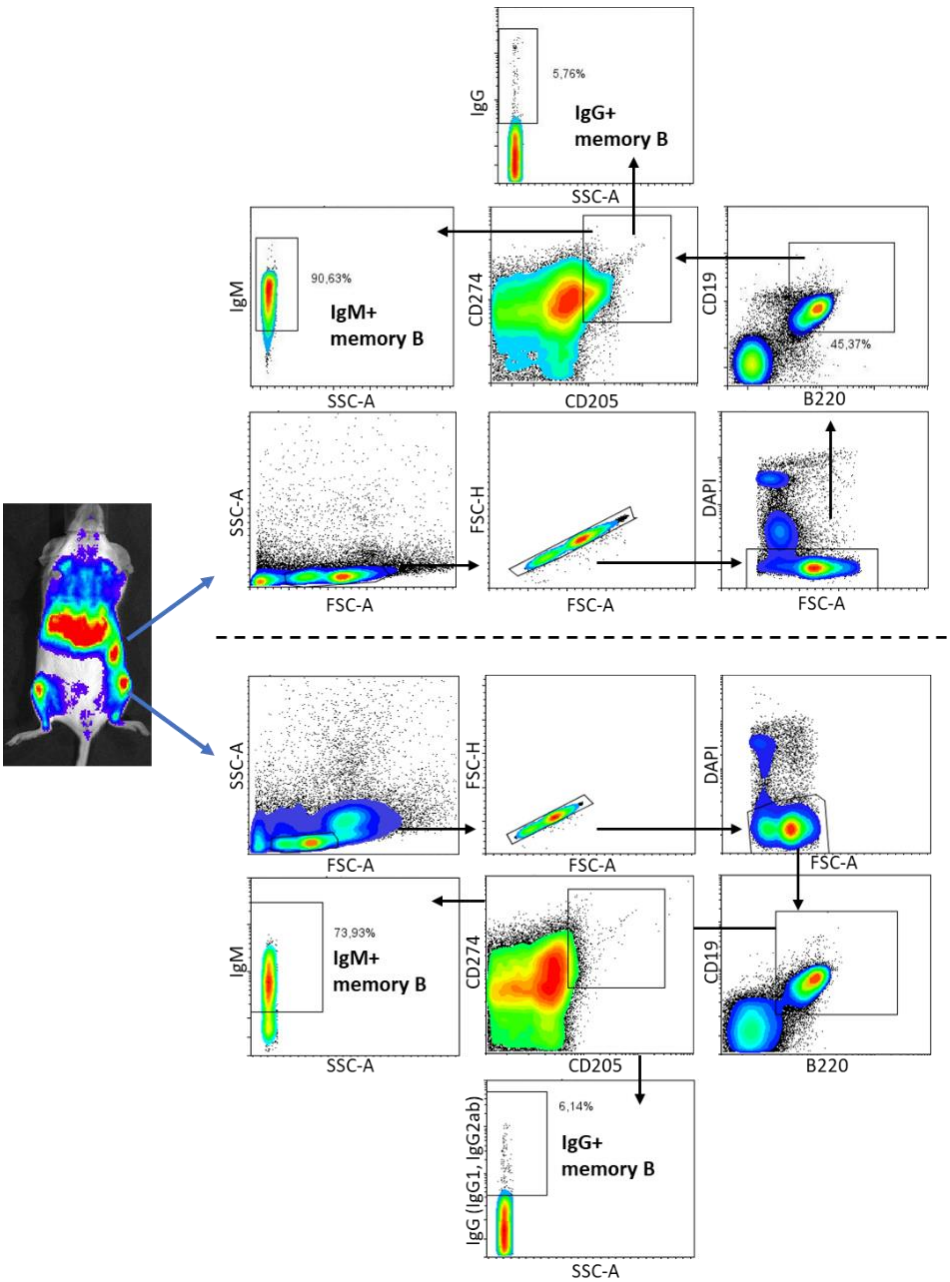

Figure 5.4. Gating strategy for memory B cells of spleen and BM using flow cytometry. The gating strategy for both spleen and BM to select IgM^+ and IgG^+ memory B cells was the same. First, a gating of forward scatter (FSC) and side scatter (SSC) was used to exclude debris followed by a gate for singlets in an FSC-H/FSC-A plot. Then, a gate for live/death cells was used resulting in selection of living cells that are $DAPI^-$. This was followed by a gate for B cells via the selection of $B220^+CD19^+$. Finally, IgM^+ and IgG^+ memory B cells were gated respectively as $CD274^+CD205^+IgM^+$ and $CD274^+CD205^+IgG^+$.

Promastigote back-transformation assay

Infected (DsRed$^+$) B cells were flow sorted into a 96-well plate containing HOMEM in a ½ serial dilution. Cell suspensions were put through a 29G needle of a 0.5 mL syringe (BD Microfine, 0.5 mL) to disrupt and free amastigotes. Plates were then placed into a 25°C incubator, where the amastigotes could transform back into proliferative promastigotes and thus confirm viability. The plates were checked 5-7 days post sorting using a conventional microscope (Leica DM2000 LED microscope).

Statistical analysis

Statistical tests were performed using GraphPad Prism 9® software. P-values $p < 0.05$ were considered as statistically significant. Comparison of % of DsRed$^+$, MFI and infection index was done using Mann-Whitney U test. Lysotracker MFI was compared using Ordinary one-way ANOVA with Tukey's multiple comparisons test. B lymphopoiesis experiments were statistically tested using Kruskal-Wallis with Dunn's multiple comparison test.

V.4 Results

VL promastigotes attach to B cells and transform to amastigotes extracellularly.

To assess whether B lymphocytes are susceptible host cells for *Leishmania*, BM and spleen cells of non-infected BALB/c mice were collected and incubated *ex vivo* with DsRed expressing *L. infantum*. After 2 hours an average of 5-10% DsRed$^+$ signal could be observed for all B cell subtypes in suspensions of both organs. A more distinct susceptibility amongst the various B lymphocytes was recorded after a 24-hour co-incubation, with a stronger association of DsRed [infection index, *i.e.* percentage of DsRed$^+$ × median fluorescence intensity (MFI)] with immature B cells of both the BM (**Figure 5.5a**) and spleen (**Figure 5.5b**). Similar results were obtained with *L. donovani* (**Figure 5.6**).

To further investigate whether DsRed$^+$ B cells are *bona fide* infected or whether the parasite is attached to or captured by the cell (**Figure 5.7**), microscopic examination and viability testing was carried out on IgM$^-$ and IgM$^+$ CD19$^+$ B cells. As documented in **Figure 5.5c**, sorted DsRed$^+$ B cells are indeed closely interacting with the parasite that underwent morphological transformation into the intracellular amastigote form. The amastigote appears attached to the cell surface rather than to reside intracellularly. The number of attached amastigotes is limited to only one or two and remains constant over time (**Figure 5.8**). This distinctive amastigote attachment was also detected *in vivo* and unrelated to the mouse strain (**Figure 5.8**). Moreover, no difference can be seen between IgM$^-$ or IgM$^+$ B cells in both BM and spleen. **Figure 5.5d** visually represents the viability test results, whereby positive promastigote back-transformation could be observed for both IgM$^-$ and IgM$^+$ B cells from the BM and spleen. These data indicate that viable *Leishmania* parasites attach to B cells in low quantities and independent of IgM expression.

To investigate the impact of this parasite interaction on B cell lysosomal activity, LysoTracker^{TM} Green was employed. DsRed$^+$ immature B cells show a higher LysoTracker^{TM} signal compared to the DsRed$^-$ population in both BM and spleen during *L. infantum* (**Figure 5.5e**) and *L. donovani* infection (**Figure 5.6**). This indicates that lysosomal activity is triggered as part of the induced immune response.

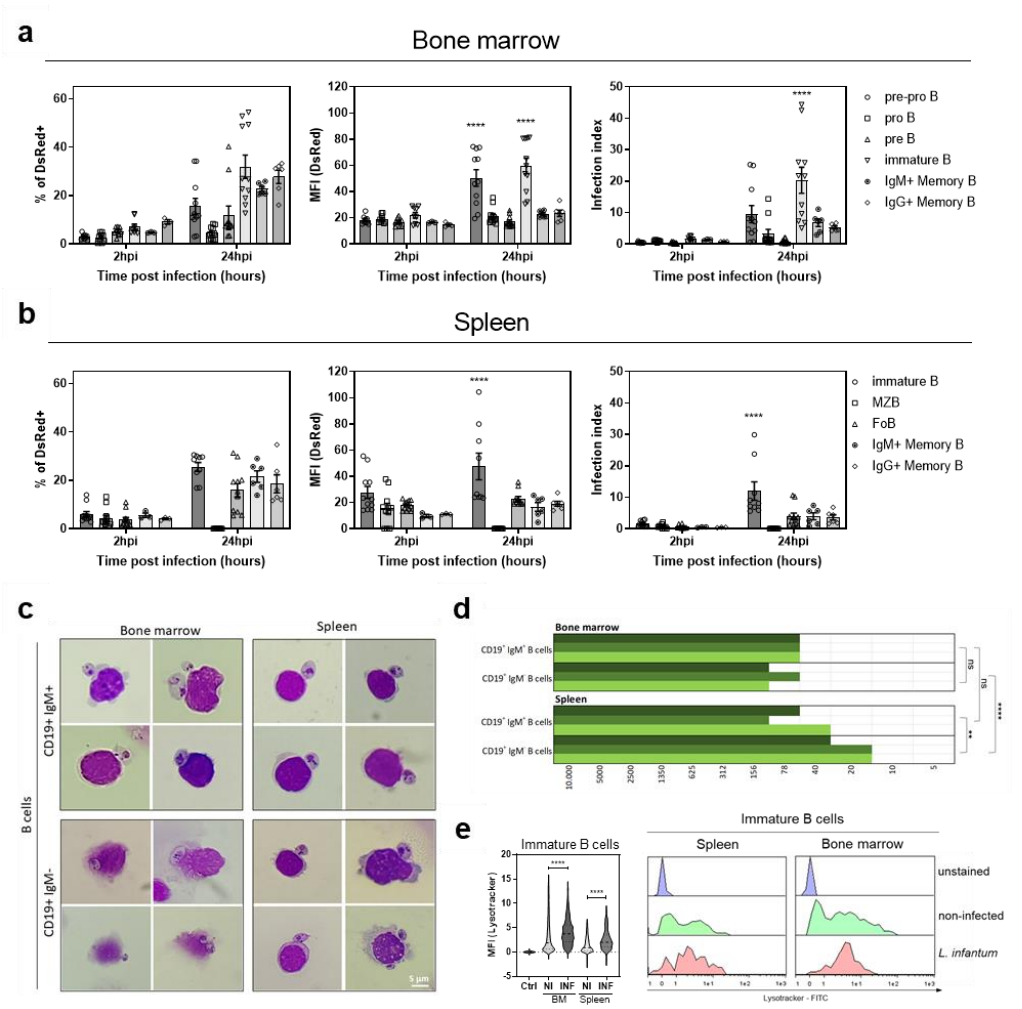

Figure 5.5. VL promastigotes attach to B cells and transform into amastigotes. (a-b) Comparison of % of DsRed+, mean fluorescence intensity (MFI) and infection index (*i.e.* % of DsRed+ × MFI) of different B cell subtypes in BM **(a)** and spleen **(b)**. Results are expressed as mean ± standard error of mean (SEM). Mann-Whitney U test. $6 < n < 11$, ****p <0.0001. **(c)** Giemsa staining of *L. infantum* infected CD19+ IgM+ and CD19+ IgM- B cells sorted from BM and spleen. Scale bar = 5 µm. **(d)** Visual representation of positive promastigote back-transformation results after sorting of DsRed+ CD19+ IgM+ and DsRed+ CD19+ IgM- B cells from BM and spleen in a ½ dilution. The number of sorted cells is indicated with a positive back-transformation shown in green. Two-way ANOVA with multiple comparisons. ns = not significant,**p <0.01 , ****p <0.0001. **(e)** LysoTracker™ MFI between DsRed- (NI) and DsRed+ immature B cells of spleen and BM after *L. infantum* infection. Ordinary one-way ANOVA with Tukey's multiple comparisons test, $359 < n < 4065$, ****p <0.0001. Unstained control is significantly lower compared to all other conditions. All results are based on at least three independent repeats performed in technical duplicate.

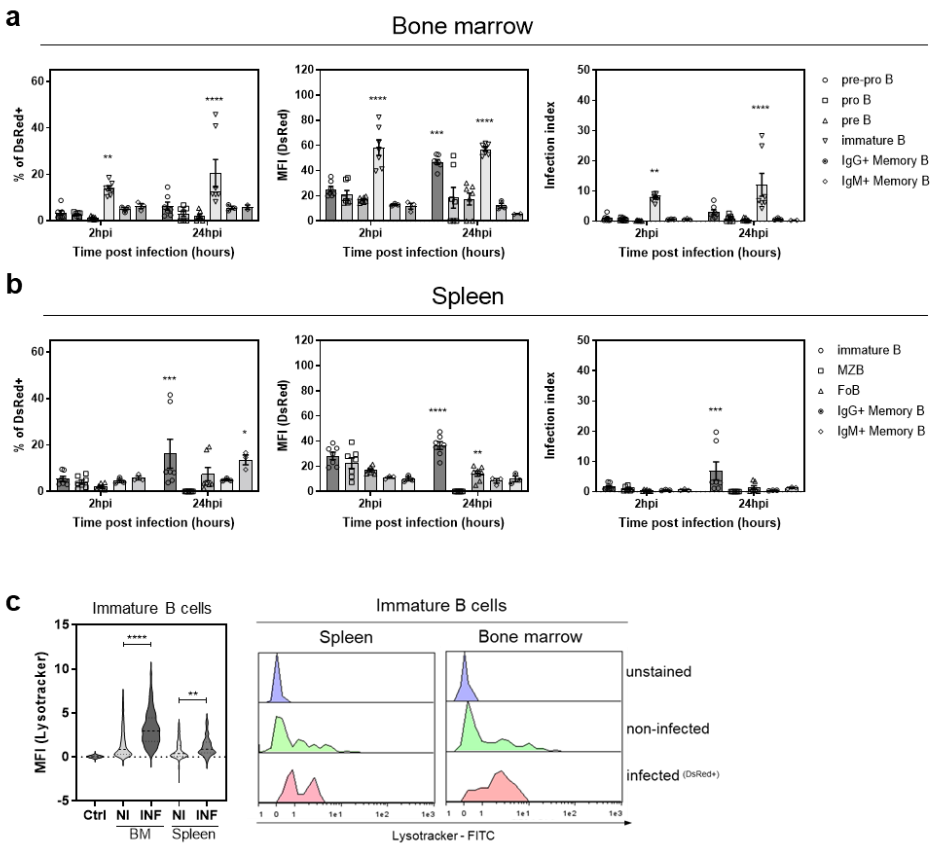

Figure 5.6. Spleen and BM infection with *L. donovani*. (a-b) Comparison of % of DsRed$^+$, mean fluorescence intensity (MFI) and infection index (*i.e.* % of DsRed$^+$ x MFI) of different B cell subtypes in BM **(a)** and spleen **(b)** infected with *L. donovani* Ldl82 WT$^{PpyRE9/DsRed}$. Results are expressed as mean ± SEM. Mann-Whitney U test. $3 < n < 7$, $*p < 0.05$, $**p < 0.01$, $****p < 0.0001$. **(c)** LysoTracker™ MFI between DsRed$^-$ (NI) and DsRed$^+$ (INF) immature B cells of spleen and BM after *L. infantum* infection. Ordinary one-way ANOVA with Tukey's multiple comparisons test, $107 < n < 4065$, $**p < 0.01$, $****p < 0.0001$. Unstained control is significantly lower compared to all other conditions ($p < 0.0001$). All results are based on at least three independent repeats.

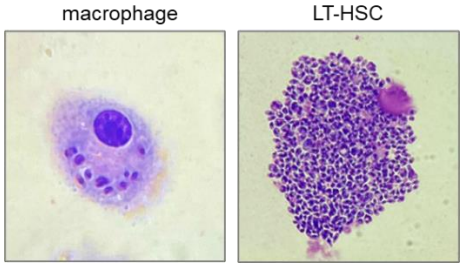

Figure 5.7. Microscopic representation of different *Leishmania* infected host cells. Giemsa staining of DsRed$^+$ sorted cells after 24 hours of *L. infantum* promastigote infection. From left to right a macrophage (CD11b$^+$F4/80$^+$), and a LT-HSC (Lin$^-$ cKit$^+$ Sca1$^+$ CD150$^+$ CD48$^-$) with intracellular amastigotes.

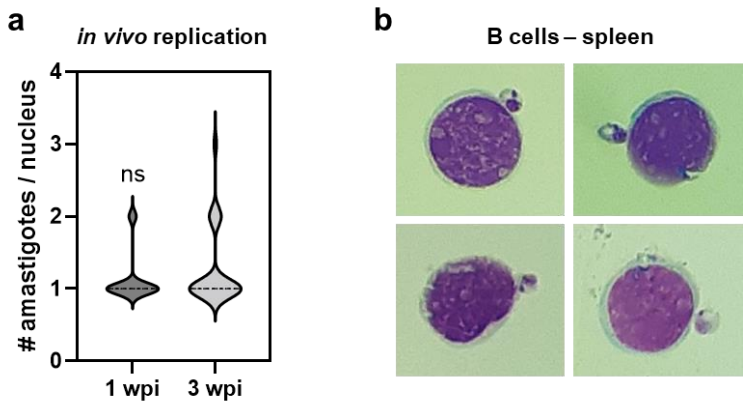

Figure 5.8. No replication of amastigotes attached to splenic B cells *in vivo*. (a) DsRed^{+} B220^{+} CD19^{+} cells in the spleen of *L. infantum* infected C57BL/6 mice were sorted after 1 and 3 weeks post-infection (wpi) and infection burden were determined microscopically. **(b)** Microscopic analysis of DsRed^{+} B220^{+} CD19^{+} cells showing a clear B cell morphology with a high nucleus/cytoplasm ratio.

VL increases B lymphopoiesis in BM and spleen.

To assess whether B cell development is affected during VL infection, as is described for African trypanosomiasis **[18, 23, 245]**, BM and spleen were collected from *L. infantum* infected BALB/c mice at predefined timepoints corresponding a non-infected condition and infection at the peak of hepatic and splenic colonization respectively, *i.e.* 0, 3 and 9 wpi (**Figure 5.9a**). During infection, an overall tendency of increase could be observed for several B cell populations in both BM (**Figure 5.9b**) and spleen (**Figure 5.9c**). Most prominently the pre-pro and pro B cells in the BM (**Figure 5.9b, d**) and FoB in the spleen (**Figure 5.9c, d**) were increased. Consistent with VL-induced splenomegaly, the amount of splenocytes consistently increased during infection, whereas BM cells were only elevated at 3 wpi (**Figure 5.9d**) **[58, 431]**. An increased number of B220^{lo} CD138^{hi} plasma cells was found in the BM of infected mice at 9 wpi. However, in the spleen these cells were reduced (**Figure 5.9b-d**).

The overall upsurge of B lymphopoiesis during VL was confirmed in an independent experiment using immunization with Alum adjuvant (**Figure 5.10**).

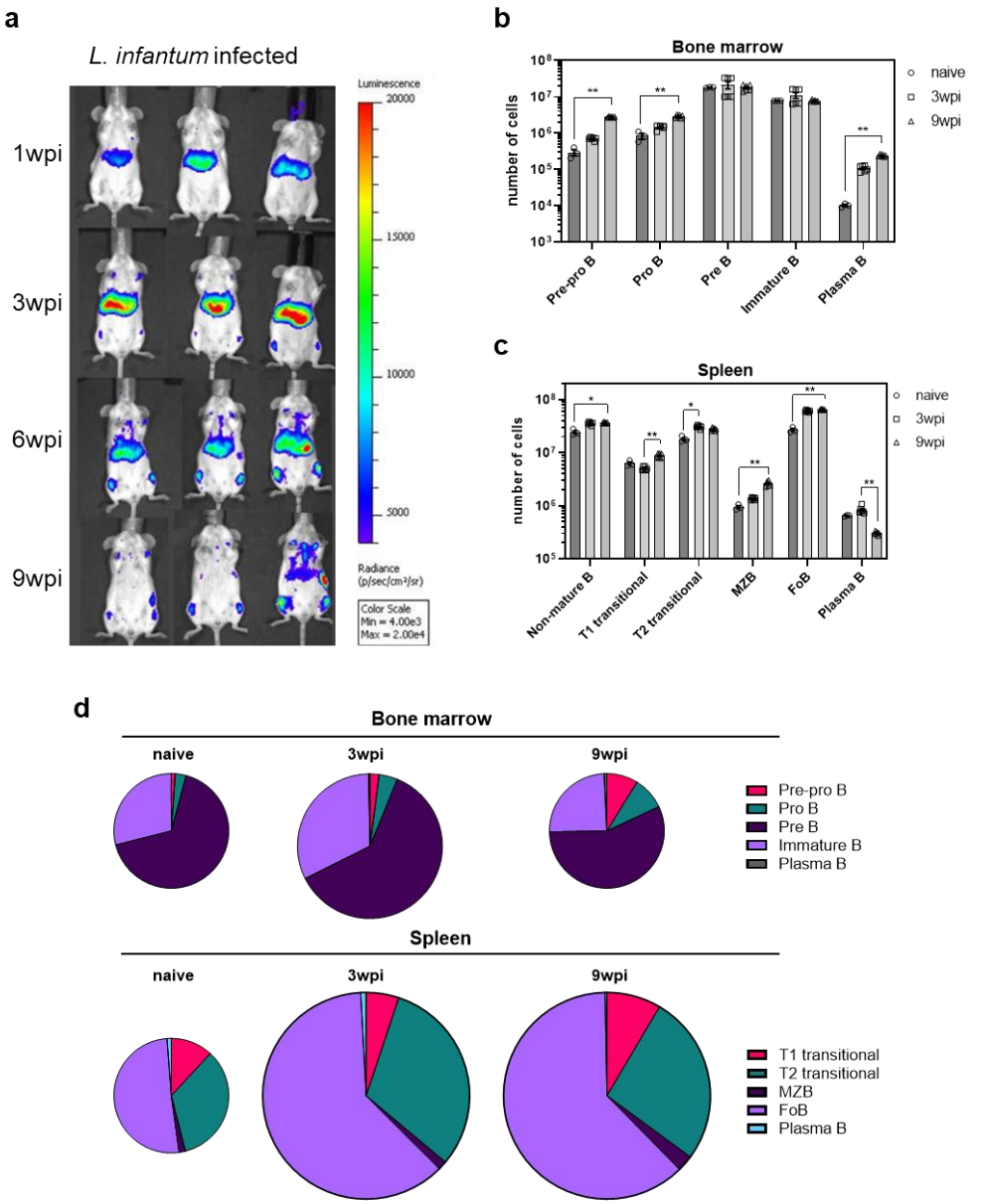

Figure 5.9. VL increases B lymphopoiesis in BM and spleen. (a) *In vivo* bioluminescent imaging using an exposure time of 15 minutes and after IP injection of D-Luciferin of *L. infantum* LEM3323 $WT^{PpyRE9/DsRed}$ infected BALB/c mice. Groups consist of 3 BALB/c mice. Mice were sacrificed at predefined timepoints (*i.e.* 3 and 9 weeks-post infection; wpi) for further analyses. **(b-c)** Absolute number of cells in BM **(b)** and spleen **(c)** of naïve (non-infected), *L. infantum* infected mice at 3 wpi and 9 wpi. Kruskal-Wallis with Dunn's multiple comparison test, $*p < 0.05$, $**p < 0.01$. **(d)** Pie charts of absolute numbers of B cell subsets in BM (top) and spleen (bottom) from (b-c). Size of pie charts is in proportion to the ratio of total number of 3 wpi or 9 wpi to naïve.

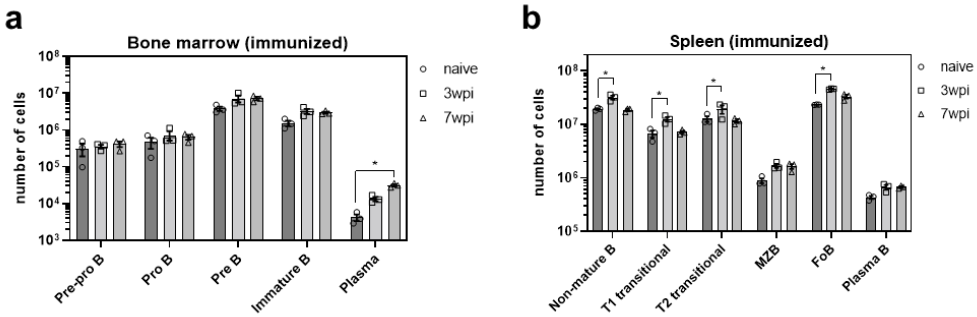

Figure 5.10. VL increases B lymphopoiesis in BM and spleen after immunization. Absolute number of cells in BM **(a)** and spleen **(b)** of immunized naïve (non-infected) and immunized *L. infantum* infected mice at 3 weeks post-infection (wpi) and 7 wpi. Groups consist of 3 BALB/c mice. Kruskal-Wallis with Dunn's multiple comparison test, $*p < 0.05$.

VL infection does not detrimentally affect pre-existing immunity

To investigate whether VL has a detrimental effect on pre-existing (vaccine-induced) immunity as described in other infections **[18, 423]**, BALB/c mice were immunized with Alum-adjuvanted fluorescent protein PE **[426]** prior to infection with *L. infantum* promastigotes (**Figure 5.11a**). During infection, mice were monitored by *in vivo* bioluminescent imaging to confirm infection burden, VL tropism and treatment outcome (**Figure 5.11b**). Animals showed a clear treatment response and relapsed by 7 wpi, consistent with the previously described post-treatment relapse model **[322] (Chapter II)**.

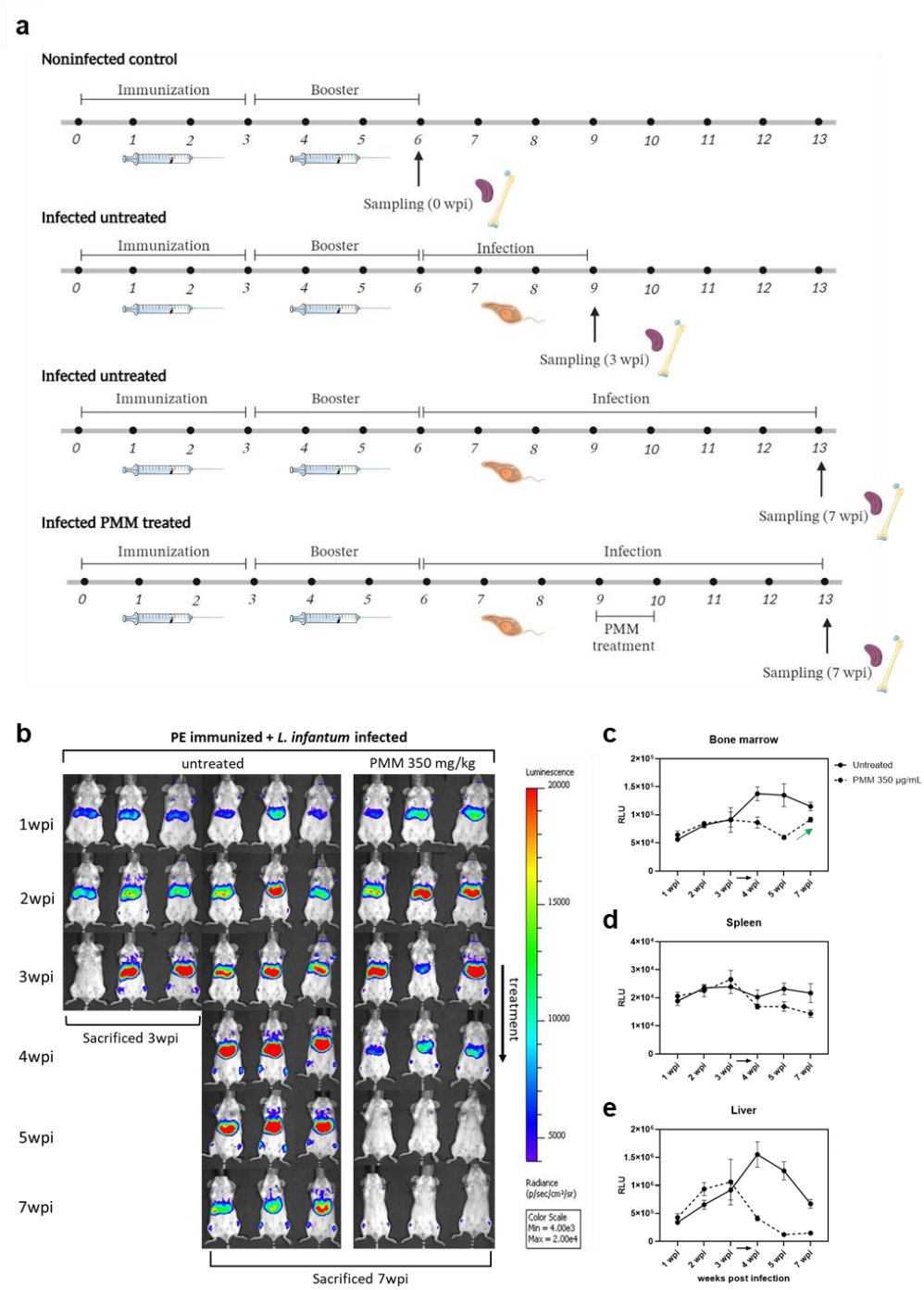

Figure 5.11. **PE specific induced immunity. (a)** Timeline of immunization protocol. Mice were immunized with an injection of PE dissolved in Imject® Alum followed by a booster injection of the same formulation three weeks later. After 6 weeks of immunization in total, mice were infected with *Leishmania* parasites. One group was treated at week 9 with PMM at 350 mg/kg body weight for 5 consecutive days. BM and spleen samples were taken at 0 wpi, 3 wpi and 7 wpi of the

noninfected control, infected untreated and infected PMM treated groups, respectively. At 0 wpi naïve non-immunized mice were additionally included as control. Groups consist of 3 BALB/c mice. This figure was created in BioRender.com. **(b)** BLI images of immunization experiment from (a). Weeks post infection (wpi). **(c-e)** Quantification of the bioluminescence signal as seen in (b) from BM, spleen and liver respectively.

To study antigen-specificity of the various B lymphocytes, BM and spleen cells were incubated with the heterologous antigen PE (used for immunization) and subjected to a specific enrichment using magnetic beads. This procedure resulted in a major enrichment of immature B cells and IgM^+ and IgG^+ memory B cells from the BM. From the spleen, especially IgM^+ and IgG^+ memory B cells were retained (**Figure 5.12**). As expected, the highest PE specific binding was observed for the memory B cells (both IgM^+ and IgG^+) and plasma cells ($B220^{lo}$ $CD138^{hi}$) of both organs, with a major increase of PE^{hi} cells after immunization as compared to non-immunized mice ($<10^2$ cells in BM, $<10^3$ cells in spleen). During infection (*i.e.* 3 and 7 wpi) PE-specific memory B cells remain stable in both BM and spleen (**Figure 5.13a-e**). Antiparasitic treatment with PMM did not change the proportion of these cells in BM and spleen. Finally, ELISA was performed to examine the impact of VL infection on antigen-specific antibody responses. A successful induction of PE-specific antibody titers was observed in immunized mice. Comparing the antibody endpoint titers, mice at 7 wpi show significantly higher PE-reactive IgG levels than non-infected mice (**Figure 5.13g-h**). It can therefore be concluded that VL infection has no major detrimental influence on pre-existing memory and even elevates circulating levels of antibodies.

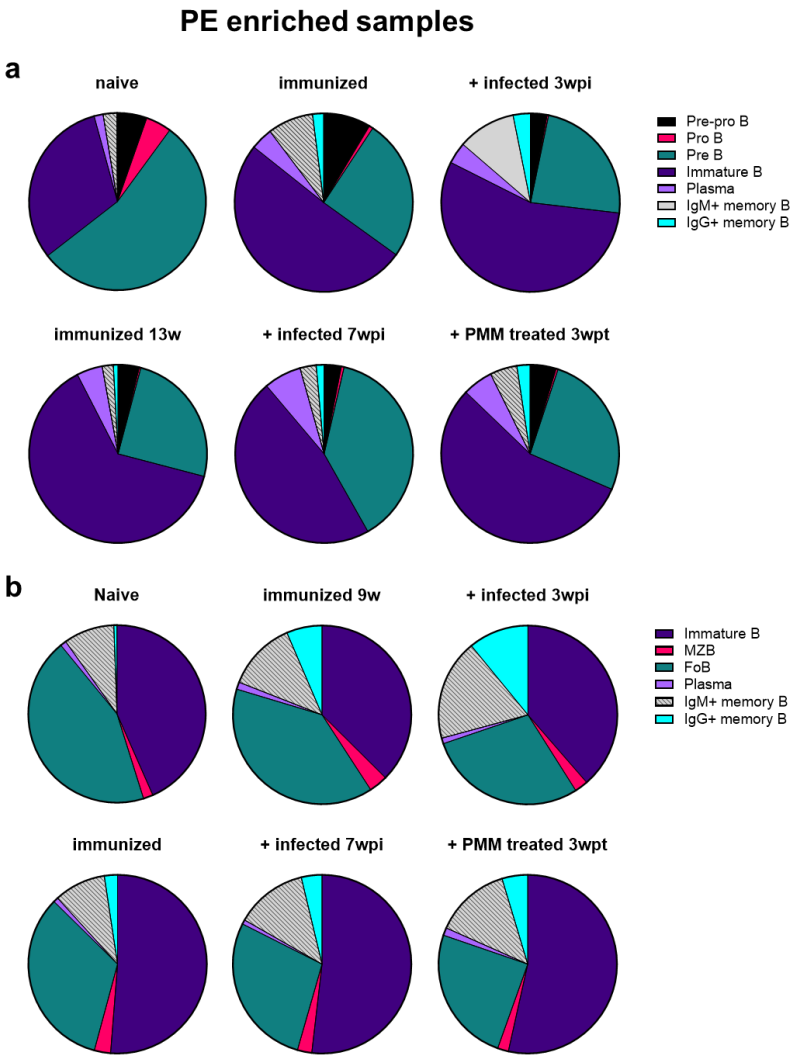

Figure 5.12. PE enrichment increases amount of immature B cells, IgM$^+$ and IgG$^+$ memory B cells. Pie charts of the absolute values of the different B cell subtypes from BM **(a)** and spleen **(b)** after PE enrichment. The comparison was made between naïve (non-immunized and non-infected), immunized, immunized + *L. infantum* infected and immunized + *L. infantum* infected mice treated with PMM. Groups consist of 3 BALB/c mice.

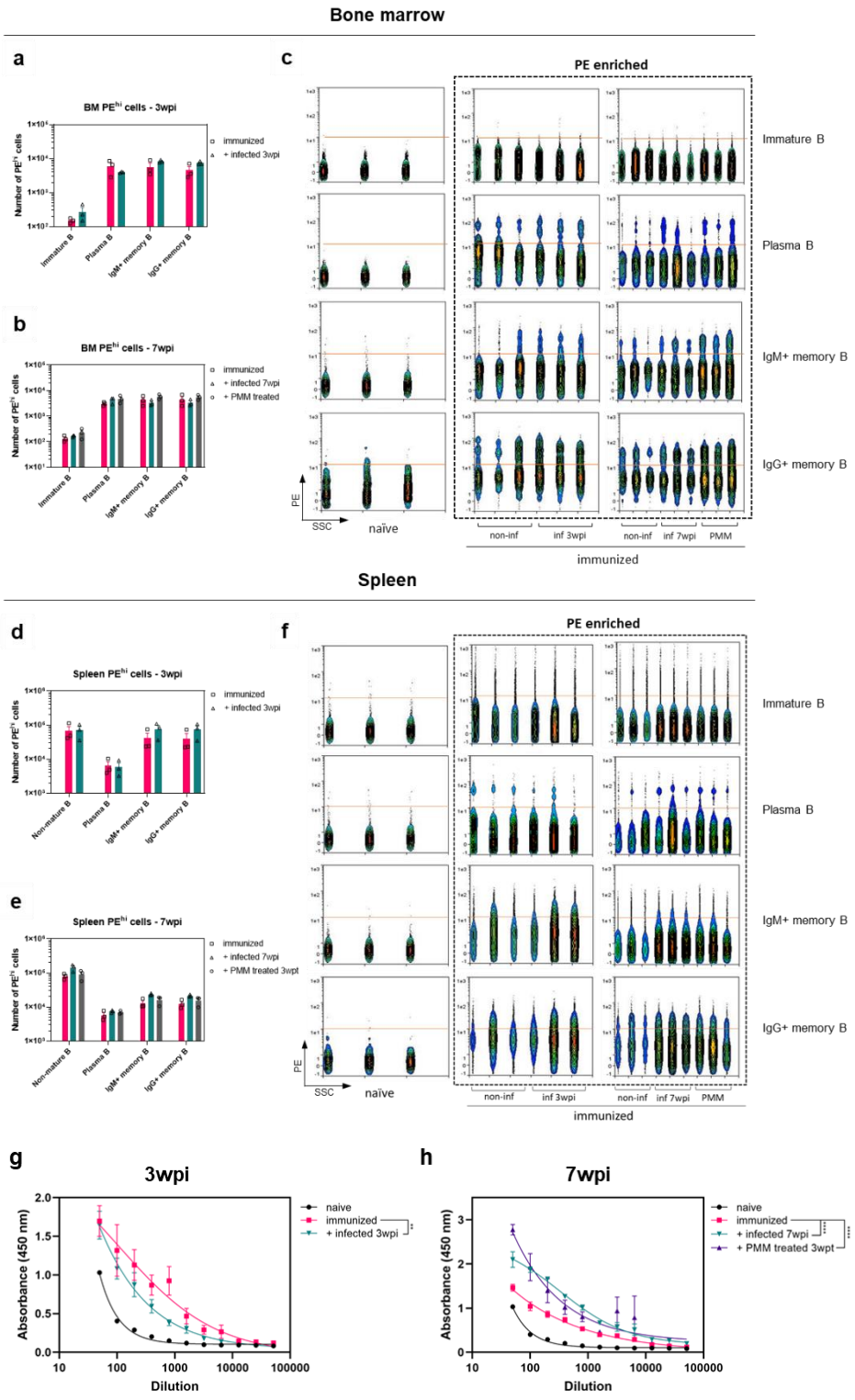
Bone marrow
a
BM PE^hi cells - 3wpi
Number of PE^hi cells
immunized
+ infected 3wpi
Immature B
Plasma B
IgM+ memory B
IgG+ memory B
b
BM PE^hi cells - 7wpi
immunized
+ infected 7wpi
+ PMM treated
c
PE enriched
Immature B
Plasma B
IgM+ memory B
IgG+ memory B
PE
SSC
naïve
non-inf
inf 3wpi
non-inf
inf 7wpi
PMM
immunized
Spleen
d
Spleen PE^hi cells - 3wpi
Non-mature B
e
Spleen PE^hi cells - 7wpi
+ PMM treated 3wpt
f
PE enriched
g
3wpi
Absorbance (450 nm)
Dilution
naive
immunized
+ infected 3wpi
h
7wpi
+ infected 7wpi
+ PMM treated 3wpt

Page 203: Figure 5.13. VL infection does not detrimentally affect antigen-specific B cell subtypes and antibody levels. Using immunization against the heterologous antigen PE, the sequelae of infection for antigen-specific B cell responses was explored. **(a-b)** Graphs of absolute numbers of PE^{hi} cells from BM after PE enrichment at 3wpi **(a)** and 7wpi **(b)**. **(c)** TitrateLogic figures showing PE^{hi} and PE^{lo} populations of immature B cells, plasma B cells, IgM^+ and IgG^+ memory B cells in BM. **(d-e)** Graphs of absolute numbers of PE^{hi} cells from spleen after PE enrichment at 3 wpi **(d)** and 7wpi **(e)**. **(f)** TitrateLogic figures showing PE^{hi} and PE^{lo} populations of immature B cells, plasma B cells, IgM^+ and IgG^+ memory B cells in spleen. **(g-h)** Tail vein serum samples were taken from naïve, PE immunized and/or *L. infantum* infected BALB/c mice and analyzed in a ½ serial dilution using PE-specific IgG detection ELISA at 3 and 7 wpi. Naïve mouse samples differed significantly from the other groups ($p < 0.0001$). Comparison of total PE-reactive IgG titers between naïve, non-infected immunized and infected immunized mice that were sacrificed at **(g)** 3 wpi and **(h)** 7 wpi. Groups consisted of 3 BALB/c mice. For all, comparisons were made between naïve (non-immunized and non-infected), immunized (non-infected), immunized + *L. infantum* infected and immunized + *L. infantum* infected mice treated with PMM using a 2-way ANOVA with Tukey's multiple comparisons test. $^{**}p < 0.01$, $^{****}p < 0.0001$.

V.5 Discussion

Although "Leishmanization" has been applied for centuries to confer long lasting immunity to leishmaniasis **[81]**, to date still no commercial human vaccine exists. Some of the challenges include finding a suitable adjuvant, the large variety of virulence and clinical manifestations of the various *Leishmania* species and strains, and the ability to produce appropriate protective long-lasting immunity **[432, 433]**. Both innate (macrophages, neutrophils, dendritic cells and natural killer cells) and adaptive immunity (T and B cells) simultaneously play a role in the antileishmanial protective immune response and disease exacerbation **[419, 434]**. In general, a protective immune response leading to parasite elimination depends on the development of a type-I immune response characterized by the initial production of IL-12 by antigen-presenting cells inducing IFN-γ-secreting Th1 cells. This will activate macrophages which in combination with recognition of glycolipids and other surface ligands through Toll-like receptors such as TLR2 **[435]** will induce the production of ROS and RNS that are highly effective in intracellular amastigote killing **[15, 16, 419, 420, 434]**. However, *Leishmania* counteracts by, for example, lipophosphoglycan (LPG) and metalloprotease GP63 that interfere with the antiparasitic signaling pathways **[17, 234, 436]**.

While the protective role of the innate immune system and Th1 cells is extensively studied, less is known about the role of B cells during leishmaniasis. Besides their polyclonal activation to generate autoreactive IgMs and IgGs, B cells represent a source of cytokines, present antigenic peptides to T cells and suppress effector memory T cell generation **[245, 250, 251, 255]**. It is not unexpected that the role of B cells in VL immunity is disregarded given the intracellular nature of the parasites. In this study, fluorescent VL strains were used for *ex vivo* infections, whereby the distinctive DsRed signal was found associated with immature B and pre-pro B cells of the BM as well as immature B cells and FoB cells of the spleen. The highest infection index was attributed to immature B cells in both organs, albeit

considerably lower compared to macrophages and LT-HSC **[322] (Chapter II)**. As corroborated in this study, promastigotes attach to B cells and even seem associated with their differentiation into amastigotes **[251, 252]**. Microscopic examination and promastigote back-transformation further revealed that amastigotes attached to $CD19^+$ B cells were viable but unable to multiply over time. De Trez *et al.* described the possibility of amastigote-transfer to other cells *in vitro* **[416]**, suggesting that B cells may function as 'carriers'. Several other pathogens use B cells for their survival or to disseminate within the body. *Brucella abortus*, for example, protects itself against bactericidal agents by targeting MZB cells **[130]**. Also *Salmonella typhimurium* can be found in splenic B cells of infected mice, in addition to pre-pro B cells, pre-B cells, immature B cells and plasma cells **[437]**. Recently, *T. cruzi* was shown to infect B cells, resulting in parasite-induced cell death which contributes to the mechanisms governing B cell depletion during infection **[438]**. *T. cruzi* is able to invade various host cells by a mechanism other than phagocytosis, such as fusion of lysosomes at the site of invasion **[54, 439]**. Hereby, the parasite takes advantage of the parasite-induced membrane damage upon cell entry, stimulating lysosomal exocytosis pathways to repair the membrane **[440]**. It was recently reported that *L. amazonensis* uses a similar mechanism to enter non-phagocytic cells, such as fibroblasts **[441]**. In our study, attachment to B cells was independent of IgM expression, contrasting the report of Bankoti *et al.* which presumed that *L. donovani* amastigote attachment to MZB was mediated by IgM acting as adhesive pockets **[251]**. Notably, we investigated the interaction with promastigotes, which represents the life cycle stage introduced by the sand fly vector. Via which route or mechanism *Leishmania* promastigotes and amastigotes can attach to or enter B cells is yet to be uncovered, but it is known that *L. donovani* amastigotes can trigger endosomal TLRs in B cells, resulting in the induction of IL-10 and type I IFN **[252]**.

Concerning the impact of VL on B cell homeostasis, an overall increase of splenic B cells, particularly FoB cells, could be observed in our mouse model. Plasma cells derived from FoB mainly produce IgG, possibly contributing to the typically

observed hypergammaglobulinemia during human VL **[245]**. The observation of an increased B lymphopoiesis in the BM can be explained as to maintain the MZB and FoB pool in the spleen. B cells participate in the immune reaction against a range of pathogens mainly as antibody-secreting cells, resulting in memory B cells that remain long after cure. However, many pathogens are able to manipulate B lymphopoiesis and responses, regardless of protective immunity **[442]**. Several related protozoan parasites such as *P. chabaudi* and *T. brucei* are capable of disrupting B lymphopoiesis by reducing the amount of pro B, pre B and immature B cells as well as induction of MZB cell apoptosis **[18, 240, 443]**. Additionally, over the last decade several pathogens have been described to hamper or deplete pre-existing immunity. Human measles infection was shown to affect the memory response to previously encountered pathogens by largely reducing previously acquired memory B cells **[19, 20, 444, 445]**. Here, a revaccination strategy with routine childhood vaccines after measles infection was implemented to rebuild the immune memory **[20]**. The gram-negative bacterium *Salmonella* produces a specific protein that selectively reduces the number of IgG-secreting plasma cells induced by vaccination or previous infections **[446, 447]**. A recent study in *T. brucei*, a pathogen closely related to *Leishmania*, confirmed that infections cause a general loss of antigen-specific splenic and BM memory B cells and a reduction in antigen-specific IgG **[423]**. In contrast, infection with *L. infantum* showed no major influence on pre-existing memory against a fluorescent heterologous antigen and even elevated circulating levels of antigen-reactive antibodies, consistent with the occurrence of hypergammaglobulinemia and large amounts of parasite-specific and non-specific antibodies **[448, 449]**. Prior reports indeed describe the polyclonal activation of B cells which leads to an increased production of low-affinity antibodies which may dilute the effects of specific, long-lived antibodies **[442, 448, 449]**. Nevertheless, VL infection does not detrimentally impair immune memory and is therefore not presumed to undermine vaccination campaigns in VL endemic areas.

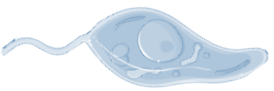

DISCUSSION AND SUMMARY

CHAPTER VI

VI. General discussion

With the ever increasing global risks of infectious diseases, cumulative related deaths and the significantly slower discovery rate of novel treatments and vaccination strategies, fundamental research remains imperative. Amongst the parasitic diseases, VL is the second leading cause of death, yet the disease remains one of the most neglected **[46]**. Infecting monocyte-derived cells from the liver, spleen and BM, VL is lethal when left untreated and is responsible for over 50,000 deaths annually **[43]**. Treatment options are scarce, and a particularly alarming situation is the increase of post-treatment relapse rates for all known antileishmanial drugs **[4, 6, 196, 197]**. Moreover, still no human vaccine exists **[450]** and information about pathogenesis and protective immunity is still scarce. Both represent an essential constraint in the development of prophylactics or long-term effective therapeutics. Given that relapse is an impediment to disease elimination and a major clinical concern, this PhD research aimed to obtain additional in-depth information on persistence of *Leishmania* parasites.

The **BM** was identified as a sanctuary site from where the host can be recolonized. In this tissue, **LT-HSC** (Lin^- $Sca1^+$ $cKit^+$ $CD48^-$ $CD150^+$) were found to constitute a hospitable cellular niche with low oxidative stress levels and harboring enormous parasite burdens, which render them more tolerant to antileishmanial drug action. As such, these cells may serve as **source of relapse**. Infected LT-HSC express a unique transcriptional signature, termed ***StemLeish***, defined by upregulated TNF/NF-kB and RGS1/TGF-β/SMAD/SKIL signaling, and a downregulated oxidative burst. Cross-species analyses demonstrated significant overlap with human VL and HIV co-infected blood transcriptomes (**Chapter II**).

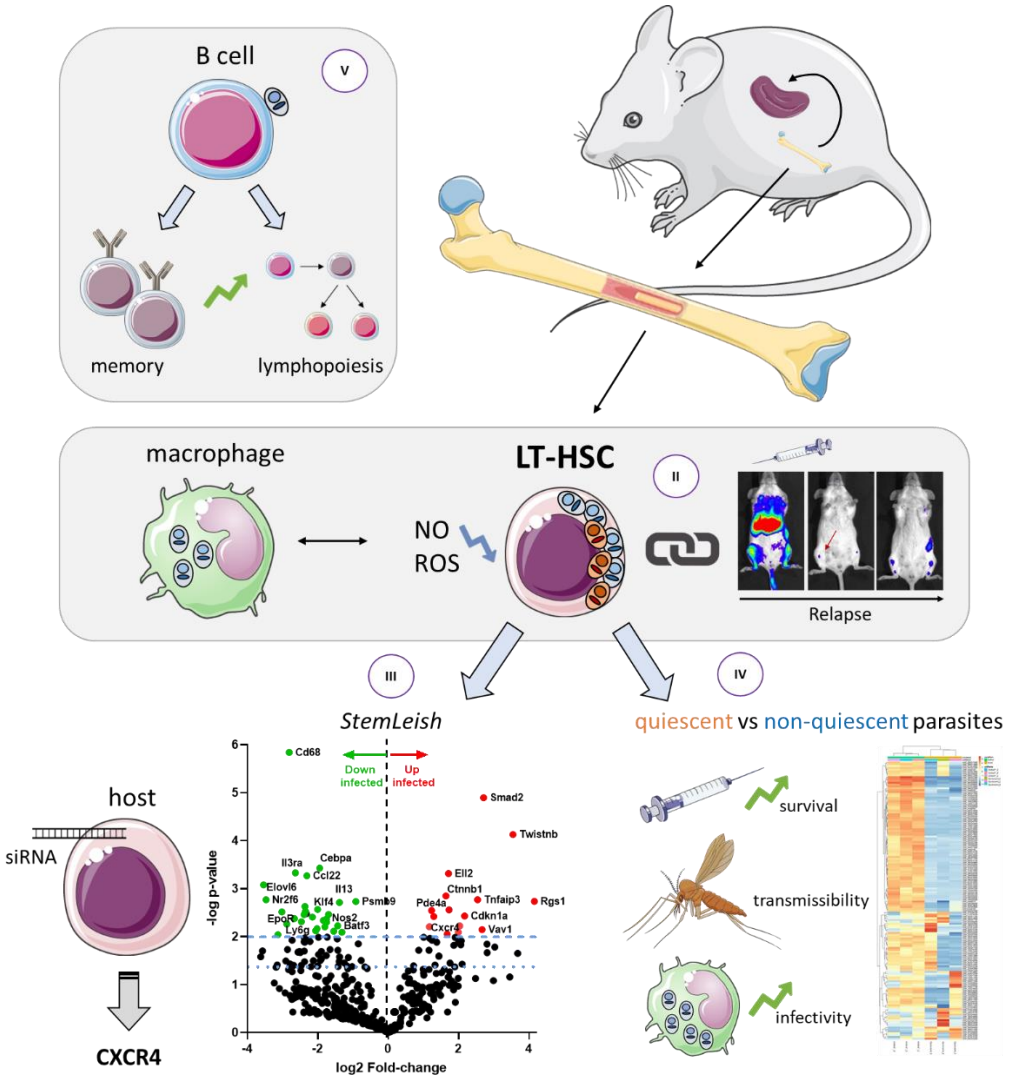

Figure 6.1. Overview of results obtained in this thesis. (II) Discovery of the LT-HSC niche linked to relapse as described in chapter II. **(III)** Defining the *StemLeish* transcriptional signature and exploring the therapeutic applications thereof as seen in chapter III. **(IV)** Parasite quiescence discovered in the LT-HSC niche and characterized in chapter IV. **(V)** *Leishmania* interacts with B cells and systemic VL infection increases B lymphopoiesis. Nitrogen oxide (NO), reactive oxygen species (ROS), small interfering RNA (siRNA).

Knockdown of major differential *StemLeish* genes *Rgs1, Cxcr4, Ell2, Vav1* and *Twistnb* confirmed their importance in regulating LT-HSC infection. Silencing *Cxcr4* partially restored the downregulated *Nos2* observed in infected LT-HSC, suggesting a central role of this gene in shaping the LT-HSC niche. *In vivo* therapeutic exploration showed that inhibition of **CXCR4** may have both beneficial or

detrimental effects depending on the used antagonist, emphasizing a pivotal balancing role in infection and pathology during VL (**Chapter III**).

Using reporter gene expression from an 18S rDNA locus as a read-out, this study unveiled that amastigotes rapidly enter **quiescence** after an estimated 4-6 divisions in LT-HSC but not in macrophages. Acquisition of a quiescent phenotype endowed parasites inside LT-HSC with a higher capacity to survive antileishmanial treatment. Parasites that transitioned through such an *in situ* quiescent stage retained a lower reporter gene expression and displayed an increased cellular infectivity and high transmission capacity through the sand fly vector. Transcriptional profiling of the two metabolic states (quiescent and non-quiescent) revealed a strongly reduced gene expression in quiescent parasites and revealed a novel set of markers and potential drivers (**Chapter IV**).

Besides the discovery of LT-HSC host cells wherein *Leishmania* thrives, also the **B cell** was found to **carry parasites**. Here, promastigotes attach independent of IgM expression and transform to the intracellular amastigote form, yet no replication could be documented. Instead of the more common negative impact of infectious diseases on B lymphopoiesis and memory development **[18-23, 423-425]**, VL infection was found to increase B cell progenitors in the BM, as well as all analyzed B cell subtypes of the spleen, which is in line with the clinical manifestation of polyclonal hypergammaglobulinemia and the occurrence of autoantibodies during VL. Using immunization against a fluorescent heterologous antigen, it was shown that VL infection does not impair immune memory, which is reassuring for vaccination campaigns in VL endemic areas (**Chapter V**).

This chapter will further reflect on specific aspects of this thesis with the intent to place the proposed findings in a broader perspective to pave the way to a future where the lethal impact of VL can be reduced.

VI. 1 Overcoming post-treatment relapse

Treatment failure of chemotherapeutic agents is a serious global health threat. Worse than receiving therapy with significant side effects is symptomatic relapse after apparent cure. Although many infectious diseases suffer from post-treatment relapse, a major knowledge gap remains regarding the underlying causes and appropriate methods to study this phenomenon. Notably, post-treatment relapse is mostly not due to reinfection, drug quality, drug exposure or drug-resistant parasites **[6, 98]** but rather due to persistence. The persistence of pathogens causing subclinical infection and subsequent relapse is common for many microorganisms **[8-12, 195, 393, 394]**. Generally, two aspects may be the underlying cause (*and these are not mutually exclusive*): pathogens residing in sanctuary sites or niches, *and/or* pathogens switching to a quiescent phenotype. The first allows pathogens to survive and escape treatment or immunity without genetic or phenotypic changes. The latter relies on phenotypic diversity, e.g. quiescent or dormant forms **[7]**. Based on our observations, treatment failure in VL most likely involves both aspects. In **Chapter II-III**, we identify a relapse-prone LT-HSC niche in the BM in which treatment is less effective, whereas in **Chapter IV** we formally link quiescent parasites residing in this particular niche to drug tolerance.

VI. 1.1 Sanctuary sites

The phenomenon of sanctuary sites or niches has been widely described for many pathogens across the microorganism spectrum. These cells and tissues provide the possibility to hide from drugs or immune responses, giving the opportunity to recolonize the host. It can be appreciated that the body comprises several potential niches ranging from specialized tissues to specific cells. Several could function as a sanctuary compartment depending on the properties of the pathogen, the concerned cell/tissue and the applied drug.

The liver can be colonized by dormant or hypnozoite stages of *P. vivax*. These stages are less susceptible to antimalarial therapies and can reactivate **[11, 293]**. The

adipose tissue has been described as a hiding place for *Trypanosoma* species, which may be less amenable for drug treatment due to a low tissue perfusion rate **[9, 294]**. Besides *Leishmania*, the BM was identified as an antibiotic-protective niche for *M. tuberculosis* where it was shown that *Mtb* can infect mesenchymal stem cells (MSC) and LT-HSC, and that they serve as reservoir **[132, 134, 292, 298]**. It was also demonstrated that even after prolonged treatment, *Mtb* survived in MSC **[8, 291]**.

It has been described that some intrinsic properties of stem cells may provide opportunities for the pathogen to evade immune responses and drug action, e.g. by avoiding the induction of cytotoxic T cell responses and by enhanced drug efflux **[122, 274]**. Here we show that VL infection substantially decreased levels of *Nos2* gene expression and of both NO and ROS in infected LT-HSC, creating a more hospitable environment for parasite survival and multiplication (**Chapter II**). This decrease in *Nos2* expression appeared to be connected to *Cxcr4*, *Twistnb* and *Vav1* upregulation (**Chapter III**). For LT-HSC, a decreased treatment response could not be linked to drug efflux and is likely related to the observed extreme high parasite burdens (**Chapter II**). Other mechanisms of the LT-HSC niche can play a role such as drug distribution to the BM **[273]**. Indeed, the concentration of drug per organ can diverge from its concentration on a cellular level, or even inside a certain niche. In general, the BM contains at least two different types of niches based on location, e.g. periosteal or perivascular. The former provides a hypoxic environment with differential sensitivity to therapy **[451]**. Zhao *et al* **[296]** showed that HSCs can be functionally distinguished into reserve HSCs and primed HSCs based on their response to chemotherapy, and which is linked to their different position in the BM niche and distance to the blood vessel. The LT-HSC are specifically in close proximity of capillary fenestrations, enabling drugs that pass through these fenestrations to directly encounter LT-HSC **[273]**. Drugs with favorable pharmacokinetic properties to target the BM would potentially be more

effective in targeting the LT-HSC burdens and prevent persistence and post-treatment relapse.

VI. 1.2 Parasite quiescence

Quiescence more commonly refers to genetically drug-susceptible, non- or slow-growing organisms that survive exposure to a given cidal drug and have the capacity to resume proliferating under specific conditions **[395]**. Investigation of the physiology of this phenotype *in vivo* is very challenging due to their scarcity and difficulty to detect them. In **Chapter IV**, we describe the rapid occurrence of quiescence in the LT-HSC niche whereby 20% of quiescent parasites could be detected within 6 hours of infection, which provided the opportunity to further investigate this phenotype. Quiescent parasites are less susceptible to chemotherapy which conceivably allows them to survive for years unnoticed in the host. A transient decreased sensitivity to drugs has been described for *T. cruzi* **[396]**, while current therapies against *T. gondii* infection are only effective against active tachyzoites and not against the dormant bradyzoites **[452]**. Both contribute to persistent infections and treatment failure without resistance **[7]**. During *Leishmania* infection, we demonstrate an increased survival of quiescent parasites in the LT-HSC niche (**Chapter IV**). Transcriptomic profiling of quiescent amastigotes revealed an overall downregulation of especially ribosomal RNA, a signature of quiescence well described in literature **[370, 399, 404, 405]**, since ribosome biosynthesis is one of the most energy intensive processes in the cell and thus a measure of the metabolic state. A large proportion of genes was downregulated in quiescent VL parasites consistent with what is found in literature on persistence. Indeed, studies have shown that DNA replication, general transcription and protein synthesis are decreased in *Plasmodium spp*. and *T. gondii* persisters **[7]**. Artificial axenic amastigote forms of *L. mexicana* and *L. braziliensis* showed downregulated synthesis of ATP, ribosomal components, proteins and alterations in membrane lipids **[14, 401]**.

Conversely, some biochemical pathways are sustained such as oxidation-reduction in *T. gondii*, *M. tuberculosis* and *P. cynomolgi* hypnozoite forms **[407-409]**. Several processes were upregulated in axenic amastigote forms of *L. braziliensis*, *i.e.* autophagy, amino acid catabolism, GP63 and amastin surface-like proteins **[370]**. In our model, the majority of consistently upregulated genes was predicted to be involved in DNA replication, cell cycle control and regulation of gene expression, however, also two metabolic genes were uncovered. These genes may serve as reliable positive markers of quiescence and may also participate in the transition of amastigotes to a quiescent state and therefore represent novel potential targets. As described before in quiescent parasites in murine lesions **[399]**, a fatty acid elongase is upregulated which may be important for maintaining a favorable parasite/host interaction as *Leishmania* polyunsaturated fatty acid metabolites are important for macrophage M2 polarization. The second gene encodes a drug/metabolite transmembrane transporter that may be implicated in conferring quiescent parasites a higher tolerance to treatment. Both positive and negative transcriptional markers or candidate drivers of entry and/or maintenance of quiescence warrant further investigation using the genetic toolbox available for *Leishmania* and may offer unprecedented insights in the universal problem of quiescence across the microorganism spectrum.

We further show that transitioning through a quiescent state has a profound impact on parasite infectivity while maintaining a high sand fly transmissibility. This suggests that the selected phenotype may pose an additional threat to leishmaniasis control programs. An increased infectivity associated with relapse of *L. donovani* infection has already been shown for MIL and Sb treatment in the Indian subcontinent **[98, 402, 403]**. Moreover, MIL and PMM resistance has also been associated with increased infectivity and higher transmissibility **[453]**, both supporting successful transmission potential of the 'enhanced' phenotype. To prevent treatment failure, we advocate that the quiescent state of *Leishmania* together with the LT-HSC niche should be considered in the early stages of the

drug discovery process. For this, the development of a performant *in vitro* assay is envisaged.

Why quiescence occurs more efficiently in the LT-HSC niche compared to macrophages remains unanswered. Initial investigation showed that individual *StemLeish* genes are not likely the direct triggers for quiescence. However, additional exploration of the transcript data of infected macrophages versus LT-HSC could be useful in elucidating the interaction of the stem cell niche and persistence. Literature describes several external triggers that induce quiescence in other pathogens, such as host immunity, drug pressure and nutritional and energetic stress **[367, 396]**. As quiescence can persist indefinitely causing lifelong infections **[7]**, scrutinizing the drivers of persistence and triggers to resume proliferation and recolonization is key to combat the precarious rise in relapse rates.

VI. 2 Versatility of VL host cells

Over the last decade, several host cells have been described for *Leishmania*, ranging from the more common macrophages, neutrophils and dendritic cells to fibroblasts and adipocytes **[52, 210]**. In **Chapter V**, another cell was found to interact with *Leishmania*, namely the B cell. More specifically, immature B and pre-pro B cells of the BM as well as immature B cells and FoB cells of the spleen. Notably, this association is markedly different than that of macrophages or LT-HSC with *Leishmania*. Here, amastigotes appear to attach to B cells extracellularly without replication, supporting a potential 'carrier' function. Microscopic examination and promastigote back-transformation further revealed that viable amastigotes were attached to $CD19^+$ B cells independent of IgM expression. This contrasts with Bankoti *et al.,* who presumed that *L. donovani* amastigote attachment on MZB was mediated by IgM acting as adhesive pockets **[251]**. DeTrez *et al.* described the possibility of amastigotes to be transferred to other cells *in vitro* **[416]**, suggesting that B cells may function as 'carriers'. B cell activation by attached *L. donovani* amastigotes was shown to trigger endosomal TLRs, resulting in the induction of

IL-10 and type I IFN **[252]**. In contrast to these studies, we investigated co-incubation with promastigotes which resulted in B cell attachment and morphological transformation into amastigotes. Via which route or mechanism *Leishmania* parasites can attach to or enter B cells is yet to uncover. *T. cruzi* can invade various host cells by a mechanism other than phagocytosis, such as fusion of lysosomes at the site of invasion **[54, 439]**, whereby the parasite takes advantage of the parasite-induced membrane damage upon cell entry, stimulating lysosomal exocytosis pathways to repair the membrane **[440]**. It was recently reported that *L. amazonensis* uses a similar mechanism to enter non-phagocytic cells, such as fibroblasts **[441]**.

What exactly propagates from the interaction of *Leishmania* with B cells remains to be clarified, although research using B cell-deficient mice shows that this interaction is beneficial for the parasite. Indeed, B cell-deficient mice are more resistant than wildtype mice to infection with *L. donovani* **[255]**. It is conceivable that B cells act as potential carrier with an extensive mobility within the host blood and lymph and capacity to enter various tissues, broadening our view of *Leishmania* as an obligate intracellular parasite targeting monocyte-derived cells.

VI. 3 Biomarkers and host-directed therapies (HDT)

Asymptomatic individuals and pre-relapse patients most likely harbor quiescent parasites in cellular niches awaiting (re)colonization, such as the LT-HSC niche in the BM **(Chapter II-IV)**. VL relapse patients have a high chance to relapse again, e.g. a recent study in Sudan using LAmB revealed that 10% of VL relapse patients had a new relapse **[196]**. Innovative detection methods are therefore needed, not only to provide proper treatment and enable accurate post-treatment follow-up, but also to tackle the dissemination of infection. Highly specific biomarkers and new host-directed therapeutic targets may serve these purposes.

In the last decade, an insurgence of studies have been conducted on the importance of biomarkers that define cure versus relapse **[454]**. As such, high post-treatment

concentrations of *Leishmania*-specific IgG1 in serum has been associated with relapse, while low (or no) concentrations are associated with cure **[455]**. Moreover, the plasma neopterin concentration, a marker of macrophage activation, has potential in identifying patients at risk of suffering an early relapse **[456]**. In **Chapter III**, we explored the role of the *StemLeish* genes, specifically *Cxcr4*, as biomarker and therapeutic target. This gene encodes for the chemokine receptor CXCR4 essential in regulating the homing and mobilization of the HSC pool **[457]**. Initial exploration already proved that *Cxcr4* is increased in the blood of VL mice and can be measured by RT-qPCR.

With the continuous risk of emerging drug resistance and the limited resources for new anti-leishmanial drug development, combining existing drugs with host immune modulators is holding promise for the future. Examples of host-directed therapies during VL infection include the combination of IL-12 and SbV, which helped in the recovery of animals infected with *L. donovani* **[202]**. Other studies were focused on promoting the production of NO and IL-12 using berberine chloride **[203]** and ROS using the biophenol oleuropein **[204]**, resulting in the improvement of immune response and promoting healing. Application of the small molecule CXCR4 inhibitor plerixafor during VL infection in mice demonstrated a beneficial reduction of the liver peak and to a lesser extent the spleen and BM burden. Further studies will be needed to explore the benefits and risks of this HDT.

VI. 4 Translation to a broader context

Experimental research is often not restricted to one pathogen, and applications may be extrapolatable to other indications. Our *StemLeish* profile (**Chapters II, III)** demonstrated a significant overlap with epigenetic and transcriptional *in vivo* signatures of both human and experimental tuberculosis. The *StemLeish* signature is significantly upregulated *in vivo* upon conversion of latent into active tuberculosis. Hence, our meta-analysis underscores the broad clinical relevance of the *StemLeish*

signature and suggests its possible use as a predictor of both *Leishmania* spp. and *M. tuberculosis* dissemination as well as therapeutic failure.

A particular gene that gained our attention is *Cxcr4*. In the last decade, CXCR4 has been described and investigated profoundly in cancer research where it plays a pivotal role in tumour development, survival, angiogenesis, metastasis, and tumour microenvironment **[458]**. In the context of HIV infection, CXCR4 is acknowledged as entry co-receptor in T-cell tropic HIV-1 strains **[459, 460]**. More recently, CXCR4 was found to be highly expressed in COVID-19 patients whereby CXCR4-positive lung 'bystander' T cells and neutrophils were correlated with disease progression and fatal outcome **[461]**, proposing the receptor as therapeutic target **[462]**. Plerixafor (AMD3100) was the first FDA-approved CXCR4 antagonist used for peripheral blood stem cell transplantation, however, toxic adverse effects after long-term administration have been described **[463]**. Fortunately, novel CXCR4 antagonists with higher safety and better pharmacological and pharmacokinetic profiles than AMD3100 are currently being developed in the context of cancer and COVID-19 research **[462, 464]**. CXCR4 antagonists are available in several different forms, including small-molecule compounds, peptides, antibodies, microRNAs and natural products, with more than ten currently in clinical trials **[465]**. The combination of plerixafor with other drugs has also been investigated with good efficacies **[466, 467]**. Innovations from these studies may accelerate progress for VL as well. While traditional drug discovery takes 6-10 years, the repurposing of drugs significantly reduces time and associated cost **[468]**, representing a spin-off opportunity for VL R&D, which unfortunately remains comparatively understudied and underfunded.

VI. 5 Future perspectives

This PhD thesis has opened multiple avenues regarding future research and application. Although much work has been done, a multitude of questions have inevitably arisen:

- What triggers relapse? What are the roles of the niche and parasite quiescence?

The *StemLeish* signature and its role in infection and relapse can be explored *in vivo* using available conditional or complete knock-out (KO) mice (e.g. $rgs1^{-/-}$ **[469]**, $cxcr4^{-/-}$) or pharmacological modulators (*i.e.* RGS-1 antagonists, CXCR4 antagonists, MAPK inhibitors). *In vivo* RNAi mediated gene silencing using modified siRNAs can be explored with lipid nanoparticle (LNP) delivery systems. Further research can be conducted to elucidate host triggers for quiescence, such as using differentially expressed genes comparing macrophage versus LT-HSC transcript data. These data can then be employed in further downstream silencing experiments. Parasite quiescence and its role in triggering relapse *in vivo* can be investigated using genetically modified parasite strains, whereby positive markers for quiescence are knocked out.

- What are parasite drivers of quiescence?

To verify that candidate parasite genes identified in **Chapter VI** are essential for quiescence, functional studies with loss-of-function mutants can be carried out using CRISPR-Cas9 and conditional knock-out systems **[470, 471]**. After identification of drivers, this information can be implemented as a prognostic tool in a biomarker context for potential relapse. Additionally, these drivers could be targeted using combination therapies to overcome relapse.

- Can we implement the LT-HSC niche and quiescence-derived parasites as drug-screening platform?

For *in vitro* screening, the collection of large numbers of LT-HSC is imperative. An *ex vivo* LT-HSC expansion protocol **[472]** could be evaluated to allow for a reliable and applicable alternative. Besides gene disruption or site-directed mutagenesis, the most promising positive marker of quiescence could be selected (based on expression level and fold change upon quiescence) to achieve *gfp*-gene tagging using the CRISPR-Cas9 methodology.

- Why is the liver resistant to recolonization after relapse in mice?

In mice, relapse specifically affects the BM and spleen, but the liver seems to have acquired a resistance to recolonization. The activation state and functional profile of $Ly6C^{hi}$ monocytes deserves further exploration. In the liver, $Ly6C^{hi}$ monocytes with a regulatory, suppressor cell-like phenotype contribute to the development of granulomas in a predominant T_h1 cytokine environment **[473]**; but in the spleen and BM, the accumulation of $Ly6C^{hi}$ monocytes seems to be detrimental to the host, resulting in higher parasite burdens **[473, 474]**.

- Can we predict relapse using host and/or parasite biomarkers?

BM and blood samples can be collected from naïve and infected mice before and after treatment, but also upon relapse from the BM. In these samples, the main *StemLeish* genes and parasite quiescence markers can be analyzed using RT-qPCR. Appropriate sensitivity and specificity and Receiver Operating Characteristic (ROC) curves to indicate diagnostic accuracy should be analyzed. Evaluation on human samples would be required for clinical validation.

- Can we improve treatment or overcome relapse by combining the *StemLeish* genes with existing antileishmanial therapy?

Several options naturally arise using inhibitors of the *StemLeish* gene products such as plerixafor (CXCR4 inhibitor) or 6NF1 (Vav1 inhibitor), or by combining RNAi mediated gene silencing with antileishmanial therapy.

- What is the biological importance of the *Leishmania* interaction with B cells and their potential carrier role?

Important to investigate is whether B cells facilitate *Leishmania* distribution throughout different host tissues using the lymphatic system and the bloodstream. The mode of attachment can be investigated using biased (pharmacological inhibitors and genetic tools) or unbiased (proteomic – interactomic) methods. On the basis of the identified interaction partners, blocking attachment *in vivo* during infection will yield basic scientific information and potentially allow therapeutic exploration.

Collectively, the results presented in this thesis provide essential fundamental insights into host-pathogen interactions and the basis of treatment failure, involving host cells and a transcriptional program of broad clinical relevance and parasite quiescence as a key metabolic feature to escape drug pressure. We propose these findings as a solid basis for new host-directed therapies in VL and as a repository for novel biomarkers of infection and relapse.

VI. 6 Summary

Visceral leishmaniasis (VL) is a lethal neglected tropical parasitic disease caused by the obligate intracellular protozoan *Leishmania* and is transmitted through the bites of female phlebotomine sand flies. In the vertebrate host, parasites propagate as amastigotes in monocyte-derived cells of the liver, spleen and bone marrow (BM), and eventually cause life-threatening complications. Treatment options are scarce, as are novel leads in the R&D pipeline. Moreover, toxicity, resistance and post-treatment relapse are common and currently no effective test-of-cure exists. There is no human vaccine available and knowledge on protective immunity is limited. All of these obstruct disease elimination and constitute a major clinical concern (**Chapter I**).

The first aim of this thesis was to unravel the origin of post-treatment relapse and make an in-depth analysis of the specific cellular tropism of *Leishmania* in the BM niche. Indeed, the BM was identified as a sanctuary site from where the host can be recolonized. A specific cell type was uncovered as source of relapse, namely the long-term hematopoietic stem cell (LT-HSC: Lin^- $Sca1^+$ $cKit^+$ $CD48^-$ $CD150^+$). An enormous number of parasites reside within this hospitable niche that is characterized by low oxidative burst levels. The excessive parasite burden renders the niche more tolerant to antileishmanial drug action. Infected LT-HSC express a unique transcriptional signature, termed *StemLeish*, defined by upregulated TNF/NF-κB and RGS1/TGF-β/SMAD/SKIL signaling. Cross-species and cross-pathology analyses revealed significant overlap with human VL and HIV co-infected blood transcriptomes, as well as tuberculosis relapse (**Chapter II**).

Using siRNA silencing, knockdown of major upregulated *StemLeish* genes *Rgs1, Cxcr4, Ell2, Vav1* and *Twistnb* confirmed their prominence in regulating LT-HSC infection. *Cxcr4* proved important for the observed decrease in oxidative burst, suggesting a central position of this gene in shaping the LT-HSC niche. *In vivo* therapeutic exploration showed that inhibition of CXCR4 presents as a double-

edged sword; both beneficial and detrimental outcomes are obtained, depending on the used antagonist. As such, CXCR4 plays a delicate and pivotal balancing role in infection and pathology during VL (**Chapter III**).

The second aim of this thesis was to evaluate post-treatment parasite characteristics and define parasite quiescence in relation with relapse. In LT-HSC, amastigotes rapidly enter quiescence after an estimated 4-6 divisions, a phenotype with a higher capacity to survive antileishmanial treatment, providing an informal link to relapse. Parasites that transitioned through such an *in situ* quiescent state displayed an increased cellular infectivity and high transmission capacity through the sand fly vector. Transcriptional profiling revealed a strongly reduced gene expression in quiescent parasites compared to their non-quiescent counterparts and revealed a novel set of markers and potential drivers for which genetic knock-outs and *gfp*-tagging is envisaged (**Chapter IV**).

The third aim of this thesis was to better understand the impact of VL on B cell lymphopoiesis and humoral immunity, and characterize the B cell-pathogen interaction. Corroborating the documented VL clinical manifestation of polyclonal hypergammaglobulinemia and the occurrence of autoantibodies, infection was found to increase B cell progenitors in the BM, as well as all analyzed B cell subtypes of the spleen. Using immunization against a fluorescent heterologous antigen, it was shown that VL infection does not impair humoral immune memory. Surprisingly, the B cell interacts with *Leishmania*, whereby it was found to carry amastigotes, extracellularly attached independent of IgM expression while remaining in a resting, non-replicative state (**Chapter V**).

Collectively, the results in this thesis deliver unprecedented insights regarding post-treatment relapse and humoral immunity during VL infection, providing novel drug targets and biomarkers for both host-directed and parasite-directed therapeutics using differential genes from quiescent amastigotes residing in a relapse-prone

niche. This data will have a direct impact on drug screening efforts tweaked to overcome relapse.

VI. 7 Samenvatting

Viscerale leishmaniasis (VL) is een dodelijke, verwaarloosde parasitaire ziekte die wordt veroorzaakt door de obligate intracellulaire protozoa *Leishmania* en wordt overgebracht door de vrouwelijke zandvlieg. In de vertebrate gastheer vermeerderen de parasieten zich als amastigoten in monocyt-afgeleide cellen van de lever, milt en beenmerg (BM), en kunnen zij uiteindelijk levensbedreigende complicaties veroorzaken. Behandelingsopties zijn schaars, evenals nieuwe geneesmiddelen in de onderzoeks- en ontwikkelingsfasen. Bovendien komen toxiciteit, resistentie en ziekte herval na behandeling (*i.e.* relapse) vaak voor en bestaat er momenteel geen doeltreffende test van genezing ('test-of-cure'). Er is geen vaccin voor mensen beschikbaar en de kennis over beschermende immuniteit is beperkt. Dit alles belemmert de eliminatie van de ziekte en vormt een groot klinisch probleem (**Hoofdstuk I**).

Het eerste doel van dit proefschrift was het ontrafelen van de oorsprong van relapse en het maken van een diepgaande analyse van het specifieke cellulaire tropisme van *Leishmania* in de BM niche. Het BM werd namelijk geïdentificeerd als een toevluchtsoord van waaruit de gastheer opnieuw gekoloniseerd kan worden. Een specifiek celtype werd ontdekt als bron van relapse, namelijk de 'lange termijn' hematopoëtische stamcel (LT-HSC: Lin- Sca1+ cKit+ CD48- CD150+). Een enorm aantal parasieten verblijft in deze gastvrije niche die gekenmerkt wordt door lage oxidatie levels. Deze enorme parasietenlast maakt de niche toleranter voor de werking van anti-*Leishmania* geneesmiddelen. Geïnfecteerde LT-HSC brengen een unieke transcriptionele signatuur tot uitdrukking, *StemLeish* genaamd, gedefinieerd door verhoogde TNF/NF-$\varkappa$B en RGS1/TGF-β/SMAD/SKIL signalering. Cross-species en cross-pathologie analyses toonden significante overlap met het

transcriptoom van humane VL en HIV co-geïnfecteerd bloed, en met tuberculose relapse (**Hoofdstuk II**).

Met behulp van siRNA silencing werden knockdowns van belangrijke opgereguleerde *StemLeish* genen *Rgs1*, *Cxcr4*, *Ell2*, *Vav1* en *Twistnb* gerealiseerd, wat hun prominente rol in het reguleren van LT-HSC infectie bevestigde. *Cxcr4* bleek belangrijk voor de waargenomen afname van de oxidatieve levels, wat een centrale positie van dit gen in de vormgeving van de LT-HSC niche suggereert. *In vivo* therapeutisch onderzoek toonde aan dat remming van CXCR4 een tweesnijdend zwaard is; zowel gunstige als nefaste resultaten werden verkregen, afhankelijk van de gebruikte antagonist. Als zodanig speelt CXCR4 een delicate en cruciale evenwichtsrol in infectie en pathologie tijdens VL (**Hoofdstuk III**).

Het tweede doel van dit proefschrift was het evalueren van de kenmerken van parasieten na behandeling en het definiëren van parasitaire quiëscentie (soort rust toestand) in relatie tot relapse. In LT-HSC transformeren amastigoten al naar een quiëscente vorm na ongeveer 4-6 delingen, een fenotype met een grotere capaciteit om anti-*Leishmania* behandeling te overleven, wat een informeel verband legt met relapse. Parasieten die dergelijke *in situ* quiëscentie toestand doormaakten, vertoonden een verhoogde cellulaire infectiviteit en een hoge transmissiecapaciteit via de zandvliegvector. Transcriptionele profilering toonde een sterk verminderde genexpressie in quiëscente parasieten in vergelijking met hun niet-quiëscente tegenhangers en onthulde een nieuwe reeks merkers en potentiële drivers waarvoor genetische knock-outs en *gfp*-tagging worden overwogen (**Hoofdstuk IV**).

Het derde doel van dit proefschrift was het beter begrijpen van de invloed van VL op de lymfopoëse van B-cellen en de humorale immuniteit, en het karakteriseren van de interactie tussen B-cellen en het pathogeen. Ter bevestiging van de gedocumenteerde klinische manifestatie van polyclonale hypergammaglobulinemie en de productie van autoantilichamen, verhoogt VL-infectie de B cel progenitors in het BM, evenals alle geanalyseerde B cel subtypen van de milt. Met behulp van

immunisatie tegen een fluorescerend heteroloog antigeen werd aangetoond dat VL-infectie het humorale immuungeheugen niet negatief aantast. Verrassend is de interactie van de B-cel met *Leishmania*, waarbij bleek dat de cel amastigoten draagt, die extracellulair gehecht zijn onafhankelijk van IgM-expressie, en in een rustende, niet-replicatieve toestand blijft (**Hoofdstuk V**).

Dit proefschrift levert ongekende inzichten op over relapse en humorale immuniteit tijdens VL-infectie, en biedt nieuwe doelwitten voor geneesmiddelen en biomerkers voor zowel gastheer- als parasietgerichte therapeutica, waarbij gebruik wordt gemaakt van differentiële genen van quiëscente amastigoten die in een relapse niche verblijven. Deze gegevens zullen een directe invloed hebben op de screening van geneesmiddelen die zijn afgestemd op het overwinnen van relapse.

References

1. Mann, S., et al., *A Review of Leishmaniasis: Current Knowledge and Future Directions.* Curr Trop Med Rep, 2021: p. 1-12.
2. (WHO), W.H.O. *leishmaniasis*. 2022 [cited 2022 december]; Available from: https://www.who.int/news-room/fact-sheets/detail/leishmaniasis.
3. Hendrickx, S., G. Caljon, and L. Maes, *Need for sustainable approaches in antileishmanial drug discovery.* Parasitol Res, 2019. **118**(10): p. 2743-2752.
4. Berbert, T.R.N., et al., *Pentavalent Antimonials Combined with Other Therapeutic Alternatives for the Treatment of Cutaneous and Mucocutaneous Leishmaniasis: A Systematic Review.* Dermatol Res Pract, 2018. **2018**: p. 9014726.
5. Jha, T.K., et al., *Randomised controlled trial of aminosidine (paromomycin) v sodium stibogluconate for treating visceral leishmaniasis in North Bihar, India.* BMJ, 1998. **316**(7139): p. 1200-5.
6. Rijal, S., et al., *Increasing failure of miltefosine in the treatment of Kala-azar in Nepal and the potential role of parasite drug resistance, reinfection, or noncompliance.* Clin Infect Dis, 2013. **56**(11): p. 1530-8.
7. Barrett, M.P., et al., *Protozoan persister-like cells and drug treatment failure.* Nat Rev Microbiol, 2019. **17**(10): p. 607-620.
8. Beamer, G., et al., *Bone marrow mesenchymal stem cells provide an antibiotic-protective niche for persistent viable Mycobacterium tuberculosis that survive antibiotic treatment.* Am J Pathol, 2014. **184**(12): p. 3170-5.
9. Ferreira, A.V., et al., *Evidence for Trypanosoma cruzi in adipose tissue in human chronic Chagas disease.* Microbes Infect, 2011. **13**(12-13): p. 1002-5.
10. Ferreira-da-Silva Mda, F., et al., *Primary skeletal muscle cells trigger spontaneous Toxoplasma gondii tachyzoite-to-bradyzoite conversion at higher rates than fibroblasts.* Int J Med Microbiol, 2009. **299**(5): p. 381-8.
11. Shanks, G.D. and N.J. White, *The activation of vivax malaria hypnozoites by infectious diseases.* Lancet Infect Dis, 2013. **13**(10): p. 900-6.
12. Tanaka, N., et al., *Use of human induced pluripotent stem cell-derived neurons as a model for Cerebral Toxoplasmosis.* Microbes Infect, 2016. **18**(7-8): p. 496-504.
13. Cabral, D.J., J.I. Wurster, and P. Belenky, *Antibiotic Persistence as a Metabolic Adaptation: Stress, Metabolism, the Host, and New Directions.* Pharmaceuticals (Basel), 2018. **11**(1).
14. Jara, M., et al., *Tracking of quiescence in Leishmania by quantifying the expression of GFP in the ribosomal DNA locus.* Sci Rep, 2019. **9**(1): p. 18951.
15. Dos-Santos, A.L., et al., *Innate immunomodulation to trypanosomatid parasite infections.* Exp Parasitol, 2016. **167**: p. 67-75.
16. Pacheco-Fernandez, T., et al., *Understanding the immune responses involved in mediating protection or immunopathology during leishmaniasis.* Biochem Soc Trans, 2021. **49**(1): p. 297-311.

17. Rossi, M. and N. Fasel, *How to master the host immune system? Leishmania parasites have the solutions!* Int Immunol, 2018. **30**(3): p. 103-111.
18. Stijlemans, B., et al., *African Trypanosomes Undermine Humoral Responses and Vaccine Development: Link with Inflammatory Responses?* Front Immunol, 2017. **8**: p. 582.
19. Petrova, V.N., et al., *Incomplete genetic reconstitution of B cell pools contributes to prolonged immunosuppression after measles.* Sci Immunol, 2019. **4**(41).
20. Mina, M.J., et al., *Measles virus infection diminishes preexisting antibodies that offer protection from other pathogens.* Science, 2019. **366**(6465): p. 599-606.
21. De Trez, C., S. Khan, and S. Magez, *T. brucei infections abrogate diverse plasma cell-mediated effector B cell responses, independently of their specificity, affinity and host genetic background.* PLoS Negl Trop Dis, 2020. **14**(6): p. e0008358.
22. Banga, S., et al., *Impact of acute malaria on pre-existing antibodies to viral and vaccine antigens in mice and humans.* PLoS One, 2015. **10**(4): p. e0125090.
23. Radwanska, M., et al., *Trypanosomiasis-induced B cell apoptosis results in loss of protective anti-parasite antibody responses and abolishment of vaccine-induced memory responses.* PLoS Pathog, 2008. **4**(5): p. e1000078.
24. Poinar, G., Jr. and R. Poinar, *Paleoleishmania proterus n. gen., n. sp., (Trypanosomatidae: Kinetoplastida) from Cretaceous Burmese amber.* Protist, 2004. **155**(3): p. 305-10.
25. Poinar, G., Jr. and R. Poinar, *Evidence of vector-borne disease of Early Cretaceous reptiles.* Vector Borne Zoonotic Dis, 2004. **4**(4): p. 281-4.
26. G, M., *The Dawn of Civilization: Egypt and Chaldæa.* Nature, 1897. **57**(1470): p. 196-197.
27. Zink, A.R., et al., *Leishmaniasis in ancient Egypt and Upper nubia.* Emerg Infect Dis, 2006. **12**(10): p. 1616-7.
28. Donovan, C., *On the possibility of the occurrence of trypanosomiasis in India. 1903.* Natl Med J India, 1994. **7**(4): p. 196, 201-2.
29. Leishman, W.B., *On the possibility of the occurrence of trypanosomiasis in India. 1903.* Natl Med J India, 1994. **7**(4): p. 196-200.
30. Steverding, D., *The history of leishmaniasis.* Parasit Vectors, 2017. **10**(1): p. 82.
31. Gibson, M.E., *The identification of kala-azar and the discovery of Leishmania donovani.* Med Hist, 1983. **27**(2): p. 203-13.
32. Abazid, N., C. Jones, and C.R. Davies, *Knowledge, attitudes and practices about leishmaniasis among cutaneous leishmaniasis patients in Aleppo, Syrian Arab Republic.* East Mediterr Health J, 2012. **18**(1): p. 7-14.
33. *The Aleppo Evil or Button.* Edinb Med J, 1875. **20**(12): p. 1142.
34. Stowers, J.H., *Case of Delhi Boil or Sore (Syn.: Oriental Sore; Aleppo Boil).* Proc R Soc Med, 1920. **13**(Dermatol Sect): p. 81-3.
35. Mans, D., A. Kent, and H. Schallig, *'Aleppo evil', 'white leprosy', 'busi yasi': biological and clinical aspects of cutaneous leishmaniasis with new insights from Suriname.* Journal of Drug Design and Research, 2016.
36. Oumeish, O.Y., *Cutaneous leishmaniasis: a historical perspective.* Clin Dermatol, 1999. **17**(3): p. 249-54.

37. Postigo, J., et al., *Global leishmaniasis surveillance: 2019–2020, a baseline for the 2030 roadmap*. 2021.
38. Parhizgari, N., N. Piazak, and E. Mostafavi, *Vector-borne diseases in Iran: epidemiology and key challenges*. Future Microbiol, 2021. **16**(1): p. 51-69.
39. Barth-Jaeggi, T. and P. Mäser, *Leishmaniasis in Europe and Central Asia: Epidemiology, Impact of Habitat and Lifestyle Changes, HIV Coinfection*, in *Neglected Tropical Diseases - Europe and Central Asia*, P. Steinmann and J. Utzinger, Editors. 2021, Springer International Publishing: Cham. p. 83-99.
40. Okwor, I. and J. Uzonna, *Social and Economic Burden of Human Leishmaniasis*. Am J Trop Med Hyg, 2016. **94**(3): p. 489-93.
41. Cloots, K., et al., *Impact of the visceral leishmaniasis elimination initiative on Leishmania donovani transmission in Nepal: a 10-year repeat survey*. Lancet Glob Health, 2020. **8**(2): p. e237-e243.
42. Sasidharan, S. and P. Saudagar, *Leishmaniasis: where are we and where are we heading?* Parasitology Research, 2021. **120**(5): p. 1541-1554.
43. Scarpini, S., et al., *Visceral Leishmaniasis: Epidemiology, Diagnosis, and Treatment Regimens in Different Geographical Areas with a Focus on Pediatrics*. Microorganisms, 2022. **10**(10).
44. de Vries, H.J.C. and H.D. Schallig, *Cutaneous Leishmaniasis: A 2022 Updated Narrative Review into Diagnosis and Management Developments*. American Journal of Clinical Dermatology, 2022. **23**(6): p. 823-840.
45. Srivastava, P., et al., *Molecular and serological markers of Leishmania donovani infection in healthy individuals from endemic areas of Bihar, India*. Trop Med Int Health, 2013. **18**(5): p. 548-54.
46. Feasey, N., et al., *Neglected tropical diseases*. Br Med Bull, 2010. **93**: p. 179-200.
47. Pace, D., *Leishmaniasis*. Journal of Infection, 2014. **69**: p. S10-S18.
48. Burza, S., S.L. Croft, and M. Boelaert, *Leishmaniasis*. Lancet, 2018. **392**(10151): p. 951-970.
49. Akhoundi, M., et al., *A Historical Overview of the Classification, Evolution, and Dispersion of Leishmania Parasites and Sandflies*. PLoS Negl Trop Dis, 2016. **10**(3): p. e0004349.
50. Kamhawi, S., *Phlebotomine sand flies and Leishmania parasites: friends or foes?* Trends Parasitol, 2006. **22**(9): p. 439-45.
51. Oliveira, F., A.M. de Carvalho, and C.I. de Oliveira, *Sand-fly saliva-leishmania-man: the trigger trio*. Front Immunol, 2013. **4**: p. 375.
52. Kaye, P. and P. Scott, *Leishmaniasis: complexity at the host-pathogen interface*. Nat Rev Microbiol, 2011. **9**(8): p. 604-15.
53. Courret, N., et al., *Biogenesis of Leishmania-harbouring parasitophorous vacuoles following phagocytosis of the metacyclic promastigote or amastigote stages of the parasites*. J Cell Sci, 2002. **115**(Pt 11): p. 2303-16.
54. Batista, M.F., et al., *The Parasitic Intracellular Lifestyle of Trypanosomatids: Parasitophorous Vacuole Development and Survival*. Front Cell Dev Biol, 2020. **8**: p. 396.
55. Pace, D., *Leishmaniasis*. J Infect, 2014. **69 Suppl 1**: p. S10-8.

56. Gossage, S.M., M.E. Rogers, and P.A. Bates, *Two separate growth phases during the development of Leishmania in sand flies: implications for understanding the life cycle.* International journal for parasitology, 2003. **33**(10): p. 1027-1034.
57. Reithinger, R., et al., *Cutaneous leishmaniasis.* Lancet Infect Dis, 2007. **7**(9): p. 581-96.
58. Torres-Guerrero, E., et al., *Leishmaniasis: a review.* F1000Res, 2017. **6**: p. 750.
59. Hendrickx, S., et al., *Experimental selection of paromomycin and miltefosine resistance in intracellular amastigotes of Leishmania donovani and L. infantum.* Parasitol Res, 2014. **113**(5): p. 1875-81.
60. Petersen, C.A. and K.J. Esch, *Reservoir Control Strategies for Leishmaniasis: Past, Present, and Future*, in *Pathogenesis of Leishmaniasis: New Developments in Research*, A. Satoskar and R. Durvasula, Editors. 2014, Springer New York: New York, NY. p. 67-75.
61. Alemayehu, B. and M. Alemayehu, *Leishmaniasis: A Review on Parasite, Vector and Reservoir Host.* Health Science Journal, 2017. **11**.
62. Medkour, H., et al., *Potential animal reservoirs (dogs and bats) of human visceral leishmaniasis due to Leishmania infantum in French Guiana.* PLoS Negl Trop Dis, 2019. **13**(6): p. e0007456.
63. Oliva, G., et al., *A randomised, double-blind, controlled efficacy trial of the LiESP/QA-21 vaccine in naive dogs exposed to two leishmania infantum transmission seasons.* PLoS Negl Trop Dis, 2014. **8**(10): p. e3213.
64. Killick-Kendrick, R., *The biology and control of phlebotomine sand flies.* Clin Dermatol, 1999. **17**(3): p. 279-89.
65. Tonelli, G.B., et al., *Sand fly behavior: much more than weak-flying.* Mem Inst Oswaldo Cruz, 2021. **116**: p. e210230.
66. Faiman, R., et al., *Studies on the flight patterns of foraging sand flies.* Acta Trop, 2011. **120**(1-2): p. 110-4.
67. Cecilio, P., A. Cordeiro-da-Silva, and F. Oliveira, *Sand flies: Basic information on the vectors of leishmaniasis and their interactions with Leishmania parasites.* Commun Biol, 2022. **5**(1): p. 305.
68. Bennis, I., et al., *Psychosocial burden of localised cutaneous Leishmaniasis: a scoping review.* BMC Public Health, 2018. **18**(1): p. 358.
69. Abadias-Granado, I., et al., *Cutaneous and Mucocutaneous Leishmaniasis.* Actas Dermosifiliogr (Engl Ed), 2021.
70. Sundar, S. and A. Singh, *Recent developments and future prospects in the treatment of visceral leishmaniasis.* Ther Adv Infect Dis, 2016. **3**(3-4): p. 98-109.
71. Saporito, L., et al., *Visceral leishmaniasis: host-parasite interactions and clinical presentation in the immunocompetent and in the immunocompromised host.* Int J Infect Dis, 2013. **17**(8): p. e572-6.
72. Karamian, M., et al., *Leishmania major infection in a patient with visceral leishmaniasis: treatment with Amphotericin B.* Parasitol Res, 2007. **101**(5): p. 1431-4.
73. Sulahian, A., et al., *Experimental pathogenicity of viscerotropic and dermotropic isolates of Leishmania infantum from immunocompromised and immunocompetent*

patients in a murine model. FEMS Immunol Med Microbiol, 1997. **17**(3): p. 131-8.
74. Kariyawasam, K., et al., *Dermotropic Leishmania donovani in Sri Lanka: visceralizing potential in clinical and preclinical studies.* Parasitology, 2018. **145**(4): p. 443-452.
75. Zijlstra, E.E., *Biomarkers in Post-kala-azar Dermal Leishmaniasis.* Front Cell Infect Microbiol, 2019. **9**: p. 228.
76. Kaufer, A., et al., *The evolution of trypanosomatid taxonomy.* Parasit Vectors, 2017. **10**(1): p. 287.
77. Kevric, I., M.A. Cappel, and J.H. Keeling, *New World and Old World Leishmania Infections: A Practical Review.* Dermatol Clin, 2015. **33**(3): p. 579-93.
78. Maurício, I.L., *Leishmania Taxonomy*, in *The Leishmaniases: Old Neglected Tropical Diseases*, F. Bruschi and L. Gradoni, Editors. 2018, Springer International Publishing: Cham. p. 15-30.
79. Pratlong, F., et al., *The Montpellier Leishmania Collection, from a Laboratory Collection to a Biological Resource Center: A 39-Year-Long Story.* Biopreserv Biobank, 2016. **14**(6): p. 470-479.
80. Younis, B.M., et al., *Safety and immunogenicity of ChAd63-KH vaccine in post-kala-azar dermal leishmaniasis patients in Sudan.* Mol Ther, 2021. **29**(7): p. 2366-2377.
81. Khamesipour, A., et al., *Leishmanization: use of an old method for evaluation of candidate vaccines against leishmaniasis.* Vaccine, 2005. **23**(28): p. 3642-8.
82. Eberhardt, E., et al., *Evaluation of a Pan-Leishmania Spliced-Leader RNA Detection Method in Human Blood and Experimentally Infected Syrian Golden Hamsters.* J Mol Diagn, 2018. **20**(2): p. 253-263.
83. Adams, E.R., et al., *Leishmaniasis direct agglutination test: using pictorials as training materials to reduce inter-reader variability and improve accuracy.* PLoS Negl Trop Dis, 2012. **6**(12): p. e1946.
84. Hagos, D.G., et al., *Performance of rapid rk39 tests for the diagnosis of visceral leishmaniasis in Ethiopia: a systematic review and meta-analysis.* BMC Infect Dis, 2021. **21**(1): p. 1166.
85. Canavate, C., et al., *Evaluation of two rK39 dipstick tests, direct agglutination test, and indirect fluorescent antibody test for diagnosis of visceral leishmaniasis in a new epidemic site in highland Ethiopia.* Am J Trop Med Hyg, 2011. **84**(1): p. 102-6.
86. Singh, O.P., et al., *Current challenges in treatment options for visceral leishmaniasis in India: a public health perspective.* Infect Dis Poverty, 2016. **5**: p. 19.
87. Alves, F., et al., *Recent Development of Visceral Leishmaniasis Treatments: Successes, Pitfalls, and Perspectives.* Clin Microbiol Rev, 2018. **31**(4).
88. Gupta, S. and Nishi, *Visceral leishmaniasis: experimental models for drug discovery.* Indian J Med Res, 2011. **133**(1): p. 27-39.
89. Hirve, S., et al., *Towards elimination of visceral leishmaniasis in the Indian subcontinent-Translating research to practice to public health.* PLoS Negl Trop Dis, 2017. **11**(10): p. e0005889.

90. Monge-Maillo, B., et al., *Visceral leishmaniasis and HIV coinfection in the Mediterranean region.* PLoS Negl Trop Dis, 2014. **8**(8): p. e3021.
91. Frezard, F., C. Demicheli, and R.R. Ribeiro, *Pentavalent antimonials: new perspectives for old drugs.* Molecules, 2009. **14**(7): p. 2317-36.
92. Reveiz, L., et al., *Interventions for American cutaneous and mucocutaneous leishmaniasis: a systematic review update.* PLoS One, 2013. **8**(4): p. e61843.
93. Pinto-Martinez, A.K., et al., *Mechanism of Action of Miltefosine on Leishmania donovani Involves the Impairment of Acidocalcisome Function and the Activation of the Sphingosine-Dependent Plasma Membrane Ca(2+) Channel.* Antimicrob Agents Chemother, 2018. **62**(1).
94. Zhang, N., et al., *Leishmania parasitophorous vacuole membranes display phosphoinositides that create conditions for continuous Akt activation and a target for miltefosine in Leishmania infections.* Cell Microbiol, 2018. **20**(11): p. e12889.
95. Kuschnir, R.C., et al., *High levels of anti-Leishmania IgG3 and low CD4(+) T cells count were associated with relapses in visceral leishmaniasis.* BMC Infect Dis, 2021. **21**(1): p. 369.
96. Horrillo, L., et al., *Clinical aspects of visceral leishmaniasis caused by L. infantum in adults. Ten years of experience of the largest outbreak in Europe: what have we learned?* Parasit Vectors, 2019. **12**(1): p. 359.
97. Hendrickx, S., et al., *Evaluating drug resistance in visceral leishmaniasis: the challenges.* Parasitology, 2018. **145**(4): p. 453-463.
98. Rai, K., et al., *Relapse after treatment with miltefosine for visceral leishmaniasis is associated with increased infectivity of the infecting Leishmania donovani strain.* mBio, 2013. **4**(5): p. e00611-13.
99. Vanaerschot, M., et al., *Treatment failure in leishmaniasis: drug-resistance or another (epi-) phenotype?* Expert Rev Anti Infect Ther, 2014. **12**(8): p. 937-46.
100. Iantorno, S.A., et al., *Gene Expression in Leishmania Is Regulated Predominantly by Gene Dosage.* mBio, 2017. **8**(5).
101. Laffitte, M.N., et al., *Plasticity of the Leishmania genome leading to gene copy number variations and drug resistance.* F1000Res, 2016. **5**: p. 2350.
102. Sterkers, Y., et al., *Novel insights into genome plasticity in Eukaryotes: mosaic aneuploidy in Leishmania.* Mol Microbiol, 2012. **86**(1): p. 15-23.
103. Dujardin, J.C., et al., *Mosaic aneuploidy in Leishmania: the perspective of whole genome sequencing.* Trends Parasitol, 2014. **30**(12): p. 554-5.
104. Lachaud, L., et al., *Constitutive mosaic aneuploidy is a unique genetic feature widespread in the Leishmania genus.* Microbes Infect, 2014. **16**(1): p. 61-6.
105. Reis-Cunha, J.L., H.O. Valdivia, and D.C. Bartholomeu, *Gene and Chromosomal Copy Number Variations as an Adaptive Mechanism Towards a Parasitic Lifestyle in Trypanosomatids.* Curr Genomics, 2018. **19**(2): p. 87-97.
106. Ponte-Sucre, A., et al., *Drug resistance and treatment failure in leishmaniasis: A 21st century challenge.* PLoS neglected tropical diseases, 2017. **11**(12): p. e0006052-e0006052.
107. Natera, S., et al., *Leishmania spp.: proficiency of drug-resistant parasites.* Int J Antimicrob Agents, 2007. **29**(6): p. 637-42.

108. Wijnant, G.-J., et al., *Tackling Drug Resistance and Other Causes of Treatment Failure in Leishmaniasis.* Frontiers in Tropical Diseases, 2022. **3**.
109. McMahon-Pratt, D. and J. Alexander, *Does the Leishmania major paradigm of pathogenesis and protection hold for New World cutaneous leishmaniases or the visceral disease?* Immunol Rev, 2004. **201**: p. 206-24.
110. Vanaerschot, M., et al., *Drug resistance in vectorborne parasites: multiple actors and scenarios for an evolutionary arms race.* FEMS Microbiol Rev, 2014. **38**(1): p. 41-55.
111. Isnard, A., M.T. Shio, and M. Olivier, *Impact of Leishmania metalloprotease GP63 on macrophage signaling.* Front Cell Infect Microbiol, 2012. **2**: p. 72.
112. de Paiva, R.M., et al., *Amastin Knockdown in Leishmania braziliensis Affects Parasite-Macrophage Interaction and Results in Impaired Viability of Intracellular Amastigotes.* PLoS Pathog, 2015. **11**(12): p. e1005296.
113. Zhang, J., et al., *Screening Novel Vaccine Candidates for Leishmania Donovani by Combining Differential Proteomics and Immunoinformatics Analysis.* Front Immunol, 2022. **13**: p. 902066.
114. Fernandes, A.P., et al., *A2 and other visceralizing proteins of Leishmania: role in pathogenesis and application for vaccine development.* Subcell Biochem, 2014. **74**: p. 77-101.
115. Aruleba, R.T., et al., *Can We Harness Immune Responses to Improve Drug Treatment in Leishmaniasis?* Microorganisms, 2020. **8**(7).
116. van Griensven, J., et al., *Leishmaniasis in immunosuppressed individuals.* Clin Microbiol Infect, 2014. **20**(4): p. 286-99.
117. Teva, A., et al., *Responses of Leishmania (Viannia) braziliensis cutaneous infection to N-methylglucamine antimoniate in the rhesus monkey (Macaca mulatta) model.* J Parasitol, 2005. **91**(4): p. 976-8.
118. Bogdan, C., et al., *Fibroblasts as host cells in latent leishmaniosis.* J Exp Med, 2000. **191**(12): p. 2121-30.
119. Scorza, B.M., et al., *Differential Activation of Human Keratinocytes by Leishmania Species Causing Localized or Disseminated Disease.* J Invest Dermatol, 2017. **137**(10): p. 2149-2156.
120. Gangneux, J.P., et al., *In vitro and ex vivo permissivity of hepatocytes for Leishmania donovani.* J Eukaryot Microbiol, 2005. **52**(6): p. 489-91.
121. Carvalho-Gontijo, R., et al., *Infection of hematopoietic stem cells by Leishmania infantum increases erythropoiesis and alters the phenotypic and functional profiles of progeny.* Cell Immunol, 2018. **326**: p. 77-85.
122. Lopes, C.S., et al., *CD271+ Mesenchymal Stem Cells as a Possible Infectious Niche for Leishmania infantum.* PLoS One, 2016. **11**(9): p. e0162927.
123. Küppers, R., *B cells under influence: transformation of B cells by Epstein-Barr virus.* Nat Rev Immunol, 2003. **3**(10): p. 801-12.
124. Shannon-Lowe, C. and M. Rowe, *Epstein Barr virus entry; kissing and conjugation.* Curr Opin Virol, 2014. **4**: p. 78-84.
125. Nothelfer, K., P.J. Sansonetti, and A. Phalipon, *Pathogen manipulation of B cells: the best defence is a good offence.* Nat Rev Microbiol, 2015. **13**(3): p. 173-84.

126. Monaco, M.C., et al., *JC virus infection of hematopoietic progenitor cells, primary B lymphocytes, and tonsillar stromal cells: implications for viral latency.* J Virol, 1996. **70**(10): p. 7004-12.
127. Remington, J.S. and E.N. Cavanaugh, *Isolation of the encysted form of Toxoplasma gondii from human skeletal muscle and brain.* N Engl J Med, 1965. **273**(24): p. 1308-10.
128. Combs, T.P., et al., *The adipocyte as an important target cell for Trypanosoma cruzi infection.* J Biol Chem, 2005. **280**(25): p. 24085-94.
129. Bechah, Y., et al., *Adipose tissue serves as a reservoir for recrudescent Rickettsia prowazekii infection in a mouse model.* PLoS One, 2010. **5**(1): p. e8547.
130. Goenka, R., et al., *B Lymphocytes provide an infection niche for intracellular bacterium Brucella abortus.* J Infect Dis, 2012. **206**(1): p. 91-8.
131. Gutiérrez-Jiménez, C., et al., *Persistence of Brucella abortus in the Bone Marrow of Infected Mice.* J Immunol Res, 2018. **2018**: p. 5370414.
132. Das, B., et al., *CD271(+) bone marrow mesenchymal stem cells may provide a niche for dormant Mycobacterium tuberculosis.* Sci Transl Med, 2013. **5**(170): p. 170ra13.
133. Reece, S.T., et al., *Mycobacterium tuberculosis-Infected Hematopoietic Stem and Progenitor Cells Unable to Express Inducible Nitric Oxide Synthase Propagate Tuberculosis in Mice.* J Infect Dis, 2018. **217**(10): p. 1667-1671.
134. Tornack, J., et al., *Human and Mouse Hematopoietic Stem Cells Are a Depot for Dormant Mycobacterium tuberculosis.* PLoS One, 2017. **12**(1): p. e0169119.
135. Bonney, K.M., et al., *Pathology and Pathogenesis of Chagas Heart Disease.* Annu Rev Pathol, 2019. **14**: p. 421-447.
136. Bourreau, E., et al., *High intralesional interleukin-10 messenger RNA expression in localized cutaneous leishmaniasis is associated with unresponsiveness to treatment.* J Infect Dis, 2001. **184**(12): p. 1628-30.
137. Katara, G.K., et al., *Foxp3 and IL-10 expression correlates with parasite burden in lesional tissues of post kala azar dermal leishmaniasis (PKDL) patients.* PLoS Negl Trop Dis, 2011. **5**(5): p. e1171.
138. Mukhopadhyay, R., et al., *Characterisation of antimony-resistant Leishmania donovani isolates: biochemical and biophysical studies and interaction with host cells.* Int J Parasitol, 2011. **41**(13-14): p. 1311-21.
139. Mukherjee, B., et al., *Antimony-resistant but not antimony-sensitive Leishmania donovani up-regulates host IL-10 to overexpress multidrug-resistant protein 1.* Proc Natl Acad Sci U S A, 2013. **110**(7): p. E575-82.
140. Peixoto, F., et al., *Evaluation of the Ability of Miltefosine Associated with Topical GM-CSF in Modulating the Immune Response of Patients with Cutaneous Leishmaniasis.* J Immunol Res, 2020. **2020**: p. 2789859.
141. Wadhone, P., et al., *Miltefosine promotes IFN-gamma-dominated anti-leishmanial immune response.* J Immunol, 2009. **182**(11): p. 7146-54.
142. Monge-Maillo, B. and R. Lopez-Velez, *Treatment Options for Visceral Leishmaniasis and HIV Coinfection.* AIDS Rev, 2016. **18**(1): p. 32-43.
143. Lindoso, J.A.L., et al., *Visceral leishmaniasis and HIV coinfection: current perspectives.* HIV AIDS (Auckl), 2018. **10**: p. 193-201.

144. Alvar, J., et al., *The relationship between leishmaniasis and AIDS: the second 10 years.* Clin Microbiol Rev, 2008. **21**(2): p. 334-59, table of contents.
145. Diro, E., et al., *High parasitological failure rate of visceral leishmaniasis to sodium stibogluconate among HIV co-infected adults in Ethiopia.* PLoS Negl Trop Dis, 2014. **8**(5): p. e2875.
146. Graepp-Fontoura, I., et al., *Epidemiological, clinical and laboratory aspects of human visceral leishmaniasis (HVL) associated with human immunodeficiency virus (HIV) coinfection: a systematic review.* Parasitology, 2018. **145**(14): p. 1801-1818.
147. Troya, J., et al., *Long term failure of miltefosine in the treatment of refractory visceral leishmaniasis in AIDS patients.* Scand J Infect Dis, 2008. **40**(1): p. 78-80.
148. Sindermann, H., et al., *Oral miltefosine for leishmaniasis in immunocompromised patients: compassionate use in 39 patients with HIV infection.* Clin Infect Dis, 2004. **39**(10): p. 1520-3.
149. Ritmeijer, K., et al., *A comparison of miltefosine and sodium stibogluconate for treatment of visceral leishmaniasis in an Ethiopian population with high prevalence of HIV infection.* Clin Infect Dis, 2006. **43**(3): p. 357-64.
150. Mahajan, R., et al., *Combination Treatment for Visceral Leishmaniasis Patients Coinfected with Human Immunodeficiency Virus in India.* Clin Infect Dis, 2015. **61**(8): p. 1255-62.
151. Diro, E., et al., *Long-term Clinical Outcomes in Visceral Leishmaniasis/Human Immunodeficiency Virus-Coinfected Patients During and After Pentamidine Secondary Prophylaxis in Ethiopia: A Single-Arm Clinical Trial.* Clin Infect Dis, 2018. **66**(3): p. 444-451.
152. Antinori, S., et al., *Leishmaniasis among organ transplant recipients.* Lancet Infect Dis, 2008. **8**(3): p. 191-9.
153. Garcia-Cordoba, F., et al., *Fatal visceral leishmaniasis, with massive bone-marrow infection, in an immunosuppressed but HIV-negative Spanish patient, after the initiation of treatment with meglumine antimoniate.* Ann Trop Med Parasitol, 2005. **99**(2): p. 125-30.
154. Moreno, D., et al., *[Visceral leishmaniasis infection in a rheumatoid arthritis patient treated with adalimumab: a case description and literature review].* Enferm Infecc Microbiol Clin, 2010. **28**(4): p. 261-2.
155. Chakravarty, J. and S. Sundar, *Current and emerging medications for the treatment of leishmaniasis.* Expert Opin Pharmacother, 2019. **20**(10): p. 1251-1265.
156. Sundar, S., et al., *Failure of pentavalent antimony in visceral leishmaniasis in India: report from the center of the Indian epidemic.* Clin Infect Dis, 2000. **31**(4): p. 1104-7.
157. Jones, C.M., S.C. Welburn, and J.D. Jones, *Treatment failure of pentavalent antimonial therapy for human visceral leishmaniasis: a meta-analysis.* Journal of Global Health Reports, 2019. **3**.
158. Carnielli, J.B.T., et al., *A Leishmania infantum genetic marker associated with miltefosine treatment failure for visceral leishmaniasis.* EBioMedicine, 2018. **36**: p. 83-91.

159. Sundar, S., et al., *Injectable paromomycin for Visceral leishmaniasis in India.* N Engl J Med, 2007. **356**(25): p. 2571-81.
160. Hailu, A., et al., *Geographical variation in the response of visceral leishmaniasis to paromomycin in East Africa: a multicentre, open-label, randomized trial.* PLoS Negl Trop Dis, 2010. **4**(10): p. e709.
161. Verrest, L., et al., *Geographical Variability in Paromomycin Pharmacokinetics Does Not Explain Efficacy Differences between Eastern African and Indian Visceral Leishmaniasis Patients.* Clin Pharmacokinet, 2021. **60**(11): p. 1463-1473.
162. Lindoso, J.A., et al., *Visceral leishmaniasis and HIV coinfection in Latin America.* PLoS Negl Trop Dis, 2014. **8**(9): p. e3136.
163. Hasker, E., et al., *Management of visceral leishmaniasis in rural primary health care services in Bihar, India.* Trop Med Int Health, 2010. **15 Suppl 2**: p. 55-62.
164. Amato, V.S., et al., *Mucosal leishmaniasis . Current scenario and prospects for treatment.* Acta Trop, 2008. **105**(1): p. 1-9.
165. Perry, M.R., et al., *Chronic exposure to arsenic in drinking water can lead to resistance to antimonial drugs in a mouse model of visceral leishmaniasis.* Proc Natl Acad Sci U S A, 2013. **110**(49): p. 19932-7.
166. Kholoud, K., et al., *Management of Leishmaniases in the Era of Climate Change in Morocco.* Int J Environ Res Public Health, 2018. **15**(7).
167. Krayem, I. and M. Lipoldova, *Role of host genetics and cytokines in Leishmania infection.* Cytokine, 2021. **147**: p. 155244.
168. Samant, M., et al., *Role of Cytokines in Experimental and Human Visceral Leishmaniasis.* Front Cell Infect Microbiol, 2021. **11**: p. 624009.
169. Perez-Cabezas, B., et al., *Understanding Resistance vs. Susceptibility in Visceral Leishmaniasis Using Mouse Models of Leishmania infantum Infection.* Front Cell Infect Microbiol, 2019. **9**: p. 30.
170. Restrepo, C.M., et al., *Gene expression patterns associated with Leishmania panamensis infection in macrophages from BALB/c and C57BL/6 mice.* PLoS Negl Trop Dis, 2021. **15**(2): p. e0009225.
171. Rijal, S., et al., *Epidemiology of Leishmania donovani infection in high-transmission foci in Nepal.* Trop Med Int Health, 2010. **15 Suppl 2**: p. 21-8.
172. Jervis, S., et al., *Variations in visceral leishmaniasis burden, mortality and the pathway to care within Bihar, India.* Parasit Vectors, 2017. **10**(1): p. 601.
173. Wondimeneh, Y., et al., *Trend analysis of visceral leishmaniasis at Addis Zemen health center, Northwest Ethiopia.* Biomed Res Int, 2014. **2014**: p. 545393.
174. Harizanov, R., et al., *Geographical distribution and epidemiological characteristics of visceral leishmaniasis in Bulgaria, 1988 to 2012.* Euro Surveill, 2013. **18**(29): p. 20531.
175. Lachaud, L., et al., *Surveillance of leishmaniases in France, 1999 to 2012.* Euro Surveill, 2013. **18**(29): p. 20534.
176. Herrador, Z., et al., *Epidemiological changes in leishmaniasis in Spain according to hospitalization-based records, 1997-2011: raising awareness towards leishmaniasis in non-HIV patients.* PLoS Negl Trop Dis, 2015. **9**(3): p. e0003594.

177. Cloots, K., et al., *Male predominance in reported Visceral Leishmaniasis cases: Nature or nurture? A comparison of population-based with health facility-reported data.* PLoS Negl Trop Dis, 2020. **14**(1): p. e0007995.
178. Satoskar, A. and J. Alexander, *Sex-determined susceptibility and differential IFN-gamma and TNF-alpha mRNA expression in DBA/2 mice infected with Leishmania mexicana.* Immunology, 1995. **84**(1): p. 1-4.
179. Travi, B.L., et al., *Gender is a major determinant of the clinical evolution and immune response in hamsters infected with Leishmania spp.* Infect Immun, 2002. **70**(5): p. 2288-96.
180. Rodriguez, N.E., et al., *Epidemiological and Experimental Evidence for Sex-Dependent Differences in the Outcome of Leishmania infantum Infection.* Am J Trop Med Hyg, 2018. **98**(1): p. 142-145.
181. Ostyn, B., et al., *Failure of miltefosine treatment for visceral leishmaniasis in children and men in South-East Asia.* PLoS One, 2014. **9**(6): p. e100220.
182. Dorlo, T.P., et al., *Failure of miltefosine in visceral leishmaniasis is associated with low drug exposure.* J Infect Dis, 2014. **210**(1): p. 146-53.
183. Rodrigues, A.M., et al., *[Factors associated with treatment failure of cutaneous leishmaniasis with meglumine antimoniate].* Rev Soc Bras Med Trop, 2006. **39**(2): p. 139-45.
184. Jara, M., et al., *Tracking of quiescence in Leishmania by quantifying the expression of GFP in the ribosomal DNA locus.* Scientific Reports, 2019. **9**(1): p. 18951.
185. Kloehn, J., et al., *Identification of Metabolically Quiescent Leishmania mexicana Parasites in Peripheral and Cured Dermal Granulomas Using Stable Isotope Tracing Imaging Mass Spectrometry.* mBio, 2021. **12**(2).
186. Windels, E.M., et al., *Antibiotics: Combatting Tolerance To Stop Resistance.* mBio, 2019. **10**(5): p. e02095-19.
187. Sundar, S. and J. Chakravarty, *Liposomal amphotericin B and leishmaniasis: dose and response.* J Glob Infect Dis, 2010. **2**(2): p. 159-66.
188. Sundar, S., et al., *Injectable Paromomycin for Visceral Leishmaniasis in India.* New England Journal of Medicine, 2007. **356**(25): p. 2571-2581.
189. Rijal, S., et al., *Increasing Failure of Miltefosine in the Treatment of Kala-azar in Nepal and the Potential Role of Parasite Drug Resistance, Reinfection, or Noncompliance.* Clinical Infectious Diseases, 2013. **56**(11): p. 1530-1538.
190. Castro, M.D., et al., *Pharmacokinetics of Miltefosine in Children and Adults with Cutaneous Leishmaniasis.* Antimicrob Agents Chemother, 2017. **61**(3).
191. Dorlo, T.P., et al., *Optimal dosing of miltefosine in children and adults with visceral leishmaniasis.* Antimicrob Agents Chemother, 2012. **56**(7): p. 3864-72.
192. Kip, A.E., et al., *Low antileishmanial drug exposure in HIV-positive visceral leishmaniasis patients on antiretrovirals: an Ethiopian cohort study.* J Antimicrob Chemother, 2021. **76**(5): p. 1258-1268.
193. Dorlo, T.P., et al., *Characterization and identification of suspected counterfeit miltefosine capsules.* Analyst, 2012. **137**(5): p. 1265-74.
194. Abtahi-Naeini, B., et al., *Gulucatime versus Glucantime: A Serious Warning on Counterfeit Medicines.* J Res Pharm Pract, 2019. **8**(4): p. 228-229.

195. McIvor, A., H. Koornhof, and B.D. Kana, *Relapse, re-infection and mixed infections in tuberculosis disease.* Pathog Dis, 2017. **75**(3).
196. Salih, N.A., et al., *Liposomal amphotericin B for complicated visceral leishmaniasis (kala-azar) in eastern Sudan: how effective is treatment for this neglected disease?* Trop Med Int Health, 2014. **19**(2): p. 146-52.
197. Atia, A.M., et al., *Sodium stibogluconate and paromomycin for treating visceral leishmaniasis under routine conditions in eastern Sudan.* Trop Med Int Health, 2015. **20**(12): p. 1674-84.
198. Naylor-Leyland, G., et al., *The increasing incidence of visceral leishmaniasis relapse in South Sudan: A retrospective analysis of field patient data from 2001-2018*. PLoS Negl Trop Dis, 2022. **16**(8): p. e0010696.
199. Adriaensen, W., et al., *Host transcriptomic signature as alternative test-of-cure in visceral leishmaniasis patients co-infected with HIV*. EBioMedicine, 2020. **55**: p. 102748.
200. Zumla, A., et al., *Host-directed therapies for infectious diseases: current status, recent progress, and future prospects.* Lancet Infect Dis, 2016. **16**(4): p. e47-63.
201. Martinez-Hernandez, J.E., et al., *Network-Based Approaches Reveal Potential Therapeutic Targets for Host-Directed Antileishmanial Therapy Driving Drug Repurposing.* Microbiol Spectr, 2021. **9**(2): p. e0101821.
202. Murray, H.W., et al., *Interleukin-12 regulates the response to chemotherapy in experimental visceral Leishmaniasis.* J Infect Dis, 2000. **182**(5): p. 1497-502.
203. Saha, P., et al., *Berberine chloride mediates its anti-leishmanial activity via differential regulation of the mitogen activated protein kinase pathway in macrophages.* PLoS One, 2011. **6**(4): p. e18467.
204. Kyriazis, I.D., et al., *The leishmanicidal activity of oleuropein is selectively regulated through inflammation- and oxidative stress-related genes.* Parasit Vectors, 2016. **9**(1): p. 441.
205. el Hag, I.A., et al., *Liver morphology and function in visceral leishmaniasis (Kala-azar).* J Clin Pathol, 1994. **47**(6): p. 547-51.
206. Murray, H.W., *Tissue granuloma structure-function in experimental visceral leishmaniasis.* Int J Exp Pathol, 2001. **82**(5): p. 249-67.
207. Kedzierski, L. and K.J. Evans, *Immune responses during cutaneous and visceral leishmaniasis.* Parasitology, 2014: p. 1-19.
208. Poulaki, A., E.T. Piperaki, and M. Voulgarelis, *Effects of Visceralising Leishmania on the Spleen, Liver, and Bone Marrow: A Pathophysiological Perspective.* Microorganisms, 2021. **9**(4).
209. Varma, N. and S. Naseem, *Hematologic changes in visceral leishmaniasis/kala azar.* Indian J Hematol Blood Transfus, 2010. **26**(3): p. 78-82.
210. Walker, D.M., et al., *Mechanisms of cellular invasion by intracellular parasites.* Cell Mol Life Sci, 2014. **71**(7): p. 1245-63.
211. Liu, D. and J.E. Uzonna, *The early interaction of Leishmania with macrophages and dendritic cells and its influence on the host immune response.* Front Cell Infect Microbiol, 2012. **2**: p. 83.

212. Lestinova, T., et al., *Insights into the sand fly saliva: Blood-feeding and immune interactions between sand flies, hosts, and Leishmania.* PLoS Negl Trop Dis, 2017. **11**(7): p. e0005600.
213. Araujo-Santos, T., et al., *Lutzomyia longipalpis saliva triggers lipid body formation and prostaglandin E(2) production in murine macrophages.* PLoS Negl Trop Dis, 2010. **4**(11): p. e873.
214. Dey, R., et al., *Gut Microbes Egested during Bites of Infected Sand Flies Augment Severity of Leishmaniasis via Inflammasome-Derived IL-1beta.* Cell Host Microbe, 2018. **23**(1): p. 134-143 e6.
215. Giraud, E., et al., *Promastigote secretory gel from natural and unnatural sand fly vectors exacerbate Leishmania major and Leishmania tropica cutaneous leishmaniasis in mice.* Parasitology, 2019. **146**(14): p. 1796-1802.
216. Dos Santos Meira, C. and L. Gedamu, *Protective or Detrimental? Understanding the Role of Host Immunity in Leishmaniasis.* Microorganisms, 2019. **7**(12).
217. Laskay, T., G. van Zandbergen, and W. Solbach, *Neutrophil granulocytes--Trojan horses for Leishmania major and other intracellular microbes?* Trends Microbiol, 2003. **11**(5): p. 210-4.
218. Wilson, M.E., et al., *Early histopathology of experimental infection with Leishmania donovani in hamsters.* J Parasitol, 1987. **73**(1): p. 55-63.
219. Moore, J.W., et al., *Functional complexity of the Leishmania granuloma and the potential of in silico modeling.* Front Immunol, 2013. **4**: p. 35.
220. Wilson, M.E., et al., *Local suppression of IFN-gamma in hepatic granulomas correlates with tissue-specific replication of Leishmania chagasi.* J Immunol, 1996. **156**(6): p. 2231-9.
221. Dutra, R.A., et al., *Splenectomy in a patient with treatment-resistant visceral leishmaniasis: a case report.* Rev Soc Bras Med Trop, 2012. **45**(1): p. 130-1.
222. Idris, M., J. Farid, and N. Gul, *Morphology Of Bone Marrow In Visceral Leishmaniasis.* J Ayub Med Coll Abbottabad, 2018. **30**(3): p. 342-344.
223. Abidin, B.M., et al., *Infection-adapted emergency hematopoiesis promotes visceral leishmaniasis.* PLoS Pathog, 2017. **13**(8): p. e1006422.
224. Pinto, A.I., et al., *TNF signalling drives expansion of bone marrow CD4+ T cells responsible for HSC exhaustion in experimental visceral leishmaniasis.* PLoS Pathog, 2017. **13**(7): p. e1006465.
225. Hammami, A., et al., *HIF-1alpha is a key regulator in potentiating suppressor activity and limiting the microbicidal capacity of MDSC-like cells during visceral leishmaniasis.* PLoS Pathog, 2017. **13**(9): p. e1006616.
226. Cotterell, S.E., C.R. Engwerda, and P.M. Kaye, *Leishmania donovani infection of bone marrow stromal macrophages selectively enhances myelopoiesis, by a mechanism involving GM-CSF and TNF-alpha.* Blood, 2000. **95**(5): p. 1642-51.
227. Cotterell, S.E., C.R. Engwerda, and P.M. Kaye, *Enhanced hematopoietic activity accompanies parasite expansion in the spleen and bone marrow of mice infected with Leishmania donovani.* Infect Immun, 2000. **68**(4): p. 1840-8.

228. Preham, O., et al., *CD4(+) T Cells Alter the Stromal Microenvironment and Repress Medullary Erythropoiesis in Murine Visceral Leishmaniasis.* Front Immunol, 2018. **9**: p. 2958.
229. Ruhland, A., N. Leal, and P.E. Kima, *Leishmania promastigotes activate PI3K/Akt signalling to confer host cell resistance to apoptosis.* Cell Microbiol, 2007. **9**(1): p. 84-96.
230. Gupta, G., S. Oghumu, and A.R. Satoskar, *Mechanisms of immune evasion in leishmaniasis.* Adv Appl Microbiol, 2013. **82**: p. 155-84.
231. Moradin, N. and A. Descoteaux, *Leishmania promastigotes: building a safe niche within macrophages.* Front Cell Infect Microbiol, 2012. **2**: p. 121.
232. Desjardins, M. and A. Descoteaux, *Inhibition of phagolysosomal biogenesis by the Leishmania lipophosphoglycan.* J Exp Med, 1997. **185**(12): p. 2061-8.
233. Lodge, R. and A. Descoteaux, *Phagocytosis of Leishmania donovani amastigotes is Rac1 dependent and occurs in the absence of NADPH oxidase activation.* Eur J Immunol, 2006. **36**(10): p. 2735-44.
234. Olivier, M., et al., *Leishmania virulence factors: focus on the metalloprotease GP63.* Microbes Infect, 2012. **14**(15): p. 1377-89.
235. Calegari-Silva, T.C., et al., *NF-kappaB-mediated repression of iNOS expression in Leishmania amazonensis macrophage infection.* Immunol Lett, 2009. **127**(1): p. 19-26.
236. Mise-Omata, S., et al., *The NF-kappaB RelA subunit confers resistance to Leishmania major by inducing nitric oxide synthase 2 and Fas expression but not Th1 differentiation.* J Immunol, 2009. **182**(8): p. 4910-6.
237. Oghumu, S., et al., *Role of chemokines in regulation of immunity against leishmaniasis.* Exp Parasitol, 2010. **126**(3): p. 389-96.
238. Ato, M., et al., *Defective CCR7 expression on dendritic cells contributes to the development of visceral leishmaniasis.* Nat Immunol, 2002. **3**(12): p. 1185-91.
239. Evans, T.G., et al., *Evaluation of antibody responses in American visceral leishmaniasis by ELISA and immunoblot.* Mem Inst Oswaldo Cruz, 1989. **84**(2): p. 157-66.
240. Bockstal, V., et al., *T. brucei infection reduces B lymphopoiesis in bone marrow and truncates compensatory splenic lymphopoiesis through transitional B-cell apoptosis.* PLoS Pathog, 2011. **7**(6): p. e1002089.
241. LeBien, T.W., Tedder, T. F., *B lymphocytes: how they develop and function.* Blood, 2008. **112**.
242. Allman, D. and S. Pillai, *Peripheral B cell subsets.* Curr Opin Immunol, 2008. **20**(2): p. 149-57.
243. LeBien, T.W. and T.F. Tedder, *B lymphocytes: how they develop and function.* Blood, 2008. **112**(5): p. 1570-80.
244. Ikeogu, N.M., et al., *Leishmania Immunity: Advancing Immunotherapy and Vaccine Development.* Microorganisms, 2020. **8**(8).
245. Silva-Barrios, S., T. Charpentier, and S. Stager, *The Deadly Dance of B Cells with Trypanosomatids.* Trends Parasitol, 2018. **34**(2): p. 155-171.

246. Elassad, A.M., et al., *The significance of blood levels of IgM, IgA, IgG and IgG subclasses in Sudanese visceral leishmaniasis patients.* Clin Exp Immunol, 1994. **95**(2): p. 294-9.
247. Soares, R.R., et al., *What do we know about the role of regulatory B cells (Breg) during the course of infection of two major parasitic diseases, malaria and leishmaniasis?* Pathog Glob Health, 2017. **111**(3): p. 107-115.
248. Hasker, E., et al., *Strong Association between Serological Status and Probability of Progression to Clinical Visceral Leishmaniasis in Prospective Cohort Studies in India and Nepal.* PLOS Neglected Tropical Diseases, 2014. **8**(1): p. e2657.
249. Woelbing, F., et al., *Uptake of Leishmania major by dendritic cells is mediated by Fcgamma receptors and facilitates acquisition of protective immunity.* J Exp Med, 2006. **203**(1): p. 177-88.
250. Cabral, S.M., et al., *A Leishmania infantum cytosolic tryparedoxin activates B cells to secrete interleukin-10 and specific immunoglobulin.* Immunology, 2008. **123**(4): p. 555-65.
251. Bankoti, R., et al., *Marginal zone B cells regulate antigen-specific T cell responses during infection.* J Immunol, 2012. **188**(8): p. 3961-71.
252. Silva-Barrios, S., et al., *Innate Immune B Cell Activation by Leishmania donovani Exacerbates Disease and Mediates Hypergammaglobulinemia.* Cell Rep, 2016. **15**(11): p. 2427-37.
253. Miles, S.A., et al., *A role for IgG immune complexes during infection with the intracellular pathogen Leishmania.* J Exp Med, 2005. **201**(5): p. 747-54.
254. Kumar, R. and S. Nylen, *Immunobiology of visceral leishmaniasis.* Front Immunol, 2012. **3**: p. 251.
255. Goncalves, R., S.M. Christensen, and D.M. Mosser, *Humoral immunity in leishmaniasis - Prevention or promotion of parasite growth?* Cytokine X, 2020. **2**(4): p. 100046.
256. Yarali, N., et al., *Myelodysplastic features in visceral leishmaniasis.* Am J Hematol, 2002. **71**(3): p. 191-5.
257. Ali, N. and S. Hussain, *Leishmania donovani bodies in bone marrow.* Clin Case Rep, 2014. **2**(5): p. 238-9.
258. Dantas Brito, M., et al., *Visceral leishmaniasis: a differential diagnosis to remember after bone marrow transplantation.* Case Rep Hematol, 2014. **2014**: p. 587912.
259. Gawade, S., et al., *Visceral leishmaniasis: A case report.* Australas Med J, 2012. **5**(2): p. 130-4.
260. Lima-Junior, D.S., et al., *Inflammasome-derived IL-1beta production induces nitric oxide-mediated resistance to Leishmania.* Nat Med, 2013. **19**(7): p. 909-15.
261. Novais, F.O., et al., *Human classical monocytes control the intracellular stage of Leishmania braziliensis by reactive oxygen species.* J Infect Dis, 2014. **209**(8): p. 1288-96.
262. Bulte, D., et al., *Miltefosine enhances infectivity of a miltefosine-resistant Leishmania infantum strain by attenuating its innate immune recognition.* PLoS Negl Trop Dis, 2021. **15**(7): p. e0009622.

263. Lo Celso, C. and D. Scadden, *Isolation and transplantation of hematopoietic stem cells (HSCs).* J Vis Exp, 2007(2): p. 157.
264. Amend, S.R., K.C. Valkenburg, and K.J. Pienta, *Murine Hind Limb Long Bone Dissection and Bone Marrow Isolation.* J Vis Exp, 2016(110).
265. Dobson, K.R., et al., *Centrifugal isolation of bone marrow from bone: an improved method for the recovery and quantitation of bone marrow osteoprogenitor cells from rat tibiae and femurae.* Calcif Tissue Int, 1999. **65**(5): p. 411-3.
266. Inaba, K., et al., *Generation of large numbers of dendritic cells from mouse bone marrow cultures supplemented with granulocyte/macrophage colony-stimulating factor.* J Exp Med, 1992. **176**(6): p. 1693-702.
267. ncbi. *Supplementary data 1.* 2022; Available from: https://www.ncbi.nlm.nih.gov/pmc/articles/PMC9233693/bin/42003_2022_3591_MOESM3_ESM.xlsx.
268. Tegazzini, D., et al., *A Replicative In Vitro Assay for Drug Discovery against Leishmania donovani.* Antimicrob Agents Chemother, 2016. **60**(6): p. 3524-32.
269. Subramanian, A., et al., *Gene set enrichment analysis: a knowledge-based approach for interpreting genome-wide expression profiles.* Proc Natl Acad Sci U S A, 2005. **102**(43): p. 15545-50.
270. Wang, P., et al., *ImmuCo: a database of gene co-expression in immune cells.* Nucleic Acids Res, 2015. **43**(Database issue): p. D1133-9.
271. Maes, L., P. Cos, and S.L. Croft, *The Relevance of Susceptibility Tests, Breakpoints, and Markers*, in *Drug Resistance in Leishmania Parasites: Consequences, Molecular Mechanisms and Possible Treatments*, A. Ponte-Sucre, E. Diaz, and M. Padrón-Nieves, Editors. 2013, Springer Vienna: Vienna. p. 407-429.
272. Van den Kerkhof, M., et al., *Antileishmanial Aminopyrazoles: Studies into Mechanisms and Stability of Experimental Drug Resistance.* Antimicrob Agents Chemother, 2020. **64**(9).
273. Mu, C.F., et al., *Targeted drug delivery for tumor therapy inside the bone marrow.* Biomaterials, 2018. **155**: p. 191-202.
274. Ng, A.P. and W.S. Alexander, *Haematopoietic stem cells: past, present and future.* Cell Death Discov, 2017. **3**: p. 17002.
275. Dittus, C. and D. Semmel, *Leishmania amastigotes visualized on bone marrow aspirate in a leishmaniasis and HIV coinfected patient presenting with pancytopenia.* Blood, 2013. **122**(26): p. 4162.
276. Zhang, G., et al., *A case of visceral leishmaniasis found by left oblique hernia: A case report.* Exp Ther Med, 2020. **19**(4): p. 2697-2701.
277. Bunting, K.D., *ABC transporters as phenotypic markers and functional regulators of stem cells.* Stem Cells, 2002. **20**(1): p. 11-20.
278. Valiathan, R., et al., *Leishmania donovani: effect of verapamil on in vitro susceptibility of promastigote and amastigote stages of Indian clinical isolates to sodium stibogluconate.* Exp Parasitol, 2006. **114**(2): p. 103-8.

279. Rodriguez, N.E., H.K. Chang, and M.E. Wilson, *Novel program of macrophage gene expression induced by phagocytosis of Leishmania chagasi.* Infect Immun, 2004. **72**(4): p. 2111-22.
280. ncbi. *Supplementary data 2*. 2022; Available from: https://www.ncbi.nlm.nih.gov/pmc/articles/PMC9233693/bin/42003_2022_3591_MOESM4_ESM.xlsx.
281. Frade, A.F., et al., *TGFB1 and IL8 gene polymorphisms and susceptibility to visceral leishmaniasis.* Infect Genet Evol, 2011. **11**(5): p. 912-6.
282. Gardinassi, L.G., et al., *Blood Transcriptional Profiling Reveals Immunological Signatures of Distinct States of Infection of Humans with Leishmania infantum.* PLoS Negl Trop Dis, 2016. **10**(11): p. e0005123.
283. Gatto, M., et al., *Transcriptional analysis of THP-1 cells infected with Leishmania infantum indicates no activation of the inflammasome platform.* PLoS Negl Trop Dis, 2020. **14**(1): p. e0007949.
284. Khouri, R., et al., *IFN-beta impairs superoxide-dependent parasite killing in human macrophages: evidence for a deleterious role of SOD1 in cutaneous leishmaniasis.* J Immunol, 2009. **182**(4): p. 2525-31.
285. Khouri, R., et al., *DETC induces Leishmania parasite killing in human in vitro and murine in vivo models: a promising therapeutic alternative in Leishmaniasis.* PLoS One, 2010. **5**(12): p. e14394.
286. Zhou, G., et al., *NetworkAnalyst 3.0: a visual analytics platform for comprehensive gene expression profiling and meta-analysis.* Nucleic Acids Res, 2019. **47**(W1): p. W234-W241.
287. Fakiola, M., et al., *Transcriptional blood signatures for active and amphotericin B treated visceral leishmaniasis in India.* PLoS Negl Trop Dis, 2019. **13**(8): p. e0007673.
288. Wauters, E., et al., *Discriminating mild from critical COVID-19 by innate and adaptive immune single-cell profiling of bronchoalveolar lavages.* Cell Res, 2021. **31**(3): p. 272-290.
289. Scriba, T.J., et al., *Sequential inflammatory processes define human progression from M. tuberculosis infection to tuberculosis disease.* PLoS Pathog, 2017. **13**(11): p. e1006687.
290. Zheng, S., et al., *Molecular transitions in early progenitors during human cord blood hematopoiesis.* Mol Syst Biol, 2018. **14**(3): p. e8041.
291. Berry, M.P., et al., *An interferon-inducible neutrophil-driven blood transcriptional signature in human tuberculosis.* Nature, 2010. **466**(7309): p. 973-7.
292. Delgobo, M., et al., *An evolutionary recent IFN/IL-6/CEBP axis is linked to monocyte expansion and tuberculosis severity in humans.* Elife, 2019. **8**.
293. Rishikesh, K. and K. Saravu, *Primaquine treatment and relapse in Plasmodium vivax malaria.* Pathog Glob Health, 2016. **110**(1): p. 1-8.
294. Trindade, S., et al., *Trypanosoma brucei Parasites Occupy and Functionally Adapt to the Adipose Tissue in Mice.* Cell Host Microbe, 2016. **19**(6): p. 837-48.
295. Frayn, K.N. and F. Karpe, *Regulation of human subcutaneous adipose tissue blood flow.* Int J Obes (Lond), 2014. **38**(8): p. 1019-26.

296. Zhao, M., et al., *N-Cadherin-Expressing Bone and Marrow Stromal Progenitor Cells Maintain Reserve Hematopoietic Stem Cells.* Cell Rep, 2019. **26**(3): p. 652-669 e6.
297. Sundar, S. and J. Chakravarty, *Investigational drugs for visceral leishmaniasis.* Expert Opin Investig Drugs, 2015. **24**(1): p. 43-59.
298. Belay, M., et al., *Detection of Mycobacterium tuberculosis complex DNA in CD34-positive peripheral blood mononuclear cells of asymptomatic tuberculosis contacts: an observational study.* Lancet Microbe, 2021. **2**(6): p. e267-e275.
299. Grinenko, T., et al., *Hematopoietic stem cells can differentiate into restricted myeloid progenitors before cell division in mice.* Nat Commun, 2018. **9**(1): p. 1898.
300. Ema, H., Y. Morita, and T. Suda, *Heterogeneity and hierarchy of hematopoietic stem cells.* Exp Hematol, 2014. **42**(2): p. 74-82 e2.
301. Seita, J. and I.L. Weissman, *Hematopoietic stem cell: self-renewal versus differentiation.* Wiley Interdiscip Rev Syst Biol Med, 2010. **2**(6): p. 640-53.
302. Gomes, A.C., M. Saraiva, and M.S. Gomes, *The bone marrow hematopoietic niche and its adaptation to infection.* Semin Cell Dev Biol, 2020.
303. Pittenger, M.F., et al., *Mesenchymal stem cell perspective: cell biology to clinical progress.* NPJ Regen Med, 2019. **4**: p. 22.
304. Ichiryu, N. and P.J. Fairchild, *Immune privilege of stem cells.* Methods Mol Biol, 2013. **1029**: p. 1-16.
305. Boulais, P.E. and P.S. Frenette, *Making sense of hematopoietic stem cell niches.* Blood, 2015. **125**(17): p. 2621-9.
306. Morrison, S.J. and D.T. Scadden, *The bone marrow niche for haematopoietic stem cells.* Nature, 2014. **505**(7483): p. 327-34.
307. Challen, G.A., et al., *Mouse hematopoietic stem cell identification and analysis.* Cytometry A, 2009. **75**(1): p. 14-24.
308. Kiel, M.J., et al., *SLAM family receptors distinguish hematopoietic stem and progenitor cells and reveal endothelial niches for stem cells.* Cell, 2005. **121**(7): p. 1109-21.
309. Sarkar, A., et al., *Monitoring of intracellular nitric oxide in leishmaniasis: its applicability in patients with visceral leishmaniasis.* Cytometry A, 2011. **79**(1): p. 35-45.
310. Murray, H.W. and C.F. Nathan, *Macrophage microbicidal mechanisms in vivo: reactive nitrogen versus oxygen intermediates in the killing of intracellular visceral Leishmania donovani.* J Exp Med, 1999. **189**(4): p. 741-6.
311. Blos, M., et al., *Organ-specific and stage-dependent control of Leishmania major infection by inducible nitric oxide synthase and phagocyte NADPH oxidase.* Eur J Immunol, 2003. **33**(5): p. 1224-34.
312. Sousa-Franco, J., et al., *Infection-induced respiratory burst in BALB/c macrophages kills Leishmania guyanensis amastigotes through apoptosis: possible involvement in resistance to cutaneous leishmaniasis.* Microbes Infect, 2006. **8**(2): p. 390-400.
313. Roma, E.H., et al., *Impact of reactive oxygen species (ROS) on the control of parasite loads and inflammation in Leishmania amazonensis infection.* Parasit Vectors, 2016. **9**: p. 193.

314. Beltran-Povea, A., et al., *Role of nitric oxide in the maintenance of pluripotency and regulation of the hypoxia response in stem cells.* World J Stem Cells, 2015. **7**(3): p. 605-17.
315. Ludin, A., et al., *Reactive oxygen species regulate hematopoietic stem cell self-renewal, migration and development, as well as their bone marrow microenvironment.* Antioxid Redox Signal, 2014. **21**(11): p. 1605-19.
316. Nogueira-Pedro, A., et al., *Nitric oxide-induced murine hematopoietic stem cell fate involves multiple signaling proteins, gene expression, and redox modulation.* Stem Cells, 2014. **32**(11): p. 2949-60.
317. Feijo, D., et al., *Dendritic Cells and Leishmania Infection: Adding Layers of Complexity to a Complex Disease.* J Immunol Res, 2016. **2016**: p. 3967436.
318. Martinez-Lopez, M., et al., *Leishmania Hijacks Myeloid Cells for Immune Escape.* Front Microbiol, 2018. **9**: p. 883.
319. Selvapandiyan, A., et al., *Innovations for the elimination and control of visceral leishmaniasis.* PLoS Negl Trop Dis, 2019. **13**(9): p. e0007616.
320. Khalil, E.A., et al., *Epidemiology and clinical manifestations of Leishmania donovani infection in two villages in an endemic area in eastern Sudan.* Trop Med Int Health, 2002. **7**(1): p. 35-44.
321. Moral, L., E.M. Rubio, and M. Moya, *A leishmanin skin test survey in the human population of l'Alacanti region (Spain): implications for the epidemiology of Leishmania infantum infection in southern Europe.* Trans R Soc Trop Med Hyg, 2002. **96**(2): p. 129-32.
322. Dirkx, L., et al., *Long-term hematopoietic stem cells as a parasite niche during treatment failure in visceral leishmaniasis.* Commun Biol, 2022. **5**(1): p. 626.
323. Wierenga, A.T., E. Vellenga, and J.J. Schuringa, *Convergence of hypoxia and TGFbeta pathways on cell cycle regulation in human hematopoietic stem/progenitor cells.* PLoS One, 2014. **9**(3): p. e93494.
324. Dirkx, L., et al., *Long-term hematopoietic stem cells as sanctuary niche with a unique transcriptional signature during treatment failure in visceral leishmaniasis, ACCEPTED.* Commun Biol, 2022.
325. Chan, K.Y.Y., et al., *R4 RGS proteins suppress engraftment of human hematopoietic stem/progenitor cells by modulating SDF-1/CXCR4 signaling.* Blood Adv, 2021. **5**(21): p. 4380-4392.
326. Xie, Z., E.C. Chan, and K.M. Druey, *R4 Regulator of G Protein Signaling (RGS) Proteins in Inflammation and Immunity.* AAPS J, 2016. **18**(2): p. 294-304.
327. Caballero-Franco, C. and S. Kissler, *The autoimmunity-associated gene RGS1 affects the frequency of T follicular helper cells.* Genes Immun, 2016. **17**(4): p. 228-38.
328. Bianchi, M.E. and R. Mezzapelle, *The Chemokine Receptor CXCR4 in Cell Proliferation and Tissue Regeneration.* Front Immunol, 2020. **11**: p. 2109.
329. Pawig, L., et al., *Diversity and Inter-Connections in the CXCR4 Chemokine Receptor/Ligand Family: Molecular Perspectives.* Front Immunol, 2015. **6**: p. 429.

330. Zhang, Y., et al., *CXCR4/CXCL12 axis counteracts hematopoietic stem cell exhaustion through selective protection against oxidative stress.* Sci Rep, 2016. **6**: p. 37827.
331. Liu, Q., et al., *CXCR4 antagonist AMD3100 redistributes leukocytes from primary immune organs to secondary immune organs, lung, and blood in mice.* Eur J Immunol, 2015. **45**(6): p. 1855-67.
332. Garcia-Bernal, D., et al., *Vav1 and Rac control chemokine-promoted T lymphocyte adhesion mediated by the integrin alpha4beta1.* Mol Biol Cell, 2005. **16**(7): p. 3223-35.
333. Montresor, A., et al., *JAK tyrosine kinases promote hierarchical activation of Rho and Rap modules of integrin activation.* J Cell Biol, 2013. **203**(6): p. 1003-19.
334. Chen, S., et al., *Transforming growth factor-beta1 increases CXCR4 expression, stromal-derived factor-1alpha-stimulated signalling and human immunodeficiency virus-1 entry in human monocyte-derived macrophages.* Immunology, 2005. **114**(4): p. 565-74.
335. Franitza, S., et al., *TGF-beta1 enhances SDF-1alpha-induced chemotaxis and homing of naive T cells by up-regulating CXCR4 expression and downstream cytoskeletal effector molecules.* Eur J Immunol, 2002. **32**(1): p. 193-202.
336. Kamir, D., et al., *A Leishmania ortholog of macrophage migration inhibitory factor modulates host macrophage responses.* J Immunol, 2008. **180**(12): p. 8250-61.
337. Van Hout, A., et al., *CXCR4-targeting nanobodies differentially inhibit CXCR4 function and HIV entry.* Biochem Pharmacol, 2018. **158**: p. 402-412.
338. De Clercq, E., *Mozobil(R) (Plerixafor, AMD3100), 10 years after its approval by the US Food and Drug Administration.* Antivir Chem Chemother, 2019. **27**: p. 2040206619829382.
339. Diener, Y., et al., *RNA-based, transient modulation of gene expression in human haematopoietic stem and progenitor cells.* Sci Rep, 2015. **5**: p. 17184.
340. Raja, M.A.G., H. Katas, and M.W. Amjad, *Design, mechanism, delivery and therapeutics of canonical and Dicer-substrate siRNA.* Asian J Pharm Sci, 2019. **14**(5): p. 497-510.
341. Stephens, B.S., et al., *Functional anatomy of the full-length CXCR4-CXCL12 complex systematically dissected by quantitative model-guided mutagenesis.* Sci Signal, 2020. **13**(640).
342. Wang, S., et al., *Emerging Importance of Chemokine Receptor CXCR4 and Its Ligand in Liver Disease.* Front Cell Dev Biol, 2021. **9**: p. 716842.
343. Garcia-Cuesta, E.M., et al., *The Role of the CXCL12/CXCR4/ACKR3 Axis in Autoimmune Diseases.* Front Endocrinol (Lausanne), 2019. **10**: p. 585.
344. Poller, W.C., M. Nahrendorf, and F.K. Swirski, *Hematopoiesis and Cardiovascular Disease.* Circ Res, 2020. **126**(8): p. 1061-1085.
345. Bernhagen, J., et al., *MIF is a noncognate ligand of CXC chemokine receptors in inflammatory and atherogenic cell recruitment.* Nat Med, 2007. **13**(5): p. 587-96.
346. Mitchell, R.A., et al., *Macrophage migration inhibitory factor (MIF) sustains macrophage proinflammatory function by inhibiting p53: regulatory role in the innate immune response.* Proc Natl Acad Sci U S A, 2002. **99**(1): p. 345-50.

347. Satoskar, A.R., et al., *Migration-inhibitory factor gene-deficient mice are susceptible to cutaneous Leishmania major infection.* Infect Immun, 2001. **69**(2): p. 906-11.
348. Richardson, J.M., et al., *Structures of Leishmania major orthologues of macrophage migration inhibitory factor.* Biochem Biophys Res Commun, 2009. **380**(3): p. 442-8.
349. Holowka, T. and R. Bucala, *Role of Host and Parasite MIF Cytokines during Leishmania Infection.* Trop Med Infect Dis, 2020. **5**(1).
350. Holowka, T., et al., *Leishmania-encoded orthologs of macrophage migration inhibitory factor regulate host immunity to promote parasite persistence.* FASEB J, 2016. **30**(6): p. 2249-65.
351. Moore, K.J. and G. Matlashewski, *Intracellular infection by Leishmania donovani inhibits macrophage apoptosis.* J Immunol, 1994. **152**(6): p. 2930-7.
352. Aragon, E., et al., *Structural basis for distinct roles of SMAD2 and SMAD3 in FOXH1 pioneer-directed TGF-beta signaling.* Genes Dev, 2019. **33**(21-22): p. 1506-1524.
353. Dayakar, A., et al., *Cytokines: Key Determinants of Resistance or Disease Progression in Visceral Leishmaniasis: Opportunities for Novel Diagnostics and Immunotherapy.* Front Immunol, 2019. **10**: p. 670.
354. Bartolome, R.A., et al., *Activation of Vav/Rho GTPase signaling by CXCL12 controls membrane-type matrix metalloproteinase-dependent melanoma cell invasion.* Cancer Res, 2006. **66**(1): p. 248-58.
355. Bustelo, X.R., *Vav family exchange factors: an integrated regulatory and functional view.* Small GTPases, 2014. **5**(2): p. 9.
356. Rodriguez-Fdez, S. and X.R. Bustelo, *The Vav GEF Family: An Evolutionary and Functional Perspective.* Cells, 2019. **8**(5).
357. Rodriguez-Fdez, S., et al., *Lysine Acetylation Reshapes the Downstream Signaling Landscape of Vav1 in Lymphocytes.* Cells, 2020. **9**(3).
358. Shilatifard, A., et al., *ELL2, a new member of an ELL family of RNA polymerase II elongation factors.* Proc Natl Acad Sci U S A, 1997. **94**(8): p. 3639-43.
359. Schier, A.C. and D.J. Taatjes, *Structure and mechanism of the RNA polymerase II transcription machinery.* Genes Dev, 2020. **34**(7-8): p. 465-488.
360. Sofia, E., et al., *Biomarkers in Leishmaniasis: From Basic Research to Clinical Application*, in *Biomarker*, B. Ghousia, Editor. 2018, IntechOpen: Rijeka. p. Ch. 11.
361. Ferreira, G.R., et al., *Biomarkers of disease severity in patients with visceral leishmaniasis co-infected with HIV*. Cytokine, 2022. **149**: p. 155747.
362. S, S.L., et al., *Biomarkers of the early response to treatment of visceral leishmaniasis: A prospective cohort study.* Parasite Immunol, 2021. **43**(1): p. e12797.
363. Sengupta, S. and M. Chatterjee, *IgG3 and IL10 are effective biomarkers for monitoring therapeutic effectiveness in Post Kala-Azar Dermal Leishmaniasis.* PLoS Negl Trop Dis, 2021. **15**(11): p. e0009906.
364. Gossage, S.M., M.E. Rogers, and P.A. Bates, *Two separate growth phases during the development of Leishmania in sand flies: implications for understanding the life cycle.* Int J Parasitol, 2003. **33**(10): p. 1027-34.

365. Lewis, K., *Persister cells.* Annu Rev Microbiol, 2010. **64**: p. 357-72.
366. Lewis, K., *Persister cells, dormancy and infectious disease.* Nat Rev Microbiol, 2007. **5**(1): p. 48-56.
367. Rittershaus, E.S., S.H. Baek, and C.M. Sassetti, *The normalcy of dormancy: common themes in microbial quiescence.* Cell Host Microbe, 2013. **13**(6): p. 643-51.
368. Ehrt, S., D. Schnappinger, and K.Y. Rhee, *Metabolic principles of persistence and pathogenicity in Mycobacterium tuberculosis.* Nat Rev Microbiol, 2018. **16**(8): p. 496-507.
369. Dworkin, J. and C.S. Harwood, *Metabolic Reprogramming and Longevity in Quiescence.* Annu Rev Microbiol, 2022. **76**: p. 91-111.
370. Jara, M., et al., *Transcriptional Shift and Metabolic Adaptations during Leishmania Quiescence Using Stationary Phase and Drug Pressure as Models.* Microorganisms, 2022. **10**(1).
371. Jumper, J., et al., *Highly accurate protein structure prediction with AlphaFold.* Nature, 2021. **596**(7873): p. 583-589.
372. Tunyasuvunakool, K., et al., *Highly accurate protein structure prediction for the human proteome.* Nature, 2021. **596**(7873): p. 590-596.
373. Hendrickx, S., et al., *Comparison of Bioluminescent Substrates in Natural Infection Models of Neglected Parasitic Diseases.* Int J Mol Sci, 2022. **23**(24).
374. Volf, P. and V. Volfova, *Establishment and maintenance of sand fly colonies.* J Vector Ecol, 2011. **36 Suppl 1**: p. S1-9.
375. Love, M.I., W. Huber, and S. Anders, *Moderated estimation of fold change and dispersion for RNA-seq data with DESeq2.* Genome Biol, 2014. **15**(12): p. 550.
376. Love, M.I., et al., *RNA-Seq workflow: gene-level exploratory analysis and differential expression.* F1000Res, 2015. **4**: p. 1070.
377. Shanmugasundram, A., et al., *TriTrypDB: An integrated functional genomics resource for kinetoplastida.* PLOS Neglected Tropical Diseases, 2023. **17**(1): p. e0011058.
378. Holm, L., et al., *DALI shines a light on remote homologs: One hundred discoveries.* Protein Science, 2023. **32**(1): p. e4519.
379. Evans, R., et al., *Protein complex prediction with AlphaFold-Multimer.* bioRxiv, 2021: p. 2021.10.04.463034.
380. Goddard, T.D., et al., *UCSF ChimeraX: Meeting modern challenges in visualization and analysis.* Protein Sci, 2018. **27**(1): p. 14-25.
381. Pettersen, E.F., et al., *UCSF ChimeraX: Structure visualization for researchers, educators, and developers.* Protein Sci, 2021. **30**(1): p. 70-82.
382. Hendrickx, S., et al., *Phenotypic adaptations of Leishmania donovani to recurrent miltefosine exposure and impact on sand fly infection.* Parasit Vectors, 2020. **13**(1): p. 96.
383. Van Bockstal, L., et al., *Impaired development of a miltefosine-resistant Leishmania infantum strain in the sand fly vectors Phlebotomus perniciosus and Lutzomyia longipalpis.* Int J Parasitol Drugs Drug Resist, 2019. **11**: p. 1-7.

384. Hendrickx, S., et al., *Comparative Fitness of a Parent Leishmania donovani Clinical Isolate and Its Experimentally Derived Paromomycin-Resistant Strain.* PLoS One, 2015. **10**(10): p. e0140139.
385. Pacakova, L., et al., *Three types of Leishmania mexicana amastigotes: Proteome comparison by quantitative proteomic analysis.* Front Cell Infect Microbiol, 2022. **12**: p. 1022448.
386. Pramanik, P.K., et al., *Bioassay-based Corchorus capsularis L. leaf-derived beta-sitosterol exerts antileishmanial effects against Leishmania donovani by targeting trypanothione reductase.* Sci Rep, 2020. **10**(1): p. 20440.
387. Sumi, M.P. and A. Ghosh, *Hsp90 in Human Diseases: Molecular Mechanisms to Therapeutic Approaches.* Cells, 2022. **11**(6).
388. Mingler, M.K., et al., *Identification of pentatricopeptide repeat proteins in Trypanosoma brucei.* Mol Biochem Parasitol, 2006. **150**(1): p. 37-45.
389. Salavati, R., et al., *KREPA4, an RNA binding protein essential for editosome integrity and survival of Trypanosoma brucei.* RNA, 2006. **12**(5): p. 819-31.
390. Kushawaha, P.K., C.D. Pati Tripathi, and A. Dube, *Leishmania donovani secretory protein nucleoside diphosphate kinase b localizes in its nucleus and prevents ATP mediated cytolysis of macrophages.* Microb Pathog, 2022. **166**: p. 105457.
391. Zappa, F., et al., *The TRAPP complex mediates secretion arrest induced by stress granule assembly.* EMBO J, 2019. **38**(19): p. e101704.
392. Pugacheva, E.N., et al., *HEF1-dependent Aurora A activation induces disassembly of the primary cilium.* Cell, 2007. **129**(7): p. 1351-63.
393. Nascimento, T.L.D., et al., *Prevalence of malaria relapse: systematic review with meta-analysis.* Rev Lat Am Enfermagem, 2019. **27**: p. e3111.
394. Madan, M. and S. Kunal, *COVID-19 reinfection or relapse: an intriguing dilemma.* Clin Rheumatol, 2020. **39**(11): p. 3189.
395. Zhang, Y., *Persisters, persistent infections and the Yin-Yang model.* Emerg Microbes Infect, 2014. **3**(1): p. e3.
396. Sanchez-Valdez, F.J., et al., *Spontaneous dormancy protects Trypanosoma cruzi during extended drug exposure.* Elife, 2018. **7**.
397. Voorberg-van der Wel, A., et al., *Transgenic fluorescent Plasmodium cynomolgi liver stages enable live imaging and purification of Malaria hypnozoite-forms.* PLoS One, 2013. **8**(1): p. e54888.
398. Deb, C., et al., *A novel in vitro multiple-stress dormancy model for Mycobacterium tuberculosis generates a lipid-loaded, drug-tolerant, dormant pathogen.* PLoS One, 2009. **4**(6): p. e6077.
399. Kloehn, J., et al., *Characterization of metabolically quiescent Leishmania parasites in murine lesions using heavy water labeling.* PLoS Pathog, 2015. **11**(2): p. e1004683.
400. Mandell, M.A. and S.M. Beverley, *Continual renewal and replication of persistent Leishmania major parasites in concomitantly immune hosts.* Proc Natl Acad Sci U S A, 2017. **114**(5): p. E801-E810.
401. Jara, M., et al., *Macromolecular biosynthetic parameters and metabolic profile in different life stages of Leishmania braziliensis: Amastigotes as a functionally less active stage.* PLoS One, 2017. **12**(7): p. e0180532.

402. Ouakad, M., et al., *Increased metacyclogenesis of antimony-resistant Leishmania donovani clinical lines.* Parasitology, 2011. **138**(11): p. 1392-9.
403. Vanaerschot, M., et al., *Linking in vitro and in vivo survival of clinical Leishmania donovani strains.* PLoS One, 2010. **5**(8): p. e12211.
404. Honeyborne, I., et al., *Profiling persistent tubercule bacilli from patient sputa during therapy predicts early drug efficacy.* BMC Med, 2016. **14**: p. 68.
405. De Virgilio, C., *The essence of yeast quiescence.* FEMS Microbiol Rev, 2012. **36**(2): p. 306-39.
406. Karamysheva, Z.N., S.A. Gutierrez Guarnizo, and A.L. Karamyshev, *Regulation of Translation in the Protozoan Parasite Leishmania.* Int J Mol Sci, 2020. **21**(8).
407. Bertschi, N.L., et al., *Transcriptomic analysis reveals reduced transcriptional activity in the malaria parasite Plasmodium cynomolgi during progression into dormancy.* Elife, 2018. **7**.
408. Kumar, A., et al., *Redox homeostasis in mycobacteria: the key to tuberculosis control?* Expert Rev Mol Med, 2011. **13**: p. e39.
409. Manger, I.D., et al., *Expressed sequence tag analysis of the bradyzoite stage of Toxoplasma gondii: identification of developmentally regulated genes.* Infect Immun, 1998. **66**(4): p. 1632-7.
410. Downing, T., et al., *Whole genome sequencing of multiple Leishmania donovani clinical isolates provides insights into population structure and mechanisms of drug resistance.* Genome Res, 2011. **21**(12): p. 2143-56.
411. D'Cruz, A.A., et al., *Structure and function of the SPRY/B30.2 domain proteins involved in innate immunity.* Protein Sci, 2013. **22**(1): p. 1-10.
412. Torres-Guerrero, E., et al., *Leishmaniasis: a review.* F1000Research, 2017. **6**: p. 750-750.
413. Bi, K., et al., *Current Visceral Leishmaniasis Research: A Research Review to Inspire Future Study.* Biomed Res Int, 2018. **2018**: p. 9872095.
414. Toepp, A.J. and C.A. Petersen, *The balancing act: Immunology of leishmaniosis.* Res Vet Sci, 2020. **130**: p. 19-25.
415. Andreani, G., et al., *Leishmania infantum amastigotes trigger a subpopulation of human B cells with an immunoregulatory phenotype.* PLoS Negl Trop Dis, 2015. **9**(2): p. e0003543.
416. De Trez, C., et al., *iNOS-producing inflammatory dendritic cells constitute the major infected cell type during the chronic Leishmania major infection phase of C57BL/6 resistant mice.* PLoS Pathog, 2009. **5**(6): p. e1000494.
417. Trigo, J., et al., *Treatment of canine visceral leishmaniasis by the vaccine Leish-111f+MPL-SE.* Vaccine, 2010. **28**(19): p. 3333-40.
418. Le Rutte, E.A., et al., *The potential impact of human visceral leishmaniasis vaccines on population incidence.* PLoS Negl Trop Dis, 2020. **14**(7): p. e0008468.
419. Rossi, M. and N. Fasel, *How to master the host immune system? Leishmania parasites have the solutions!* International immunology, 2018. **30**(3): p. 103-111.
420. Sunter, J. and K. Gull, *Shape, form, function and Leishmania pathogenicity: from textbook descriptions to biological understanding.* Open Biol, 2017. **7**(9).

421. Ronet, C., et al., *Regulatory B cells shape the development of Th2 immune responses in BALB/c mice infected with Leishmania major through IL-10 production.* J Immunol, 2010. **184**(2): p. 886-94.
422. Deak, E., et al., *Murine visceral leishmaniasis: IgM and polyclonal B-cell activation lead to disease exacerbation.* Eur J Immunol, 2010. **40**(5): p. 1355-68.
423. Moon, S., et al., *Detrimental Effect of Trypanosoma brucei brucei Infection on Memory B Cells and Host Ability to Recall Protective B-cell Responses.* J Infect Dis, 2022. **226**(3): p. 528-540.
424. Wykes, M.N., et al., *Plasmodium yoelii can ablate vaccine-induced long-term protection in mice.* J Immunol, 2005. **175**(4): p. 2510-6.
425. Strickland, G.T. and P.C. Sayles, *Depressed antibody responses to a thymus-dependent antigen in toxoplasmosis.* Infect Immun, 1977. **15**(1): p. 184-90.
426. Pape, K.A., et al., *Different B cell populations mediate early and late memory during an endogenous immune response.* Science, 2011. **331**(6021): p. 1203-7.
427. Martensson, I.L., et al., *The pre-B cell receptor checkpoint.* FEBS Lett, 2010. **584**(12): p. 2572-9.
428. Bergmann, B., et al., *Memory B cells in mouse models.* Scand J Immunol, 2013. **78**(2): p. 149-56.
429. Bhattacharya, M. *Understanding B lymphocyte development: a long way to go*. 2019; Available from: https://www.intechopen.com/chapters/62616.
430. Anderson, S.M., et al., *New markers for murine memory B cells that define mutated and unmutated subsets.* J Exp Med, 2007. **204**(9): p. 2103-14.
431. de Melo, C.V.B., et al., *Phenotypical Characterization of Spleen Remodeling in Murine Experimental Visceral Leishmaniasis.* Front Immunol, 2020. **11**: p. 653.
432. Srivastava, S., et al., *Possibilities and challenges for developing a successful vaccine for leishmaniasis.* Parasit Vectors, 2016. **9**(1): p. 277.
433. Hohman, L.S. and N.C. Peters, *CD4(+) T Cell-Mediated Immunity against the Phagosomal Pathogen Leishmania: Implications for Vaccination.* Trends Parasitol, 2019. **35**(6): p. 423-435.
434. Elmahallawy, E.K., A.A.M. Alkhaldi, and A.A. Saleh, *Host immune response against leishmaniasis and parasite persistence strategies: A review and assessment of recent research.* Biomed Pharmacother, 2021. **139**: p. 111671.
435. Halliday, A., et al., *Toll-like receptor 2 (TLR2) plays a role in controlling cutaneous leishmaniasis in vivo, but does not require activation by parasite lipophosphoglycan.* Parasit Vectors, 2016. **9**(1): p. 532.
436. Rosazza, T., et al., *Dynamic imaging reveals surface exposure of virulent Leishmania amastigotes during pyroptosis of infected macrophages.* J Cell Sci, 2020. **134**(5).
437. Castro-Eguiluz, D., et al., *B cell precursors are targets for Salmonella infection.* Microb Pathog, 2009. **47**(1): p. 52-6.
438. Dos Santos, M.A., et al., *Human B cells infected by Trypanosoma cruzi undergo F-actin disruption and cell death via caspase-7 activation and cleavage of phospholipase Cgamma1.* Immunobiology, 2020. **225**(3): p. 151904.

439. Andrews, N.W., *Living dangerously: how Trypanosoma cruzi uses lysosomes to get inside host cells, and then escapes into the cytoplasm.* Biol Res, 1993. **26**(1-2): p. 65-7.
440. Fernandes, M.C., et al., *Trypanosoma cruzi subverts the sphingomyelinase-mediated plasma membrane repair pathway for cell invasion.* Journal of Experimental Medicine, 2011. **208**(5): p. 909-921.
441. Cavalcante-Costa, V.S., et al., *Leishmania amazonensis hijacks host cell lysosomes involved in plasma membrane repair to induce invasion in fibroblasts.* J Cell Sci, 2019. **132**(6).
442. Nothelfer, K., P.J. Sansonetti, and A. Phalipon, *Pathogen manipulation of B cells: the best defence is a good offence.* Nature Reviews Microbiology, 2015. **13**(3): p. 173-184.
443. Bockstal, V., N. Geurts, and S. Magez, *Acute Disruption of Bone Marrow B Lymphopoiesis and Apoptosis of Transitional and Marginal Zone B Cells in the Spleen following a Blood-Stage Plasmodium chabaudi Infection in Mice.* J Parasitol Res, 2011. **2011**: p. 534697.
444. Laksono, B.M., et al., *Measles pathogenesis, immune suppression and animal models.* Curr Opin Virol, 2020. **41**: p. 31-37.
445. Laksono, B.M., et al., *Studies into the mechanism of measles-associated immune suppression during a measles outbreak in the Netherlands.* Nat Commun, 2018. **9**(1): p. 4944.
446. Männe, C., et al., *Salmonella SiiE prevents an efficient humoral immune memory by interfering with IgG(+) plasma cell persistence in the bone marrow.* Proc Natl Acad Sci U S A, 2019. **116**(15): p. 7425-7430.
447. Takaya, A., T. Yamamoto, and K. Tokoyoda, *Humoral Immunity vs. Salmonella.* Frontiers in immunology, 2020. **10**: p. 3155-3155.
448. Smelt, S.C., et al., *B cell-deficient mice are highly resistant to Leishmania donovani infection, but develop neutrophil-mediated tissue pathology.* J Immunol, 2000. **164**(7): p. 3681-8.
449. Amezcua Vesely, M.C., et al., *B-Cell Response during Protozoan Parasite Infections.* Journal of Parasitology Research, 2012. **2012**: p. 362131.
450. Parkash, V., et al., *Vaccines against leishmaniasis: using controlled human infection models to accelerate development.* Expert Rev Vaccines, 2021. **20**(11): p. 1407-1418.
451. Pajonk, F. and E. Vlashi, *Characterization of the stem cell niche and its importance in radiobiological response.* Semin Radiat Oncol, 2013. **23**(4): p. 237-41.
452. Dunay, I.R., et al., *Treatment of Toxoplasmosis: Historical Perspective, Animal Models, and Current Clinical Practice.* Clin Microbiol Rev, 2018. **31**(4).
453. Hendrickx, S., et al., *Evidence of a drug-specific impact of experimentally selected paromomycin and miltefosine resistance on parasite fitness in Leishmania infantum.* J Antimicrob Chemother, 2016. **71**(7): p. 1914-21.
454. Carrillo, E. and J. Moreno, *Editorial: Biomarkers in Leishmaniasis.* Front Cell Infect Microbiol, 2019. **9**: p. 388.

455. Marlais, T., et al., *Visceral Leishmaniasis IgG1 Rapid Monitoring of Cure vs. Relapse, and Potential for Diagnosis of Post Kala-Azar Dermal Leishmaniasis.* Front Cell Infect Microbiol, 2018. **8**: p. 427.
456. Kip, A.E., et al., *Macrophage Activation Marker Neopterin: A Candidate Biomarker for Treatment Response and Relapse in Visceral Leishmaniasis.* Front Cell Infect Microbiol, 2018. **8**: p. 181.
457. Sugiyama, T., et al., *Maintenance of the hematopoietic stem cell pool by CXCL12-CXCR4 chemokine signaling in bone marrow stromal cell niches.* Immunity, 2006. **25**(6): p. 977-88.
458. Shi, Y., D.J. Riese, 2nd, and J. Shen, *The Role of the CXCL12/CXCR4/CXCR7 Chemokine Axis in Cancer.* Front Pharmacol, 2020. **11**: p. 574667.
459. Mostashari Rad, T., L. Saghaie, and A. Fassihi, *HIV-1 Entry Inhibitors: A Review of Experimental and Computational Studies.* Chem Biodivers, 2018. **15**(10): p. e1800159.
460. Choi, W.T., et al., *Targeting chemokine receptor CXCR4 for treatment of HIV-1 infection, tumor progression, and metastasis.* Curr Top Med Chem, 2014. **14**(13): p. 1574-89.
461. Zimmermann, J., et al., *Dual anti-viral and immunomodulatory activity of the CXCR4 inhibitor Balixafortide (POL6326) in preclinical in vitro and in vivo SARS-CoV2 infection models.* Swiss Medical Weekly, 2021. **151**: p. 14s-14s.
462. Daoud, S. and M. Taha, *Ligand-based Modeling of CXC Chemokine Receptor 4 and Identification of Inhibitors of Novel Chemotypes as Potential Leads towards New Anti- COVID-19 Treatments.* Med Chem, 2022. **18**(8): p. 871-883.
463. Choi, H.Y., C.S. Yong, and B.K. Yoo, *Plerixafor for stem cell mobilization in patients with non-Hodgkin's lymphoma and multiple myeloma.* Ann Pharmacother, 2010. **44**(1): p. 117-26.
464. Song, J.S., et al., *A highly selective and potent CXCR4 antagonist for hepatocellular carcinoma treatment.* Proc Natl Acad Sci U S A, 2021. **118**(13).
465. Zhao, R., et al., *Recent Advances in CXCL12/CXCR4 Antagonists and Nano-Based Drug Delivery Systems for Cancer Therapy.* Pharmaceutics, 2022. **14**(8).
466. Jang, Y.G., et al., *Resveratrol inhibits DHT-induced progression of prostate cancer cell line through interfering with the AR and CXCR4 pathway.* J Steroid Biochem Mol Biol, 2019. **192**: p. 105406.
467. Chen, Z., et al., *The combination of G-CSF and AMD3100 mobilizes bone marrow-derived stem cells to protect against cisplatin-induced acute kidney injury in mice.* Stem Cell Res Ther, 2021. **12**(1): p. 209.
468. Pillaiyar, T., et al., *A medicinal chemistry perspective of drug repositioning: Recent advances and challenges in drug discovery.* Eur J Med Chem, 2020. **195**: p. 112275.
469. Moratz, C., et al., *Abnormal B-cell responses to chemokines, disturbed plasma cell localization, and distorted immune tissue architecture in Rgs1-/- mice.* Mol Cell Biol, 2004. **24**(13): p. 5767-75.
470. Yagoubat, A., et al., *Gene Editing in Trypanosomatids: Tips and Tricks in the CRISPR-Cas9 Era.* Trends Parasitol, 2020. **36**(9): p. 745-760.

471. Yagoubat, A., et al., *Universal highly efficient conditional knockout system in Leishmania, with a focus on untranscribed region preservation.* Cell Microbiol, 2020. **22**(5): p. e13159.
472. Wilkinson, A.C., et al., *Long-term ex vivo expansion of mouse hematopoietic stem cells.* Nat Protoc, 2020. **15**(2): p. 628-648.
473. Cotterell, S.E.J., C.R. Engwerda, and P.M. Kaye, *Leishmania donovani infection of bone marrow stromal macrophages selectively enhances myelopoiesis, by a mechanism involving GM-CSF and TNF-a.* Blood, 2000. **95**(5): p. 1642-1651.
474. Abidin, B.M., et al., *Infection-adapted emergency hematopoiesis promotes visceral leishmaniasis.* PLoS Pathogens, 2017. **13**(8): p. e1006422.

Laura Dirkx

PhD student

+32495321000

Laura.Dirkx@uantwerpen.be

Antwerp, Belgium

www.linkedin.com/in/laura-dirkx/

https://www.sciencefiguredout.be/playing-hide-and-seek-parasites

PERSONALIA

Date of Birth	23rd of January 1995
Place of Birth	Genk
Driver's license	Passenger car (B)
Languages	Dutch (mother tongue)
	English (Fluent)
	French (Good)
	German (Notion)

EDUCATION

Master tropical and infectious diseases
University of Antwerp
2016-2018
Greatest distinction

Bachelor biomedical sciences
University of Antwerp
2013-2016
Distinction

ASO – Latin mathematics
OLV lyceum Genk
2007-2013
Distinction

COURSES AND CERTIFICATES

Felasa C
University of Antwerp, **2017**

Basic principles of statistics
University of Antwerp, StatUA, **2019**

Pitch workshop "Science Figured Out"
Selected candidate. Project by Scriptie vzw. Brussels, **2019**

Attest medical blood sampling
Technique of venous blood sampling with vacutainer system.
UZA, Antwerp, **2023**

VOLUNTEERWORK

Exchange student 2011-2013
Comeniusproject, Europe | Exchange in Madrid, Spain, May 2012

Chiro leader 2012-2015
Chiro Mozaïek Winterslag, Genk

Internship (biomedical sciences, University of Antwerp) September 2016
AUREA, NKO-UZA – led by Professor Floris Wuyts | Knowledge and experience in clinical tests of balance

INTERNATIONAL

Erasmus student November 2017 – June 2018
Porto, Portugal – i3S Instituto de Investigação e Inovação em Saúde, under guidance of professor Ana Tomás | **Master Thesis**

Research stay November – December 2022
Incheon, South-Korea – IGC Incheon global campus, university of Ghent, under guidance of professor Stefan Magez | **PhD Thesis**

SCIENTIFIC AWARDS AND GRANTS

Prize for best MSc thesis, biomedical sciences class of 2018, University of Antwerp.

PhD fellowship strategic basic research (1S30721N), 2019-2022, The Research Foundation – Flanders (FWO), Belgium.

Zoetis Travel grant, granted BSPP meeting 30/11/2022 for the WorldLeish conference in Colombia (08/2022), Belgium.

L /D Laura Dirkx
PhD student

+32495321000
Laura.Dirkx@uantwerpen.be
Antwerp, Belgium
www.linkedin.com/in/laura-dirkx/

SCIENTIFIC OUTPUT

Publications

Van Bockstal L., Bulté D., Van den Kerkhof M., **Dirkx L.**, Mabille D., Hendrickx S., Delputte P., Maes L., Caljon G. *Interferon alpha favors macrophage infection by visceral Leishmania species through upregulation of sialoadhesin expression.*
Frontier Immunol. 2020 Jun 9;11:1113. doi: 10.3389/fimmu.2020.01113. PMID: 32582193; PMCID: PMC7296180.
IF: 8.79

Bulté D., Van Bockstal L., **Dirkx L.**, Van den Kerkhof M., De Trez C., Timmermans J-P., Hendrickx S., Maes L., Caljon G. *Miltefosine enhances infectivity of miltefosine-resistant Leishmania infantum by attenuating innate immune recognition.*
PLoS Negl Trop Dis. 2021 Jul 22;15(7):e0009622. doi: 10.1371/journal.pntd.0009622. PMID: 34292975; PMCID: PMC8330912.
IF: 4.52

Vanderhaeghen T., Timmermans S., Watts D., Paakinaho V., Eggermont M., Vandewalle J., Wallaeys C., Van Wyngene L., Van Looveren K., Nuyttens L., Dewaele S., Vanden Berghe J., Lemeire K., De Backer J., **Dirkx L.**, Vanden Berghe W., Caljon G., Ghesquire B., De Bosscher K., Wielockx B., Palvimo J., Beyaert R., and Libert C. *Reprogramming of glucocorticoid receptor function by hypoxia.* **EMBO Rep**. 2022 Jan 5;23(1):e53083. doi: 10.15252/embr.202153083. Epub 2021 Oct 26. PMID: 34699114; PMCID: PMC8728616.
IF: 8.81

Wijnant G-J., Dumetz F., **Dirkx L.**, Bulté D., Cuypers B., Van Bocxlaer K., Hendrickx H. *Tackling drug resistance and other causes of treatment failure in leishmaniasis*. **Front. Trop. Dis**. 2022 May 12. Sec. Antimicrobial Resistance Volume 3. doi: 10.3389/fitd.2022.837460.
Review.

Dirkx L., Hendrickx S., Merlot M., Bulté D., Starick M., Elst J., Bafica A., Ebo D. G., Maes L., Van Weyenbergh J, Caljon G. *Long-term hematopoietic stem cells as a parasite niche during treatment failure in visceral leishmaniasis.*
Commun Biol. 2022 Jun 25;5(1):626. doi: 10.1038/s42003-022-03591-7. PMID: 35752645; PMCID: PMC9233693.
IF: 6.55

Mabille D., **Dirkx L.**, Thys S., Vermeersch M., Montenye D., Govaerts M., Hendrickx S., Takac P., Van Weyenbergh J., Pintelon I., Delputte P., Maes L., Pérez-Morga D., Timmermans J-P., Caljon G. *Pulmonary African trypanosomes: parasitological observations, immunological correlates and effects on lung function.*
Nat Commun. 2022 Nov 18;13(1):7083. doi: 10.1038/s41467-022-34757-w. PMID: 36400767; PMCID: PMC9674601.
IF: 17.69

Hendrickx S, Bulté D, Mabille D, Mols R, Claes M, Ilbeigi K, Ahmad R, **Dirkx L**, Van Acker SI, Caljon G. *Comparison of Bioluminescent Substrates in Natural Infection Models of Neglected Parasitic Diseases.*
Int J Mol Sci. 2022 Dec 16;23(24):16074. doi: 10.3390/ijms232416074. PMID: 36555716; PMCID: PMC9781651.
IF: 6.21

L /D Laura Dirkx
PhD student

+32495321000
Laura.Dirkx@uantwerpen.be
Antwerp, Belgium
www.linkedin.com/in/laura-dirkx/

SCIENTIFIC OUTPUT

Oral presentations

Dirkx L., Bulté D., Hendrickx S., Maes L. and Caljon G. Treatment failure in visceral leishmaniasis: What do bioluminescent infection models reveal about subcurative paromomycin treatment? *Trypanosomatid Meeting*, 28-30/10/2019, Paris, France.

Dirkx L., Hendrickx S., Maes L. and Caljon G. Long-term hematopoietic stem cells as sanctuary niche during treatment failure in visceral leishmaniasis. *EMOP Meeting*, 12-16/10/2021, Belgrade, Serbia.

Dirkx L., Hendrickx S., Maes L. and Caljon G. Identification of long-term hematopoietic stem cells as sanctuary niche with a unique transcriptional signature during treatment failure in visceral leishmaniasis. *BSPP Meeting*, 30/11/2021, Antwerp, Belgium.

Dirkx L., Hendrickx S., Ebo D. G., Van Weyenbergh J., Maes L. and Caljon G. Long-term hematopoietic stem cells as sanctuary niche during treatment failure in visceral leishmaniasis. *WorldLeish*, 1-6/08/2022, Cartagena, Colombia.

Dirkx L., Nicolaes Y., Merlot M., Ebo D. G., Maes L., Van Weyenbergh J., Hendrickx S., Caljon G. Stem cells at the basis of parasite quiescence and treatment failure in visceral leishmaniasis. *Research Day FBD*, 28/10/2022, Antwerp, Belgium.

Dirkx L., Nicolaes Y., Hendrickx S., Maes L. and Caljon G. Characterizing the bone marrow as a parasitological niche responsible for antileishmanial treatment failure. GUGC seminar, 28/11/2022, Incheon, South-Korea.

Dirkx L., Nicolaes Y., Hendrickx S., Maes L. and Caljon G. The bone marrow as a parasitological niche responsible for antileishmanial treatment failure. BSP Spring meeting, 11-14/04/2023, Edinburgh, United Kingdom.

Poster presentations

Dirkx L., Nicolaes Y., Hendrickx S., Maes L. and Caljon G. The bone marrow as a parasitological niche responsible for antileishmanial treatment failure. BSP Spring meeting, 11-14/04/2023, Edinburgh, United Kingdom.

Supervision of students

PhD student

Yasmine Nicolaes, UAntwerpen, 2022-present. *Treatment failure in leishmaniasis: host sanctuary sites and parasite quiescence.* FWO 1123523N.

Master thesis students

Femke Wollaert, UAntwerpen, 2018-2019. *Infection tropism and treatment relapse in visceral leishmaniasis.*

Sylvie Vanden Bossche, UAntwerpen, 2020-2021. *B cells and the CXCL12/CXCR4-axis during post-treatment persistence of visceral leishmaniasis in the major lymphoid target organs.*

Jill Hannes, UGent, 2021-2022. *De monitoring en allopurinol behandeling van leishmaniasis bij muis en hond.*

Marlotte Loyens, UAntwerpen, 2021-2022. *The role of B cells in visceral leishmaniasis in the major lymphoid target organs.*

Yasmine Nicolaes, UAntwerpen, 2021-2022. *Unravelling the molecular immunological basis for persistence of visceral Leishmania species in long term hematopoietic stem cells.*

Bachelor thesis students

Shivani Jibodh, UAntwerpen, 2019-2020. *De rol van het beenmerg in behandelingsfalen en relapse van infectieziekten, zoals viscerale leishmaniasis.*

Michael Rheinberger, FH Campus Wien, Austria, 2020-2021. *Involvement of bone marrow in treatment failure and relapse during visceral leishmaniasis infection.*

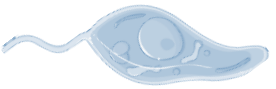

ACKNOWLEDGEMENTS

Antwerp, May 2023

At the end of every PhD thesis an acknowledgement section is customarily added, the part of any thesis that is read the most – or even the only part, let's be honest. Most of you will not even read this part and just scan the pages to see if your name is mentioned somewhere specifically. Don't feel ashamed – that's how I read acknowledgments too. Sufficed to say that this puts a lot of pressure on writing something that should come from the heart. Unfortunately for me, I am not good at expressing gratitude on paper. I am however, very very very grateful for many people in my life, and without their support I would not be writing this today. Disclaimer: there will be an excessive amount of 'thank you's in this section (17 to be exact!) – my apologies beforehand.

I would like to articulate my genuine gratitude to all of those whom, somehow, contributed to the development of this thesis.

Before I start, I would like to express my appreciation to the members of my doctoral committee and external jury members, **prof. dr. Kristel Sleegers**, **prof. dr. Tom Vanden Berghe**, **prof. dr. ir. Stefan Magez**, **prof. dr. Ana Tomàs**, and **prof. dr. ir. Yann Sterckx**, for their invested time, profound evaluation, and constructive feedback.

Guy Caljon, I am very grateful for the effort that you put into helping me to complete this thesis, your contributions were of irreplaceable value. Your suggestions and expertise guided me through a very challenging time! I really appreciate your dedication to your teaching, supervising, and exceptional ambition. I was very fortunate to have had the benefit of learning from you. Throughout the years you always had an open-door policy and were always available. Under your supervision I had the opportunity to write projects, review papers, mentor students and in general bring this thesis to a higher level. I would like to express my sincere

appreciation for all the stimulating discussions, for always encouraging me to push my limits, for granting me the opportunity to go abroad, and giving me the space and trust to work independently.
You once told me that 'time seems to work different for me', and even though I wish that were true, time seems to pass quicker than I would like – I still can't believe I finished. Once again, thank you for everything, and I'm excited to see what the future brings!

Louis Maes, I would not be here if it were not for your trust in me. After completing the oral exams for Preclinical Drug Research and Parasitology the first semester of the first master year, I was asked the question; 'What do you want to do after your masters? Are you interested in doing a PhD? Because we would like you in our team.' I will never forget those words. Completely shocked, but extremely happy I left the exam and spent the next year working hard to have high grades and a great thesis. Thank you for always showing interest in the subject of this thesis, for always believing in the bone marrow as a niche and for all the advice and assistance you have given me during this period.

I believe my PhD journey already started during my MSc internship at i3s in Porto. Here, **Ana Tomàs** stimulated independence and critical thinking, and gave me the opportunity to work out my own little project. After this, I was fully prepared to embark on my journey as a PhD student.

When I first arrived at LMPH, I was greatly supported by my fellow parasitologists **Sarah**, **Dorien, Magali**, **Lieselotte** and **Dimitri**. **Sarah**, thank you for teaching me everything there is to know about our favorite parasite *Leishmania*. For sharing the love for swoon-worthy romantic movies, Nicholas Sparks books and Miraculous Ladybug. **Lieselotte**, thank you for the sleepwalking gift you once gave me during a conference (haha!), and for our fun afterwork activities such as Zumba, interval training, and self-defense. **Dimitri**, thank you for showing me the wonders of flow cytometry and Nutella biscuits. **Magali**, thank you for always being so kind and

patient. You once called me a 'bubbly' person, and to this day I still think of it as one of the sweetest compliments I ever received.

After my first year, the famous *second-year-blues* started. Everybody doing a PhD knows this as the year where you realize you will nót change the world with your thesis, you already wasted one year of your precious little four years, and you still have no idea how to progress in your work. On top of that, the infamous COVID-19 put a stop to any lab work for months, again depriving us of precious time.

There comes a time in everybody's life when they must resort to stronger methods to stay focused and awake: **Coffee**. I want to thank coffee for being there on many late-night lab days, for keeping me motivated and alert. This is around the time we founded the 'What Else?' group. After convincing our PI to purchase a Nespresso machine – because it would obviously increase our work effort – we started our mini bar of syrups, cocoa powder, and cinnamon sugar. Thousands of latte art trials later, we decided to stick with science. Our coffee breaks (only one in the afternoon of course!) are the fuel I look forward to everyday.

I will always remember these last two years as a time spent with a golden group of remarkable people. Doing a PhD can often feel very lonely. The greatest gift you can have in this journey is supporting, loving, and enjoyable colleagues. **Dorien**, **Margot**, **Mathieu**, **Sara**, **Kayhan**, and **Rokaya**, thank you for all the laughs, good times, relatable memes, and shared misery. **Mathieu**, Anakin Skywalker is the greatest Jedi to have every existed, his midi-chlorian count is off the charts. That being said, I always enjoyed our talks, discussions, laughs and shared interests in 'nerdy' stuff, for which I want to thank you. **Sara**, thank you for being the postdoc I never knew I needed, for the deep conversations but also the 'superficial' laughs that we shared (America can be defined in a single word?). **Kayhan**, thank you for being my work hubby, and for letting me take a piece of tape every day without having to pay.

Yasmine (Esq.), in the last year I had the privilege to mentor you as a MSc student and now as a junior PhD student, as the 'successor' to the LT-HSC story. There are not many people in life that can make you laugh to the point of crying (at least not for me), but with you, every day in the lab there is something to laugh about #rokwama. I look forward to our partnership in the LT journey, our Anakin marathons, and to more kdrama episodes during long melody days. I am sure my StemLeish baby is in good hands.

I would also like to thank everyone else working at **LMPH**, from bacteriology and virology, to all labtechs. I always enjoyed LMPH-days, barbecues, summer lunches in the sun, the snackening, the snackening 2.0 and every happy moment together in the lab.

In my last months I was granted the great opportunity to go to Incheon, South-Korea, to the lab of professor **Stefan Magez** and professor **Magdalena Radwanska**. Their unquestionable knowledge on the subject of B cell immunity greatly helped in finalizing the data analysis of chapter V of this thesis. Here I met the sweetest people who became great friends. **Hien**, **Phil**, **Boyoon**, **Hang**, **Isaac**, **Tseggy** and **Odongo**, thank you all for making me feel at home and indulging me in the Korean lifestyle, food (hotpot!), traditional palaces, kdramas (of course), and just in general for giving me the warmest welcome I could ever wish for. 감사합니다

Over the past five years, some colleagues became irreplaceable friends;

Ju Li Moon, who shares my love for Japan, introduced me to the wonders of Ghibli and with whom I spend many evenings painting, watching movies, and eating the absolute best noodles ever. Thank you for being you, 愛してるよ.

My fellow Outlanders; **Dorien** and **Margot**. Dorien, thank you for making me an auntie to the sweetest Liene (mijn dikke vriend), for the great synergistic top team and lab vibes, and for always being there to talk. Margot, when you joined LMPH, it was the first time I didn't feel alone in my ibs journey. Finally, there was someone

who understood the misery of terrible bowls. On top of that, I had someone who could share my misery of the FACSMelody – the sorter that we, for some reason, use every day but somehow never works. Words cannot describe how grateful I am for having you both in my life. Or at least not my words, so I'll say it in the words of our favorite Scotsman; *when the day shall come, that we do part, if my last words are not 'I love you' – ye'll ken it was because I didna have time.*

Tati, my forever bestie, where do I even start? We've been best friends for almost 10 years now, supporting each other through every exam period, every stressful day, every high and every low both at home and at work. I have no idea what I would have done or would do without you. Every movie night, painting session, dance practice, BTS sing-along, foodie moment, or even work-out in your living room, are all very precious to me. Special thanks for helping me with digitalizing my drawings that are at the beginning of each chapter in this thesis. You've been an amazing support these last months, and I hope to do the same for you when you're finishing. I believe in you! Saranghae.

Burnie en **Siesert**, mijn mede big brain siblings, dankjulliewel voor alle etentjes en brunchkes waar we gewoon over belachelijke dingen konden lachen en babbelen. Liesa, jij hebt zo ongelofelijk veel doorzettingsvermogen, daar kan ik alleen maar naar opkijken. Bertje, jouw grote hart en ambitieuze toekomstplannen doen me geloven in de term 'dream big!'. Ik ben super trots om jullie zus te zijn.

Mama en **papa**, ik kan jullie nooit genoeg bedanken voor alles wat jullie voor mij gedaan hebben, doen en zullen blijven doen. Wat ik ook had gedaan met mijn leven tot nu toe, ik weet dat jullie altijd trots zouden zijn geweest. Of ik nu mijn doctoraat in de biomedische wetenschappen aflegde of stofzuigers verkocht deur-aan-deur, ik weet dat jullie me altijd zouden hebben gesteund. Ik ben ongelofelijk dankbaar voor de lange weekends die ik thuis kon spenderen afgelopen jaren om even een pauze te hebben van het PhD-leven en gewoon terug als kind thuis kon zijn. De vele snackjes, drankjes, series en knuffels. Ik hou van jullie.

Bert, we startte onze PhD samen 5 jaar geleden, toen we nog maar net samen waren. Daarbovenop kwam dan ook nog eens covid. Toch heeft het ons dichter bij elkaar gebracht, omdat we samen konden delen in de 'miserie' van lange werkdagen en weekenden, dagelijkse stress en prestatiedruk voor resultaten. Zonder jouw lekkere kookkunsten, dagelijkse Caprisun, en knuffels van onze **Bumi**, was er niet veel van mij over gebleven. Dankjewel voor alle steun en begrip die je mij gegeven hebt in deze periode en ik hoop – nee beloof, dat ik jou hetzelfde zal geven wanneer jij aflegt.

Liefs, Laura